AWARD NUMBER: W81XWH-18-1-0547

TITLE: Brigatinib and Its Combination with INK-128 as a Novel Treatment for *NF2*-Deficient Meningioma

PRINCIPAL INVESTIGATOR: Long-Sheng Chang, Ph.D.

CONTRACTING ORGANIZATION: The Research Institute at Nationwide Children's Hospital, Columbus, Ohio 43205-2696

REPORT DATE: October 2019

TYPE OF REPORT: Annual

PREPARED FOR: U.S. Army Medical Research and Materiel Command
Fort Detrick, Maryland 21702-5012

DISTRIBUTION STATEMENT: Approved for Public Release;
Distribution Unlimited

The views, opinions and/or findings contained in this report are those of the author(s) and should not be construed as an official Department of the Army position, policy or decision unless so designated by other documentation.

REPORT DOCUMENTATION PAGE

Form Approved
OMB No. 0704-0188

Public reporting burden for this collection of information is estimated to average 1 hour per response, including the time for reviewing instructions, searching existing data sources, gathering and maintaining the data needed, and completing and reviewing this collection of information. Send comments regarding this burden estimate or any other aspect of this collection of information, including suggestions for reducing this burden to Department of Defense, Washington Headquarters Services, Directorate for Information Operations and Reports (0704-0188), 1215 Jefferson Davis Highway, Suite 1204, Arlington, VA 22202-4302. Respondents should be aware that notwithstanding any other provision of law, no person shall be subject to any penalty for failing to comply with a collection of information if it does not display a currently valid OMB control number. **PLEASE DO NOT RETURN YOUR FORM TO THE ABOVE ADDRESS.**

1. REPORT DATE	2. REPORT TYPE	3. DATES COVERED
October 2019	Annual	15 Sept. 2018 – 14 Sept. 2019

4. TITLE AND SUBTITLE

Brigatinib and Its Combination with INK-128 as a Novel Treatment for *NF2*-Deficient Meningiomas

5a. CONTRACT NUMBER

5b. GRANT NUMBER
W81XWH-18-1-0547

5c. PROGRAM ELEMENT NUMBER

6. AUTHOR(S)

Long-Sheng Chang, Ph.D.

E-Mail: Long-Sheng.Chang@nationwidechildrens.org

5d. PROJECT NUMBER

5e. TASK NUMBER

5f. WORK UNIT NUMBER

7. PERFORMING ORGANIZATION NAME(S) AND ADDRESS(ES)

Research Institute at Nationwide Children's Hospital
700 Children's Drive
Columbus, OH 43205-2696

8. PERFORMING ORGANIZATION REPORT NUMBER

9. SPONSORING / MONITORING AGENCY NAME(S) AND ADDRESS(ES)

U.S. Army Medical Research and Materiel Command
Fort Detrick, Maryland 21702-5012

10. SPONSOR/MONITOR'S ACRONYM(S)

11. SPONSOR/MONITOR'S REPORT NUMBER(S)

12. DISTRIBUTION / AVAILABILITY STATEMENT

Approved for Public Release; Distribution Unlimited

13. SUPPLEMENTARY NOTES

14. ABSTRACT

Presently, an FDA-approved medical therapy for the treatment of *NF2*-deficient meningiomas is not available. In our continued efforts to identify novel targeted therapies for NF2-assoicated tumors, we, as members of the Synodos for NF2 Consortium in collaboration with the National Center for Advancing Translational Sciences (NCATS), have identified Brigatinib, a potent inhibitor of anaplastic lymphoma kinase (ALK) and other receptor tyrosine kinases (RTKs), to be effective as a single agent in inhibiting proliferation of *NF2*-deficient meningioma cells and suppressing tumor growth in an orthotopic, quantifiable meningioma animal model. Our additional studies showed that INK-128, a dual mTORC1/2 inhibitor, synergized with Brigatinib to potently suppress meningioma cell proliferation *in vitro*. Based on these data, we have proposed to further evaluate the Brigatinib/INK-128 combination as an effective treatment for *NF2*-deficient meningiomas and investigate their mechanisms of action. During this report period, we demonstrated that *NF2*-deficient meningiomas did not express ALK and that Brigatinib potently suppressed the growth of *NF2*-deficient tumors via inhibition of multiple RTKs and non-RTKs, such as focal adhesion kinase (FAK), which has previously been recognized as an oncoprotein in NF2-related tumors. We have also determined the maximal tolerable doses (MTDs) for the Brigatinib and INK-128 drug combination and are in the process of generating mice bearing intracranial sporadic meningioma xenografts for the efficacy study. In addition, we are developing another xenograft animal model using an NF2-associated meningioma.

15. SUBJECT TERMS

Neurofibromatosis type 2 (NF2), *NF2* gene, meningioma, Brigatinib, anaplastic lymphoma kinase (ALK), receptor tyrosine kinase (RTK), INK-128, mTORC1/2, inhibitor, imaging

16. SECURITY CLASSIFICATION OF:			17. LIMITATION OF ABSTRACT	18. NUMBER OF PAGES	19a. NAME OF RESPONSIBLE PERSON
a. REPORT	b. ABSTRACT	c. THIS PAGE			USAMRMC
Unclassified	Unclassified	Unclassified	Unclassified	15 + Appendix	19b. TELEPHONE NUMBER *(include area code)*

Table of Contents

	Page
Cover…….……...……	1
SF298……..……	2
Table of Content…….……...	3
1. Introduction…….……..…...	4
2. Keywords……..	4
3. Overall Project Summary...……...…….……	4 - 5
4. Key Research Accomplishments...……...	5 - 10
5. Impact……..…….……	10
6. Changes/Problems…….…….……	11
7. Publications, Abstracts, and Presentations…….……	11 - 13
6. Participants and Other Collaborating Organizations…….	13 - 14
9. Reportable Outcomes……..……	14
10. Other Achievements……	14
11. References…….……	14 - 15
12. Appendices…….……...	15

1. INTRODUCTION *Narrative that briefly (one paragraph) describes the subject, purpose and scope of the research*

Meningiomas, originating from the meningothelial cells of the arachnoid layer lining the brain, are the most common brain tumors (Ostrom et al., 2018). These tumors can occur spontaneously in the general population or frequently found in patients with Neurofibromatosis Type 2 (NF2), an autosomal-dominant genetic disorder caused by mutations in the *NF2* tumor suppressor gene (Rouleau et al., 1993; Trofatter et al., 1993). Current treatment options for NF2-associated meningiomas are limited to surgery and radiation; however, these treatments could cause severe complications, such as seizure, intracranial bleeding, and stroke (Suppiah et al., 2019). As patients with NF2 often develop multiple meningiomas, surgery may not be possible due to too many tumors or the locations that are difficult to operate, such as in the skull base. Also, incomplete tumor resection is not uncommon and is a main cause of tumor recurrence. In addition, radiation therapy may induce malignant transformation of benign tumors and increase risk for secondary malignancies. Together, these factors underscore the importance of developing effective medical therapies that stop tumor growth or completely eradicate these NF2-associated tumors. To accelerate drug development for NF2-related tumors, the Children's Tumor Foundation previously sponsored the establishment of the multi-institutional Synodos for NF2 Consortium (Synodos for NF2 Consortium, 2018). In collaboration with the NIH – National Center for Advancing Translational Sciences (NCATS), the Synodos for NF2 team, which included us, conducted high-throughput drug screening of isogenic pairs of *NF2*-deficient and *NF2*-expressing disease-relevant cells to identify actionable drug targets for the treatment of both NF2-related tumors. Using this approach, the team established the FDA-approved, multi-receptor tyrosine kinase (RTK) inhibitor, Brigatinib, as a potent inhibitor of *NF2*-deficient meningioma growth, both *in vitro* and *in vivo*. In addition, we, together with Dr. Vijaya Ramesh who was also a member of the Synodos for NF2 Consortium at Massachusetts General Hospital (MGH), found that INK-128, a high-potent inhibitor of both mTORC1 and mTORC2 kinases previously shown to be aberrantly activated in *NF2*-deficient meningiomas, synergizes with Brigatinib to suppress the growth of *NF2*-deficient meningioma cells *in vitro*. Based on these findings, we (Dr. Chang and Dr. Ramesh) have proposed to evaluate Brigatinib and INK-128 as a novel drug combination to treat *NF2*-deficient meningiomas and to investigate their molecular mechanisms of action. It is hoped that the results to be obtained from this study will potentially lead to an effective combination treatment approach for NF2.

2. KEYWORDS (Limit to 20 words)

Neurofibromatosis type 2 (NF2), *NF2* gene, meningioma, Brigatinib, anaplastic lymphoma kinase (ALK), receptor tyrosine kinase (RTK), INK-128, mTORC1/2, inhibitor, imaging

3. OVERALL PROJECT SUMMARY

Presently, an FDA-approved medical therapy is not available for the treatment of *NF2*-deficient meningiomas. To identify novel targeted therapies, either alone or in combination, for these tumors, we, as members of the Synodos NF2 team in collaboration with Dr. Marc Ferrer of the NCATS, previously identified Brigatinib, an inhibitor of anaplastic lymphoma kinase (ALK) and several other RTKs that are frequently activated in NF2-associated tumors, to be effective as a single agent in inhibiting proliferation of primary human meningioma cells and suppressing meningioma growth in an intracranial *NF2*-deficient meningioma model. In addition, together with Dr. Ramesh of MGH, we found that INK-128, a potent inhibitor of both mTORC1 and

mTORC2 complexes previously shown to be aberrantly activated in *NF2*-deficient meningiomas, synergizes with Brigatinib to suppress the growth of *NF2*-deficient meningioma cells *in vitro*. Based on these findings, we have proposed to further evaluate the Brigatinib/INK-128 combination as an effective treatment for *NF2*-deficient meningiomas. The **objective** of this research is to investigate the mechanistic aspects of Brigatinib activity either alone or in combination with INK-128 in *NF2*-null *in vitro* and *in vivo* meningioma models with the ultimate goal of translating this therapy into the clinic for treating these NF2-associated tumors. To achieve this goal, the following two specific aims are proposed:

Aim 1 will evaluate the mechanism by which Brigatinib inhibits proliferation of *NF2*-null meningioma cells and to understand the synergy between Brigatinib and INK-128 in growth inhibition. Brigatinib was originally designed as a highly selective and potent inhibitor of ALK. It also has activity against ROS1 and other RTKs (Huang et al., 2016; Zhang et al., 2016). We hypothesize that mutation-independent activation of ALK/ROS1 is likely in *NF2*-null meningioma cells. To test this hypothesis, we will examine the expression and activation of ALK and ROS1 upon *NF2* loss and to address whether Brigatinib functions in an ALK/ROS1-dependent manner or as an inhibitor of other RTKs. Further, we will address the question how Brigatinib synergizes with the dual mTORC1/2 inhibitor INK-128 by examining the bypass signaling after single and combination treatment with these two drugs.

Aim 2 will determine the anti-tumor activity of Brigatinib and INK-128 combination in orthotopic *NF2*-deficient meningioma models. We have found that as a single agent, INK-128 also effectively suppresses intracranial Ben-Men-1 meningioma growth in mice (Angus et al., 2018). We hypothesize that combined Brigatinib and INK-128 treatment restrains activation of bypass signaling pathways, such as the AKT-mTOR pathway, resulting in efficient tumor inhibition. We plan to evaluate the antitumor effects of the Brigatinib/INK-128 combination in *NF2*-deficient sporadic as well as NF2-associated meningiomas. We will analyze treated tumors for inhibition of any bypass signaling pathways.

Brigatinib is an FDA-approved drug, and a recent Phase I clinical study of INK-128 has demonstrated tolerability and encouraging tumor responses (Ghobrial et al., 2016). Should the proposed Brigatinib/INK-128 combination show impressive anti-tumor efficacy in *NF2*-deficient meningiomas, the results could be quickly translated to human evaluation. Identification of a medical therapy that effectively eradicates NF2-related tumors would significantly advance our current approach to NF2 treatment and greatly improve the clinical care and long-term treatment outcomes for these patients.

4. KEY RESEARCH ACCOMPLISHMENTS:

(i) What were the major goals of the project?

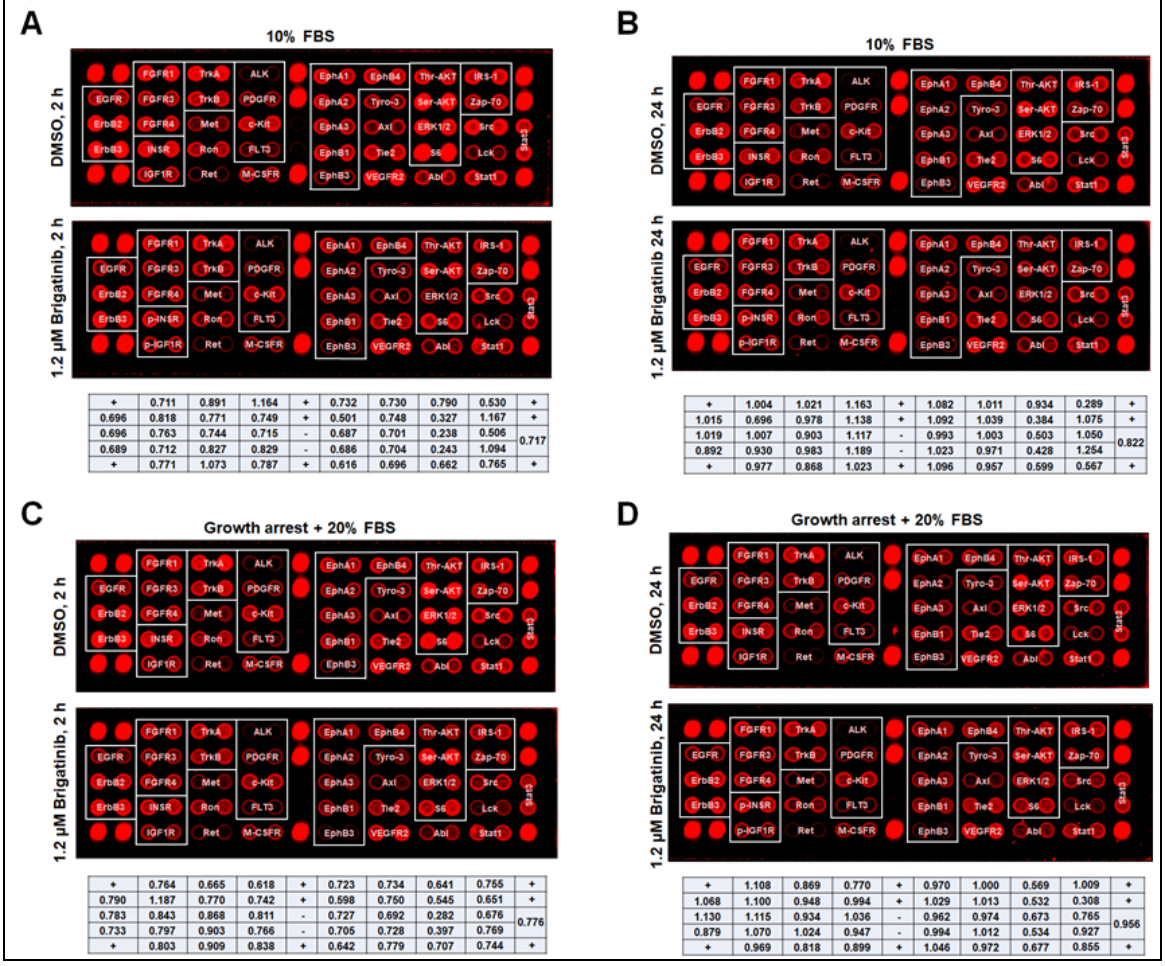
The major **goals** of this project are to evaluate Brigatinib and INK-128 as a novel drug combination to treat *NF2*-deficient meningiomas and to investigate their molecular mechanisms of action.

(ii) What was accomplished under these goals?

Previously, we, as members of the Synodos for NF2 team, demonstrated that Brigatinib potently suppressed the growth of *NF2*-deficient meningioma growth both *in vitro* and in a preclinical animal model. With this grant support, we further investigated its

mechanism of action. Using the PathScan® RTK Signaling Antibody Array, we profiled the expression of 28 phospho-RTKs (p-RTKs) and 11 downstream signaling nodes in *NF2*-deficient Ben-Men-1 meningioma cells treated with one-IC_{50} dose of Brigatinib or DMSO under active growth conditions in 10% FBS or in growth-arrested cells stimulated with 20% serum. Intriguingly, while Brigatinib has been described as a potent ALK inhibitor and is used clinically for the treatment of ALK+ non-small cell lung carcinoma (Huang et al., 2016; Zhang et al., 2016), we did not detect any ALK signal in Ben-Men-1 cells with or without Brigatinib treatment under both growth conditions (Figure 1).

Figure 1. Inhibition of multiple RTKs and non-RTKs in Brigatinib-treated Ben-Men-1 cells grown under various conditions. PathScan® RTK signaling antibody array analysis was conducted using cells grown in 10% FBS and treated with 1x IC_{50} of brigatinib for 2h (A) and 24 h (B) or in growth-arrested cells stimulated with 20% FBS in the presence of 1x IC_{50} of brigatinib for 2h (C) and 24 h (D).). The numeric table below each pair of arrays displays the fold-change in fluorescence detected for each phospho-protein expressed in cells treated with brigatinib relative to DMSO control after subtraction of the fluorescence in the background control spots (indicated as "-"). Positive control spots are denoted as "+".



Western blot analysis confirmed that ALK expression was not detected in Ben-Men-1 cells (Figure 2A) or normal meningeal cells, three *NF2*-deficient meningioma cell lines, and four primary meningioma cell cultures with or without *NF2* loss (Figure 3). Similarly, we also did not detect ALK expression in primary schwannoma cells and cell lines as well as schwannoma tumors (data not shown). In contrast, we observed a broad range of kinases that were active in Ben-Men-1 cells, with similar patterns of activity between logarithmically growing cells and growth-arrested cells stimulated with 20% serum

(Figures 1A and 1C). Notably, strong expression of phosphorylated ErbB2, ErbB3, INSR, FGFR1, TRKA, c-Kit, VEGFR2, and several EPH receptors was observed. Importantly, Brigatinib treatment reduced the levels of most of these p-RTKs with the most significant reduction in EGFR, ErbB2, ErbB3, VEGFR2, and EPH receptors, particularly in cells treated for 2h. In addition, Brigatinib treatment led to attenuation of the downstream signals from these RTKs, including p-AKT(S473 and T308) and p-ERK1/2. The phosphorylation of most of the Brigatinib-inhibited RTKs showed some recovery to baseline levels after 24h, although some of their downstream signaling proteins, such as ERK1/2, AKT, and S6, remained markedly suppressed (compare Figures 1A and 1C with Figures 1B and 1D).

Figure 2. Brigatinib inhibits multiple RTKs, non-RTKs, and their downstream signals. (A) Western blot analysis was conducted to detect ALK expression in Ben-Men-1 cells grown under various growth conditions and with or without brigatinib treatment. (B) Brigatinib treatment greatly reduced phosphorylation of non-RTKs FER and FAK, RTKs EPHA2 and ErbB3, and their downstream signaling molecules AKT, ERK1/2, and S6 in active growing Ben-Men-1 cells or growth-arrested cells stimulated with 20% serum. (C) Brigatinib blocked phosphorylation of EGFR, ErbB3, and IGF1R in growth-arrested Ben-Men-1 cells stimulated with each cognate ligand.

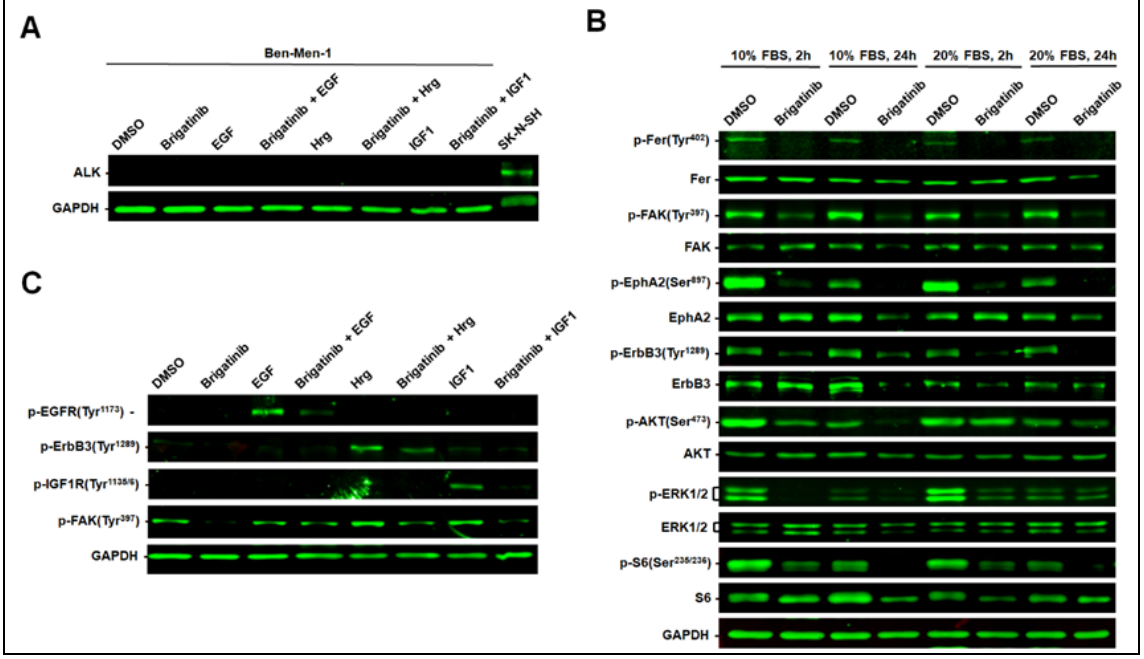
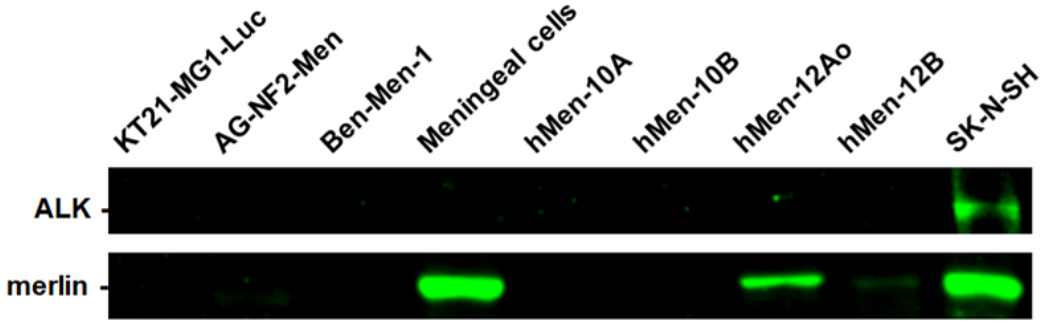
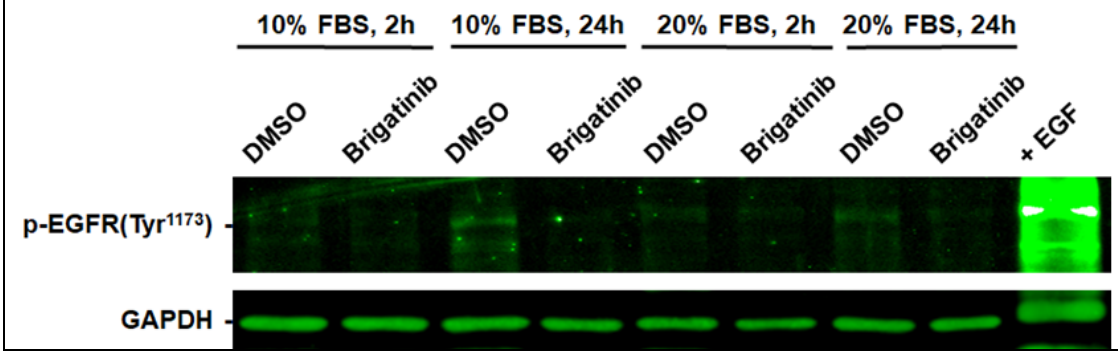


Figure 3. ALK was not detected in normal meningeal and meningioma cells with or without *NF2* expression. Equal amounts of protein lysates from three human meningioma cell lines (KT21-MG1-Luc, AG-NF2-Men, and Ben-Men-1), normal meningeal cells, and four primary meningioma cultures (hMen-10A, hMen-10B, hMen-12Ao, hMen-12B) were used in Western blot analysis to probe ALK and merlin expression. SK-N-SH neuroblastoma cells, which express ALK, were used as a positive control.



Further, Western blot analysis corroborated that phosphorylation of the non-RTKs FAK/PTK2 and FER were noticeably reduced in Brigatinib-treated Ben-Men-1 cells under active growth conditions in 10% FBS or in growth-arrested cells stimulated with 20% serum (Figure 2B). Similar to p-RTK array analysis, we observed reduced phosphorylation of ErbB3 and EphA2 in Brigatinib-treated cells. Also, their downstream signaling nodes ERK1/2, AKT, and S6 were all markedly decreased. However, under the same growth conditions, the basal levels of p-EGFR were minimally detectable and were lost following Brigatinib treatment particularly after 24h (Figure 4). Additionally, we did not detect p-IGF1R under these growth conditions (data not shown). Therefore, we investigated the effects of Brigatinib in ligand-induced activation of IGF1R, EGFR, and ErbB3 in Ben-Men-1 cells. Upon each cognate ligand stimulation, p-EGFR, p-ErbB3, and p-IGF1R were readily detected in Ben-Men-1 cells, and Brigatinib treatment abrogated their phosphorylation (Figure 2C).

Figure 4. Ben-Men-1 cells expressed low levels of p-EGFR, which was abolished by brigatinib treatment. Western blot analysis revealed that while phosphorylated EGFR was robustly induced in EGF-stimulated Ben-Men-1 cells, only very low levels of p-EGFR were detected in actively-growing cells or growth-arrested cells stimulated with 20% serum for 24h. Brigatinib treatment diminished p-EGFR expression.



Taken together, these results indicate that Brigatinib possessed potent anti-tumor activity against *NF2*-deficient tumors via inhibition of multiple RTKs frequently activated in these tumors, but not ALK, as well as blockade of several non-RTKs, such as FAK (focal adhesion kinase), which has previously been recognized as an oncoprotein in NF2-related tumors (Ammoun and Hanemann, 2011; Blakeley and Plotkin, 2016). The results presented here together with the findings obtained previously by the Synodos for NF2 team have been combined and written into a manuscript to be submitted for publication (please see the attached manuscript in Appendix). In addition, we have presented these findings to the 2018 and 2019 NF Conferences (also see Appendix).

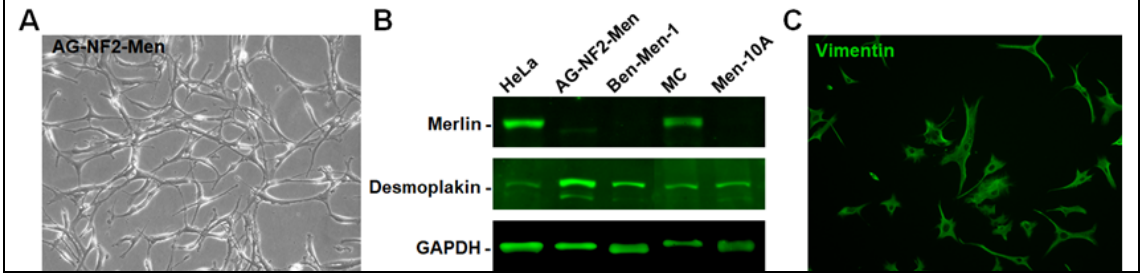
It should be mentioned that the Synodos for NF2 team also demonstrated anti-tumor activity of Brigatinib in a genetically-engineered mouse model for NF2-associated schwannoma. A clinical trial is being planned to evaluate Brigatinib as a new treatment for both meningioma and schwannoma in patients with NF2.

During this past year, we have also worked with the Human Research Protection Office (HRPO) of the US Army Medical Research and Materiel Command (USAMRMC) Office of Research Protections (OPR) and received approval for our IRB-approved Human Subjects protocol. In addition, we submitted ACURO Animal Use Appendix for Research Involving Animals to the Animal Care and Use Review Office (ACURO) and received approval for our animal study. With these approvals, we have begun to test the maximal tolerable doses (MTDs) for the Brigatinib and INK-128 drug combination. We found that

immunodeficient NSG (*NOD.Cg-Prkdc*^{scid} *Il2rg*^{tmlWjl}*/SzJ*) mice tolerate Brigatinib at 50 mg/kg/day (formulated in 90% polyethylene glycol and 10% 1-methyl-2-pyrrolidinone) and INK-128 at 0.75 mg/mg/kg/day (prepared in 5% 1-methyl-2-pyrrolidinone, 15% polyvinylpyrrolidone, and 80% water), either alone or in combination. We are presently generating a cohort of NSG mice bearing *NF2*-deficient Ben-Men-1-LucB sporadic meningioma xenografts at the skull base for the efficacy study.

In addition, we have generated a meningioma cell line from a grade I tumor from an NF2 patient by telomerase immortalization. This NF2-associated meningioma cell line, named AG-NF2-Men, retained many characteristics of the original tumor; it was slow growing and morphologically looked fibroblastic in culture (Figure 5A). Western blot analysis confirmed that AG-NF2-Men cells did not express the NF2 protein, indicating that they are *NF2*-null (Figure 5B). Also, AG-NF2-Men cells expressed several meningioma markers, including desmoplakin and vimentin (Figures 5B and 5C). It should be pointed out that AG-NF2-Men represents the first NF2-associated, grade-I meningioma cell line.

Figure 5. AG-NF2-Men, a telomerase-immortalized meningioma cell line established from a grade I tumor from an NF2 patient. (A) Morphology of AG-NF2-Men cells in culture, exhibiting a spider web-like growth pattern. (B) Western blot analysis confirmed that like Ben-Men-1 meningioma cells, established from a sporadic grade I tumor (Püttmann et al., 2005; Burns et al., 2013), AG-NF2-Men cells did not express merlin, the NF2 gene product. In contrast, normal meningeal cells (MC) and HeLa cervical carcinoma cells, readily express merlin. Also, the NF2/merlin protein was not detected in a primary meningioma cell culture prepared from a sporadic grade I meningioma (Men-10A). Desmoplakin, a component of desmosomes previously reported to be expressed in meningioma cells, was detected in AG-NF2-Men, Ben-Men-1, MC, and primary Men-10A cells. (C) Immunofluorescence staining confirmed that AG-NF2-Men cells also expressed vimentin, a marker commonly found in meningiomas.



To generate a quantifiable, orthotopic animal model for NF2-associated meningioma, we transduced AG-NF2-Men cells with Lenti-CMV-Luc lentiviruses, which carry a luciferase-expressing cassette as we did for Ben-Men-1 cells previously (Burns et al., 2013). We are presently characterizing lentivirus-transduced clones for luciferase expression. The clone with the highest luciferase activity, once identified, will be used in stereotactic injection into the skull base to generate tumor-bearing mice for drug evaluation.

(iii) What opportunities for training and professional development has the project provided?

This project was not intended to provide training and professional development opportunities; therefore, we have "Nothing to Report."

(iv) How were the results disseminated to communities of interest?

The results obtained over the last year and presented above have been combined with the data obtained previously by the Synodos for NF2 team, which includes us, and written into a manuscript to be submitted for publication (see Appendix). In addition, we have presented these findings to the 2018 and 2019 NF Conferences (also see

Appendix). As the Synodos for NF2 team also demonstrated anti-tumor activity of Brigatinib in a genetically-engineered mouse model for NF2-associated schwannoma, a clinical trial is being planned to evaluate Brigatinib as a new treatment for both meningioma and schwannoma in patients with NF2.

(v) What do you plan to do during the next reporting period to accomplish the goals?

As mentioned above, our RTK Signaling Antibody Array and Western blot analyses demonstrated that Brigatinib suppressed the growth of *NF2*-deficient meningioma via inhibition of multiple RTKs, but not ALK, as well as blockade of several non-RTKs, such as FAK. We are presently conducting experiments to investigate how Brigatinib synergizes with the mTOR kinase inhibitor INK-128 to further restrain meningioma cell proliferation. Also, we are generating intracranial Ben-Men-1-LucB sporadic meningioma xenografts in NSG mice to evaluate the anti-tumor efficacy of the Brigatinib and INK-128 combination. In addition, we are developing an orthotopic NF2-associated meningioma model using the AG-NF2-Men cell line that we have established.

5. IMPACT

(i) What was the impact on the development of the principal discipline(s) of the project?

Identification of a medical therapy that effectively eradicates NF2-related tumors would significantly advance our current approach to NF2 treatment and greatly improve the clinical care and long-term treatment outcomes for these patients. Brigatinib is an FDA-approved drug, and a recent Phase I clinical study of INK-128 has demonstrated tolerability and encouraging tumor responses (Ghobrial et al., 2016). As we have found that Brigatinib caused tumor shrinkage in *NF2*-deficient meningiomas, a clinical trial is being planned to evaluate it as a new treatment for patients with NF2. If the proposed Brigatinib/INK-128 combination shows impressive anti-tumor efficacy in *NF2*-deficient meningiomas, the results could also be quickly translated to human evaluation.

(ii) What was the impact on other disciplines?

As we have found that Brigatinib suppressed the growth *NF2*-deficient tumors via inhibition of multiple RTKs and non-RTKs, including FAK. Many of these kinases have also been found to be activated in other human cancers, including malignant peripheral nerve sheath tumors (MPNSTs) which are frequently found in patients with NF1. Indeed, we also found that Brigatinib exhibited anti-tumor effects in MPNSTs. These results will be presented at the 2019 NF Conference in San Francisco (see Appendix).

(iii) What was the impact on technology transfer?

Nothing to report.

(iv) What was the impact on society beyond science and technology?

Nothing to report.

6. CHANGES/PROBLEMS:

(i) Changes in approach and reasons for change

None

(ii) Actual or anticipated problems or delays and actions or plans to resolve them

None

(iii) Changes that had a significant impact on expenditures

None

(iv) Significant changes in use or care of human subjects

None

(v) Significant changes in use or care of vertebrate animals

None

(vi) Significant changes in use of biohazards and/or select agents

None

7. Publications, Abstracts, and Presentations

(1) Journal publications or manuscripts under review

The works described in the following publications or manuscripts under review were supported, in part, by this grant. We have acknowledged the DOD support in these papers (please see Appendices).

(i) Fuse MA, Dinh CT, Vitte J, Kirkpatrick J, Mindos T, Plati SK, Young JI, Huang J, Carlstedt A, Franco MC, Brnjos K, Nagamoto J, Petrilli A, Copik AJ, Soulakova JN, Bracho O, Yan D, Mittal R, Shen R, Telischi FF, Morrison H, Giovannini M, Liu XZ, Chang LS, Fernandez-Valle C. 2019. Preclinical Assessment of MEK1/2 Inhibitors for Neurofibromatosis Type 2-Associated Schwannomas Reveals Differences in Efficacy and Drug Resistance Development. Neuro-Oncol. 21:486-497. PMID: 30615146

To identify an effective treatment for NF2-associated schwannomas, we collaborated with Dr. Cristina Fenandez-Valle at the University of Central Florida to investigate repurposing drugs targeting MEK1/2 kinases as merlin, the *NF2* gene product, has been shown to modulate activity of the Ras/Raf/MEK/ERK pathway. Among six MEK inhibitors examined, trametinib, PD0325901, and cobimetinib were most effective in reducing the viability of merlin-deficient mouse and human Schwann cells. Also, the three inhibitors slowed the growth of schwannoma allografts. However, when we analyzed drug-treated tumors, we found decreased pERK1/2 levels only in the tumors treated with PD0325901 and cobimetinib but not

trametinib. Similarly, tumor burden and average tumor size were reduced in trametinib-treated NF2 transgenic mice, and we also did not find reduced pERK1/2 in treated mouse tumors. The results show that MEK inhibitors exhibited differences in anti-tumor efficacy resistance in schwannoma models with possible emergence of trametinib resistance.

(ii) Chang L-S, Oblinger JL, Smith A, Ferrer M, Angus S, Petrilli AM, Beauchamp RL, Riecken LB, Erdin S, Poi M, Huang J, Bessler W, Zhang X, Rajarshi G, Thomas C, Burns SS, Jiang L, Li X, Lu Q, Yuan J, He Y, Masters A, Jones DR, Yates CW, Haggarty Stephen J, La Rosa S, Welling DB, Stemmer-Rachamimov AO, Plotkin SR, Blakeley JO, Gusella JF, Morrison H, Ramesh V, Fernandez-Valle C, Johnson GL, Clapp DW, on behalf of the Synodos for NF2 Consortium. 2019. Brigatinib causes tumor shrinkage in both *NF2*-deficient meningioma and schwannoma through inhibition of multiple tyrosine kinases but not ALK. To be submitted to Cancer Discovery.

We, as members of the Synodos for NF2 Consortium in collaboration with the NIH-NCATS, conducted high-throughput drug screening of isogenic pairs of *NF2*-deficient and *NF2*-expressing disease-relevant cells and identified several actionable drug targets for the treatment of both NF2-related schwannomas and meningiomas. We further showed that Brigatinib, developed for inhibition of ALK, potently suppressed the growth of *NF2*-deficient meningioma and schwannoma cells *in vitro* and of established xenograft and spontaneous *NF2*-deficient meningiomas and schwannomas *in vivo*. With this support, we found that Brigatinib specifically inhibited multiple RTKs and non-RTKs, such as focal adhesion kinase, but not ALK, in *NF2*-deficient tumor cells. These findings represent a major advance for the development of a treatment of NF2-related malignancies and demonstrate the power of a *de novo* unbiased approach to drug development.

(iii) Chang L-S, Oblinger JL, Burns SS, Huang J, Anderson LW, Hollingshead MG, Shen R, Pan L, Agarwal G, Ren Y, Roberts R, O'Keefe BR, Kinghorn AD, Collins JM. 2019. Targeting protein translation by rocaglamide and didesmethylrocaglamide to treat MPNST and other sarcomas. Submitted to Mol Cancer Ther.

Previously we showed that malignant schwannomas, such as malignant peripheral nerve sheath tumors (MPNSTs) which are frequently found in patients with NF1, and benign schwannoma including those commonly seen in patients with NF2, often overexpress eIF4F components, and the eIF4A inhibitor silvestrol potently suppresses MPNST growth (Oblinger JL et al. Neuro-Oncol. 2016;18:1265-1277). However, silvestrol has suboptimal drug-like properties, including a bulky structure, poor oral bioavailability, sensitivity to MDR1 efflux, and pulmonary toxicity in dogs. We compared 10 silvestrol-related rocaglates lacking the dioxanyl ring and found that didesmethylrocaglamide (DDR) and rocaglamide (Roc) had growth-inhibitory activity comparable to silvestrol. Both DDR and Roc arrested MPNST cells at G_2/M, increased the sub-G_1 population, induced cleavage of caspases and poly(ADP-ribose) polymerase, and elevated the levels of the DNA-damage response marker γH2A.X, while decreasing the expression of AKT and ERK1/2, consistent with translation inhibition. Unlike silvestrol, DDR and Roc were not sensitive to MDR1 inhibition and pharmacokinetic analysis confirmed that Roc had 50% oral bioavailability. Importantly, Roc, when administered intraperitoneally or orally, showed potent anti-tumor effects in an orthotopic MPNST mouse model and did not induce pulmonary toxicity in dogs as found with silvestrol. Treated tumors displayed degenerative changes and had more cleaved caspase 3-positive cells, indicative of

increased apoptosis. Furthermore, Roc effectively suppressed the growth of osteosarcoma, Ewing sarcoma, and rhabdomyosarcoma cells and patient-derived xenografts. Both Roc- and DDR-treated sarcoma cells showed decreased levels of multiple oncogenic kinases, including IGF-1R. The more favorable drug-like properties of DDR and Roc and the potent anti-tumor activity of Roc suggest that these rocaglamides could become viable treatments for MPNST and other sarcomas.

(2) Abstracts presented at national/international conferences

The following nine abstracts were presented at the annual Neurofibromatosis (NF) Conferences. We have acknowledged the DOD support in these abstracts (please see Appendices).

(i) Chang L-S, SS Burns, JL Oblinger, M Ferrer, J Huang, M Poi, V Ramesh, On behalf of the Synodos for NF2 Consortium. 2018. Novel drug discovery for NF2-deficient meningiomas: Brigatinib causes tumor shrinkage in NF2-deficient meningiomas. The 2018 Joint Global NF Conference, Paris, France. (Platform presentation)

(ii) Chang L-S, JL Oblinger, SS Burns, J Huang, L Anderson, R Shen, L Pan, Y Ren, BR O'Keefe, AD Kinghorn, JM Collins. 2018. Identification of silvestrol-related rocaglates with better bioavailability and high potency against malignant peripheral nerve sheath tumors. The 2018 Joint Global NF Conference, Paris, France. (Poster presentation)

(iii) Fernandez-Valle C, M Fuse, C Dinh, J Vitte, J Kirkpatrick, T Mindos, S Campion, K Brnjos, MC Franco, J Huang, J Young, A Petrilli, D Yan, R Mittal, R Shen, F Telischi, L-S Chang, H Morrison, M Giovannini, X-Z Liu. 2018. Preclinical Assessment of MEK1/2 Inhibitors for Neurofibromatosis Type 2-Associated Schwannomas Reveals Differences in Efficacy and Drug Resistance Development. The 2018 Joint Global NF Conference, Paris, France. (Platform presentation)

(iv) Welling DB, SS Burns, JL Oblinger, B Miles-Markley, A Quinkert, J Blakeley, BA Neff, RK Jackler, L-S Chang. 2018. Phase 1 and Phase 0 studies of AR-42, a pan histone deacetylase inhibitor, in subjects with neurofibromatosis type 2 (NF2)-associated vestibular schwannomas and meningiomas. The 2018 Joint Global NF Conference, Paris, France. (Poster presentation)

(v) Oblinger J, L-S Chang. 2019. Brigatinib as a potential therapy for malignant peripheral nerve sheath tumors. The 2019 NF Conference, San Francisco, CA. (Poster presentation)

(vi) Chang L-S, JL Oblinger, SS Burns, J Huang, L Anderson, R Shen, L Pan, Y Ren, R Roberts, BR O'Keefe, AD Kinghorn, JM Collins. Targeting protein translation with rocaglamide and didesmethylrocaglamide to treat NF1 and NF2 tumors. The 2019 NF Conference, San Francisco, CA. (Platform presentation)

8. PARTICIPANTS & OTHER COLLABORATING ORGANIZATIONS

(i) What individuals who have worked on the project

The Research Institute at Nationwide Children's Hospital
Long-Sheng Chang, Ph.D., Professor, Principal Investigator - 1.8 Calendar Months
Janet Oblinger, Ph.D., Research Associate - 2.7 Calendar Months
Massachusetts General Hospital
Vijaya Ramesh, Ph.D., Professor, Site Principal Investigator - 10% effort
Roberta Beauchamp, M.S., Research Associate - 25% effort

(ii) Has there been a change in the active other support of the PD/PI(s) or senior/key personnel since the last reporting period?

Nothing to report.

(iii) What other organizations were involved as partners

Massachusetts General Hospital - Vijaya Ramesh, Ph.D., Site Principal Investigator

9. Reportable Outcome

One peer-reviewed publication, two manuscripts under review, and six abstracts at national/international conferences.

10. Other Achievements

Nothing to report.

11. References

Ammoun S, Hanemann CO. 2011. Emerging therapeutic targets in schwannomas and other merlin-deficient tumors. Nat Rev Neurol. 2011;7:392-399. https://www.ncbi.nlm.nih.gov/pubmed/21647202

Angus SP, Oblinger JL, Stuhlmiller TJ, DeSouza PA, Beauchamp RL, Witt L, Chen X, Jordan JT, Gilbert TSK, Stemmer-Rachamimov A, Gusella JF, Plotkin SR, Haggarty SJ, Chang LS, Johnson GL, Ramesh V; Children's Tumor Foundation Synodos for NF2 Consortium. EPH receptor signaling as a novel therapeutic target in NF2-deficient meningioma. Neuro Oncol. 2018;20:1185-1196. https://www.ncbi.nlm.nih.gov/pubmed/29982664

Blakeley JO, Plotkin SR. Therapeutic advances for the tumors associated with neurofibromatosis type 1, type 2, and schwannomatosis. Neuro Oncol. 2016;18:624-638. https://www.ncbi.nlm.nih.gov/pubmed/26851632

Burns SS, Akhmametyeva EM, Oblinger JL, Bush ML, Huang J, Senner V, Chen C-S, Jacob A, Welling DB, Chang L-S. 2013. AR-42, a Histone Deacetylase Inhibitor, Differentially Affects Cell-Cycle Progression of Meningeal and Meningioma Cells and Potently Inhibits $NF2^{-}$ Meningioma Growth. Cancer Res. 73:792-804. http://www.ncbi.nlm.nih.gov/pubmed/23151902

Ghobrial IM, Siegel DS, Vij R, Berdeja JG, Richardson PG, Neuwirth R, Patel CG, Zohren F, Wolf JL. TAK-228 (formerly MLN0128), an investigational oral dual TORC1/2 inhibitor: A phase I dose escalation study in patients with relapsed or refractory multiple myeloma, non-Hodgkin lymphoma, or Waldenström's macroglobulinemia. Am J Hematol.

2016;91:400-405. https://www.ncbi.nlm.nih.gov/pubmed/26800393
Huang WS, Liu S, Zou D, Thomas M, Wang Y, Zhou T, Romero J, Kohlmann A, Li F, Qi J, Cai L, Dwight TA, Xu Y, Xu R, Dodd R, Toms A, Parillon L, Lu X, Anjum R, Zhang S, Wang F, Keats J, Wardwell SD, Ning Y, Xu Q, Moran LE, Mohemmad QK, Jang HG, Clackson T, Narasimhan NI, Rivera VM, Zhu X, Dalgarno D, Shakespeare WC. Discovery of Brigatinib (AP26113), a Phosphine Oxide-Containing, Potent, Orally Active Inhibitor of Anaplastic Lymphoma Kinase. J Med Chem. 2016; 59:4948-4964. https://www.ncbi.nlm.nih.gov/pubmed/27144831
Ostrom QT, Gittleman H, Truitt G, Boscia A, Kruchko C, Barnholtz-Sloan JS. CBTRUS Statistical Report: Primary Brain and Other Central Nervous System Tumors Diagnosed in the United States in 2011-2015. Neuro Oncol. 2018;20(suppl_4):iv1-iv86. https://www.ncbi.nlm.nih.gov/pubmed/30445539
Püttmann S, Senner V, Braune S, Hillmann B, Exeler R, Rickert C, Paulus W. 2005. Establishment of a benign meningioma cell line by hTERT-mediated immortalization. Lab Invest. 85:1163-1171. http://www.ncbi.nlm.nih.gov/pubmed/15965488
Rouleau GA, Merel P, Lutchman M, Sanson M, Zucman J, Marineau C, Hoang-Xuan K, Demczuk S, Desmaze C, Plougastel B, et al. Alteration in a new gene encoding a putative membrane-organising protein causes neurofibromatosis type 2. Nature 1993;363:515-521. http://www.ncbi.nlm.nih.gov/pubmed/8379998
Suppiah S, Nassiri F, Bi WL, Dunn IF, Hanemann CO, Horbinski CM, Hashizume R, James CD, Mawrin C, Noushmehr H, Perry A, Sahm F, Sloan A, Von Deimling A, Wen PY, Aldape K, Zadeh G; International Consortium on Meningiomas. Molecular and translational advances in meningiomas. Neuro Oncol. 2019;21(Supplement_1):i4-i17. https://www.ncbi.nlm.nih.gov/pubmed/30649490
Synodos for NF2 Consortium, Allaway R, Angus SP, Beauchamp RL, Blakeley JO, Bott M, Burns SS, Carlstedt A, Chang LS, Chen X, Clapp DW, Desouza PA, Erdin S, Fernandez-Valle C, Guinney J, Gusella JF, Haggarty SJ, Johnson GL, La Rosa S, Morrison H, Petrilli AM, Plotkin SR, Pratap A, Ramesh V, Sciaky N, Stemmer-Rachamimov A, Stuhlmiller TJ, Talkowski ME, Welling DB, Yates CW, Zawistowski JS, Zhao WN. Traditional and systems biology based drug discovery for the rare tumor syndrome neurofibromatosis type 2. PLoS One. 2018;13:e0197350. https://www.ncbi.nlm.nih.gov/pubmed/29897904
Trofatter JA, MacCollin MM, Rutter JL, Murrell JR, Duyao MP, Parry DM, Eldridge R, Kley N, Menon AG, Pulaski K, Haase VH, Ambrose CM, Munroe D, Bove C, Haines JL, Martuza RL, MacDonald ME, Seizinger BR, Short MP, Buckler AJ, Gusella JF. A novel moesin-, ezxrin-, radixin-like gene is a candidate for the neurofibromatosis 2 tumor-suppressor. Cell 1993;72:791-800. http://www.ncbi.nlm.nih.gov/pubmed/8453669
Zhang S, Anjum R, Squillace R, Nadworny S, Zhou T, Keats J, Ning Y, Wardwell SD, Miller D, Song Y, Eichinger L, Moran L, Huang WS, Liu S, Zou D, Wang Y, Mohemmad Q, Jang HG, Ye E, Narasimhan N, Wang F, Miret J, Zhu X, Clackson T, Dalgarno D, Shakespeare WC, Rivera VM. The Potent ALK Inhibitor Brigatinib (AP26113) Overcomes Mechanisms of Resistance to First- and Second-Generation ALK Inhibitors in Preclinical Models. Clin Cancer Res. 2016;22:5527-5538. https://www.ncbi.nlm.nih.gov/pubmed/27780853

12. Appendices

The attachment includes one publication, two manuscripts, and six abstracts.

Neuro-Oncology
21(4), 486–497, 2019 | doi:10.1093/neuonc/noz002 | Advance Access date 6 January 2019

Preclinical assessment of MEK1/2 inhibitors for neurofibromatosis type 2–associated schwannomas reveals differences in efficacy and drug resistance development

Marisa A. Fuse, Christine T. Dinh, Jeremie Vitte, Joanna Kirkpatrick, Thomas Mindos, Stephani Klingeman Plati, Juan I. Young, Jie Huang, Annemarie Carlstedt, Maria Clara Franco, Konstantin Brnjos, Jackson Nagamoto, Alejandra M. Petrilli, Alicja J. Copik, Julia N. Soulakova, Olena Bracho, Denise Yan, Rahul Mittal, Rulong Shen, Fred F. Telischi, Helen Morrison, Marco Giovannini, Xue-Zhong Liu, Long-Sheng Chang, and Cristina Fernandez-Valle

Burnett School of Biomedical Sciences, College of Medicine, University of Central Florida (UCF), Orlando, Florida, USA (M.A.F., S.K.P., M.C.F., K.B., J.N., A.P., A.J.C., J.N.S., C.F-V.); Department of Otolaryngology, University of Miami Miller School of Medicine, Miami, Florida, USA (C.T.D., O.B., D.Y., R.M., F.F.T., X.Z-L.); Department of Head and Neck Surgery, David Geffen School of Medicine at UCLA and Jonsson Comprehensive Cancer Center, University of California at Los Angeles (UCLA), Los Angeles, California, USA (J.V., M.G.); Leibniz Institute on Aging, Fritz Lipmann Institute, Jena, Germany (J.K., T.M., A.C., H.M.); Department of Human Genetics, University of Miami Miller School of Medicine, Miami, Florida, USA (J.I.Y., X.-Z.L.); Center for Childhood Cancer and Blood Diseases, Nationwide Children's Hospital (J.H., L-S.C.) and Departments of Pediatrics (J.H., L.-S.C.) and Pathology, The Ohio State University (R.S.), Columbus, Ohio, USA

Corresponding Author: Cristina Fernandez-Valle, Ph.D., Burnett School of Biomedical Sciences, College of Medicine, University of Central Florida, 6900 Lake Nona Blvd, Orlando, FL 32827 (cfv@ucf.edu).

Abstract

Background. Neurofibromatosis type 2 (NF2) is a genetic tumor-predisposition disorder caused by *NF2*/merlin tumor suppressor gene inactivation. The hallmark of NF2 is formation of bilateral vestibular schwannomas (VS). Because merlin modulates activity of the Ras/Raf/mitogen-activated protein kinase kinase (MEK)/extracellular signal-regulated kinase (ERK) pathway, we investigated repurposing drugs targeting MEK1 and/or MEK2 as a treatment for NF2-associated schwannomas.

Methods. Mouse and human merlin-deficient Schwann cell lines (MD-MSC/HSC) were screened against 6 MEK1/2 inhibitors. Efficacious drugs were tested in orthotopic allograft and *NF2* transgenic mouse models. Pathway and proteome analyses were conducted. Drug efficacy was examined in primary human VS cells with *NF2* mutations and correlated with DNA methylation patterns.

Results. Trametinib, PD0325901, and cobimetinib were most effective in reducing MD-MSC/HSC viability. Each decreased phosphorylated pERK1/2 and cyclin D1, increased p27, and induced caspase-3 cleavage in MD-MSCs. Proteomic analysis confirmed cell cycle arrest and activation of pro-apoptotic pathways in trametinib-treated MD-MSCs. The 3 inhibitors slowed allograft growth; however, decreased pERK1/2, cyclin D1, and Ki-67 levels were observed only in PD0325901 and cobimetinib-treated grafts. Tumor burden and average tumor size were reduced in trametinib-treated *NF2* transgenic mice; however, tumors did not exhibit reduced pERK1/2 levels. Trametinib and PD0325901 modestly reduced viability of several primary human VS cell cultures with *NF2* mutations. DNA methylation analysis of PD0325901-resistant versus -susceptible VS identified genes that could contribute to drug resistance.

© The Author(s) 2019. Published by Oxford University Press on behalf of the Society for Neuro-Oncology. All rights reserved.
For permissions, please e-mail: journals.permissions@oup.com

Downloaded from https://academic.oup.com/neuro-oncology/article-abstract/21/4/486/5274482 by Medical Library 244 ED user on 10 August 2019

Conclusion. MEK inhibitors exhibited differences in antitumor efficacy resistance in schwannoma models with possible emergence of trametinib resistance. The results support further investigation of MEK inhibitors in combination with other targeted drugs for NF2 schwannomas.

Key Points

1. Cobimetinib and trametinib reduced NF2 schwannoma model cell proliferation in vitro and in vivo.
2. Biochemical/proteome analyses reveal cell cycle arrest and apoptosis of trametinib-treated cells.
3. Human vestibular schwannoma cell viability is modestly inhibited by PD0325901 and trametinib.

Importance of the Study

There are currently no FDA-approved drug therapies for the treatment of NF2-associated schwannomas. Clinical trials for selumetinib and cobimetinib are ongoing for assessment of efficacy for NF2-associated tumors and hearing loss; however, little preclinical data have been published. Here, we evaluated 6 MEK1/2 inhibitors for efficacy in mouse and human cell and animal models as well as patient-derived vestibular schwannoma cells with *NF2* mutations. We observed differences in efficacy among the inhibitors as well as the possibility of drug resistance development. Our work highlights the importance of comprehensive drug screening in multiple model systems and supports further investigation of MEK inhibitors alone and in combination with other targeted therapies.

Neurofibromatosis type 2 (NF2) is caused by mutations in the *NF2* gene encoding the merlin tumor suppressor.[1,2] NF2 patients classically present with bilateral vestibular schwannomas (VS) involving the cochleovestibular nerves important for hearing and balance, and can develop additional peripheral schwannomas, meningiomas, and ependymomas.[3] Management of NF2 requires a complex, multidisciplinary approach focused on balancing tumor control and nerve function preservation to improve quality of life and maximize survival.[4] Whereas microsurgical resection of tumors risks permanent nerve injury, radiation therapy increases the chance of malignant transformation of benign tumors and secondary malignancies.[5–10] Therefore, there is an ongoing search for effective drug therapies for NF2.

Schwann cells with loss of merlin tumor suppressor function have elevated levels of Ras/Raf/mitogen-activated protein kinase kinase (MEK)/extracellular signal-regulated kinase (ERK) signaling that promotes cell proliferation.[11–13] Sixteen small molecule MEK inhibitors have entered clinical trials for various cancers.[14] Among these MEK inhibitors, selumetinib (AZD6244) was recently granted Orphan Drug Designation by the FDA for treatment of inoperable plexiform neurofibromas in children with NF1.[15] Additionally, selumetinib reduced growth of an in vitro human schwannoma model.[16,17] This success has prompted additional trials of selumetinib for NF1 and NF2 (NCT numbers: 01089101, 01362803, 02839720, 03259633, 03095248).

Trametinib (Mekinist, GSK1120212, JTP-74057, GlaxoSmithKline) is an allosteric, second-generation, adenosine triphosphate non-competitive reversible MEK1/2 inhibitor that also blocks Raf-dependent phosphorylation of MEK Ser218.[14] Trametinib promotes cell cycle arrest and caspase cleavage in cultured colorectal cells, and demonstrates more potent antitumor activity than other second-generation MEK inhibitors, PD0325901 and selumetinib. It is FDA approved for metastatic melanoma and is in phase I clinical trial for NF1-associated plexiform neurofibromas (NCT02124772).[18]

PD0325901 (Pfizer) is also an allosteric MEK1/2 inhibitor and is a synthetic analog of the first-generation MEK1/2 inhibitor, CI-1040.[14,19] In an *Nf1* genetically engineered mouse model, PD0325901 prolonged survival of mice with malignant peripheral nerve sheath tumors and decreased neurofibroma size in over 80% of mice.[20] Tumor regrowth was observed when treatment was suspended.[21] A phase II open-label study is ongoing for PD0325901 in NF1 (NCT02096471).[14]

Cobimetinib (XL518, GDC-0973, Cotellic, Exelixis/Genentech) is derived from methanone and was FDA approved in 2015 for use in combination with vemurafenib, a BRAF inhibitor, for advanced melanoma with *BRAF* mutations.[22,23] Cobimetinib inhibited growth of tumors with *BRAF* and *KRAS* mutations in xenograft models.[24–26] Phase I studies of cobimetinib for solid tumors reported a manageable toxicity profile with signs of efficacy in tumors with $BRAF^{V600E}$ mutations.[27] Cobimetinib is in clinical trial for pediatric and young adult patients with rasopathies, including NF2 (NCT02639546), treated previously for solid tumors.

Here, we used mouse and human merlin-deficient Schwann cell lines (MD-MSC/HSC) and animal models to evaluate the growth-inhibitory and antitumor activities of a panel of MEK inhibitors. Also, we assessed their efficacy in primary human VS with NF2 mutations.

Downloaded from https://academic.oup.com/neuro-oncology/article-abstract/21/4/486/5274482 by Medical Library 244 ED user on 10 August 2019

Materials and Methods

Cell Culture

Wild-type (WT)-MSCs and MD-MSCs were generated and characterized in 2010.[28] MD-MSCs were transduced with lentiviral luciferase as previously reported.[29] MD-schwannoma (MD-SCN) cells were derived from paraspinal schwannomas of *Periostin-Cre*:*Nf2*$^{flox2/flox2}$ mice with *Nf2* inactivation (provided by Dr Wade Clapp, Indiana University). Human Schwann cells (HSCs) were purchased from ScienCell Research Laboratories (catalog #1700, lot #7228), and the generation of a merlin-deficient HSC (MD-HSC) line using lentiviral short hairpin (sh)RNA targeting *NF2* (Sigma Mission, SHCLNV-TRCN0000237845) was previously described.[30] Cells were tested monthly for *Mycoplasma* contamination (Lookout *Mycoplasma* PCR Detection Kit, Sigma).

Mouse Model Systems

NSG (*NOD.Cg-Prkdcscid Il2rgtmlWjl/SzJ*) mice were used at 6–10 weeks of age. *P0-SCH-Δ(39–121)-27* transgenic mice[31] in the BALB/c background were used as a genetically engineered mouse (GEM) model of NF2 schwannomas. Animal use was approved by the Institutional Animal Care and Usage Committees of UCF and UCLA, and the Animal Care and Use Review Office of the United States Army Medical Research and Materiel Command.

Human VS Samples

Through an institutional review board (IRB) approved protocol, the University of Miami Tissue Bank Core Facility (UM-TBCF) consented patients undergoing surgery for brain tumors to harvest samples for research purposes. De-identified fresh human VS were obtained from UM-TBCF through an IRB-exempt protocol. Primary VS cells were prepared and cultured as previously reported.[29,30]

Drug Formulations

MEK inhibitors were purchased from MedChemExpress. Drugs were prepared in dimethyl sulfoxide (DMSO) (stock 10 mM) and diluted to final concentrations in cell culture medium for in vitro work. For animal studies, drugs were solubilized in DMSO at 50–100 mg/mL and diluted in 0.1 M citrate buffer (pH 3) for oral dosing.

Cell Viability Assays

Cells were seeded in 384-well CellBind plates (Corning) at 2000–2500 cells/well in phenol red-free growth medium. WT-MSCs were seeded at 15 000 cells/well in 96-well plates coated with poly-L-lysine (200 μg/mL) and laminin (25 μg/mL). Attached cells were treated with drug or DMSO for 48 h (mouse) or 72 h (human); viability was measured with the CellTiter-Fluor Assay (Promega). Primary human VS cells were seeded (passage 1 or 2) in 96-well plates at 10 000 cells/well. After 24 hours, cells were treated with drug or DMSO for 72 h. Crystal violet assay was performed using a SpectraMax 190 microplate reader (Molecular Devices) to assess cell number, as previously described.[29,30]

Membrane Asymmetry Assay

MD-MSCs were grown at 200 000 cells/well in 12-well CellBind plates (Corning). When at ~80% confluency, cells were treated with drug for 18–24 h, then harvested with 0.05% trypsin and resuspended in Hanks Balanced Salt Solution. The Violet Ratiometric Membrane Asymmetry Assay (Invitrogen) was used to detect apoptosis per the manufacturer's instructions. Cell populations were measured by flow cytometry (Cytoflex, Beckman Coulter) and analyzed with CytExpert software (Beckman Coulter).

Mouse Studies

For pharmacokinetic analysis, at each timepoint 3 mice received drug (1 mg/kg trametinib, 1.5 mg/kg PD0325901, or 20 mg/kg cobimetinib); one mouse received vehicle alone (0.1 M citrate, pH 3, 2% DMSO). Mice were sacrificed after 0.5–32 h; blood and sciatic nerve samples were collected and analyzed by mass spectrometry at Sanford Burnham Prebys Medical Discovery Institute (Lake Nona, Florida).

The orthotopic allograft model using luciferase-expressing MD-MSCs was generated as previously described.[29] Upon confirmation of successful grafting, mice were randomized into treatment groups and received drug or vehicle at the above concentrations daily by oral gavage. Mice were imaged weekly for bioluminescence using the In Vivo Imaging System (IVIS, Caliper) or Bruker MI Imaging System. After 13–14 days of treatment, mice were sacrificed; grafts and contralateral sciatic nerves were removed, weighed, and photographed. Grafts were fixed overnight in 4% paraformaldehyde and stored in 30% sucrose (0.02% azide in phosphate buffered saline) at 4°C. List of antibodies used is provided in Supplementary Methods.

Four-week-old *P0-SCH-Δ(39–121)-27* transgenic mice[31] were treated daily with trametinib (1 mg/kg) or vehicle (0.1 M citrate buffer pH 3, 0.2% DMSO) by oral gavage for 8 weeks. Spinal nerve roots were histopathologically scored at the endpoint as previously described.[32] Following a blind procedure, measurements of tumors and nerve root areas were performed using Zeiss Axiovision software on hematoxylin and eosin stained parasagittal sections of cervical, thoracic, lumbar, and sacral spinal cord segments. The total area of nerve root analyzed was comparable between the trametinib and vehicle-treated groups ($P = 0.1541$).

Western Blotting

Western blots were performed as previously described.[29] Protein was extracted from human VS tumors using radioimmunoprecipitation buffer with protease and phosphatase inhibitors (ThermoFisher). Human VS blots were blocked in 3% bovine serum albumin and incubated

Downloaded from https://academic.oup.com/neuro-oncology/article-abstract/21/4/486/5274482 by Medical Library 244 ED user on 10 August 2019

overnight in primary antibody solution at 4°C, followed by incubation with Alexa Fluor 488 and 647 conjugated secondary antibodies (1:200; ThermoFisher) for 2 hours at room temperature and imaged using the ImageQuant LAS 4000 Imager (GE Healthcare).

NF2 Mutation Analysis

Total DNA was extracted from fresh tumor tissues using the QIAamp DNA Mini Kit (Qiagen) and purified using the QIAquick PCR Purification Kit (Qiagen). All VS were tested for mutations within the NF2 gene with multiplex ligation-dependent probe amplification using the Salsa MLPA NF2 Kit (MRC-Holland) per the manufacturer's instructions. Copy number alterations in all 17 exons of the NF2 gene (NM_000268.3) were analyzed with Coffalyser. Additional details are provided in the Supplementary Methods.

DNA Methylation Analysis

High-throughput DNA methylation analysis was performed for 7 human VS tumors using the Infinium MethylationEPIC Kit (Illumina) according to the manufacturer's instructions. Methylation patterns were compared between VS that had a statistically significant decrease in cell number following a 72 hour incubation with 3 μM PD0325901 and those with no response. Additional details are provided in Supplementary Methods.

Proteome

Protein from cell pellets of MD-MSCs treated with trametinib or vehicle was extracted, denatured and prepared for liquid chromatography–tandem mass spectrometry (LC-MS/MS) as described in the Supplementary Methods. MS/MS spectra were searched against the *Mus Musculus* Swiss-Prot entries of the Uniprot KB (database release 2016_01, 16755 entries) using the Andromeda search engine.[33] The specific search criteria and analytics used are provided in Supplementary Methods. Protein differential expression between the trametinib and vehicle control samples was evaluated using the Limma package.[34]

Statistics

Using GraphPad Prism 6, ANOVA with Bonferroni posttest, or Kruskal–Wallis test with Dunn's comparison was applied to all in vitro data. For in vivo allograft studies, we used SAS version 9.4 to test the overall differences in median tumor weight and median fold change in flux after 14 days treatment among the 4 cohorts (vehicle treatment served as the control). Nonparametric ANOVA with Bonferroni adjustments were used to adjust for small group sample sizes and non-normal distributions. The ANOVA for the median tumor weight and median fold change in flux indicated the overall significance differences. We tested 1-tailed hypothesis of improvements. For the *P0-SCH-Δ(39–121)-27* NF2 mouse model, 2-tailed unpaired Student's *t*-test was used to compare tumor burden and sizes in the trametinib- and vehicle-treated groups.

Results

We screened selumetinib, trametinib, PD0325901, MEK162, cobimetinib, and refametinib for effectiveness in reducing viability of 9 WT and MD-MSC/HSC lines after 48-hour (mouse) and 72-hour (human) treatments. Based upon 50% inhibitory concentration (IC_{50}) values, the inhibitors were overall more effective in MSCs compared with HSCs. Maximum loss of cell viability at 10 μM observed for all inhibitors tested was ~90–95% in MD-MSCs, compared with ~60% in MD-HSCs (Fig. 1A–B). The lowest inhibitor concentration tested produced a 20–40% reduction in MD-MSC viability. MEK inhibitors promoted a dose-dependent decrease in incorporation of 5-ethynyl-2'-deoxyuridine in both MD-MSC and MD-HSC (Supplementary Fig. 1). All 6 MEK inhibitors also exhibited less selectivity between WT- and MD-HSCs compared with MSC lines (2–5 fold compared with 6–15 fold; Fig. 1A–B and Supplementary Fig. 2).

Trametinib, PD0325901, and cobimetinib were further evaluated in vitro and in an allograft mouse model because each reduced viability of both MD-MSCs and MD-HSCs with submicromolar IC_{50} values and had some selectivity in HSCs. Each drug decreased phosphorylated pERK levels in MD-MSCs at 5 and 24 hours of treatment (Fig. 2A–B, Supplementary Fig. 3). Trametinib was the most potent, as pERK was not detected in the 0.001 μM sample. Among these 3 MEK1/2 inhibitors, cobimetinib was the least effective, based on sustained reduction of pERK levels over 24 hours. Higher cobimetinib concentrations (0.3–1 μM) were required to achieve an equivalent pERK reduction observed with 0.001 μM trametinib and PD0325901. As reported in other cell types, MEK inhibition is associated with a compensatory increase in pMEK levels (Fig. 2A–B, Supplementary Fig. 3).[35] In MD-MSCs, a more robust increase in pMEK levels was observed in cells treated with cobimetinib at 5 hours and PD0325901 at 24 hours. Because trametinib uniquely blocks Raf-dependent MEK phosphorylation,[14] the lowest increase in pMEK was observed in trametinib-treated cells. MD-HSCs also exhibited decreased pERK and increased pMEK following MEK inhibition, but at higher drug concentrations compared with MD-MSCs (Supplementary Fig. 4).

An examination of downstream MEK/ERK effectors in MD-MSCs treated with these inhibitors revealed decreased levels of cyclin D1, and increased $p27^{kip1}$ and cleaved caspase 3 levels (Fig. 2C–D). Membrane asymmetry assays confirmed an increase in apoptotic cell populations from ~2% in DMSO-treated to 20% and 45% in trametinib- and cobimetinib-treated MD-MSCs, respectively (Fig. 2E, Supplementary Fig. 4).

A proteomic analysis of trametinib-treated MD-MSCs was conducted to assess global changes in protein expression. The results were consistent with effective inhibition of MEK1/2 and downstream effectors and induction of apoptotic pathways. Trametinib-treated MD-MSCs had reduced expression of Ras/Raf/MEK/ERK pathway effectors including cyclin D1 and c-Myc and increased expression of pro-apoptotic proteins such as Bcl-2 interacting protein 3 like (BNIP3L) at 24 hours, compared with DMSO control (Fig. 3A). Ingenuity Pathway Analysis identified upstream regulators whose

Downloaded from https://academic.oup.com/neuro-oncology/article-abstract/21/4/486/5274482 by Medical Library 244 ED user on 10 August 2019

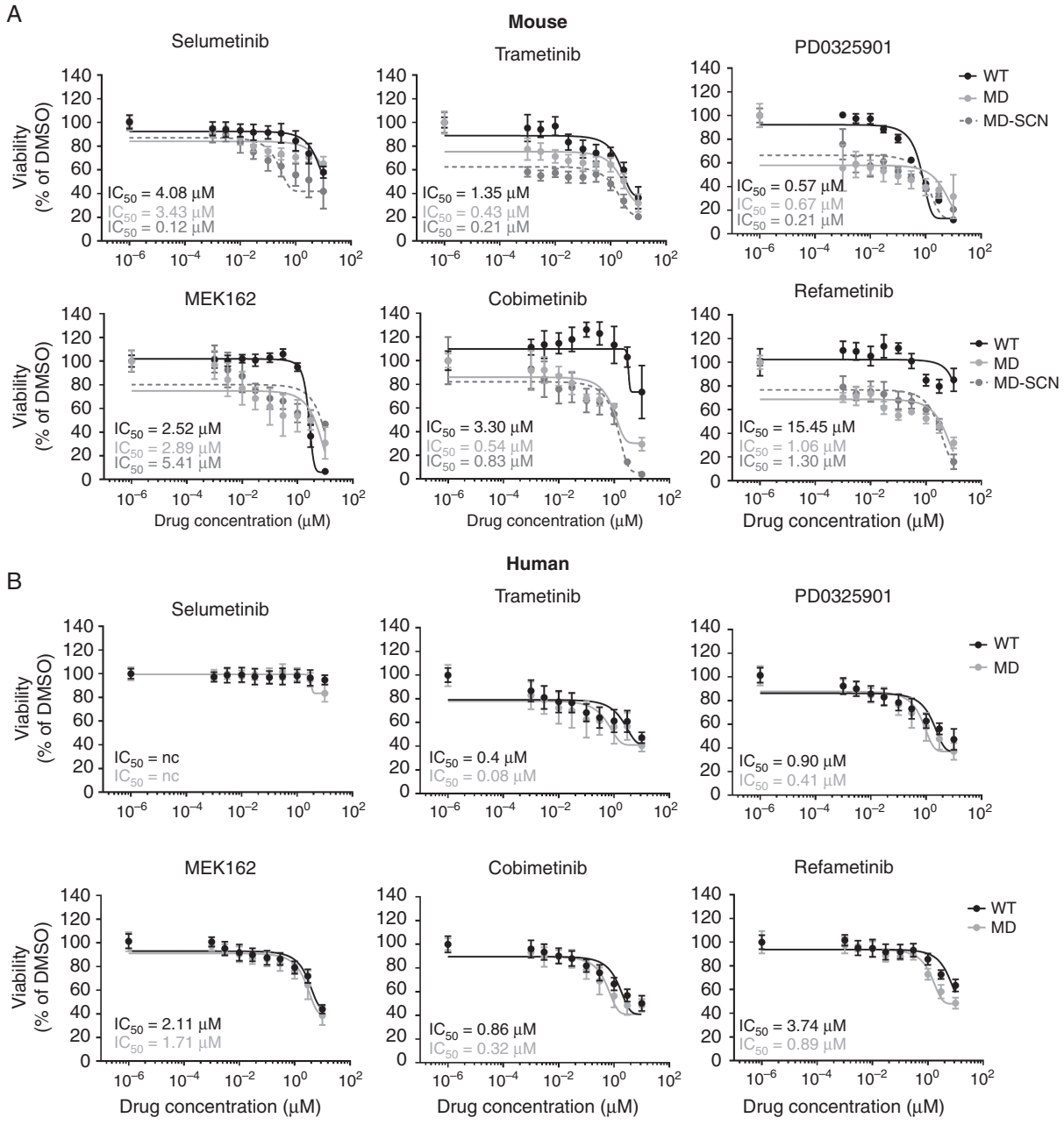


Fig. 1 MEK inhibitors reduce MD-MSC and MD-HSC viability. Screen of 6 MEK inhibitors against (A) mouse and (B) human WT and MD-SC lines treated for 48–72 h. Mean viability is plotted with IC_{50} values (n = 1–3 independent experiments; 8 replicates each).

modulation is consistent with the observed changes in protein levels. These included transforming growth factor beta (TGFβ), specificity protein 1, and p53 levels, whose levels were higher in trametinib-treated MD-MSCs compared with DMSO-treated controls (Fig. 3B–D).

To assess in vivo efficacy, we employed an orthotopic allograft model by grafting luciferase-expressing MD-MSCs into the sciatic nerves of NSG mice. Pharmacokinetic studies revealed that trametinib and cobimetinib had long $t_{1/2}$ values (~8 h and 4.8 h, respectively) and their nerve/plasma ratios increased with time (Fig. 4A). Upon confirmation of successful grafting (Supplementary Fig. 5), mice were gavaged daily for 14 days with trametinib (1 mg/ kg), PD0325901 (1.5 mg/ kg), or cobimetinib (20 mg/kg). All 3 MEK inhibitors significantly reduced the median tumor weight by 60–70% and the median fold change in flux from 0 to 14 days

Downloaded from https://academic.oup.com/neuro-oncology/article-abstract/21/4/486/5274482 by Medical Library 244 ED user on 10 August 2019

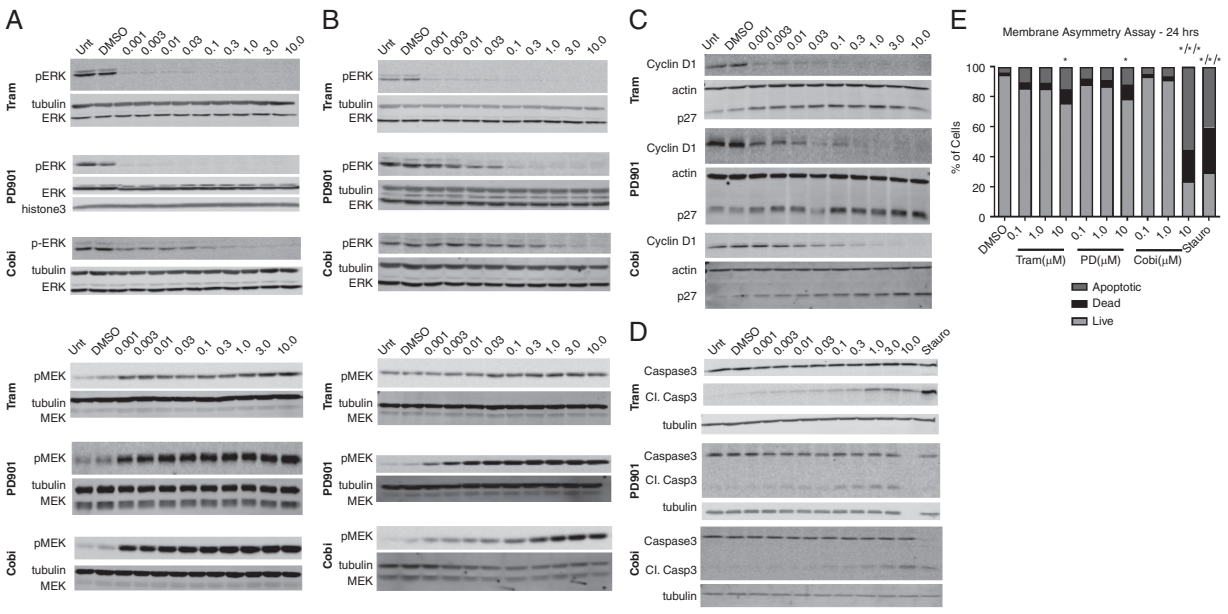


Fig. 2 MEK inhibitors promote G1 arrest and caspase-dependent apoptosis of MD-MSC in vitro. pERK1/2, pMEK1/2, cyclin D1, p27, and caspase-3 western blots of MD-MSC treated as indicated for (A) 5 h and (B-D) 24 h. All western blots are representative of 3–5 independent experiments. (E) Quantitation of membrane asymmetry assay of MD-MSC treated for 20 h with MEK inhibitors. Staurosporine (0.1 μM) served as a positive control for apoptosis ($n = 3$ independent experiments, 2-way ANOVA, $^*P < 0.05$).

by at least 80% compared with controls (Fig. 4B–D, Supplementary Fig. 6). Immunohistochemical analysis revealed that PD0325901 and cobimetinib were superior to trametinib in reducing pERK levels compared with the vehicle-treated group (Fig. 4E). Additionally, both inhibitors caused a more robust decrease in Ki-67 and cyclin D1 than trametinib, suggesting they were more potent inhibitors of graft growth in vivo. None of the inhibitors produced detectable caspase 3 cleavage nor did they affect vascularity as evidenced by CD31 staining (Fig. 4E).

Because trametinib is a well-tolerated FDA-approved drug and outperformed cobimetinib in cell assays, we assessed its efficacy in an 8-week study using the *P0-SCH-Δ(39–121)-27 NF2* schwannoma mouse model.[31,32] In this GEM model, trametinib efficacy was assessed by comparing the tumor burden, as defined by the percentage of tumor area versus total spinal nerve root area. Overall, trametinib promoted a 25% reduction in tumor burden ($P < 0.0001$) and a 37% decrease of average tumor size ($P = 0.0023$) (Fig. 5). Phosphorylated ERK immunohistochemistry of tumor samples revealed equivalent staining in trametinib- and vehicle-treated mice (data not shown), consistent with the allograft findings.

To examine the effect of MEK inhibition on human VS cells, primary cultures from 7 VS tumors were prepared and treated with PD0325901 or trametinib. All 7 VS tumors demonstrated ≥1 mutation in the *NF2* gene (Supplementary Table 1) and varying degrees of MEK1/2, pMEK, and pERK expression (Fig. 6A–B). Compared with DMSO-treated cells, trametinib (3 μM) moderately reduced cell viability of 2 of 7 VS, whereas PD0325901 (3 μM) reduced cell viability of 5 of the 7 VS tested (Fig. 6C–D). No significant correlations between viabilities and MEK1/2 and pMEK protein expression levels were identified, suggesting that drug response was independent of MEK expression.

To assess whether aberrant DNA methylation of the genome was associated with a lack of drug response, we compared methylation profiles of 2 VS with no response to PD0325901 tumors (VS27 and VS32) to the remaining 5 PD0325901-responsive tumors. In an unbiased evaluation, we identified 17 299 single cytosine-phosphate-guanine (CpG) sites with significantly different methylation levels ($P < 0.05$) between the drug responsive and nonresponsive VS. Among significant CpG sites, 4773 were hypermethylated (covering 3090 genes) and 12 526 were hypomethylated (covering 8051 genes) in the PD0325901-resistant compared with drug-sensitive VS. Supplementary Table 2 displays the top 20 hypermethylated and hypomethylated genes between the 2 groups. However, when false discovery rate (FDR) <0.05 was applied, *ELMOD1* (NM_001130037; Engulfment and cell motility domain 1) was the only gene that contained a CpG site (cg22355889) in the promoter region that was significantly hypermethylated in the PD0325901 nonresponsive VS.

Neighboring CpG sites often display closely related methylation patterns. To account for spatial correlations, we identified 34 differentially methylated regions (DMRs) with at least 5 consecutive

Downloaded from https://academic.oup.com/neuro-oncology/article-abstract/21/4/486/5274482 by Medical Library 244 ED user on 10 August 2019

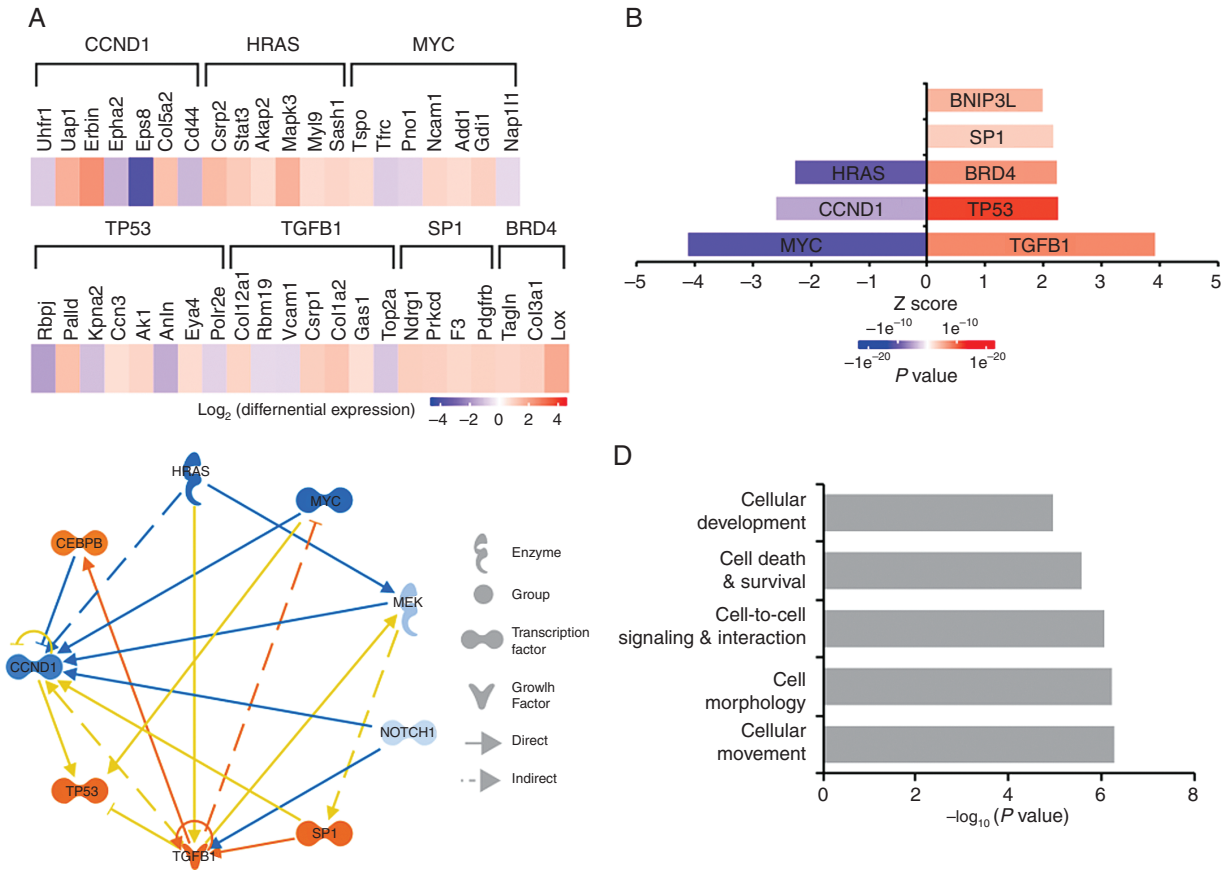


Fig. 3 Trametinib reduces signaling through Ras, Myc, and cyclin D1, and increases signaling through TP53 and TGFβ1. (A) Proteomic heat map showing differences in protein abundance in trametinib- versus DMSO-treated cells as determined by LC-MS/MS (blue: decreased expression, red: increased expression). (B) Predictions of upstream signaling pathways modulated by trametinib treatment. (C) Focus molecules and their connectivity based on Ingenuity Pathway Analysis of differentially expressed proteins in trametinib-treated versus DMSO-treated MD-MSC. (D) Differentially expressed proteins function in the indicated cellular processes ($n = 5$ replicate experiments).

hypermethylated or hypomethylated CpG loci in the PD0325901-nonresponsive compared with responsive VS (Supplementary Table 3). When examining individual DMRs, PD0325901 nonresponsive VS had DMRs in genes involved in non-MEK merlin signaling, including the *ATF6B* (activating transcription factor 6) and RXR (retinoid x receptor) genes associated with the phosphoinositide 3-kinase (PI3K/Akt) pathway and ATP6V1C1 (V-type proton ATPase subunit C1) of the mammalian target of rapamycin pathway. Gene ontology pathway analysis revealed no significant enrichment pathways for DMRs. However, when using a targeted approach assessing genes associated with merlin signaling, cancer, drug resistance, cell death, and survival, additional DMRs were identified. ARCHS4 pathway analysis revealed significant enrichment in epidermal growth factor receptor and tumor suppressor RPS6KA2 (ribosomal protein S6 kinase A2) human kinase pathways (http://amp.pharm.mssm.edu/Enrichr/. Accessed January 20, 2019).

Discussion

NF2 is a genetic disorder involving the development of multiple nervous system tumors that each impact neurological functions. Individuals affected by NF2 develop bilateral VS that cause severe hearing loss, disabling imbalance, and even life-threatening hydrocephalus from brainstem and cerebellar compression. Observation of tumor growth rate and hearing is standard as enthusiasm for microsurgical resection in NF2 is low due to consequential and irreversible limitations on nerve function and quality of life.[8] In the same respect, the long-term sequelae of utilizing radiotherapy is not so uncommon to disregard the risk of developing malignant transformation of benign tumors.[5–7,9,10] Off-label use of select FDA-approved chemotherapeutic agents for NF2 in clinical trials show moderate tumor control at best and hearing stabilization in only some NF2 patients.[36–41] However, even small effects

Downloaded from https://academic.oup.com/neuro-oncology/article-abstract/21/4/486/5274482 by Medical Library 244 ED user on 10 August 2019

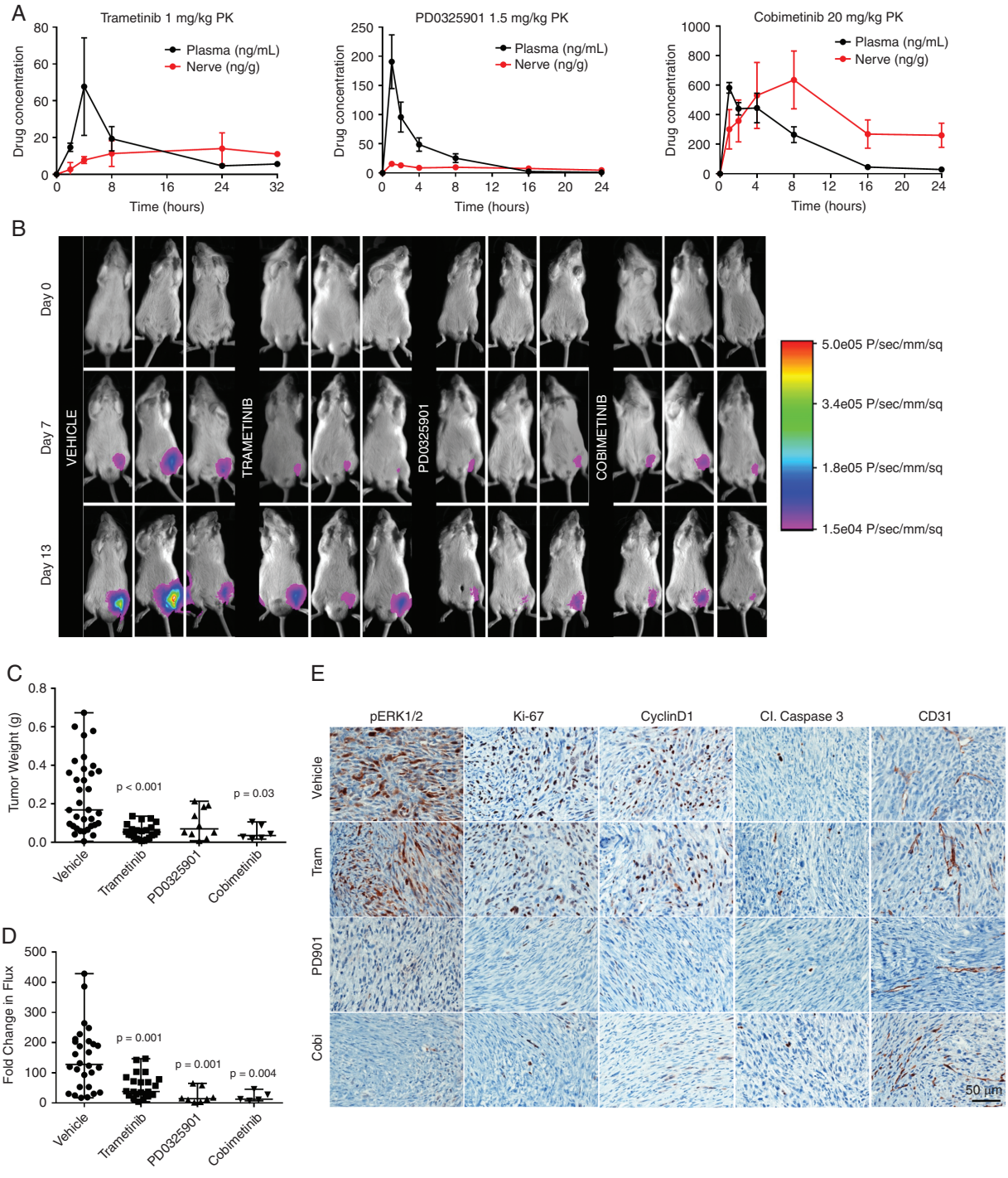


Fig. 4 MEK inhibitors slow MD-MSC growth in NSG mice. (A) Pharmacokinetic analysis for plasma and nerve following a single drug dose. (B) Representative bioluminescent (BL) images for indicated times. (C) Median tumor weights after 14 days of drug treatment compared with vehicle (n = 6–35 mice, nonparametric ANOVA). (D) BL signals were normalized to day 0 for each mouse and fold change in flux (photons/sec) after 14 days of treatment is shown (nonparametric ANOVA, median values shown). (E) Representative graft immunohistochemistry images for pERK1/2, Ki-67, cyclin D1, cleaved caspase 3, and CD31.

Downloaded from https://academic.oup.com/neuro-oncology/article-abstract/21/4/486/5274482 by Medical Library 244 ED user on 10 August 2019

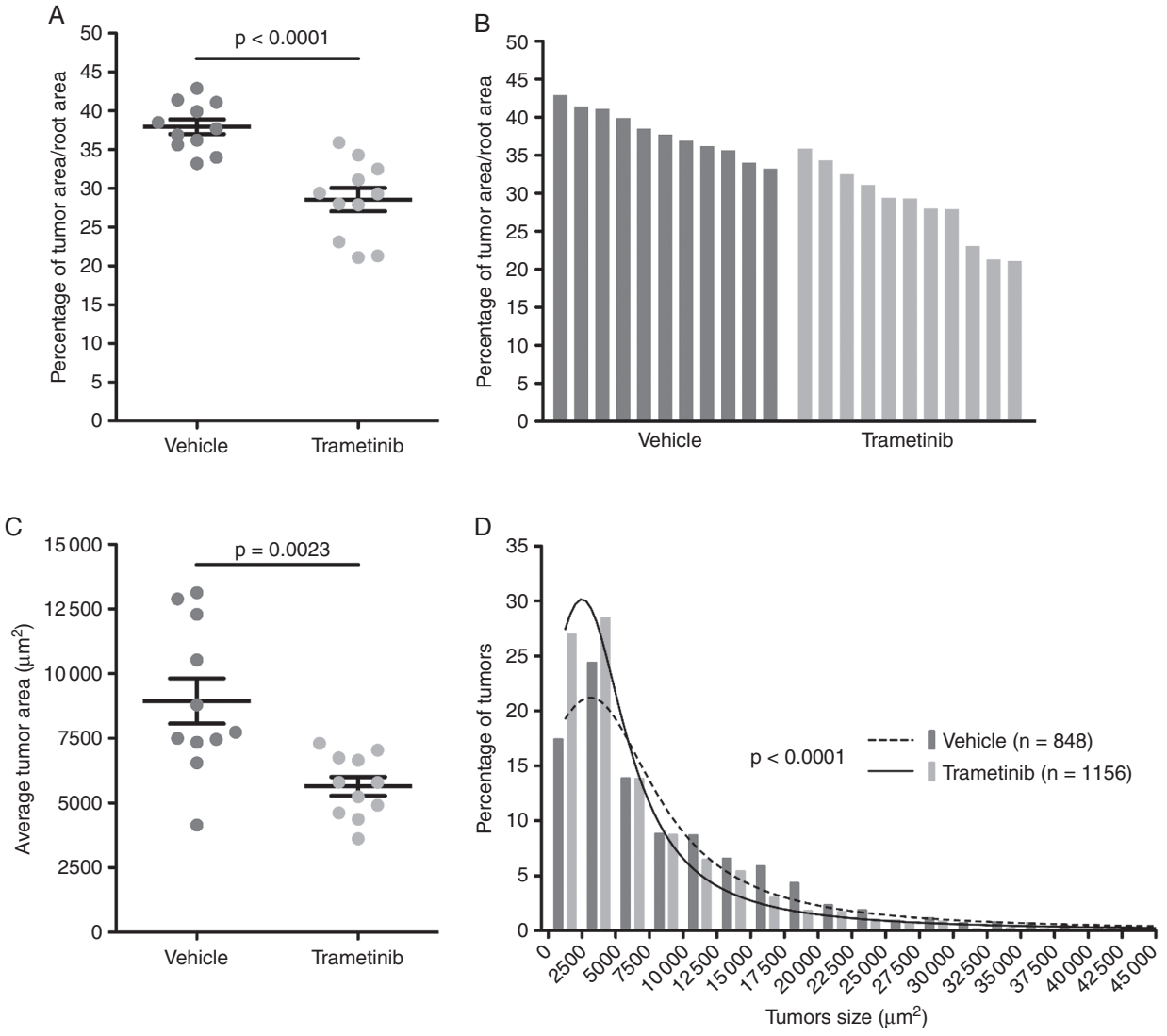


Fig. 5 Trametinib reduces schwannoma growth in the *P0-SCH-Δ(39–121)-27* NF2 mouse model. *P0-SCH-Δ(39–121)-27* mice were treated daily with trametinib (1 mg/kg, p.o., 7 d/wk) for 8 weeks starting at 4 weeks of age. (A) Reduction by 25% of the average tumor burden, calculated as percentage of tumor area versus total spinal nerve root area for trametinib-treated mice ($n = 11$) compared with vehicle-treated mice ($n = 11$). (B) Waterfall plot showing tumor burden for each vehicle- and trametinib-treated mouse. (C) Treatment with trametinib reduced average tumor size by 37% in trametinib-treated compared with vehicle-treated mice. (D) Histogram of tumor size distribution demonstrated a significantly higher percentage of smaller tumors in trametinib-treated ($n = 1156$ tumors) compared with vehicle-treated ($n = 848$ tumors) mice.

can impact survival and quality of life in individual NF2 patients. Therefore, the discovery of effective NF2 drug therapies is critical.

Currently, 2 clinical trials are enrolling pediatric NF2 patients to test effectiveness of selumetinib and cobimetinib in reducing tumor volume and preserving hearing (NCT03095248 and NCT02639546). However, the preclinical efficacies for selumetinib and cobimetinib have not been established. These trials are supported by knowledge that merlin loss is associated with increased mitogen-activated protein kinase signaling, and[42] success of selumetinib in shrinking plexiform neurofibromas in NF1 children.[15] Our study is the first to evaluate a panel of MEK inhibitors in mouse and human NF2 schwannoma models.

Of the 6 inhibitors screened against multiple mouse and human SC lines, trametinib, PD0325901, and cobimetinib reduced MD-SC viability at submicromolar IC_{50} values and were the most effective in non-immortalized human MD-SCs (Fig. 1A). Notably, selumetinib was the least effective in MD-HSCs and was not a top performer in MD-MSCs (based on maximum effect and IC_{50} values). In vitro, trametinib, PD0325901, and cobimetinib reduced pERK levels, modulated cyclin D1 and p27 levels in a manner consistent with a G_1/S cell cycle arrest, and induced caspase-dependent apoptosis in MD-MSCs. The proteomic study conducted in

Downloaded from https://academic.oup.com/neuro-oncology/article-abstract/21/4/486/5274482 by Medical Library 244 ED user on 10 August 2019

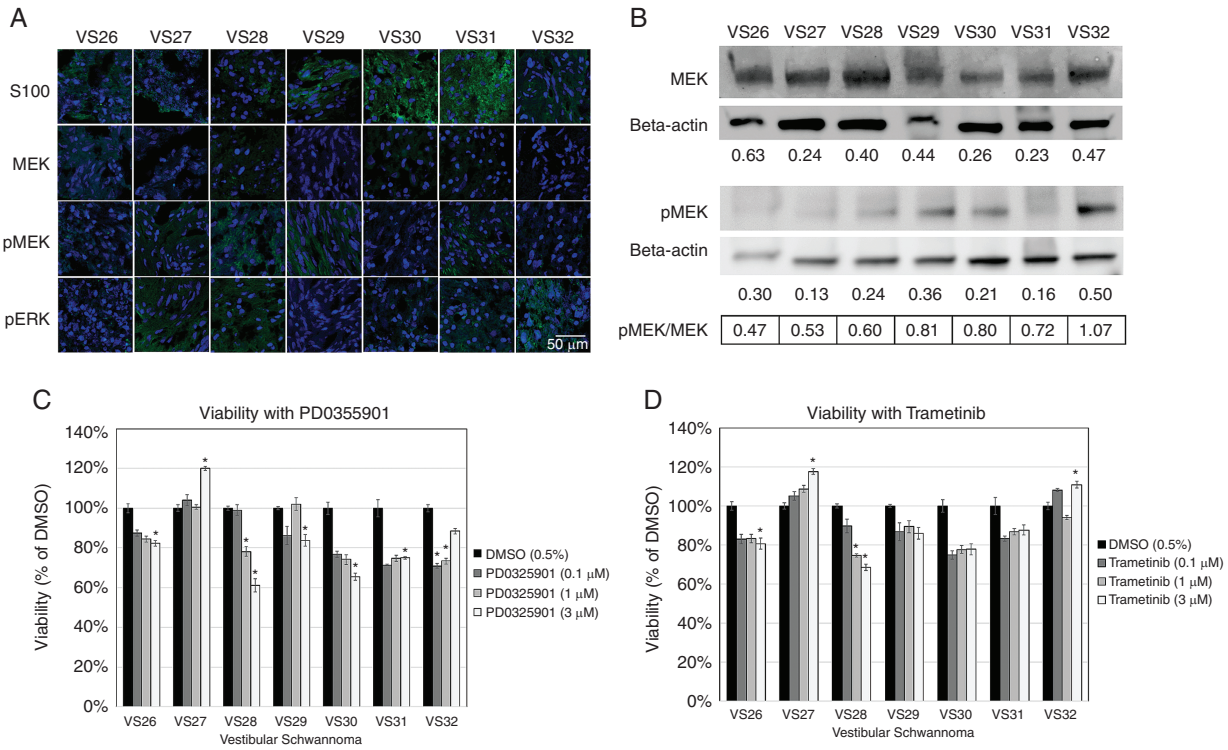


Fig. 6 MEK inhibitors reduce viability of a subset of primary human VS cells. (A) Immunohistochemistry shows S100 positivity and variable expression levels of MEK, pMEK, and pERK (green) in VS tumors (4′,6′-diamidino-2-phenylindole nuclear stain, blue). (B) Western blots demonstrate expression of MEK and pMEK for VS with beta-actin as the standard. Relative expression levels of MEK and pMEK were displayed and expressed as a ratio of pMEK/MEK. (C–D) Cell viability assays for PD0325901 and trametinib were performed and viability was normalized to 0.5% DMSO controls.

trametinib-treated MD-MSC further corroborated this conclusion by revealing decreased signaling in the Ras-ERK-cyclin D1 pathway and increased signaling from BNIP3L, a pro-apoptotic subfamily in the Bcl-2 family of proteins.

We used 2 in vivo models to evaluate drug efficacy: a 2-week treatment protocol aimed at slowing growth of established MD-MSCs nerve grafts in NSG mice, and an 8-week chemoprevention protocol aimed at preventing appearance of schwannomas in a GEM model. In the nerve grafts, PD0325901 and cobimetinib produced a stronger reduction in MD-MSC growth compared with trametinib, likely from persistent inhibition of pERK, cyclin D1, and Ki-67 levels.Trametinib did not significantly decrease pERK, cyclin D1 and Ki-67 levels in allografts at the study endpoint when compared with vehicle-treated controls, supporting the conclusion that cells in the allografts were developing resistance to trametinib. Similar responses to trametinib were obtained with the GEM model. Although the number and size of schwannomas were reduced in the GEM model following 8 weeks of trametinib treatment, immunohistochemically, pERK levels in trametinib-treated schwannomas were equivalent to controls. An adaptive response to trametinib has been reported in triple-negative breast cancer.[43] Trametinib treatment resulted in degradation of c-Myc and in assembly of bromodomain containing 4 (BRD4)-containing transcriptional enhancers on promoters of adaptive response genes, resulting in activation of compensatory pathways associated with drug resistance.[43] Our proteomic analysis similarly revealed decreased c-Myc levels and increased BRD4 levels in MD-MSCs treated with trametinib (Fig. 3). BRD4 in trametinib-induced adaptive response promoter complexes can be displaced by treatment with bromodomain and extraterminal domain family (BET) bromodomain inhibitors.[44] A study of BET bromodomain inhibitors in ovarian cancer revealed reduced activation of ERK, Akt, and Src kinase following treatment, suggesting that these pathways may be activated by bromodomain-containing transcriptional enhancers.[45] Additionally, BET family bromodomains were involved in reactivation of the Src/focal adhesion kinase pathway in breast cancer cells following inhibition of ErbB2 with lapatinib.[46] Collectively, these studies suggest that trametinib treatment may promote assembly of BRD-containing transcriptional enhancers that can activate compensatory proliferative pathways. Future studies examining the effects of bromodomain and Src inhibitors in combination with MEK inhibitors are warranted.

Of the 7 primary human VS cultures tested, only a subset responded to either PD0325901 or trametinib by reducing cell viability by 15–40% of controls. Although the trend of response to both drugs was similar within individual VS cultures, the differing response rate to the drugs was

Downloaded from https://academic.oup.com/neuro-oncology/article-abstract/21/4/486/5274482 by Medical Library 244 ED user on 10 August 2019

71% versus 29%, respectively, and did not correlate with baseline MEK or pMEK expression (Fig. 6A–D). The differing response rate can be attributed to the 10-fold higher potency of cobimetinib compared with PD0325901 (Fig. 6C–D).[18,19] VS cells also demonstrated a large variety of *NF2* mutations, which can have differential effects on merlin-dependent cell proliferation and survival pathways. Methylome exploration identified *ELMOD1* as the single gene with a hypermethylated promoter and an FDR <0.05 in nonresponsive VS compared with responsive VS. ELMOD1 is a GTPase activator for small GTPases in the ADP ribosylation factor (Arf) and Arf-like families (Arl2). In PD0325901 nonresponsive VS, a hypermethylated promoter in *ELMOD1* is expected to reduce ELMOD1 expression, increase Arl2 activity, and alter normal microtubule dynamics.[47] This may allow VS cells to circumvent traditional mechanisms of cell cycle arrest and cell death.[47] Further investigation into how tumor heterogeneity in NF2 contributes to drug resistance and disease progression is imperative for identifying treatment modalities to overcome resistance to MEK inhibition.

We present a comprehensive preclinical analysis of MEK inhibitors in mouse and human NF2 schwannoma models and primary human VS. Although differences in response were observed between drugs, species, and models, our cumulative results support MEK inhibitors for the treatment of a subset of NF2 schwannomas. We demonstrate that differences in treatment response to MEK inhibitors depends on genetic and epigenetic differences between tumors that can impact downstream merlin signaling, drug resistance mechanisms, and adaptive pathways to evade cell death or arrest. By understanding the mechanisms of drug response and resistance to MEK inhibitors in individual tumors, we can identify optimal combination therapies to maximize tumor control, determine important genetic and molecular biomarkers to predict patient outcomes, and develop precision medicine algorithms for NF2 treatment.

Supplementary Material

Supplementary data are available at *Neuro-Oncology* online.

Keywords

merlin tumor suppressor | methylome | NF2 transgenic mice | MEK inhibitors | patient-derived vestibular schwannomas

Funding

This work was supported by Department of Defense Congressionally Directed Medical Research Program (W81XWH-15-1-0446 to CFV and W81XWH-16-1-0104 to LSC), National Institutes of Health/National Institute on Deafness and Other Communication Disorders (R0-DC005575 and R01-DC012115 to XZL), and the Children's Tumor Foundation with contracts to CFV and MAF.

Acknowledgments

We thank Drs Jacques Morcos and Michael Ivan for their efforts harvesting human VS tumors and patients for donated tumor samples. We acknowledge Anthony Griswold, PhD, Division Head of the Center for Genetic Epidemiology and Statistical Genetics at the University of Miami Miller School of Medicine, for bioinformatics and statistical analysis of DNA methylation experiments.

Conflict of interest statement. CFV is a named inventor on unrelated patents. MG and JV receive research funding from Recursion Pharmaceuticals. Other authors report that no conflicts of interest exist.

Authorship statement. *Designed experiments*: CFV, MCF, MAF, JV, MG, JK and CTD. *Supervised work:* CFV, CTD, MG, HM, and LSC. *Cell and allograft studies*: MAF, SKP, JN, KB, AP, MCF. *Human VS work*: CTD, OB, RM, DY, XL, FT, JIY. *GEM model*: MG, JV. *Proteome analysis*: AC, JK, TM, HM. *Histology*: LSC, RS, JH. *Flow cytometry analysis*: AJC. *Statistical analysis*: JNS. CFV, MAF and LSC wrote the initial draft and all authors edited the manuscript.

Portions of Figs. 1, 3, and 5 were presented at the annual Neurofibromatosis Conference in Washington DC in June 2017.

References

1. Rouleau GA, Merel P, Lutchman M, et al. Alteration in a new gene encoding a putative membrane-organizing protein causes neuro-fibromatosis type 2. *Nature*. 1993;363(6429):515–521.
2. Trofatter JA, MacCollin MM, Rutter JL, et al. A novel moesin-, ezrin-, radixin-like gene is a candidate for the neurofibromatosis 2 tumor suppressor. *Cell*. 1993;72(5):791–800.
3. Evans DG. Neurofibromatosis type 2 (NF2): a clinical and molecular review. *Orphanet J Rare Dis*. 2009;4:16.
4. Blakeley JO, Evans DG, Adler J, et al. Consensus recommendations for current treatments and accelerating clinical trials for patients with neurofibromatosis type 2. *Am J Med Genet A*. 2012;158A(1):24–41.
5. Chung LK, Nguyen TP, Sheppard JP, et al. A systematic review of radiosurgery versus surgery for neurofibromatosis type 2 vestibular schwannomas. *World Neurosurg*. 2018;109:47–58.
6. Evans DG, Birch JM, Ramsden RT, Sharif S, Baser ME. Malignant transformation and new primary tumours after therapeutic radiation for benign disease: substantial risks in certain tumour prone syndromes. *J Med Genet*. 2006;43(4):289–294.
7. Kim BS, Seol HJ, Lee JI, et al. Clinical outcome of neurofibromatosis type 2-related vestibular schwannoma: treatment strategies and challenges. *Neurosurg Rev*. 2016;39(4):643–653.

Downloaded from https://academic.oup.com/neuro-oncology/article-abstract/21/4/486/5274482 by Medical Library 244 ED user on 10 August 2019

8. Nowak A, Dziedzic T, Czernicki T, et al. Strategy for the surgical treatment of vestibular schwannomas in patients with neurofibromatosis type 2. *Neurol Neurochir Pol*. 2015;49(5):295–301.
9. Seferis C, Torrens M, Paraskevopoulou C, Psichidis G. Malignant transformation in vestibular schwannoma: report of a single case, literature search, and debate. *J Neurosurg*. 2014;121(Suppl):160–166.
10. Sun S, Liu A. Long-term follow-up studies of Gamma Knife surgery for patients with neurofibromatosis type 2. *J Neurosurg*. 2014;121(Suppl):143–149.
11. Hilton DA, Ristic N, Hanemann CO. Activation of ERK, AKT and JNK signalling pathways in human schwannomas in situ. *Histopathology*. 2009;55(6):744–749.
12. Morrison H, Sperka T, Manent J, Giovannini M, Ponta H, Herrlich P. Merlin/neurofibromatosis type 2 suppresses growth by inhibiting the activation of Ras and Rac. *Cancer Res*. 2007;67(2):520–527.
13. Petrilli AM, Fernández-Valle C. Role of merlin/NF2 inactivation in tumor biology. *Oncogene*. 2016;35(5):537–548.
14. McDermott L, Qin C. Allosteric MEK1/2 inhibitors for the treatment of cancer: an overview. *J Drug Res Dev*. 2015;1:1–9. doi: 10.16966/jdrd.101.
15. Dombi E, Baldwin A, Marcus LJ, et al. Activity of selumetinib in neurofibromatosis type 1–related plexiform neurofibromas. *N Engl J Med*. 2016;375(26):2550–2560.
16. Ammoun S, Schmid MC, Ristic N, et al. The role of insulin-like growth factors signaling in merlin-deficient human schwannomas. *Glia*. 2012;60(11):1721–1733.
17. Ammoun S, Schmid MC, Triner J, Manley P, Hanemann CO. Nilotinib alone or in combination with selumetinib is a drug candidate for neurofibromatosis type 2. *Neuro Oncol*. 2011;13(7):759–766.
18. Yamaguchi T, Kakefuda R, Tajima N, Sowa Y, Sakai T. Antitumor activities of JTP-74057 (GSK1120212), a novel MEK1/2 inhibitor, on colorectal cancer cell lines in vitro and in vivo. *Int J Oncol*. 2011;39(1):23–31.
19. Barrett SD, Bridges AJ, Dudley DT, et al. The discovery of the benzhydroxamate MEK inhibitors CI-1040 and PD 0325901. *Bioorg Med Chem Lett*. 2008;18(24):6501–6504.
20. Jessen WJ, Miller SJ, Jousma E, et al. MEK inhibition exhibits efficacy in human and mouse neurofibromatosis tumors. *J Clin Invest*. 2013;123(1):340–347.
21. Jousma E, Rizvi TA, Wu J, et al. Preclinical assessments of the MEK inhibitor PD-0325901 in a mouse model of Neurofibromatosis type 1. *Pediatr Blood Cancer*. 2015;62(10):1709–1716.
22. Signorelli J, Shah Gandhi A. Cobimetinib. *Ann Pharmacother*. 2017;51(2):146–153.
23. Wong H, Vernillet L, Peterson A, et al. Bridging the gap between preclinical and clinical studies using pharmacokinetic-pharmacodynamic modeling: an analysis of GDC-0973, a MEK inhibitor. *Clin Cancer Res*. 2012;18(11):3090–3099.
24. Choo EF, Ng CM, Berry L, et al. PK-PD modeling of combination efficacy effect from administration of the MEK inhibitor GDC-0973 and PI3K inhibitor GDC-0941 in A2058 xenografts. *Cancer Chemother Pharmacol*. 2013;71(1):133–143.
25. Hoeflich KP, Merchant M, Orr C, et al. Intermittent administration of MEK inhibitor GDC-0973 plus PI3K inhibitor GDC-0941 triggers robust apoptosis and tumor growth inhibition. *Cancer Res*. 2012;72(1):210–219.
26. Rice KD, Aay N, Anand NK, et al. Novel carboxamide-based allosteric MEK inhibitors: discovery and optimization efforts toward XL518 (GDC-0973). *ACS Med Chem Lett*. 2012;3(5):416–421.
27. Rosen LS, LoRusso P, Ma WW, et al. A first-in-human phase I study to evaluate the MEK1/2 inhibitor, cobimetinib, administered daily in patients with advanced solid tumors. *Invest New Drugs*. 2016;34(5):604–613.
28. Petrilli AM, Fuse MA, Donnan MS, et al. A chemical biology approach identified PI3K as a potential therapeutic target for neurofibromatosis type 2. *Am J Transl Res*. 2014;6(5):471–493.
29. Fuse MA, Plati SK, Burns SS, et al. Combination therapy with c-Met and Src inhibitors induces caspase-dependent apoptosis of merlin-deficient schwann cells and suppresses growth of schwannoma cells. *Mol Cancer Ther*. 2017;16(11):2387–2398.
30. Petrilli AM, Garcia J, Bott M, et al. Ponatinib promotes a G1 cell-cycle arrest of merlin/NF2-deficient human schwann cells. *Oncotarget*. 2017;8(19):31666–31681.
31. Giovannini M, Robanus-Maandag E, Niwa-Kawakita M, et al. Schwann cell hyperplasia and tumors in transgenic mice expressing a naturally occurring mutant NF2 protein. *Genes Dev*. 1999;13(8):978–986.
32. Giovannini M, Bonne NX, Vitte J, et al. mTORC1 inhibition delays growth of neurofibromatosis type 2 schwannoma. *Neuro Oncol*. 2014;16(4):493–504.
33. Cox J, Neuhauser N, Michalski A, Scheltema RA, Olsen JV, Mann M. Andromeda: a peptide search engine integrated into the MaxQuant environment. *J Proteome Res*. 2011;10(4):1794–1805.
34. Smyth GK, Michaud J, Scott HS. Use of within-array replicate spots for assessing differential expression in microarray experiments. *Bioinformatics*. 2005;21(9):2067–2075.
35. Gilmartin AG, Bleam MR, Groy A, et al. GSK1120212 (JTP-74057) is an inhibitor of MEK activity and activation with favorable pharmacokinetic properties for sustained in vivo pathway inhibition. *Clin Cancer Res*. 2011;17(5):989–1000.
36. Blakeley JO, Plotkin SR. Therapeutic advances for the tumors associated with neurofibromatosis type 1, type 2, and schwannomatosis. *Neuro Oncol*. 2016;18(5):624–638.
37. Goutagny S, Raymond E, Esposito-Farese M, et al. Phase II study of mTORC1 inhibition by everolimus in neurofibromatosis type 2 patients with growing vestibular schwannomas. *J Neurooncol*. 2015;122(2):313–320.
38. Karajannis MA, Legault G, Hagiwara M, et al. Phase II trial of lapatinib in adult and pediatric patients with neurofibromatosis type 2 and progressive vestibular schwannomas. *Neuro Oncol*. 2012;14(9):1163–1170.
39. Karajannis MA, Legault G, Hagiwara M, et al. Phase II study of everolimus in children and adults with neurofibromatosis type 2 and progressive vestibular schwannomas. *Neuro Oncol*. 2014;16(2):292–297.
40. Plotkin SR, Halpin C, McKenna MJ, Loeffler JS, Batchelor TT, Barker FG 2nd. Erlotinib for progressive vestibular schwannoma in neurofibromatosis 2 patients. *Otol Neurotol*. 2010;31(7):1135–1143.
41. Plotkin SR, Merker VL, Halpin C, et al. Bevacizumab for progressive vestibular schwannoma in neurofibromatosis type 2: a retrospective review of 31 patients. *Otol Neurotol*. 2012;33(6):1046–1052.
42. Yi C, Troutman S, Fera D, et al. A tight junction-associated merlin-angiomotin complex mediates merlin's regulation of mitogenic signaling and tumor suppressive functions. *Cancer Cell*. 2011;19(4):527–540.
43. Bevill SM, Zawistowski JS, Johnson GL. Enhancer remodeling regulates epigenetic adaptation and resistance to MEK1/2 inhibition in triple-negative breast cancer. *Mol Cell Oncol*. 2017;4(6):e1300622.
44. Zawistowski JS, Bevill SM, Goulet DR, et al. Enhancer remodeling during adaptive bypass to MEK inhibition is attenuated by pharmacologic targeting of the P-TEFb complex. *Cancer Discov*. 2017;7(3):302–321.
45. Kurimchak AM, Shelton C, Duncan KE, et al. Resistance to BET bromodomain inhibitors is mediated by kinome reprogramming in ovarian cancer. *Cell Rep*. 2016;16(5):1273–1286.
46. Stuhlmiller TJ, Miller SM, Zawistowski JS, et al. Inhibition of lapatinib-induced kinome reprogramming in ERBB2-positive breast cancer by targeting BET family bromodomains. *Cell Rep*. 2015;11(3):390–404.
47. Zhou C, Cunningham L, Marcus AI, Li Y, Kahn RA. Arl2 and Arl3 regulate different microtubule-dependent processes. *Mol Biol Cell*. 2006;17(5):2476–2487.

Downloaded from https://academic.oup.com/neuro-oncology/article-abstract/21/4/486/5274482 by Medical Library 244 ED user on 10 August 2019

Brigatinib causes tumor shrinkage in both *NF2*-deficient meningioma and schwannoma through inhibition of multiple tyrosine kinases but not ALK

Chang, Long-Sheng[1,*] (Long-Sheng.Chang@nationwidechildrens.org),
Oblinger, Janet L.[1] (Janet.Oblinger@nationwidechildrens.org),
Smith, Abbi[2] (asmith@iu.edu),
Ferrer, Marc[3] (marc.ferrer@nih.gov),
Angus, Steven P.[4] (steven.angus@unc.edu),
Petrilli, Alejandra M.[5] (Alejandra.Petrilli@ucf.edu),
Beauchamp, Roberta L.[6] (beauch@helix.mgh.harvard.edu),
Riecken, Lars Björn[7] (lars.riecken@leibniz-fli.de),
Erdin, Serkan[8] (SERDIN@mgh.harvard.edu),
Poi, Ming[9] (Ming.Poi@osumc.edu),
Huang, Jie[1] (Jie.Huang@nationwidechildrens.org),
Bessler, Waylan K.[2] (wbessler@iu.edu),
Zhang, Xiaohu [3] (xiaohu.zhang@nih.gov),
Rajarshi Guha[3] (rajarshi.guha@gmail.com),
Thomas, Craig [3] (craigt@mail.nih.gov),
Burns, Sarah S.[1] (Sarah.Burns@nationwidechildrens.org),
Jiang, Li[2] (ljiang@iu.edu),
Li, Xiaohong[2] (xli@iu.edu),
Lu, Qingbo[2] (qlu@iu.edu),
Yuan, Jin[2] (jyuan@iu.edu),
He, Yongzheng[2] (yhe@iu.edu),
Masters, Andi[2] (amasters@iu.edu),
Jones, David R.[2] (drjones1@iupui.edu),
Yates, Charles W.[10] (cyates3@iuhealth.org),
Haggarty, Stephen J.[6] (haggarty@chgr.mgh.harvard.edu),
La Rosa, Salvatore[11] (slarosa@ctf.org),
Welling, D. Bradley[12] (Brad_Welling@meei.harvard.edu),
Stemmer-Rachamimov, Anat O.[13] (ASTEMMERRACHAMIMOV@mgh.harvard.edu),
Plotkin, Scott R.[6] (SPLOTKIN@partners.org),
Blakeley, Jaishri O.[14] (jblakel3@jhmi.edu),
Gusella, James F.[15] (gusella@helix.mgh.harvard.edu),
Morrison, Helen[7] (Helen.Morrison@leibniz-fli.de),
Ramesh, Vijaya[6] (ramesh@chgr.mgh.harvard.edu),
Fernandez-Valle, Cristina[5] (cfv@ucf.edu),
Johnson, Gary L.[4] (gary_johnson@med.unc.edu),
Clapp, D. Wade[2,*] (dclapp@iu.edu),
on behalf of the Synodos for NF2 Consortium (http://dx.doi.org/10.7303/syn2343195)

[1]Center for Childhood Cancer & Blood Diseases, The Research Institute at Nationwide Children's Hospital and Department of Pediatrics, The Ohio State University College of Medicine, Columbus, OH 43205, USA;
[2]Department of Pediatrics, Indiana University, School of Medicine, Indianapolis, IN 46202, USA;

[3]*Division of Preclinical Innovation, National Center for Advancing Translational Sciences, NIH, Bethesda, MD;*
[4]*University of North Carolina School of Medicine, Chapel Hill, NC 27599, USA;*
[5]*Burnett School of Biomedical Sciences, College of Medicine, University of Central Florida, Lake Nona-Orlando, FL 32827, USA;*
[6]*Department of Neurology, Massachusetts General Hospital and Harvard Medical School, Boston, MA 02114, USA;*
[7]*Leibniz Institute on Aging – Fritz-Lipmann Institute (FLI), Jena 07745, Germany;*
[8]*Center for Genomic Medicine, Massachusetts General Hospital, Boston, MA 02114, USA;*
[9]*Division of Pharmacy Practice and Science, The Ohio State University College of Pharmacy*
[10]*Department of Otolaryngology & Head/Neck Surgery, Indiana University School of Medicine, Indianapolis, IN 46202;*
[11]*Children's Tumor Foundation, New York, NY 10005, USA;*
[12]*Department of Otolaryngology, Massachusetts Eye and Ear Infirmary, Massachusetts General Hospital and Harvard University, Boston, MA 02114, USA;*
[13]*Department of Pathology, Massachusetts General Hospital and Harvard Medical School, Boston, MA 02114;*
[14]*Departments of Neurology, Neurosurgery and Oncology, Johns Hopkins University School of Medicine, Baltimore, MD 21287, USA;*
[15]*Department of Genetics, Massachusetts General Hospital and Harvard Medical School, Boston, MA 02114;*

Precis: An unbiased, systems-based approach was used to identify brigatinib as a novel therapy for the treatment of NF2-associated schwannomas and meningiomas

Running title: Brigatinib as a potential treatment for schwannoma and meningioma

Key words: Neurofibromatosis type 2 (NF2), schwannoma, meningioma, brigatinib, receptor tyrosine kinase (RTK), anaplastic lymphoma kinase (ALK), focal adhesion kinase (FAK)

*Corresponding authors:
Long-Sheng Chang, Center for Childhood Cancer & Blood Diseases, The Research Institute at Nationwide Children's Hospital, 700 Children's Drive, Columbus, OH 43205; Phone: 614-355-2658; e-mail: Long-Sheng.Chang@nationwidechildrens.org) and
D. Wade Clapp, Department of Pediatrics, Indiana University, School of Medicine, 705 Riley Hospital Drive, Indianapolis, IN 46202; Phone: 317-944-7810; e-mail: dclapp@iu.edu

Disclosure of Potential Conflicts of Interest: No potential conflicts of interest were disclosed.

Data availability: Processed data used in this study is available at doi:10.7303/syn18463554.3 or as a supplemental file. Raw data associated with this study is available at the Synodos NF2 project on the Synapse data repository (doi: 10.7303/syn2343195)

Word Counts: Abstract (148 words); Statement of Significance (50 words); Text including Abstract, Statement of Significance, Methods, Results, Discussion, and Acknowledgements (5,915 words)

Abstract

Neurofibromatosis Type 2 (NF2) is an autosomal-dominant genetic syndrome caused by mutations in the *NF2* tumor suppressor gene with no FDA-approved chemotherapeutics for treatment. Patients develop multiple tumors of neural crest-derived origin, prototypically schwannomas and meningiomas. High-throughput drug screening of isogenic pairs of *NF2*-deficient and *NF2*-expressing disease-relevant cells identified actionable drug targets for the treatment of both NF2-related schwannomas and meningiomas. Brigatinib, developed for inhibition of anaplastic lymphoma kinase (ALK), targeted multiple receptor tyrosine kinases (RTKs) and potently suppressed the growth of *NF2*-deficient meningioma and schwannoma cells *in vitro* and of established xenograft and spontaneous *NF2*-deficient meningiomas and schwannomas *in vivo*, independent of ALK expression. Kinases specifically inhibited by brigatinib included multiple RTKs and non-RTKs, such as focal adhesion kinase. These findings represent a major advance for the development of a treatment of NF2-related malignancies and demonstrate the power of a *de novo* unbiased approach to drug development.

Statement of significance

Using an unbiased, systems-based approach including high-throughput drug screening of isogenic *NF2*-deficient and -expressing disease-relevant cells, we identified the ALK inhibitor brigatinib to potently suppress NF2-related schwannoma and meningioma growth. Surprisingly, ALK was not detected in NF2-related tumors, and instead brigatinib suppressed multiple RTKs and non-RTKs, including focal adhesion kinase.

Introduction

Neurofibromatosis Type 2 (NF2) is a rare disease in which biallelic loss of the *NF2* gene leads to the development of tumors of neural crest-derived origin (Blakeley et al., 2012; Evans, 2015). *NF2* encodes the tumor suppressor merlin, whose biochemical function is incompletely understood. Bilateral vestibular schwannomas are pathognomonic for NF2 and the disease is also commonly associated with the development of multiple meningiomas. Further, 95% of sporadic schwannomas and 50% of sporadic meningiomas, the most common intracranial tumors in humans, have homozygous loss of *NF2*. These tumors are unresponsive to traditional chemotherapy, and surgery is associated with major morbidity.

Sponsored by the Children's Tumor Foundation, the Synodos for NF2 Consortium was a multi-institutional collaboration established to accelerate drug development in NF2 tumors (Synodos for NF2 Consortium, 2018). In this study, we selected a systems biology approach to: (1) utilize high-throughput drug screens to identify FDA-approved or late-stage development compounds active against *NF2*-deficient schwannoma and meningioma cells, (2) integrate data from kinome and transcriptome profiling to prioritize targets for future development, (3) utilize a genetically-engineered mouse model and tumor xenograft model to establish preclinical efficacy data for a subset of compounds identified in the drug screen, and (4) identify at least one drug to move forward into a clinical trial.

Using this approach, we have identified for the first time, single and combinatorial agents that positively impact the treatment of both schwannomas and meningiomas. Importantly, we established the FDA-approved, multi-receptor tyrosine kinase (RTK)

inhibitor, brigatinib, as a potent inhibitor of *NF2*-deficient schwannoma and meningioma growth, both *in vitro* and in preclinical animal models. Interestingly, neither *NF2*-deficient schwannoma nor meningioma cells express the primary published target of brigatinib, anaplastic lymphoma kinase (ALK). Instead, we demonstrate that mechanistically, brigatinib inhibits multiple other RTKs and non-RTKs, including focal adhesion kinase (FAK), which has previously been recognized as an oncoprotein in NF2-related tumors (Ammoun and Hanemann, 2011; Blakeley and Plotkin, 2016). These data represent an effective systems approach to preclinical therapeutic development for orphan disease tumors and support the advancement of brigatinib as a multi-RTK/non-RTK inhibitor into clinical trials for the treatment of NF2.

Materials and Methods

Compound library and screening

The MIPE (Mechanism Interrogation Plates) oncology compound library 4.0, consisting of 745 FDA-approved drugs, 420 Phase I-III investigational agents, and 767 preclinical molecules (Mathews Griner et al., 2014) was screened at the National Center for Advancing Translational Sciences (NCATS), NIH. All compounds in the library have been annotated for their known nominal target, representing diverse and redundant mechanisms of action. Also, the library contains several compounds per target, allowing target-based enrichment analysis of responses.

A panel of NF2 tumor-relevant cells, including the isogenic pairs of *NF2*-expressing HS11 and *NF2*-deficient HS01 Schwann cells and *NF2*-expressing Syn1 and *NF2*-null Syn5 arachnoidal cells as well as human *NF2*-deficient meningioma Ben-Men-1, mouse

Postn-Cre;*Nf2*$^{flox/flox}$ schwannoma MS02, and primary human meningioma and schwannoma cells, was used for drug evaluation (Püttmann et al., 2005; Burns et al., 2013; Beauchamp et al., 2015; Gehlhausen et al., 2015; Petrilli et al., 2017; Synodos for NF2 Consortium, 2018). Detailed information regarding compound screening, hit selection, compound combination matrix screening, and *in vitro* confirmation of compound efficacy and synergism is provided in Supplementary Methods.

Kinome profiling and Transcriptome analysis

Multiplexed kinase inhibitor beads and mass spectrometry (MIB/MS) was conducted to quantitate the dynamic behavior of the expressed kinome in response to drug treatment (Duncan et al., 2012; Stuhlmiller et al., 2015). Detailed procedures for kinome and transcriptome analysis are summarized in Supplementary Methods.

Phospho-receptor tyrosine kinase (RTK) array, Western blot, and immunohistochemistry analyses

Ben-Men-1 cells were growth-arrested without serum for two days, followed by growth stimulation with 20% fetal bovine serum (FBS) in the presence of 1xIC_{50} concentration of brigatinib or DMSO. Also, cells grown in 10% FBS were treated with 1xIC_{50} concentration of brigatinib or DMSO for 2 or 24h. Protein lysates from treated cells were incubated with the PathScan RTK Antibody Array (#7949; Cell Signaling) according to the manufacturer's instructions (see Supplementary Methods).

Western blotting and immunohistochemistry were performed as previously described (Synodos for NF2 Consortium, 2018). Antibodies used are appended in Supplementary

Methods.

Pharmacokinetic (PK) analysis

For PK analysis of brigatinib and MK-2206, NSG mice (The Jackson Laboratory) were fed a single oral dose of each drug or their combination at the predetermined maximal tolerated dose (MTD). Prior to and at various times after dosing (n=3), whole blood was collected for plasma preparation and mice were euthanized for brain harvesting. Both the plasma and brain samples were frozen at -80ºC until ultra-high-pressure LC tandem-MS (UHPLC-MS/MS) analysis (Supplementary Methods).

For PK analysis of brigatinib and dasatinib, plasma samples were acidified and extracted in hexane:ethyl acetate (50:50, v/v). After solvent evaporation, mobile phase (acetonitrile:5mM ammonium acetate; 70:30, v/v) was mixed with residual sample and injected into an Agilent 1290 HPLC system with an Eskigent Autosampler. MS was performed using an ABSciex 5500 Q-TRAP.

Quantifiable orthotopic meningioma model

NSG mice bearing luciferase-expressing Ben-Men-1-LucB xenografts were established as described (Burns et al., 2013) and randomized into four groups: MK-2206, brigatinib, MK-2206/brigatinib combination, or vehicle (n=10). Treatment schedule and bioluminescence imaging (BLI) are described in Supplementary Methods.

Schwannoma model and hearing tests

The methodologies of tumor and hearing assessment for the *PostnCre; Nf2*$^{flox/flox}$

mice were used as previously described (Gehlhausen et al., 2015).

Results

Discovery of novel drug combinations for NF2-associated meningiomas and schwannomas.

To identify novel chemotherapeutic agents for *NF2*-associated tumors, we screened the NCATS MIPE library 4.0 of 1,932 compounds in a high-throughput dose-response format using the isogenic pairs of *NF2*-expressing HS11 and *NF2*-deficient HS01 Schwann cells and *NF2*-expressing Syn1 and *NF2*-null Syn5 arachnoidal cells, as well as *Nf2*$^{-/-}$ mouse MS02 schwannoma cells and human Ben-Men-1 meningioma cells (Syn6). The cells were selected to assess selectivity of pharmacological responses based on *NF2* status and to distinguish the differences in compound responses between human and mouse NF2-related tumor cells to better predict the drug activity in animal models. We first screened the MIPE library, as single agents in dose-response mode, to determine the potency (IC_{50}), efficacy (maximum % inhibition), and area under the curve (AUC) for each compound in each cell line (Fig. 1A). Active compounds were selected using dose-response curve analysis algorithms, which assign each tested compound a Curve Response Class (CRC) number (Ferrer et al., 2018). This method classified primary hits into different categories according to their IC_{50}, magnitude of response, quality of curve fitting (r^2), and number of asymptotes. For example, a CRC of -1.1 represents a compound with a complete curve and with high efficacy; a CRC of -1.2 represents a compound with a complete curve but with partial efficacy. Compounds with CRC 4 are inactive. Compounds with CRCs of -1.1, -1.2, and a maximum response of

<30% cell viability were considered for further testing in combination screen. Shown in Fig. 1B is a heat map of the maximal % activity clustered using the hierarchical clustering function in Spotfire Tibco. The results of this single-agent screen demonstrated that the pharmacological responses clustered cells by tumor type (meningioma vs schwannoma) and that there were no major differences between the *NF2*-expressing and *NF2*-deficient cells. Figure 1C provides a view of the pharmacological responses according to different relevant targets and cellular pathways and mechanisms, based on the AUC parameters which include both potency and efficacy of the compounds. This high-level biological analysis of pharmacological responses confirms that all cells behaved very similarly and that compounds targeting proteasome, chaperone, topoisomerase, RTK, serine-threonine kinase (STK), phosphatidylinositol 3-kinase (PI3K), and tubulin are the most active. 62 and 82 compounds were active in all cells by maximum response criteria of <30% cell viability and CRC of -1.1 and -1.2, respectively. Compounds with CRC -1.1 were considered cytotoxic, while those with CRC -1.2 could either be cytostatic or induce senescence and slow cell growth. Targets enriched for these active compounds included inhibitors of histone deacetylase (HDAC), proteasome, Janus kinase 2 (JAK2), tubulin, mammalian target of rapamycin (mTOR), and cyclin-dependent kinase 1 (CDK1), PI3K, and topoisomerase (Fig. 1D).

Based on compound potency and efficacy in each cell line, targets in key merlin pathways, and the mechanisms of interest previously identified based on genomic and kinome data on the various NF2 tumor-relevant cell models, we selected 45 compounds for further combination screening. These compounds were first tested using the

CellTiterGlo assay for 72-h treatment, in 6x6 concentrations, all vs all dose-response matrices, for a total of 990-pairwise combinations (Fig. 1E), with concentrations customized to include a range > 4-fold and < 4-fold the IC_{50}, to better determine possible synergies with Syn1 and Syn5 cells as the meningioma cell model and HS11 and HS01 cells as the schwannoma cell model. Synergistic combinations were ranked based on the Delta Bliss Sum Negative (DBSumNeg) values (Borisy et al., 2003) for each pairwise combination matrix on the *NF2*-deficient cells. We detected 33 combinations, which had a DBSumNeg value of <-2 in Syn5 cells, and 69 combinations, which had a DBSumNeg of <-2 in HS01 cells. A heat map of hierarchical clustering of DBSumNeg for each pairwise compound combination in each cell line was generated, showing that meningioma and schwannoma cells each clustered separately by DBSumNeg synergy scores, regardless of NF2 status (Fig. 1F). Next, we selected 176 pairwise compound combinations based on DBSumNeg values, synergy selectivity for *NF2*-deficient cells, mechanisms of interest, and clinical interest and tested them in 10x10 dose-response matrix format with the same set of meningioma and schwannoma cell models using both a cell proliferation readout (CellTiterGlo at 72h) and an apoptosis readout (CaspaseGlo, 20h). Based on differential drug synergy in *NF2*-deficient vs *NF2*-expressing cells, the stage of drug development, and compound performance in prior preclinical and clinical evaluations including pharmacology, response rate, toxicity, and availability, we selected and ranked the top three drug combinations for each NF2 tumor type. For meningioma, the combinations of cabozantinib (an inhibitor of RTKs, including vascular endothelial growth factor receptor 2 [VEGFR2] and hepatocyte growth factor receptor MET) with danusertib (an Aurora kinase inhibitor), dasatinib (an inhibitor of

BCR-ABL and SRC-family TKs) with GSK2126458 (a dual PI3K/mTOR inhibitor), and ALK-IN-1 (an inhibitor of ALK and multiple other TKs) with MK-2206 (an AKT inhibitor) were selected (Fig. 2A). For schwannoma, the combinations of ALK-IN-1 with dasatinib, TAE226 (a dual FAK/IGF-1R inhibitor) with dasatinib, and dasatinib with simvastatin (an HMG-CoA reductase inhibitor) were chosen (Fig. 2E).

ALK-IN-1 and its derivative brigatinib synergized with MK-2206 and dasatinib to inhibit *NF2*-deficient meningioma and schwannoma cell proliferation, respectively.

ALK-IN-1 is a chemical analogue of the FDA-approved ALK inhibitor brigatinib (AP26113. ALUNBRIG®) (Markham, 2017). As ALK-IN-1 is no longer in clinical development, we compared brigatinib with ALK-IN-1 for their ability to synergize with MK-2206 or dasatinib to inhibit proliferation of *NF2*-deficient cells. Similar to ALK-IN-1, brigatinib inhibited proliferation of *NF2*-deficient Syn5 arachnoidal and Ben-Men-1 meningioma cells and two different primary meningioma cells with *NF2* loss, MN612 and MN621. MK-2206 alone showed little growth-inhibitory activity (Figs. 2B/C); however, when combined with brigatinib, it exhibited mild synergy in growth inhibition of these meningioma cells (Fig. 2D and Supplementary Fig. S1).

Similarly, as a single agent, brigatinib inhibited proliferation of mouse *Nf2*$^{-/-}$ schwannoma MS02 and human *NF2*-deficient HS01 Schwann cells (Fig. 2G). Mouse MS02 cells appeared more sensitive to brigatinib inhibition than human HS01 cells. As with ALK-IN-1, brigatinib demonstrated significant synergy with dasatinib in reducing proliferation of both HS01 and MS02 cells (Fig. 2H and Supplementary Fig. S2). Also,

we observed some synergy in growth inhibition of these Schwann and schwannoma cells when dasatinib was combined with simvastatin (Supplementary Fig. S3).

Based on these results, we further evaluated brigatinib and its combination with MK-2206 or dasatinib *in vivo*.

Kinome profiling revealed strong inhibition of non-RTKs, such as FER and PTK2/FAK, in brigatinib-treated cells.

Brigatinib has been described as a potent ALK inhibitor and is used clinically for the treatment of ALK+ non-small cell lung carcinoma; however, it has multiple other kinase targets as well (Huang et al., 2016). To investigate the protein targets of brigatinib in schwannoma and meningioma cells, we conducted kinome profiling in isogenic NF2-related cell panels with or without drug treatment using MIB/MS. The MIBs are designed to bind kinases when they are in the “Asp-Phe-Gly (DFG)-in” (active) conformation. Kinases inhibited by brigatinib would not be bound by MIBs, while those bound are subsequently identified via MS (Duncan et al., 2012; Stuhlmiller et al., 2015). A comparison of the kinome profiles of *NF2*-expressing Syn1 arachnoidal cells treated with brigatinib or DMSO for 24h identified the loss of MIB binding to several non-RTKs in brigatinib-treated cells, including the Fps/Fes-related kinase (FER), tyrosine kinase non-receptor 2/activated p21CDC42 kinase (TNK2/ACK), protein tyrosine kinase 2 /focal adhesion kinase (PTK2/FAK), and JAK1, in addition to several STK, such as cyclin G-associated kinase (GAK), microtubule-associated protein-microtubule affinity regulating kinase (MARK) 1 and 3, and ribosomal protein S6 kinase α3/ribosomal S6 kinase 2 (RPS6KA3/RSK2) (Fig. 3A). The *NF2*-null Syn5 line exhibited MIB binding loss

of essentially the same kinases observed in the Syn1 line, albeit with increased significance (Fig. 3B). Treatment with MK-2206 alone did not lead to significant changes in either Syn1 or Syn5 cells (data not shown). When Syn1 or Syn5 cells were treated with the brigatinib/MK-2206 combination, the top affected kinases included the non-receptor PTK2B/FAK2 and several other STKs, such as Aurora kinase A (AURKA), maternal embryonic leucine zipper kinase (MELK), and Ste20-like kinase (SLK) 1 and 2, similar to brigatinib monotherapy (Figs. 3C/3D). To better define the direct targets of brigatinib, Ben-Men-1 cells were treated with 10nM and 100nM of brigatinib for 2h. A similar set of non-RTKs, including FER, PTK2B/FAK2, and PTK2/FAK, and STKs, such as TNK2, STK33, and GAK, displayed strongly reduced MIB binding (Fig. 3E). Surprisingly, under these treatment conditions, we did not observe any changes in the MIB binding of active EGFR, IGF-1R, and INSR in treated Ben-Men-1 cells. Also, we did not detect any ALK or its related ROS1.

Transcriptome analysis of the Syn1 and Syn5 cells confirmed the lack of expression of both *ALK* and *ROS1* and the exaggerated response of the merlin-null Syn5 cells compared to the merlin-expressing Syn1 cells to brigatinib treatment (Supplementary Table S1). The former showed more than 4.5 times as many differentially expressed genes (DEGs; Bonferroni-corrected $p < 0.05$), which included most of the DEGs observed in the latter (Supplementary Fig. S4A). Similar to the kinome results, treatment of the arachnoidal cells with MK-2206 did not result in any significant DEGs. The brigatinib+MK2206 combination showed mildly more DEGs for Syn1 and less for Syn5 than did brigatinib alone. Pathway analysis of the drug-treated Syn5 DEGs (Supplementary Table S2) showed that those overlapping with Syn1 DEGs were

enriched most significantly in pathways related to DNA replication (e.g., GO:0006260~DNA replication, GO:0000082~G1/S transition of mitotic cell cycle, and GO:0006270~DNA replication initiation), while those seen only in Syn5 were enriched most significantly in pathways related to RNA [GO:0005730~nucleolus, GO:0005654~nucleoplasm, and GO:0044822~poly(A) RNA binding]. Of the kinome differences noted above, only MELK (downregulated in both Syn1 and Syn 5 by brigatinib or brigatinib+MK-2206) and PTK2B (upregulated only in Syn5 by brigatinib or brigatinib+MK-2206) showed a significant difference at the mRNA level. A comparison of untreated Syn5 and Syn1 cells revealed the number of DEGs caused by the loss of merlin to be comparable to the number elicited in Syn5 by drug treatment. Interestingly, of the DEGs associated with brigatinib or brigatinib+MK-2206 treatment of Syn5, those also associated with loss of merlin were moved overwhelmingly in the direction of Syn1 expression, with genes upregulated by merlin-loss being downregulated by drug treatment and genes downregulated by merlin-loss being upregulated by drug treatment (Supplementary Fig. S4B).

We also analyzed the kinome profiles of tumors formed at dorsal root ganglions (DRGs) or control sciatic nerves from *Postn-Cre*;*Nf2*$^{flox/flox}$ mice (Fig. 3F and Supplementary Fig. S5A). Ptk2/Fak and Gak MIB binding was dramatically affected by brigatinib treatment in lysates from both the tumor and control sciatic nerve tissues. To implement a co-clinical trial of brigatinib in the murine NF2 model, *Postn-Cre*;*Nf2*$^{flox/flox}$ mice with DRG tumors were treated with brigatinib for 3 or 7 days and compared to vehicle-treated controls by MIB/MS kinome profiling (Fig. 3G). Consistent with our prior observations, the tumors from brigatinib-treated mice showed significant MIB binding

loss of predominantly Ptk2/Fak and Gak. In addition, the STKs RPS6KA3/Rsk2 and Mark3 were also affected after 7-day treatment (Fig. 3H). Notably, brigatinib treatment did not result in an increased MIB binding of any kinase at either time point.

Kinome analysis of HS01 and HS11 cells treated with 1μM brigatinib, 0.6μM dasatinib or 1μM simvastatin, alone or in combination, showed by principal component analysis (normalized MIB binding) that dasatinib and brigatinib were the distinguishing drivers of the combination drug effects (Supplementary Figs. S5B/C). When HS01 and HS11 cells were treated with brigatinib alone, the top 20 kinases with loss of MIB binding included FER, TNK2, PTK/FAK, PTK2B/FAK2, and the targets identified in other cell line models and tissues described above (Fig. 3H). However, treatment of HS01 and HS11 cells with brigatinib did not significantly disrupt the transcriptome, while treatment with either dasatinib or simvastatin had modest effects (Supplementary Table S1 and Supplementary Fig. S4C). The brigatinib+dasatinib combination showed more robust effects, with DEGs in HS01 Schwann cells being enriched most significantly in cytoplasmic pathways, in contrast to the arachnoidal cells (Supplementary Table S2)

Collectively, these results indicate that brigatinib consistently inhibits unanticipated non-RTK targets, such as PTK2/FAK and FER, and the STK GAK across the various NF2-related meningioma and schwannoma cell lines and tissues.

Brigatinib effectively suppressed phosphorylation of FER, FAK, EPHA2, EGFR, ErbB3, and IGF1R.

To corroborate the findings from MIB/MS and to further identify any additional kinases perturbed by brigatinib treatment, we profiled the expression of 28 phospho-

RTKs and 11 downstream signaling nodes using PathScan® RTK Signaling Antibody Array in Ben-Men-1 cells treated with 1xIC_{50} dose of brigatinib or DMSO under active growth conditions in 10% FBS or in growth-arrested cells stimulated with 20% serum. Consistent with MIB/MS analysis, we did not detect any ALK signal in Ben-Men-1 cells with or without brigatinib treatment under both growth conditions (Supplementary Fig. S6). Western blot analysis confirmed that ALK expression was not detected in Ben-Men-1 cells (Fig. 4A) or normal meningeal cells, three *NF2*-deficient meningioma cell lines, and four primary meningioma cell cultures with or without *NF2* loss (Supplementary Fig. S7).

In contrast, we observed a broad range of kinases that were active in Ben-Men-1 cells, with similar patterns of activity between logarithmically growing cells and growth-arrested cells stimulated with 20% serum (Supplementary Figs. S6A/C). Notably, strong expression of phosphorylated ErbB2, ErbB3, INSR, FGFR1, TRKA, c-Kit, VEGFR2, and several EPH receptors was observed. Importantly, brigatinib treatment reduced the levels of most of these phospho-RTKs with the most significant reduction in EGFR, ErbB2, ErbB3, VEGFR2, and EPH receptors, particularly in cells treated for 2h. In addition, brigatinib treatment led to attenuation of the downstream signals from these RTKs, including p-AKT(S473 and T308) and p-ERK1/2. The phosphorylation of most of the brigatinib-inhibited RTKs showed some recovery to baseline levels after 24h, although some of their downstream signaling proteins, such as ERK1/2, AKT, and S6, remained markedly suppressed (compare Supplementary Figs. S6A/C with S6B/D).

Western blot analysis corroborated that phosphorylation of the non-RTKs FAK/PTK2 and FER were noticeably reduced in brigatinib-treated Ben-Men-1 cells under active

growth conditions in 10% FBS or in growth-arrested cells stimulated with 20% serum (Fig. 4B). Similar to p-RTK array analysis, we observed reduced phosphorylation of ErbB3 and EphA2 in brigatinib-treated cells. Also, their downstream signaling nodes ERK1/2, AKT, and S6 were all markedly decreased. However, under the same growth conditions, the basal levels of p-EGFR were minimally detectable and were lost following brigatinib treatment particularly after 24h (Supplementary Fig. S8). Additionally, we did not detect p-IGF1R under these growth conditions (data not shown). Therefore, we investigated the effects of brigatinib in ligand-induced activation of IGF1R, EGFR, and ErbB3 in Ben-Men-1 cells. Upon each cognate ligand stimulation, p-EGFR, p-ErbB3, and p-IGF1R were readily detected in Ben-Men-1 cells, and brigatinib treatment abrogated their phosphorylation (Fig. 4C).

Similarly, we did not detect ALK expression in human Schwann and schwannoma cells by Western blots (Supplementary Fig. S9). Treatment of *Nf2*-null Schwann cells with brigatinib resulted in a reduction in FAK phosphorylation as well as reductions in p-ERK1/2, p-AKT, and p-S6 (Fig. 4D). In *NF2*-deficient HS01 human Schwann cells, brigatinib reduced phosphorylation of FAK, ERK1/2, MEK, AKT, S6RP, and IGR (Fig. 4E).

Together, these results validate the MIB/MS findings that brigatinib inhibits multiple non-RTKs, such as FAK, in both schwannoma and meningioma cells *in vitro*.

Brigatinib and MK-2206 showed favorable plasma and brain PK profiles in mice.

To evaluate the anti-tumor activity of the brigatinib and MK-2206 combination in meningioma, we first characterized the PK of brigatinib and MK-2206 in mice. When a

single MTD of MK-2206 or brigatinib was given orally, the mean concentration of MK-2206 quickly reached the maximum (C_{max}) of ~2.2μg/ml in the plasma at T_{max} = 1h, while brigatinib reached the plasma C_{max} of ~1.3μg/ml at ~4h (Fig. 5A and Supplementary Fig. S10). The concentrations of both compounds gradually declined in the plasma over 24h, and the plasma half-life ($T_{½}$) for MK-2206 and brigatinib was estimated to be ~5.6 and 7.2h, respectively. In a similar trend, both MK-2206 and brigatinib reached the C_{max} in the brain at ~4 h after oral dosing. The estimated half-life for MK-2206 and brigatinib in the brain was ~6 and 6.2h, respectively. To evaluate if there are any PK interactions between MK-2206 and brigatinib, we administered mice with an oral dose of both compounds at their MTDs and harvested blood and brain tissues 12h after dosing. The mean concentrations of both compounds when given in combination were found to be comparable to those when given alone in both sets of plasma and brain samples (Fig. 5A). These results indicate that there are no PK changes when brigatinib and MK-2206 were given in combination.

Brigatinib alone or in combination with MK-2206 caused tumor shrinkage in an intracranial *NF2*-deficient meningioma model.

To assess the *in vivo* efficacies of brigatinib and MK-2206, either alone or in combination, mice bearing established luciferase-expressing Ben-Men-1-LucB tumors, as defined by an increase in BL signal over at least two time points (Burns et al., 2013), were treated with brigatinib, MK-2206, or their combination at the MTDs, or vehicle. BLI showed that compared with vehicle-treated tumors, which grew steadily over time (an average of 670% after 12 weeks), brigatinib alone effectively blocked meningioma

growth over the 12-week treatment period (Figs. 5B-C), with the average size of treated tumors reduced to ~62% of pretreated tumors (Fig. 5C and Supplementary Fig. S11). In contrast, tumors treated with MK-2206 alone continued to increase in size over time; however, their growth was slower than that of vehicle-treated tumors. Most significantly, combined treatment with brigatinib and MK-2206 further shrank meningiomas to ~37% of the original tumor size after 12 weeks. Immunohistochemistry analysis revealed that tumors treated with brigatinib or its combination with MK-2206 had a marked decrease in the numbers of Ki67-, p-S6-, and p-ERK-positive cells, compared with vehicle-treated tumors. In contrast, tumors treated with MK-2206 alone exhibited modestly-reduced staining for these signaling molecules (Fig. 5E). These results are consistent with tumor inhibition by brigatinib and its combination with MK-2206.

To evaluate potential tumor regrowth after cessation of treatment and the efficacy of re-treatment, we stopped treating one cage each of mice that had been treated with brigatinib or the brigatinib/MK-2206 combination for 14 weeks and continued monitoring tumor growth by BLI for another 12 weeks. Upon cessation of treatment, the brigatinib-treated tumors steadily regrew over time (Fig. 5D). Similarly, following cessation of treatment, brigatinib/MK-2206-treated gradually regrew, albeit at much slower rates than those treated with brigatinib alone. However, treatment re-initiation resulted in tumor shrinkage again, suggesting that the meningioma xenografts were still drug-sensitive.

Brigatinib inhibited schwannoma growth and slowed down hearing loss in *Postn-Cre;Nf2$^{flox/flox}$* mice.

To assess therapeutic response of the selected compounds in schwannomas *in*

vivo, *Postn-Cre*;*Nf2*$^{flox/flox}$ mice were treated for 12 weeks with brigatinib and dasatinib, as single agents and in combination, as well as dasatinib in combination with simvastatin, another FDA approved therapeutic which demonstrated synergy with dasatinib in our drug screens (Fig. 2E). Mice treated with brigatinib alone received the MTD of 50mg/kg. Due to *in vivo* toxicity in this model, the dose of brigatinib in the brigatinib/dasatinib combination had to be reduced to 15mg/kg. The lower dosing regimen and decreased half-life of brigatinib led to significant reduction in total drug exposure as measured by AUC in the combination group (Fig. 6A). Brigatinib alone, but not in combination with dasatinib, protected mice from development of sensorineural hearing loss over the 12-week treatment (Fig. 6B). Brigatinib alone significantly decreased the volume of tumor-bearing DRG tissue (Fig. 6C). Finally, tissues treated with brigatinib exhibited Schwann cell hypercellularity at the end of a 12-week treatment protocol, but had far fewer areas of discrete schwannoma when compared to the other treatment conditions (Fig. 6D). The brigatinib/dasatinib combination also reduced the DRG volume, albeit by a smaller magnitude. Western blot analysis showed that DRGs from *Postn-Cre*;*Nf2*$^{flox/flox}$ mice treated with brigatinib or brigatinib+dasatinib had reduced p-FAK, p-AKT, and p-S6, substantiating that brigatinib inhibits non-RTKs, such as FAK (Supplementary Fig. S12). These results indicate that brigatinib also possesses anti-tumor effects in spontaneous *NF2*-deficient schwannomas *in vivo*.

Discussion

In this study, we undertook an unbiased, systems-based approach to identify brigatinib, an inhibitor of ALK and other RTKs, as a novel therapy for the treatment of

NF2-related schwannomas and meningiomas. The reasoning behind relying on an unbiased, systems based screen to identify novel therapeutics for NF2 was driven in part by our lack of understanding of the complex biochemical functions of merlin which has hampered our prior abilities to advance therapeutics for this disease using a more traditional data and hypothesis driven approach (Evans et al., 2009; Blakeley et al., 2012). To this end, we would not have anticipated an ALK inhibitor demonstrating preclinical efficacy in either schwannoma or meningioma, given that ALK is not detected in either tumor type.

Our work began with a series of cell-based drug screens. From single-agent screening of the MIPE 4.0 oncology collection of ~2,000 compounds using an isogenically-matched panel of cell lines for schwannoma and meningioma, we identified the most active compounds based on the compound's IC_{50} and maximum % inhibition. Remarkably, among the top 40 most active compounds, there were seven inhibitors each of proteasome and HDAC. We and others previously showed HDAC inhibitors to potently suppress the growth of NF2-related tumors (Jacob et al., 2012; Burns et al., 2013; Petrilli et al., 2014; Synodos for NF2 Consortium, 2018). In addition, consistent with our previous study of 19 drugs with targets relevant to NF2 biology (Synodos for NF2 Consortium, 2018), we observed no major difference overall between *NF2*-expressing and *NF2*-deficient cells in terms of drug sensitivity, rather it was clustered by tumor type (meningioma vs schwannoma). These results suggest that drugs that do not directly target known merlin-regulated pathways should also be considered as potential treatments for NF2 tumors. Thus, evaluation of selective proteasome inhibitors in these tumors is warranted.

Along the notion of tumor type difference in drug response, we also identified different sets of drug combinations with the highest growth-inhibitory synergy in meningioma and schwannoma cells (Figs. 2A and 2E). Among the top three drug combinations selected for meningiomas, we decided not to evaluate the cabozantinib/danusertib combination due to previous findings on the tolerability for cabozantinib and Aurora kinase inhibitors and the poor efficacy for Aurora kinase inhibitors (Schöffski et al., 2015; Cohen et al., 2017; ClinicalTrials.gov Identifier: NCT01482962; Bersanelli et al., 2018; Rabinowits et al., 2018). For the dasatinib/GSK2126458 combination, we previously tested dasatinib in combination with the mTOR kinase inhibitor INK128, instead of the dual PI3K/mTOR inhibitor GSK2126458 due to toxicity issues (Grilley-Olson et al., 2016; Synodos for NF2 Consortium, 2018). We showed that the dasatinib/INK128 combination suppresses meningioma growth (Angus et al., 2018). We chose not to pursue ALK-IN-1 directly as a therapeutic because ALK-IN-1 was originally generated as a part of a series of structural analogs which could inhibit ALK. Ultimately therapeutic development of that series of molecules favored a different analog, AP26113, now known as brigatinib (Huang et al., 2016). We confirmed that brigatinib had efficacy comparable to ALK-IN-1 in slowing the growth of meningioma and schwannoma cell lines and also exhibited some synergy in growth inhibition in meningioma cells when combined with MK-2206.

For the other top combinatorial therapies for schwannoma discovered from our screening, we pursued dasatinib, both alone and in combination with brigatinib and simvastatin, but not the TAE226/dasatinib combination for preclinical studies. Our rationale for this prioritization is that while TAE226 is a FAK inhibitor in preclinical

development, we have data demonstrating that both brigatinib and dasatinib inhibit FAK activation in Schwann cells and both are FDA-approved. Therefore, given the lack of any effective experimental therapeutics for NF2 tumors, we chose to prioritize the three compounds which already have FDA approval in other contexts.

Following up on the unexpected finding that ALK was not detected in either schwannoma and meningioma, we demonstrated that under our cell-culture conditions, the kinases most potently inhibited by brigatinib were non-RTKs (FER, PTK2B/FAK2, and PTK2/FAK) and STKs (TNK2, STK33, and GAK). Similarly, the non-RTK PTK2/FAK and the STKs GAK, RPS6KA3/RSK2, and MARK3 were also found to be greatly suppressed in brigatinib-treated DRGs.

From the New Drug Application (NDA) information submitted to the FDA (https://www.accessdata.fda.gov/drugsatfda_docs/nda/2017/208772Orig1s000TOC.cfm), we learned that while brigatinib has an IC_{50} of ~1nM against ALK, it potently inhibits at relatively low IC_{50} values (≤ 10nM) other RTKs like ROS1 and FLT3, several non-RTKs including FER, FES/FPS, FAK/PTK2, and breast tumor kinase/protein tyrosine kinase 6 (BRK/PTK6), and the STKs STK22D and checkpoint kinase 2 (CHK2). Brigatinib is also active at IC_{50} ≤ 100nM against several RTKs (including the various EGFR-family members, VEGFR3, RET, and IGF-1R), non-RTKs (such as YES and PTK2B/FAK2), and a number of STKs. In addition, it inhibits at >100nM but at concentrations (e.g., low micromolar) that have been achieved clinically many other RTKs, including various fibroblast growth factor receptors (FGFRs) and several EPH receptors, and a few non-RTKs and STKs. Using a proteome-wide drug screening approach, it was confirmed that brigatinib strongly interacts with ALK, PTK2/FAK, and PTK2B/FAK2 and has a

medium affinity to IGF1R and EGFR (Zhou et al., 2016). These results suggest that the non-RTKs FAK/PTK2 and FER, which are strongly inhibited by brigatinib in *NF2*-deficient meningioma and schwannoma cells, are important for the growth and survival of these tumors. However, the multiple other targets of brigatinib in signaling pathways linked to merlin could also underlie the drug's therapeutic efficacy.

It should be emphasized that even though we did not detect changes in the RTKs frequently activated in NF2-related tumors by MIB/MS (Fig. 3), we were able to demonstrate suppression of phosphorylated EGFR, ErbB3, and IGF1R in cells treated with 1xIC_{50} concentration of brigatinib under ligand-induced growth conditions (Fig. 4C). At this brigatinib concentration, we also detected inhibition of EPHA2, which we previously showed increased expression and activation of this RTK in *NF2*-deficient cells (Angus et al., 2018). Consequently, activation of all these RTKs and non-RTKs leads to downstream activation of both PI3K-AKT and MEK-ERK signaling. Collectively, our results suggest that the anti-tumor activity of brigatinib in schwannoma and meningioma is mediated through blockade of multiple RTKs and non-RTKs.

Consistent with previous reports (Yap et al., 2011; Huang et al., 2016), brigatinib and MK-2206 exhibited overall favorable PK profiles. In the blood, brigatinib reached an average of 2.2μM when given orally (C_{max}=1,311ng/ml; Supplementary Fig. S8), which is above the IC_{50} in Ben-Men-1 cells. Our PK data also showed effective blood-brain penetration and further suggests no drug-drug interaction between brigatinib and MK-2206 (Fig. 5A). These results should guide optimization of the dosing regimen for these drugs in a future clinical trial. Importantly, brigatinib monotherapy induced tumor regression in meningioma and its combination with MK-2206 resulted in further tumor

shrinkage. Although meningiomas regrew upon cessation of treatment, these tumors remained responsive to brigatinib, either alone or in combination with MK-2206. These results suggest that it is possible to have short breaks from treatment while maintaining therapeutic responses to retreatment, particularly after treatment with the brigatinib/MK-2206 combination.

Brigatinib as a single agent was also very well-tolerated in the NF2 GEM model. We observed a nearly 40% reduction in average DRG volume after 12 weeks of brigatinib treatment and those mice did not develop detectable sensorineural hearing loss over the course of the study. The two combinatorial therapeutics of brigatinib+dasatinib and dasatinib+simvastatin which we identified in the drug screen and tested *in vivo* were also efficacious in reducing schwannoma growth, albeit to a lesser extent than what was observed with brigatinib alone at a higher concentration. Of note, significant toxicity was observed in the brigatinib/dasatinib treatment group, and consequently we had to reduce the dose of brigatinib from 50 mg/kg to 15 mg/kg for this combination. The lower dose of brigatinib in the combination treatment significantly reduced total drug exposure as measured by AUC (Fig. 6A). The magnitude of the reduction in average DRG volume observed in the brigatinib-treated mice is the largest we have seen for any treatment in this NF2 GEM model. So the reduction in efficacy of the brigatinib/dasatinib combination therapy over the brigatinib single-agent treatment may be a result of the greater than 3-fold reduction in brigatinib dosing given to the combination-treated mice.

Based on the data presented here, brigatinib possessed potent anti-tumor activity against *NF2*-deficient tumors via inhibition of multiple RTKs frequently activated in these tumors, but not ALK, as well as blockade of several non-RTKs and STKs. Given the fact

that brigatinib caused tumor shrinkage in both schwannoma and meningioma, a clinical trial is being planned to evaluate it as a new treatment for patients with NF2.

ACKNOWLEDGMENTS

This study was supported by grants from Children's Tumor Foundation for the Synodos for NF2 project (#2014-18-001A to GLJ; 2014-18-001B to JFG; 2014-18-001C to JOB; 2014-18-001D to DWC; 2014-18-001E to DWB; 2014-18-001F to CFV; 2014-18-001G to HM; 2014-18-001H to LSC; 2014-04-008 to JG) and the US Department of Defense (W81XWH-18-1-0547 to LSC and VR). We sincerely thank Tracy Galloway, mother of an NF2 patient and acting patient representative on the project, and the CTF management team for their support.

References

Ammoun S, Hanemann CO. 2011. Emerging therapeutic targets in schwannomas and other merlin-deficient tumors. Nat Rev Neurol. 2011;7:392-399.

Angus SP, Oblinger JL, Stuhlmiller TJ, DeSouza PA, Beauchamp RL, Witt L, Chen X, Jordan JT, Gilbert TSK, Stemmer-Rachamimov A, Gusella JF, Plotkin SR, Haggarty SJ, Chang LS, Johnson GL, Ramesh V; Children's Tumor Foundation Synodos for NF2 Consortium. EPH receptor signaling as a novel therapeutic target in NF2-deficient meningioma. Neuro Oncol. 2018;20:1185-1196.

Beauchamp RL, James MF, DeSouza PA, Wagh V, Zhao WN, Jordan JT, et al. A high-throughput kinome screen reveals serum/glucocorticoid-regulated kinase 1 as a therapeutic target for NF2-deficient meningiomas. Oncotarget. 2015;6: 16981-16997.

Bersanelli M, Leonardi F, Buti S. Spotlight on cabozantinib for previously untreated advanced renal cell carcinoma: evidence to date. Cancer Manag Res. 2018;10:3773-3780.

Blakeley JO, Evans DG, Adler J, Brackmann D, Chen R, Ferner RE, Hanemann CO, Harris G, Huson SM, Jacob A, Kalamarides M, Karajannis MA, Korf BR, Mautner VF, McClatchey AI, Miao H, Plotkin SR, Slattery W 3rd, Stemmer-Rachamimov AO, Welling DB, Wen PY, Widemann B, Hunter-Schaedle K, Giovannini M. Consensus recommendations for current treatments and accelerating clinical trials for patients with neurofibromatosis type 2. Am J Med Genet A. 2012;158A:24-41.

Blakeley JO, Plotkin SR. Therapeutic advances for the tumors associated with neurofibromatosis type 1, type 2, and schwannomatosis. Neuro Oncol. 2016;18:624-638.

Borisy AA, Elliott PJ, Hurst NW, Lee MS, Lehar J, Price ER, Serbedzija G, Zimmermann GR, Foley MA, Stockwell BR, Keith CT. Systematic discovery of multicomponent therapeutics. Proc Natl Acad Sci USA 2003;100:7977-7982.

Burns SS, Akhmametyeva EM, Oblinger JL, Bush ML, Huang J, Senner V, et al. Histone deacetylase inhibitor AR-42 differentially affects cell-cycle transit in meningeal and meningioma cells, potently inhibiting NF2-deficient meningioma growth. Cancer Res. 2013;73: 792-803.

Cohen JB, Maddocks KJ, Huang Y, Christian BA, Jaglowski SM, Flowers CR, Blum KA. A phase 2 trial of alisertib in patients with relapsed or refractory B-cell non-Hodgkin lymphoma. Leuk Lymphoma. 2017;58:1-2.

Cox J, Hein MY, Luber CA, Paron I, Nagaraj N, Mann M**.** Accurate proteome-wide label-

free quantification by delayed normalization and maximal peptide ratio extraction, termed MaxLFQ**.** Mol Cell Proteomics. 2014;13:2513-2526**.**

DeLuca DS, Levin JZ, Sivachenko A, Fennell T, Nazaire MD, Williams C, Reich M, Winckler W, Getz G. RNA-SeQC: RNA-seq metrics for quality control and process optimization. Bioinformatics 2012;28:1530-1532.

Di Veroli GY, Fornari C, Wang D, Mollard S, Bramhall JL, Richards FM, Jodrell DI. Combenefit: an interactive platform for the analysis and visualization of drug combinations. Bioinformatics. 2016;32:2866-2868.

Dobin A, Davis CA, Schlesinger F, Drenkow J, Zaleski C, Jha S, Batut P, Chaisson M, Gingeras TR. STAR: ultrafast universal RNA-seq aligner. Bioinformatics 2013;29:15-21.

Duncan JS, Whittle MC, Nakamura K, Abell AN, Midland AA, Zawistowski JS, Johnson NL, Granger DA, Jordan NV, Darr DB, Usary J, Kuan PF, Smalley DM, Major B, He X, Hoadley KA, Zhou B, Sharpless NE, Perou CM, Kim WY, Gomez SM, Chen X, Jin J, Frye SV, Earp HS, Graves LM, Johnson GL. Dynamic reprogramming of the kinome in response to targeted MEK inhibition in triple-negative breast cancer. Cell. 2012;149:307-321.

Evans DG. Neurofibromatosis type 2. Handb Clin Neurol. 2015;132:87-96.

Evans DG, Kalamarides M, Hunter-Schaedle K, Blakeley J, Allen J, Babovic-Vuskanovic D, Belzberg A, Bollag G, Chen R, DiTomaso E, Golfinos J, Harris G, Jacob A, Kalpana G, Karajannis M, Korf B, Kurzrock R, Law M, McClatchey A, Packer R, Roehm P, Rubenstein A, Slattery W 3rd, Tonsgard JH, Welling DB, Widemann B, Yohay K, Giovannini M. 2009. Consensus recommendations to

accelerate clinical trials for neurofibromatosis type 2. Clin Cancer Res. 2009;15:5032-5039.

Ferrer M, Gosline SJC, Stathis M, Zhang X, Guo X, Guha R, Ryman DA, Wallace MR, Kasch-Semenza L, Hao H, Ingersoll R, Mohr D, Thomas C, Verma S, Guinney J, Blakeley JO. Pharmacological and genomic profiling of neurofibromatosis type 1 plexiform neurofibroma-derived schwann cells. Sci Data. 2018;5:180106.

Gehlhausen JR, Park SJ, Hickox AE, Shew M, Staser K, Rhodes SD, et al. A murine model of neurofibromatosis type 2 that accurately phenocopies human schwannoma formation. Hum Mol Genet. 2015;24: 1-8.

Grilley-Olson JE, Bedard PL, Fasolo A, Cornfeld M, Cartee L, Razak AR, Stayner LA, Wu Y, Greenwood R, Singh R, Lee CB, Bendell J, Burris HA, Del Conte G, Sessa C, Infante JR. A phase Ib dose-escalation study of the MEK inhibitor trametinib in combination with the PI3K/mTOR inhibitor GSK2126458 in patients with advanced solid tumors. Invest New Drugs. 2016;34:740-749.

Hirai H, Sootome H, Nakatsuru Y, Miyama K, Taguchi S, Tsujioka K, Ueno Y, Hatch H, Majumder PK, Pan BS, Kotani H. MK-2206, an allosteric Akt inhibitor, enhances antitumor efficacy by standard chemotherapeutic agents or molecular targeted drugs in vitro and in vivo. Mol Cancer Ther. 2010;9:1956-1967.

Huang da W, Sherman BT, Lempicki RA. Systematic and integrative analysis of large gene lists using DAVID bioinformatics resources. Nat Protoc. 2009;4:44-57.

Huang WS, Liu S, Zou D, Thomas M, Wang Y, Zhou T, Romero J, Kohlmann A, Li F, Qi J, Cai L, Dwight TA, Xu Y, Xu R, Dodd R, Toms A, Parillon L, Lu X, Anjum R, Zhang S, Wang F, Keats J, Wardwell SD, Ning Y, Xu Q, Moran LE, Mohemmad QK, Jang

HG, Clackson T, Narasimhan NI, Rivera VM, Zhu X, Dalgarno D, Shakespeare WC. Discovery of Brigatinib (AP26113), a Phosphine Oxide-Containing, Potent, Orally Active Inhibitor of Anaplastic Lymphoma Kinase. J Med Chem. 2016; 59:4948-4964.

Jacob A, Oblinger J, Bush ML, Brendel V, Santarelli G, Chaudhury AR, Kulp S, La Perle KM, Chen CS, Chang LS, Welling DB. Preclinical validation of AR42, a novel histone deacetylase inhibitor, as treatment for vestibular schwannomas. Laryngoscope. 2012;122:174-189.

Li H, Handsaker B, Wysoker A, Fennell T, Ruan J, Homer N, Marth G, Abecasis G, Durbin R; 1000 Genome Project Data Processing Subgroup. The Sequence Alignment/Map format and SAMtools. Bioinformatics 2009;25:2078-2079

Markham A. 2017. Brigatinib: First Global Approval. Drugs. 77:1131-1135.

Mathews Griner LA, Guha R, Shinn P, Young RM, Keller JM, Liu D, Goldlust IS, Yasgar A, McKnight C, Boxer MB, Duveau DY, Jiang JK, Michael S, Mierzwa T, Huang W, Walsh MJ, Mott BT, Patel P, Leister W, Maloney DJ, Leclair CA, Rai G, Jadhav A, Peyser BD, Austin CP, Martin SE, Simeonov A, Ferrer M, Staudt LM, Thomas CJ. High-throughput combinatorial screening identifies drugs that cooperate with ibrutinib to kill activated B-cell-like diffuse large B-cell lymphoma cells. Proc Natl Acad Sci U S A. 2014;111:2349-2354.

Petrilli AM, Fuse MA, Donnan MS, Bott M, Sparrow NA, Tondera D, Huffziger J, Frenzel C, Malany CS, Echeverri CJ, Smith L, Fernandez-Valle C. A chemical biology approach identified PI3K as a potential therapeutic target for neurofibromatosis type 2. Am J Transl Res 2014;6:471-493.

Petrilli AM, Garcia J, Bott M, Klingeman Plati S, Dinh CT, Bracho OR, et al. Ponatinib

promotes a G1 cell-cycle arrest of merlin/NF2-deficient human schwann cells. Oncotarget. 2017;8:31666-31681.

Plowman J, Camalier R, Alley M, Sausville E, Schepartz S. US-NCI testing procedures. In: Feibig HH, Burger AM (eds), Relevance of Tumor Models for Anticancer Drug Development. Contrib Oncol. Basel, Karger, 1999;54:21-135.

Püttmann S, Senner V, Braune S, Hillmann B, Exeler R, Rickert CH, Paulus W. Establishment of a benign meningioma cell line by hTERT-mediated immortalization. Lab Invest. 2005;85:1163-1171.

Rabinowits G, Lezcano C, Catalano PJ, McHugh P, Becker H, Reilly MM, Huang J, Tyagi A, Thakuria M, Bresler SC, Sholl LM, Shapiro GI, Haddad R, DeCaprio JA**.** Cabozantinib in Patients with Advanced Merkel Cell Carcinoma**.** Oncologist. 2018;23:814-821**.**

Robinson MD, McCarthy DJ, Smyth GK. edgeR: a Bioconductor package for differential expression analysis of digital gene expression data. Bioinformatics 2010;26:139-140.

Schöffski P, Besse B, Gauler T, de Jonge MJ, Scambia G, Santoro A, Davite C, Jannuzzo MG, Petroccione A, Delord JP. Efficacy and safety of biweekly i.v. administrations of the Aurora kinase inhibitor danusertib hydrochloride in independent cohorts of patients with advanced or metastatic breast, ovarian, colorectal, pancreatic, small-cell and non-small-cell lung cancer: a multi-tumour, multi-institutional phase II study. Ann Oncol. 2015;26:598-607.

Siaw JT, Wan H, Pfeifer K, Rivera VM, Guan J, Palmer RH, Hallberg B. Brigatinib, an anaplastic lymphoma kinase inhibitor, abrogates activity and growth in ALK-positive neuroblastoma cells, Drosophila and mice. Oncotarget. 2016;7:29011-29022.

Stuhlmiller TJ, Miller SM, Zawistowski JS, Nakamura K, Beltran AS, Duncan JS, Angus SP, Collins KA, Granger DA, Reuther RA, Graves LM, Gomez SM, Kuan PF, Parker JS, Chen X, Sciaky N, Carey LA, Earp HS, Jin J, Johnson GL. Inhibition of Lapatinib-Induced Kinome Reprogramming in ERBB2-Positive Breast Cancer by Targeting BET Family Bromodomains. Cell Rep. 2015;11:390-404.

Synodos for NF2 Consortium, Allaway R, Angus SP, Beauchamp RL, Blakeley JO, Bott M, Burns SS, Carlstedt A, Chang LS, Chen X, Clapp DW, Desouza PA, Erdin S, Fernandez-Valle C, Guinney J, Gusella JF, Haggarty SJ, Johnson GL, La Rosa S, Morrison H, Petrilli AM, Plotkin SR, Pratap A, Ramesh V, Sciaky N, Stemmer-Rachamimov A, Stuhlmiller TJ, Talkowski ME, Welling DB, Yates CW, Zawistowski JS, Zhao WN. Traditional and systems biology based drug discovery for the rare tumor syndrome neurofibromatosis type 2. PLoS One. 2018;13:e0197350.

Wang L, Wang S, Li W. RSeQC: quality control of RNA-seq experiments. Bioinformatics 2012;28:2184-2185.

Yap TA, Yan L, Patnaik A, Fearen I, Olmos D, Papadopoulos K, Baird RD, Delgado L, Taylor A, Lupinacci L, Riisnaes R, Pope LL, Heaton SP, Thomas G, Garrett MD, Sullivan DM, de Bono JS, Tolcher AW. First-in-man clinical trial of the oral pan-AKT inhibitor MK-2206 in patients with advanced solid tumors. J Clin Oncol. 2011;29:4688-4695.

Zhou Y, Liu Z, Rothschild KJ, Lim MJ. Proteome-wide drug screening using mass spectrometric imaging of bead-arrays. Sci Rep. 2016;6:26125.

Figure Legends

Figure 1. Single-agent dose response and matrix HTS of the oncology MIPE 4.0 collection in meningioma and schwannoma cells. (A) Schematic diagram of the workflow for the discovery of novel drugs and drug combinations for the treatment of NF2-associated tumors. (B) Heat map of pharmacological responses (as % cell viability at the maximum dose tested, 46 μM, also called maximum response) of the MIPE 4.0 library in *NF2*-expressing Syn1 and *NF2*-null Syn5 human arachnoidal cells, *NF2*-deficient Ben-Men-1 meningioma cells, *NF2*-expressing HS11 and *NF2*-knockdown HS01 human Schwann cells, and *Nf2*$^{-/-}$ MS02 mouse schwannoma cells. Responses were clustered using a Hierarchical Clustering in Spotfire TIBCO. Red indicates low % cell viability and blue is high viability. (C) Cell survival responses to all MIPE 4.0 library agents (as judged by relative AUCs) binned per mechanistic classes with mechanistic superclasses listed in order from top to bottom: transcriptional regulation, physiological homeostasis, other, metabolism, DNA repair, cell surface protein, cell signaling, cell growth, antimicrobial. Solid dots represent the median response for all the compounds, in each mechanistic class, and for each cell line. (D) Target enrichment plots for pan active hits selected by % viability at the maximum concentration of compound tested (MAXR) <30% for both cell lines and all assay modes (top panel) and for pan active hits selected by CRCs -1.1 or -1.2 for both cell lines and all assay modes (bottom). The -log p-values were calculated as follows: given a selection of compounds, the annotated targets for these compounds were identified and the enrichment for each target computed, compared to background, using the Fishers exact test. For this test, the background was defined as all the targets annotated in the MIPE collection. The p-value

from the test was adjusted for multiple hypothesis testing using the Benjamini-Hochberg method. A -log p-value >1 was used as a cut-off to consider a target or processed being overrepresented. (E) Number of combinations tested and assays used for the 6x6 and 10x10 matrix combination HTS. Delta bliss 6x6 and 10x10 matrix plots for the combination of MK-2206 and ALK-IN-1 in Syn5 cells, using the CellTiterGlo viability assay. Darker color indicates higher DeltaBliss scores for synergy. (F) Heat map of DeltaBliss Sum Negative for the 990 6x6 all vs all pairwise combinations of the 45 drugs selected from the single-agent testing. The IC_{50} and maximum % inhibition of each compound in each indicated cell line were calculated. Responses were clustered using a Hierarchical Clustering in Spotfire TIBCO. Red indicates low % cell viability and blue is high viability.

Figure 2. Like ALK-IN-1, brigatinib exhibited growth-inhibitory synergy with MK-2206 or dasatinib in meningioma and schwannoma cells, respectively. (A) The top synergistic drug combinations identified for *NF2*-deficient meningioma cells. (B) 10x10 dose-viability response matrix of ALK-IN-1 vs MK-2206 in Syn1 and Syn5 cells, assessed at 72h. (C) Single-drug dose-response curves (DRCs) for MK-2206 (left) or brigatinib (right) were generated for human *NF2*-null cell lines, including Syn5, Ben-Men-1, and two primary meningiomas (MN612, MN621). Drug concentrations are outlined under supplementary methods. n.d., not determined. Data is expressed as +/- SEM. (D) Combination treatment of Ben-Men-1 cells was carried out in a 10x10 dose-matrix format using the same increasing concentration range of MK-2206 and brigatinib as with single DRCs. Heatmaps were generated on a colorimetric scale using Combenefit software, which calculates the drug interaction effects (relative to

vehicle/DMSO control). (E) The top synergistic drug combinations identified for NF2-related schwannoma cells. (F) 10x10 dose-viability response matrix of ALK-IN-1 vs dasatinib in HS11 and HS01 cells, assessed at 72h. (G) Brigatinib dose-response in mouse MS02 and human HS01 cells at 60 and 72h, respectively. (H) Loewe and highest single agent (HSA) synergy matrix analysis of brigatinib vs dasatinib in HS01 cells treated for 72h.

Figure 3. MIB/MS kinome profiling reveals brigatinib target specificity in multiple *NF2*-deficient cell models. (A-D) MIB/MS kinome profiling was performed following treatment of Syn1 and Syn5 cells with vehicle (DMSO), brigatinib (1μM) or the combination of MK-2206 (0.5μM) and brigatinib (1μM) for 24h in biological triplicate. MIB binding (log2LFQ intensities) were used for comparisons and the volcano plots indicate log2 difference and significance (5% FDR, indicated by dashed line). (E) MIB/MS kinome profiling was performed following treatment of Ben-Men-1 cells with vehicle (DMSO) or brigatinib (10nM, blue or 100nM, red) for 2h in biological duplicate. The log2 difference in MIB binding (LFQ intensity) was calculated and plotted relative to vehicle for each replicate. (F) Tumor lysates from the *Postn-Cre*;*Nf2*$^{flox/flox}$ mouse model were prepared and equal amounts of total protein were incubated for 2h with vehicle (0.001% ethanol) or brigatinib (10nM, blue; 100nM, red; 1000nM, green) in biological duplicate prior to MIB/MS kinome profiling. The log2 difference in MIB binding (LFQ intensity) was calculated and plotted relative to vehicle for each replicate. (G) *Postn-Cre*;*Nf2*$^{flox/flox}$ mice were treated with vehicle or brigatinib for 3 or 7 days (gold and blue, respectively, for indicated kinases). Tumors were harvested and subjected to MIB/MS kinome profiling. MIB binding (log2LFQ intensities) was determined and used for

comparisons of brigatinib to vehicle treatment. The volcano plot indicates log2 difference and significance (5% FDR, indicated by dashed line). (H) HS11 and HS01 cells were treated with vehicle (DMSO) or brigatinib (1μM) for 24h prior to MIB/MS kinome profiling. MIB binding (log2LFQ intensities) was determined and the top 20 kinases with decreased MIB binding compared to vehicle are shown as a stacked bar plot for the two cell lines.

Figure 4. Brigatinib inhibits multiple RTKs, non-RTKs, and their downstream signals. (A) Western blot analysis was conducted to detect ALK expression in Ben-Men-1 cells grown under various growth conditions and with or without brigatinib treatment. (B) Brigatinib treatment greatly reduced phosphorylation of non-RTKs FER and FAK, RTKs EPHA2 and ErbB3, and their downstream signaling molecules AKT, ERK1/2, and S6 in active growing Ben-Men-1 cells or growth-arrested cells stimulated with 20% serum. (C) Brigatinib blocked phosphorylation of EGFR, ErbB3, and IGF1R in growth-arrested Ben-Men-1 cells stimulated with each cognate ligand. (D) Brigatinib reduced the levels of p-FAK, p-ERK1/2, p-AKT, p-S6, and p-Gsk in . (E) Brigatinib blocked phosphorylation of FAK, ERK1/2, MEK, AKT, S6RP, and IGR in *NF2*-deficient HS01 human Schwann cells

Figure 5. Brigatinib and its combination with MK-2206 effectively shank intracranial meningioma xenografts. (A) PK analysis was conducted to determine the concentrations of brigatinib and MK-2206 in mouse plasma and brain. Mice were treated with a single MTD of brigatinib or MK-2206. Prior to and at various times after dosing (n=3 per time point), blood and brain from each dosed mouse were collected for UHPLC-MS/MS analysis according to Supplementary Methods. The mean

concentration of each drug at each indicated time point with standard deviation was plotted. Also, mice were treated with a combined dose of brigatinib and MK-2206 at their MTD (n=3), and the drug concentration in the plasma and brain determined (indicated with arrows). (B-C) Mice with established meningioma xenografts were treated with vehicle, brigatinib, MK-2206, or brigatinib+MK-2206 by oral gavage (n=10 each) and tumor growth was monitored by BLI. (B) Shown are representative BL images of tumor-bearing mice acquired prior to (PreTx) and 12 weeks (wks) after treatment. (C) The relative tumor-emitted BL signals were quantified and denoted as % of total flux after treatment relative to the total flux prior to treatment designated as one (100%). The data are shown as mean ± standard deviation. At least seven mice from each group completed the entire 12-week treatment. (D) Upon cessation of treatment, tumors in mice that had been treated with brigatinib or brigatinib+MK-2206 for 14 weeks (n=4 each) regrew. However, tumor shrinkage was observed when the treatment was re-initiated. Data shown for mice treated with brigatinib or brigatinib+MK-2206 are only from the cage of mice that had undergone cessation of treatment and retreatment. (E) Representative images of immunostained sections of the heads of tumor-bearing mice after 12-week treatment with vehicle, MK-2206, brigatinib, or MK-2206+brigatinib for Ki67, p-S6, p-ERKs, and cleaved caspase 3 (CC3) expression.

Figure 6. Schwannoma mouse model. (A) . (B) . (C) . (D) .

Supplementary Figure Legends

Supplementary Figure S1. Single and combination drug treatment of meningioma-related cell lines. Drug treatment of the *NF2*-expressing Syn1(+) and *NF2*-null Syn5(-) cells (A), Ben-Men-1 cells (B), and two primary meningioma cultures MN612 and MN621 (C) was performed using the same drug doses as for Figs. 2C/D. Single drug DRCs and combination drug heatmaps were generated using Combenefit software. Note that heatmap data for Ben-Men-1 (B) is the same as shown in Fig. 2D.

Supplementary Figure S2. Brigatinib and dasatinib synergized to reduce *NF2*-deficient Schwann cell viability. (A) *Nf2*$^{-/-}$ mouse MS02 schwannoma and *NF2*-deficient human HS01 Schwann cells were plated and tested in dose-response 10x10 matrix format as described in Methods. Shown are single-agent dose response curves for ALK-IN-1 and brigatinib. (B) Brigatinib/dasatinib combination matrix analyses was conducted with HS01 cells. Shown are the brown-scale viability and synergy matrix plots with modeled surface synergy distributions in Loewe, Bliss, and HSA models. (C) Brigatinib/dasatinib combination matrix were analyzed with MS02 cells as described in Supplementary Fig. S2B.

Supplementary Figure S3. Brigatinib and simvastatin synergized to reduce the viability of Schwann and schwannoma cells. 10x10 matrix dose-response analysis was performed for *NF2*-deficient HS01 (A) and *NF2*-expressing HS11 (B) human Schwann cells and *Nf2*$^{-/-}$ mouse schwannoma MS02 cells (C) treated with the brigatinib/simvastatin combination. Shown are the viability (brown scale) and synergy matrix (blue to red scale) plots with modeled surface synergy distributions in Loewe, Bliss, and HSA models.

Supplementary Figure S4. Gene expression changes caused by drug treatments. (A) Significant (Bonferroni-adjusted $p < 0.05$) changes in gene expression in Syn5 and Syn1 arachnoidal cells, which show extensive overlap with an overall greater response in the Syn5 merlin-null cells, are caused by brigatinib or brigatinib + MK-2206 treatment, but not by MK-2206 alone. (B) Genes whose expression is altered both by lack of merlin in Syn5 and by treatment of Syn5 with either brigatinib or brigatinib+MK-2206 treatment overwhelmingly show the expression change in opposite directions. (C) Significant changes in gene expression in HS01 and HS11 Schwann cells are limited in single drug treatments and most pronounced with the brigatinib+dasatinib combination. (D) The small number of genes differentially expressed in HS01 as a result of merlin expression do not overlap extensively with those altered in HS01 by the brigatinib+dasatinib treatment, and those overlaps that do occur are concordant in direction, contrasting with the arachnoidal cells.

Supplementary Figure S5. MIB/MS kinome profiling reveals dasatinib and brigatinib target specificity. (A) Control sciatic nerve tissues from ____ mice were used to prepare lysates. Equal amount of protein lysates (1mg) was incubated with vehicle (0.001% ethanol) or brigatinib (10nM, blue; 100nM, red; 1000nM, green) for 2h in biological duplicate. The log2 difference in MIB binding (LFQ intensity) was calculated and plotted relative to vehicle for each replicate. (B) HS11 and HS01 cells were treated with vehicle or brigatinib (1μM) for 24h prior to MIB/MS kinome profiling. MIB binding (log2LFQ intensities) was determined and PCA performed in Perseus. (C) HS11 and HS01 cells were treated with vehicle or dasatinib (0.6μM) for 24h prior to MIB/MS kinome profiling. MIB binding (log2LFQ intensities) was determined and the top 20

kinases with decreased MIB binding compared to vehicle are shown as a stacked bar plot for the two cell lines.

Supplementary Figure S6. Inhibition of multiple RTKs and non-RTKs in Ben-Men-1 cells treated with 1x IC_{50} of brigatinib under various growth conditions. PathScan® RTK signaling antibody array analysis was conducted according to Supplementary Methods using cells grown in 10% FBS and treated with 1x IC_{50} of brigatinib for 2h (A) and 24 h (B) or in growth-arrested cells stimulated with 20% FBS in the presence of 1x IC_{50} of brigatinib for 2h (C) and 24 h (D). The numeric table below each pair of arrays displays the fold-change in fluorescence detected for each phospho-protein expressed in cells treated with brigatinib relative to DMSO control after subtraction of the fluorescence in the background control spots (indicated as "-"). Positive control spots are denoted as "+".

Supplementary Figure S7. ALK was not detected in normal meningeal and meningioma cells with or without *NF2* expression. Equal amounts of protein lysates from three human meningioma cell lines (KT21-MG1-Luc, AG-NF2-Men, and Ben-Men-1), normal meningeal cells, and four primary meningioma cultures (hMen-10A, hMen-10B, hMen-12Ao, hMen-12B) were used in Western blot analysis to probe ALK and merlin expression. SK-N-SH neuroblastoma cells, which express ALK, were used as a positive control.

Supplementary Figure S8. Ben-Men-1 cells expressed low levels of p-EGFR, which was abolished by brigatinib treatment. Western blot analysis revealed that while phosphorylated EGFR was robustly induced in EGF-stimulated Ben-Men-1 cells, only very low levels of p-EGFR were detected in actively-growing cells or growth-

arrested cells stimulated with 20% serum for 24h. Brigatinib treatment diminished p-EGFR expression.

Supplementary Figure S9. ALK expression was not detected in Schwann and schwannoma cells. (A) Western blotting was performed to detect ALK expression in human Schwann cells, four primary vestibular schwannoma cultures (hVS-16H, hVS-16S, hVS-12J, hVS-12Ga), and SK-N-SH neuroblastoma cells. Tubulin was used as a loading control. (B) Western blotting for ALK was also performed using extracts from nine vestibular schwannoma tumors. GAPDH was used as a loading control

Supplementary Figure S10. Mouse PK parameters following a single oral dose of brigatinib or MK-2206 at the MTD. Mice were orally fed 50 mg/kg of brigatinib or 120 mg/kg of MK-2206. PK analysis was performed according to Supplementary Methods.

Supplementary Figure S11. Relative tumor sizes in meningioma-bearing mice prior to or after treatment with MK-2206 and brigatinib, either alone or in combination, for 12 weeks. Detailed drug treatment and tumor measurement were as described in Figs. 5B/C and Supplementary Methods.

Supplementary Figure S12. Brigatinib inhibited p-FAK, p-AKT, and p-S6 target pathways in *Postn-Cre;Nf2$^{flox/flox}$* mice. DRGs from *Postn-Cre;Nf2$^{flox/flox}$* mice treated with the indicated drug or drug combination were used in Western blotting as described in Supplementary Methods.

Supplementary Methods:

Compounds

Brigatinib (CAS: 1197953-54-0), MK-2206 (CAS: 1032350-13-2), dasatinib (CAS: 302962-49-8), and simvastatin (CAS: 79902-63-9) were synthesized by Proactive Molecular Research with purities of greater than 98-99% as determined by liquid chromatography-mass spectrometry (LC-MS) and nuclear magnetic resonance spectroscopy. ALK-IN-1 (CAS: 1197958-12-5) was obtained from NCATS and Advanced ChemBlocks, and dasatinib-d_8 (CAS: 1132093-70-9) was purchased from Cayman Chemical. For *in vitro* studies, all compounds were dissolved in DMSO as 10mM stock solutions and diluted in medium prior to adding to cells with DMSO concentration kept constant at 0.1%.

Compound screening

HS11 and HS01 Schwann cells, Syn1 and Syn5 arachnoidal cells, and Ben-Men-1 cells were seeded in white 1536-well plates (Corning) at a density of 500 cells/well (5µl) using a Multidrop Combi Reagent dispenser with a small pin cassette (ThermoFisher). The next day, compounds were added and cells treated for 72h. Compounds were tested at doses starting with a stock concentration of 10mM in DMSO (final concentration = 46µM) serially diluted 3-fold with DMSO for a total of 11 compound concentrations. Cell viability was measured using CellTiterGlo (5µl) (Promega), and relative luminescence units (RLUs) were measured with the Viewlux (Perkin Elmer) after 15-min incubation at room temperature. RLUs for each well were normalized to the median RLUs from the DMSO control wells as 100% viability, and median RLUs from

control wells with media only denoted as 0% viability.

Hit selection from dose-response single-agent high-throughput screening (HTS)

Activity of the compounds from the dose response HTS screen was determined based on three parameters (Ferrer et al., 2018): i) % viability at the maximum concentration of compound tested (MAXR); and ii) Curve Response Class (CRC) classification from dose-response HTS, in which normalized data were fitted to a 4-parameter dose response curve using a custom grid-based algorithm to generate a CRC score for each compound dose response. CRC values of -1.1, -1.2, -2.1, -2.2 are considered highest quality hits; CRC values of -1.3, -1.4, -2.3, -2.4 and -3 are inconclusive hits; and a CRC value of 4 are inactive compounds. iii) An Area under the Curve (AUC) was also calculated using the trapezoidal method applied to the dose responses. The AUC is a useful measure since it implicitly incorporates potency and efficacy. Processed dose-response HTS data parameters for each compound screened in each cell line can be found in the supplemental data file or at the doi:10.7303/syn18463554.3..

Compound combination matrix screening

For combination matrix screen, protocols were as described above. Briefly, compounds were pre-plated using an acoustic dispenser ATS-100 (EDC Biosystems). A total of 5 nL of each compound solubilized in DMSO, as well as DMSO control wells, were dispensed with 3-fold dilution for the 6x6 dose response matrices and 2-fold dilutions to generate the 10x10 dose-response matrices. Cell suspension (500 cells/well

in 5 µl) was added directly to the plate immediately after compounds were pre-plated. For cell proliferation assays, cells were incubated with the compounds for 72 h, and 5 µl of CellTiterGlo reagent added; for the apoptosis assay, cells were incubated with the compounds for 20 h, and 5 µl of CaspaseGlo reagent added. RLUs were measured with the Viewlux after 15-min incubation at room temperature. Processed data for each 6x6 and 10x10 combination in each cell line can be found in the supplemental data file or at the doi:10.7303/syn18463554.3.

In vitro confirmation of compound efficacy and synergism

Meningioma-relevant cells, including Syn1, Syn5, Ben-Men-1, and primary cultures of *NF2*-null meningioma cells, were seeded in 384-well plates as previously described (Synodos for NF2 Consortium, 2018) and treated the next day with serial dilutions of brigatinib, MK-2206, or the combination of MK-2206 with brigatinib for 72 h. For single drug treatment, dose-response curves (DRCs) were generated using 9 dilution points (3-fold serial dilution) of drug ranging from 1.5nM to 10µM. Cells were treated with 0.1% DMSO as the vehicle control. Combination drug treatment was performed in 384-well plates as previously described (Angus et al., 2018) using a 10x10 dose-matrix screening approach carried out in duplicate, and drug treatment concentrations and time were the same as single drug treatments above. Cell viability was measured using CellTiter-Glo (Promega).

For the schwannoma-relevant cell panel, HS01, HS11, and MS02 were seeded in 384-well plates overnight and incubated with various dilutions of ALK-IN-1, brigatinib, dasatinib, or the combination of dasatinib with ALK-IN-1 or brigatinib in the 10x10 matrix

format. Cell viability was measured after 60 or 72 h of treatment for mouse MS02 or human HS01 and HS11 cells, respectively, using CellTiter-Fluor (Promega). A similar study to validate the efficacy of dasatinib, simvastatin, and their combination was also conducted.

For both cell types, dose-response measurements were normalized to vehicle controls, and DRCs and IC_{50}/EC_{50} were generated using either GraphPad Prism 7 or Combenefit software. Drug combination synergy was analyzed using the Loewe additivity, Bliss independence, and highest single agent (HSA) reference models as previously described using the Combenefit software (Di Veroli et al., 2016).

Kinome profiling and transcriptome analysis

MIB/MS was conducted to quantitate the dynamic behavior of the expressed kinome in response to drug treatment (Duncan et al., 2012; Stuhlmiller et al., 2015). Briefly, lysates of cells or flash-frozen animal tissues treated with the indicated concentrations of each drug or drug combination for various times were prepared, normalized for total protein input, and loaded onto the column containing MIBs. Kinase-bound inhibitor beads were stringently washed, followed by protein purification, overnight trypsin digestion, ethyl acetate extraction, and peptide clean-up with C-18 spin column (Thermo). Peptide suspensions were separated using an EASY nLC-1000 System with an Easy-Spray C-18 column (ThermoFisher). Raw files were searched using MaxQuant-MaxLFQ (Cox et al., 2014) and mouse or human Uniprot database. LFQ intensities were log_2 transformed and missing values were imputed using Perseus for comparison. Log_2 LFQ intensities were used for Student's t-tests (with BH correction)

and principal components analysis in Perseus or plotted as $\log_2$ difference. The entire kinome data can be found in the supplemental data file or at the doi:10.7303/syn18463554.3.

For transcriptome analysis, RNA was isolated from meningioma and schwannoma-relevant human cell lines treated in triplicate with single and combination drugs and used to prepare RNA libraries for RNAseq using Illumina HiSeq2000 and 2500 platforms as previously described (Synodos for NF2 Consortium, 2018). Sequence reads were aligned to human reference genome Ensembl GRCh37 (v. 75) using STAR (v. 2.5.2a) (Dobin et al., 2013) with parameters "-outSAMunmapped Within -outFilterMultimapNmax 1 -outFilterMismatchNoverLmax 0.1 -alignIntronMin 21 -alignIntronMax 0 -alignEndsType Local -quantMode GeneCounts -twopassMode Basic". In this step, STAR also generated gene level counts for all libraries. Quality checking of alignments was assessed by a custom script utilizing Picard Tools (http://broadinstitute.github.io/picard/), RNASeQC (DeLuca et al., 2012), RSeQc (Wang et al., 2012), and samTools (Li et al., 2009). These analyses identified two samples, Syn1_1 and Syn1_11 (Brigatinib), as outlier samples as they failed to pass the following thresholds: exonic rate ≥ 0.8 and intergenic rate ≤ 0.1, and thus they were excluded from further analysis. Differentially expressed genes in pairwise comparisons were identified by edgeR's quasi-likelihood F test (v. 3.18.1) (Robinson et al., 2010), which was run at the R platform (v. 3.4) on genes with greater than 10 counts across replicates per condition in pairwise comparisons. Gene ontology (GO) enrichment analysis for each comparison was performed on differentially expressed genes at

Bonferroni adjusted p values < 0.05, where all the analyzed genes in a given comparison were used as a background list, using DAVID (v. 6.8) (Huang da et al., 2009). GO terms with Benjamini Hochberd adjusted p value < 0.05 were reported as significantly enriched for a given gene list.

Phospho-RTK array

Ben-Men-1 cells were plated in Dulbecco modified Eagle medium (DMEM) containing 10% fetal bovine serum (FBS). The following day, cells were growth-arrested in medium without serum for two days. Serum-starved cells were stimulated with 20% FBS-containing medium in the presence of 1x IC_{50} concentration of brigatinib or DMSO vehicle. Also, cells grown in 10% FBS were treated with 1x IC_{50} concentration of brigatinib or DMSO in fresh medium containing 10% FBS. After treatment for 2 or 24 hours, the dishes were immediately placed on ice, rinsed once with cold PBS, lysed in 500 µL of 1x Cell Lysis buffer (#9803; Cell Signaling) supplemented with 1 mM freshly added PMSF. The lysates were sonicated for 12 seconds using a Model 705 Sonic Dismembrator (Fisher Scientific) with a probe and amplitude setting at “1”, followed by centrifugation for 10 minutes at 14,000 x g. The total protein content of clear lysates was assessed by microBCA assay (#23235; Thermo). The PathScan RTK Antibody Array (#7949; Cell Signaling) was prepared according to manufacturer’s instructions. All incubations and rinses were performed on a laboratory rocker. Briefly, 150 µg of total protein was added to each chamber of array. The arrays were incubated overnight at 4 °C and then rinsed four times in 1x Array Wash Buffer for 5 minutes at room temperature. Detection Antibody Cocktail (150 µL) was added to each array, and the

arrays were incubated for 1 hour at room temperature. Following rinsing four times with Array Wash Buffer, DyLight-680-linked streptavidin (150 µL) was added to each array for 30 minutes at room temperature in a light-protected box. Unbound streptavidin was removed by four rinses in Array Wash Buffer, followed by 10 seconds in deionized water. The arrays were air-dried completely at room temperature in the dark, and the fluorescent signal was detected by scanning in the 700-nm channel on an Odyssey CLx near-infrared scanner (LI-COR) using a resolution of 21 µm and medium quality image acquisition. Quantitation was performed using Image Studio software (LI-COR). The remaining protein lysates from the above treated cells were analyzed by Western blotting to validate array findings. Phospho-RTK array measurement data can be found at the doi:10.7303/syn18463554.3.

Western blot analysis

In addition to the protein lysates prepared for phospho-RTK arrays, Ben-Men-1 cells were growth-arrested in medium without serum for two days and then pretreated for 2 hours with 1.5 µM of brigatinib or DMSO vehicle in serum-free DMEM, followed by incubation for 10 minutes with 50 ng/mL each of the following ligands: epidermal growth factor (EGF) (#PHG0311; ThermoFisher), heregulin (HRG) (#100-03; PeproTech), or insulin-like growth factor 1 (IGF1) (#1150-01; Gold Biotechnology). Following ligand stimulation, cells were placed on ice, lysed in cold RIPA buffer containing protease/phosphatase inhibitor cocktail (#78440; Sigma-Aldrich), and sonicated. Also, lysates were prepared from primary human meningioma and schwannoma cells (including NF2 and sporadic tumors), Ben-Men-1 cells, normal

human meningeal and Schwann cells (ScienCell), as well as human SK-N-SH neuroblastoma cells. The protein concentration of each lysate was determined as described above, and equal amounts of protein were resolved on SDS-polyacrylamide gels, followed by electroblotting to PVDL-FL membranes (Burns et al., 2013). The PVDF-FL blots were blocked in 5% milk/TBS and probed with the following antibodies: anti-ALK (#3633), Fer (#4268), FAK (#3285), p-EphA2(Ser^{897}) (#6347), EphA2 (#6997), p-ErbB3(Tyr^{1289}) (#4791), p-AKT(Ser^{473}) (#4060), AKT (#9272), p-ERK1/2(Thr^{202}/Tyr^{204}) (#4370), ERK1/2 (#4695), p-S6(Ser$^{235/236}$) (#4858), S6 (#2270), p-EGFR(Tyr^{1173}) (#4407), EGFR (#4267), p-IGF1R(Tyr$^{1135/1136}$) (#3024), IGF1R (#9750) [all from Cell Signaling]; p-Fer(Tyr^{402}) (#ab79573; Abcam), p-FAK(Tyr^{397}) (#700255; ThermoFisher), ErbB3 (#sc-285; Santa Cruz Biotechnology), and GAPDH (#5174; Cell Signaling or #sc-32233; Santa Cruz Biotechnology). Bound primary antibodies were labelled with goat anti-rabbit or anti-mouse secondary antibodies that were conjugated with the fluorophore IRDye-800CW or IRDye-680RD (LI-COR). Fluorescent signals were detected by scanning in the 700- and 800-nm fluorescent channels of an Odyssey CLx imager, using a resolution of 84 μm and medium quality image acquisition.

Immunohistochemistry

The heads of drug- or vehicle-treated mice bearing meningiomas were decalcified, followed by paraffin embedding as described previously (Burns et al., 2013). Serial 5-μm sections were cut and stained with hematoxylin and eosin to localize the tumor. Then, the sections containing tumors were processed for immunohistochemical staining using antibodies against Ki67 (RM-9106-S, Neomarkers), phospho-S6 (p-S6[Ser$^{235/236}$];

#4858, Cell Signaling), p-ERK1/2(Thr^{202}/Tyr^{204}) (#4370, Cell Signaling), and cleaved caspase 3 (CC3; #9664, Cell Signaling). Negative control slides were treated with the same procedures but without the primary antibody.

Drug formulation and MTD determination

For animal dosing, MK-2206 was dissolved in 30% Captisol® and brigatinib was formulated in 90% polyethylene glycol 300 and 10% 1-methyl-2-pyrrolidinone. The MTD was determined as described (Plowman et al., 1999). Briefly, eight-to-12 week-old NSG (NOD-SCID gamma or *NOD.Cg-Prkdc^{scid} Il2rg^{tmlWjl}/SzJ*) mice (The Jackson Laboratory) were treated with various doses of MK-2206 every other day or brigatinib every day by oral gavage for two weeks (three mice per dose). The starting doses for MK-2206 and brigatinib were based on those used previously (Hirai et al., 2010; Siaw et al., 2016). The MTD was determined to be 50mg/kg/day for brigatinib and 120mg/kg every other day for MK-2206 by oral gavage in NSG mice. Also, these mice appeared to tolerate the combination of 50mg/kg of Brigatinib daily and 120mg/kg of MK-2206 every other day.

Pharmacokinetic (PK) analysis

For PK analysis of brigatinib and MK-2206, mice were fed a single oral dose of brigatinib, MK-2206, or their combination at the MTD. Prior to and at various times after dosing (n=3 per time point), whole blood was collected from the facial vein into EDTA-containing Microtainer® (Becton Dickinson, Franklin Lakes, NJ). Plasma samples were obtained by centrifugation. Immediately after blood sampling, mice were euthanized for brain harvesting. Both the plasma and brain samples were frozen at -80 ^{o}C until

analysis of compound concentrations using ultra-high pressure liquid chromatography tandem-mass spectrometry (UHPLC-MS/MS). For calibration in plasma matrix, the brigatinib analogue ALK-IN-1 (CAS: 1197958-12-5; Advanced Chemblocks) and dasatinib-d_8 (CAS: 1132093-70-9; Cayman Chemical) were used as the internal standard (I.S.) for brigatinib and MK-2206, respectively. A serially-diluted calibration solutions containing both brigatinib and MK-2206 at the concentrations of 50, 100, 200, 500, 1,000, 2,000, 5,000, and 10,000 ng/ml in methanol and a mixed internal standard solution comprised of the brigatinib analogue and dasatinib-d_8 at 500 ng/ml each in methanol were freshly prepared on the day of analysis. Forty five-µl blank plasma were mixed with 5-µl calibration solution or 5-µl internal standard solution to yield final concentrations of calibration sample were 0, 5, 10, 20, 50, 100, 200, 500, and 1,000 ng/mL for both brigatinib and MK 2206 and 50 ng/mL for both internal standards. Also, a set of quality control samples were prepared in a similar manner at 10, 100, 600, and 1,000 ng/ml. Each mixture was extracted with 500-µl cold acetonitrile and centrifuged at 23,000 x g for 20 min to separate the organic layers. The supernatant was collected and dried under a gentile nitrogen flow. Then the residues were reconstituted in 50-µl 70% methanol. Following another centrifugation at 23,000 x g for 20 min, 3 µl of each sample was injected into the UHPLC-MS/MS system. For measuring plasma concentrations of brigatinib in dosed mice, 45-µl plasma and 5-µl brigatinib internal standard solution were mixed and analyzed as above. For measuring MK-2206 concentrations, 10-µl plasma was mixed with 35-µl blank plasma and 5-µl dasatinib-d_8 internal standard.

For calibration in brain matrix, the whole brain tissue from an untreated mouse was placed in pure water (5-ml H_2O per gram of brain) and homogenized using a

BeadBug™ Microtube Homogenizer (Benchmark Scientific). Fifty-µl brain homogenate was mixed with 5-µl calibration solution containing brigatinib and MK2206 each at the concentrations of 20, 50, 100, 200, 500, 1,000, 2,000, and 5,000 ng/ml in methanol or a mixed internal standard solution comprised of the brigatinib analogue and dasatinib-d_8 at 100 ng/ml each in methanol and analyzed as described above. The final concentrations of calibration samples were 0, 2, 5, 10, 20, 50, 100, 200, and 500 ng/ml for both brigatinib and MK 2206, and 10 ng/ml for both internal standards. The quality controls (QCs) samples were prepared in a similar manner at 2, 20, 200 and 500 ng/ml. For brain sample detection, each brain tissue was homogenized in water and 45-µl brain homogenate was mixed with 5-µl internal standard solution for analysis as described above.

Separation was carried out using an ACQUITY UPLC CSH C18 column (1.7 µm particle size, 2.1 mm x 100 mm; Waters) with column temperature at 40°C. The isocratic mobile phase (A: 5 mM ammonium formate/0.1% formic acid in water and B: 0.1% formic acid in acetonitrile) was delivered to the column at a flow rate of 0.3 ml/min and the autosampler temperature set at 8°C. The mass spectrometer was operated using heated electrospray ionization (HESI) with a capillary voltage of +3.5 kV. Sheath gas was delivered at 35 arb and auxiliary gas was 10 arb. The ion transfer tube temperature of 325°C and the vaporize temperature of 275°C were recorded. The following selected reaction monitoring (SRM) parameters were used in tandem MS.

Compound	Precursor (m/z)	Product (m/z)	Collision Energy (V)	RF Lens (V)
MK-2206	408.2	380.2	22	87
Dasatinib-d8	496.3	406.2	30	137

(MK-2206 I.S.)				
ALK-IN-1 (Brigatinib I.S.)	529.2	484.2	27	110
Brigatinib	584.3	484.2	30	121

Mass spectrometer was tuned daily to its optimum sensitivity and the precision and accuracy of the assay were established by analyzing each quality control (QC) solution. Multiple replicates of each QC were measured in separate analytical runs within one day. The precision calculated as the coefficient of variation (CV, %) within a single run (intra-day) and the accuracy as the percentile difference between nominal and measured concentration were determined and the assay was found to be reproducible with adequate accuracy, precision, and specificity.

Quantifiable orthotopic meningioma model

The Institutional Animal Care and Use Committee at Nationwide Children's Hospital approved this animal study. Following deep anesthesia, each eight-to-12 week-old NSG mouse was injected with approximately 10^6 luciferase-expressing Ben-Men-1-LucB cells into the skull base (Burns et al., 2013). The coordinates used were 1.5 mm anterior and 1.5 mm to the right of the bregma and 4.5 mm below the skull surface. The injected mice were monitored for tumor growth by bioluminescence imaging (BLI) every two weeks using a Xenogen IVIS® Spectrum imaging system (Perkin Elmer, Bradford, CT). Mice with successful tumor engraftment were randomized into four groups (n = 10 each) and treated with MK-2206, brigatinib, MK-2206/brigatinib combination, or a mixture of

the corresponding vehicles in which MK-2206 and brigatinib were formulated (1:1 ratio) by oral gavage. BLI was performed biweekly to assess the effects on tumor growth. Previously we showed that the BL signal detected in luciferase-expressing tumor xenografts correlates with the tumor size (Burns et al., 2013). The luminescence detected in each mouse was normalized to its pretreatment signal and expressed as the mean normalized luminescence ± standard deviation for each treatment group. After 14 weeks of treatment, we stopped treating a cage of mice (n = 4) that had received brigatinib or the MK-2206/brigatinib combination and monitored possible tumor regrowth for 12 more weeks. Then, we retreated these mice to examine the effects of retreatment. Mouse tumor luminescence data can be found in the supplemental data file or at the doi:10.7303/syn18463554.3.

Schwannoma model and hearing tests

The animal study using *Postn-Cre*;*Nf2*$^{flox/flox}$ mice was carried out in accordance with, and approval of, the Institutional Animal Care and Use Committee of Indiana University Medical School. The methodologies of tumor and hearing assessment on *Postn-Cre*;*Nf2*$^{flox/flox}$ mice with or without drug treatment were conducted as previously described (Gehlhausen et al., 2015).

Fig. 1

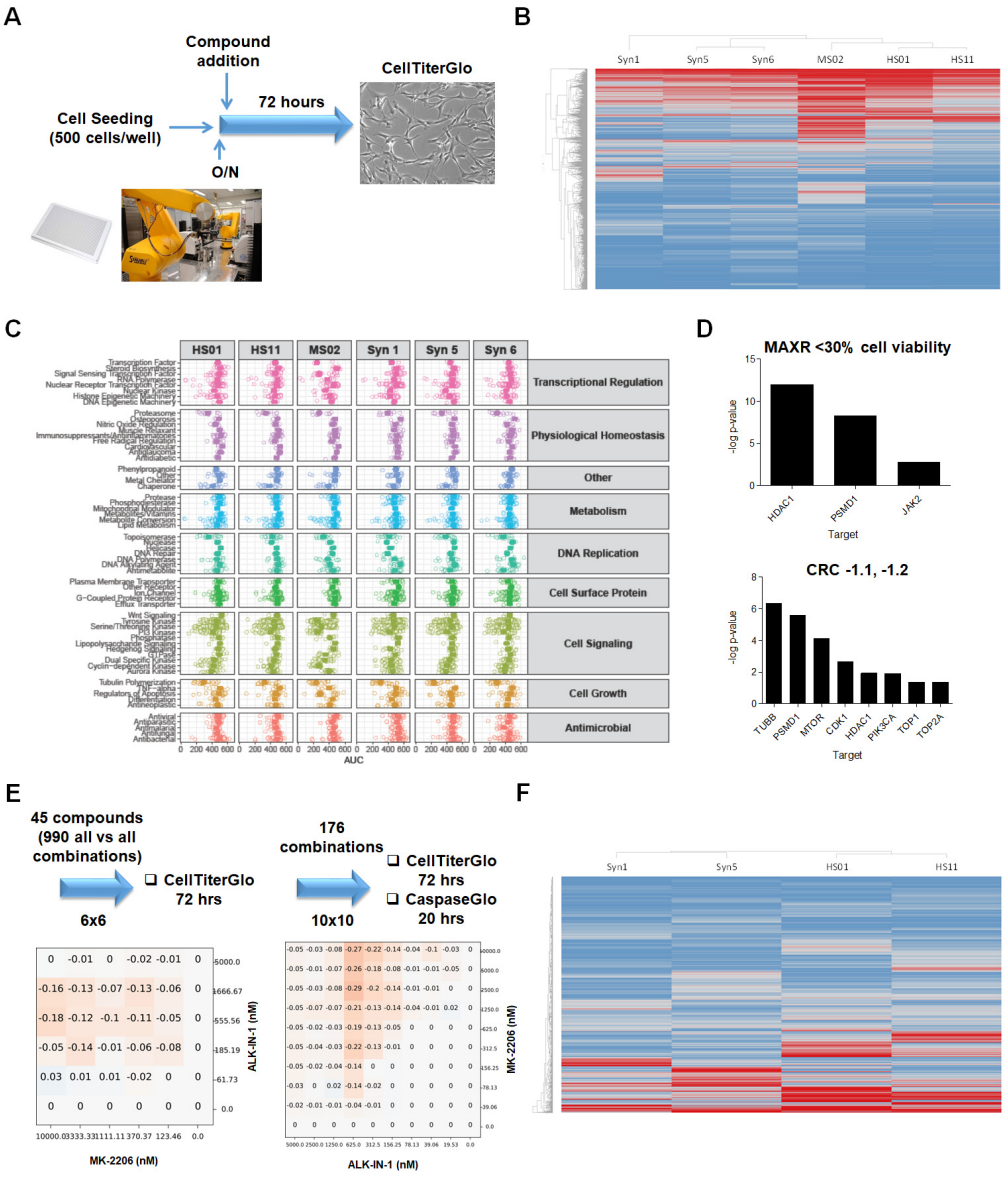
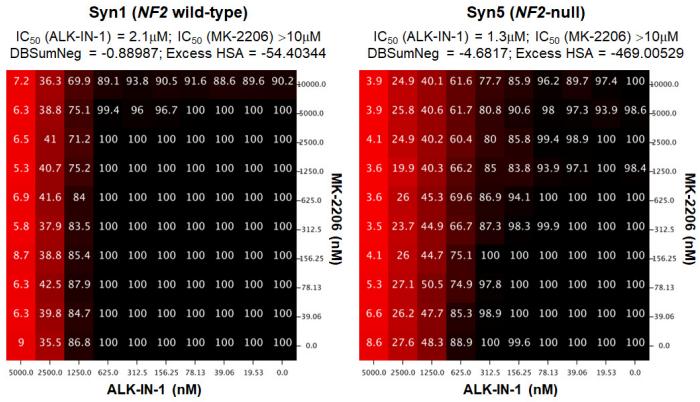

A
Compound addition
72 hours
CellTiterGlo
Cell Seeding (500 cells/well)
O/N
B
Syn1
Syn5
Syn6
MS02
HS01
HS11
C
HS01
HS11
MS02
Syn 1
Syn 5
Syn 6
Transcriptional Regulation
Physiological Homeostasis
Other
Metabolism
DNA Replication
Cell Surface Protein
Cell Signaling
Cell Growth
Antimicrobial
AUC
D
MAXR <30% cell viability
-log p-value
HDAC1
PSMD1
JAK2
Target
CRC -1.1, -1.2
TUBB
PSMD1
MTOR
CDK1
HDAC1
PIK3CA
TOP1
TOP2A
E
45 compounds (990 all vs all combinations)
CellTiterGlo 72 hrs
6x6
176 combinations
CellTiterGlo 72 hrs
CaspaseGlo 20 hrs
10x10
MK-2206 (nM)
ALK-IN-1 (nM)
F
Syn1
Syn5
HS01
HS11

Fig. 2

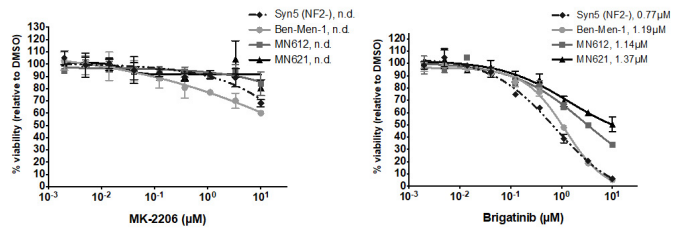
A

Ranking	Drug combination	Targets	DBSumNeg in Syn1 ($NF2^+$) cells	DBSumNeg in Syn5 ($NF2^-$) cells
1	Cabozantinib/Danusertib	VEGFR2/AURKa,b,c	-4.55567	-9.56327
2	Dasatinib/GSK2126458	BCR-ABL/PI3K	-0.3212	-4.90171
3	MK-2206/ALK-IN-1	AKT/ALK	-0.88987	-4.68107

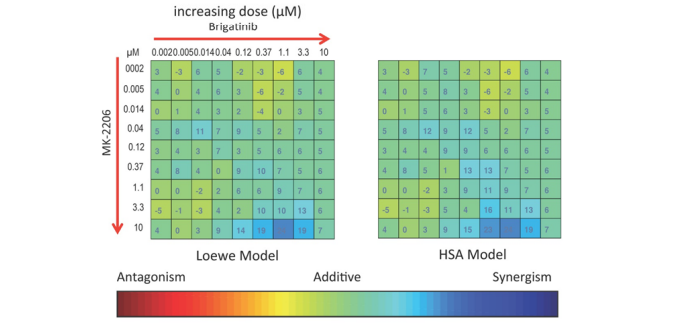
B



C



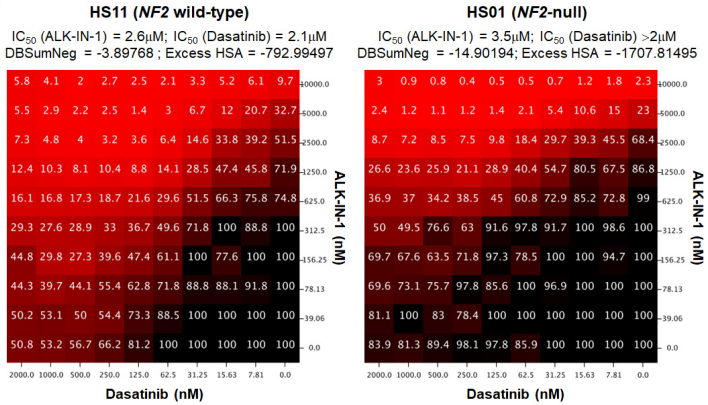
D



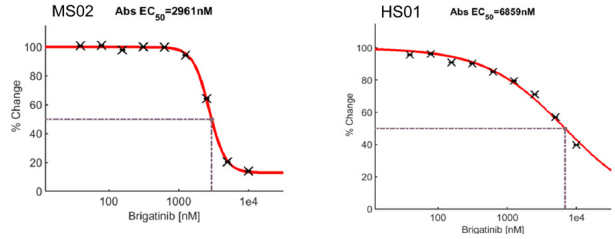
E

Ranking	Drug combination	Targets	DBSumNeg in HS11 ($NF2^+$) cells	DBSumNeg in HS01 ($NF2^-$) cells
1	ALK-IN-1/Dasatinib	ALK/BCR-ABL	-3.89768	-14.90194
2	TAE226/Dasatinib	FAK/BCR-ABL	-3.16579	-8.93415
3	Dasatinib/Simvastatin	BCR-ABL/HMG CoA Reductase	-2.79717	-7.11969

F



G



H

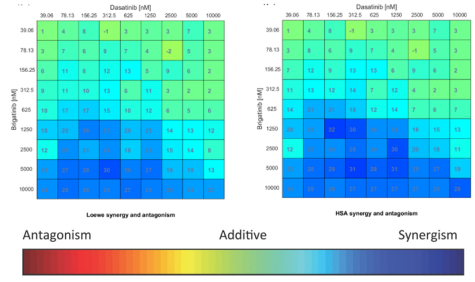


Fig. 3

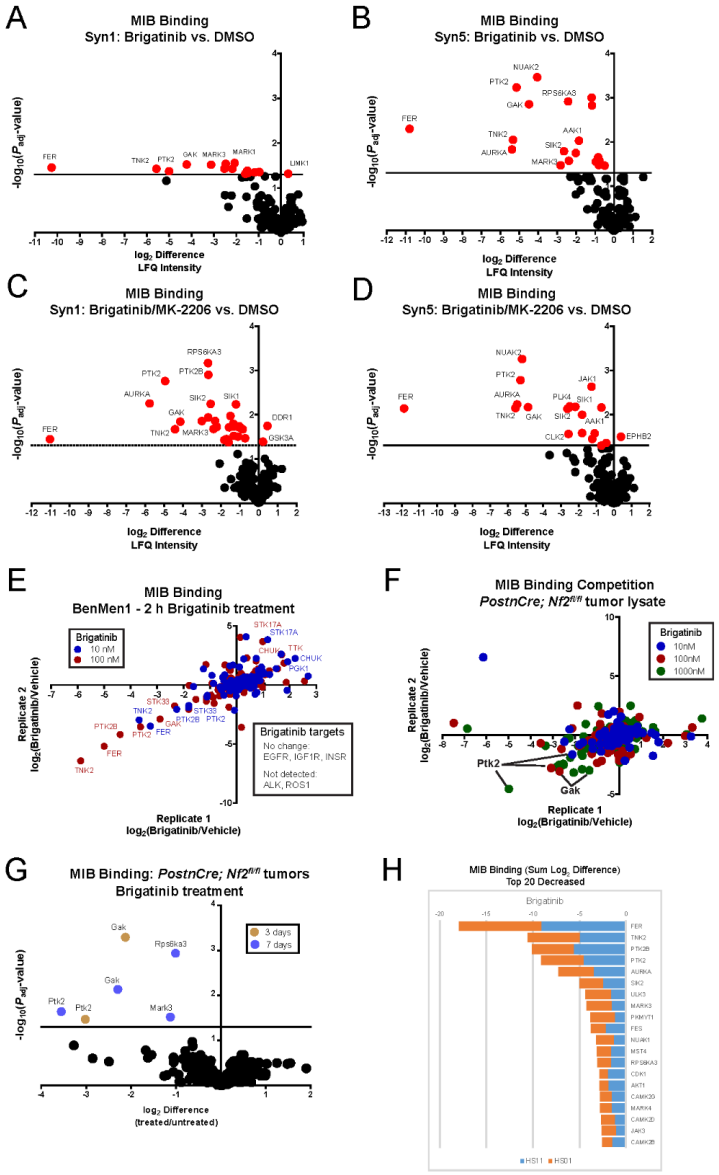

A
MIB Binding
Syn1: Brigatinib vs. DMSO
B
MIB Binding
Syn5: Brigatinib vs. DMSO
C
MIB Binding
Syn1: Brigatinib/MK-2206 vs. DMSO
D
MIB Binding
Syn5: Brigatinib/MK-2206 vs. DMSO
E
MIB Binding
BenMen1 - 2 h Brigatinib treatment
Brigatinib
10 nM
100 nM
Brigatinib targets
No change:
EGFR, IGF1R, INSR
Not detected:
ALK, ROS1
F
MIB Binding Competition
PostnCre; Nf2fl/fl tumor lysate
Brigatinib
10nM
100nM
1000nM
G
MIB Binding: PostnCre; Nf2fl/fl tumors
Brigatinib treatment
3 days
7 days
H
MIB Binding (Sum Log2 Difference)
Top 20 Decreased
Brigatinib

Fig. 4

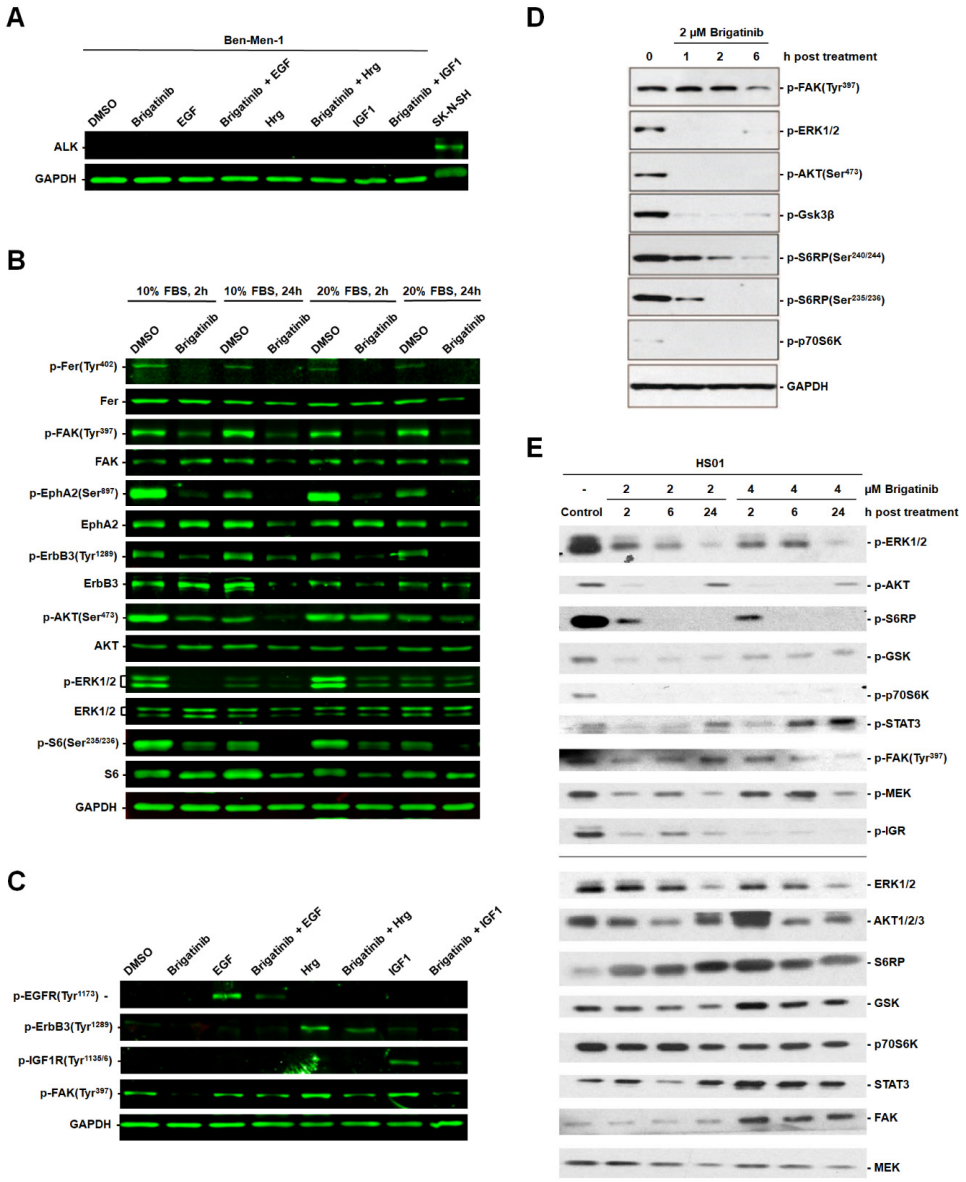

A
Ben-Men-1
DMSO
Brigatinib
EGF
Brigatinib + EGF
Hrg
Brigatinib + Hrg
IGF1
Brigatinib + IGF1
SK-N-SH
ALK
GAPDH
B
10% FBS, 2h
10% FBS, 24h
20% FBS, 2h
20% FBS, 24h
DMSO
Brigatinib
p-Fer(Tyr402)
Fer
p-FAK(Tyr397)
FAK
p-EphA2(Ser897)
EphA2
p-ErbB3(Tyr1289)
ErbB3
p-AKT(Ser473)
AKT
p-ERK1/2
ERK1/2
p-S6(Ser235/236)
S6
GAPDH
C
DMSO
Brigatinib
EGF
Brigatinib + EGF
Hrg
Brigatinib + Hrg
IGF1
Brigatinib + IGF1
p-EGFR(Tyr1173)
p-ErbB3(Tyr1289)
p-IGF1R(Tyr1135/6)
p-FAK(Tyr397)
GAPDH
D
2 μM Brigatinib
0
1
2
6
h post treatment
p-FAK(Tyr397)
p-ERK1/2
p-AKT(Ser473)
p-Gsk3β
p-S6RP(Ser240/244)
p-S6RP(Ser235/236)
p-p70S6K
GAPDH
E
HS01
-
2
2
2
4
4
4
μM Brigatinib
Control
2
6
24
2
6
24
h post treatment
p-ERK1/2
p-AKT
p-S6RP
p-GSK
p-p70S6K
p-STAT3
p-FAK(Tyr397)
p-MEK
p-IGR
ERK1/2
AKT1/2/3
S6RP
GSK
p70S6K
STAT3
FAK
MEK

Fig. 5

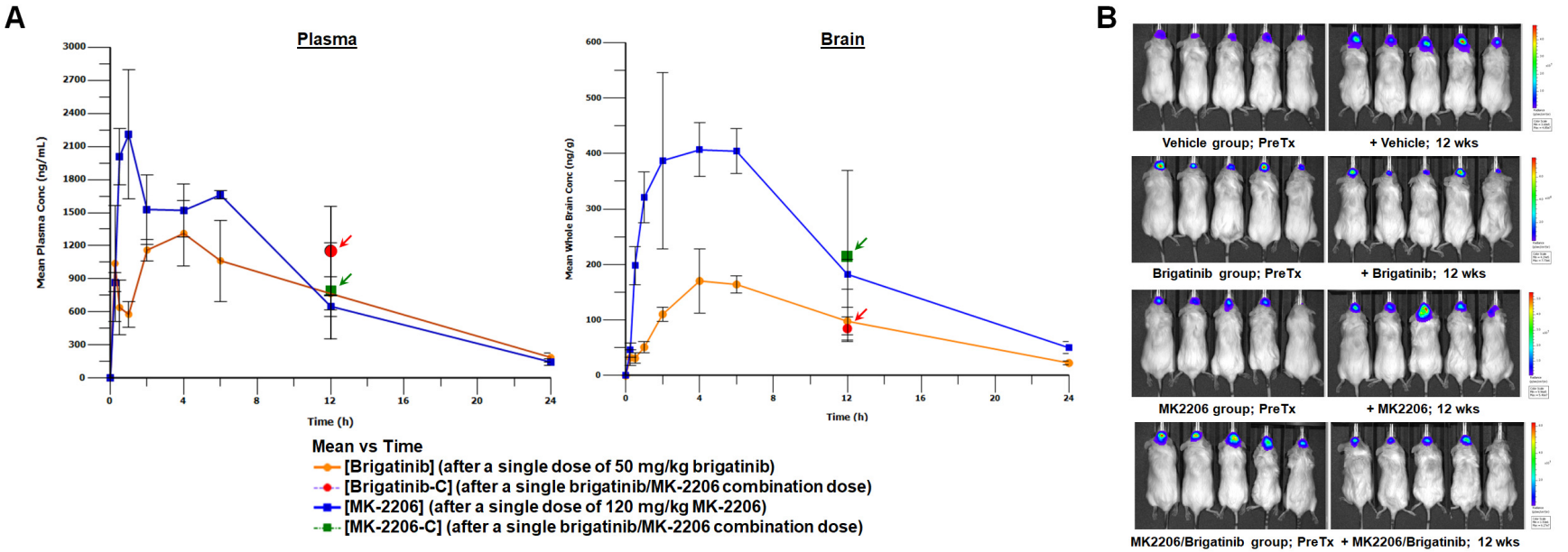
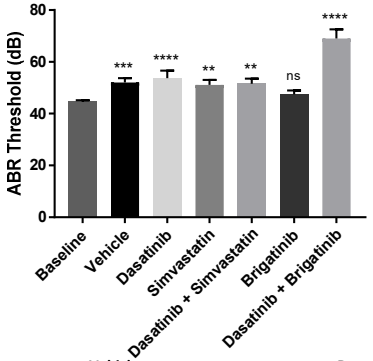

A
Plasma
Brain
Mean Plasma Conc (ng/mL)
Mean Whole Brain Conc (ng/g)
Time (h)
Mean vs Time
[Brigatinib] (after a single dose of 50 mg/kg brigatinib)
[Brigatinib-C] (after a single brigatinib/MK-2206 combination dose)
[MK-2206] (after a single dose of 120 mg/kg MK-2206)
[MK-2206-C] (after a single brigatinib/MK-2206 combination dose)
B
Vehicle group; PreTx
+ Vehicle; 12 wks
Brigatinib group; PreTx
+ Brigatinib; 12 wks
MK2206 group; PreTx
+ MK2206; 12 wks
MK2206/Brigatinib group; PreTx
+ MK2206/Brigatinib; 12 wks
C
Vehicle
MK-2206
Brigatinib
MK-2206+Brigatinib
Normalized luminescence (x100%)
Treatment (weeks)
D
Brigatinib
MK2206+Brigatinib
Vehicle
+ drugs
No drugs
+ Treatment
No treatment
+ Treatment
Normalized luminescence (x100%)
Treatment schedule (weeks)
E
Ki67
p-S6
p-ERKs
CC3
+ Vehicle
+ MK-2206
+ Brigatinib
+ MK-2206/Brigatinib

Fig. 6

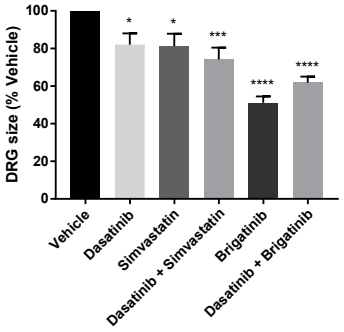
A

Compound	Dosage (mg/kg)	C_{max} (ng/mL)	t_{max} (hours)	$AUC_{0-\infty}$ ($ng*mL^{-1}*hr$)	$t_{½}$ (hours)	Cl/F (L/hr)	Vd_{ss}/F (L)
Brigatinib (alone)	50	2819	4	54907	8.8	0.019	0.26
Brigatinib (+Dasatinib)	15	818	1	9529	6.3	0.034	0.32
Dasatinib (alone)	20	115	1	537	0.94	0.82	2.32
Dasatinib (+Brigatinib)	20	507	1	2406	4.3	0.18	1.09

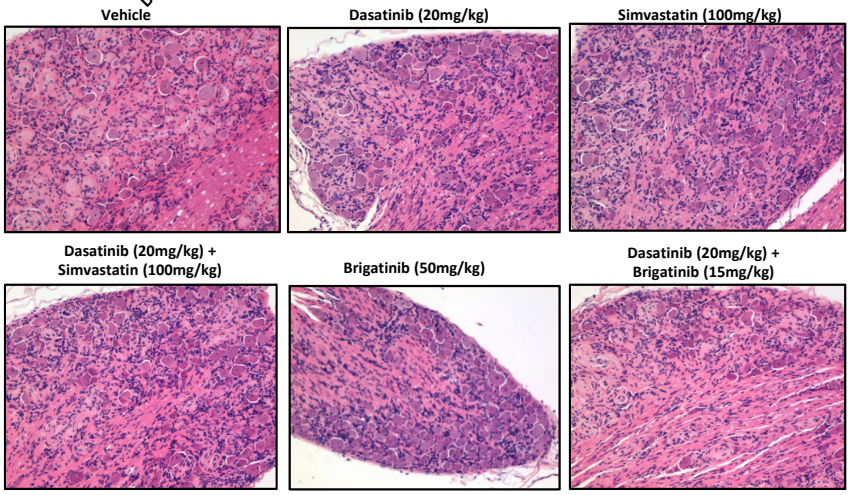
B



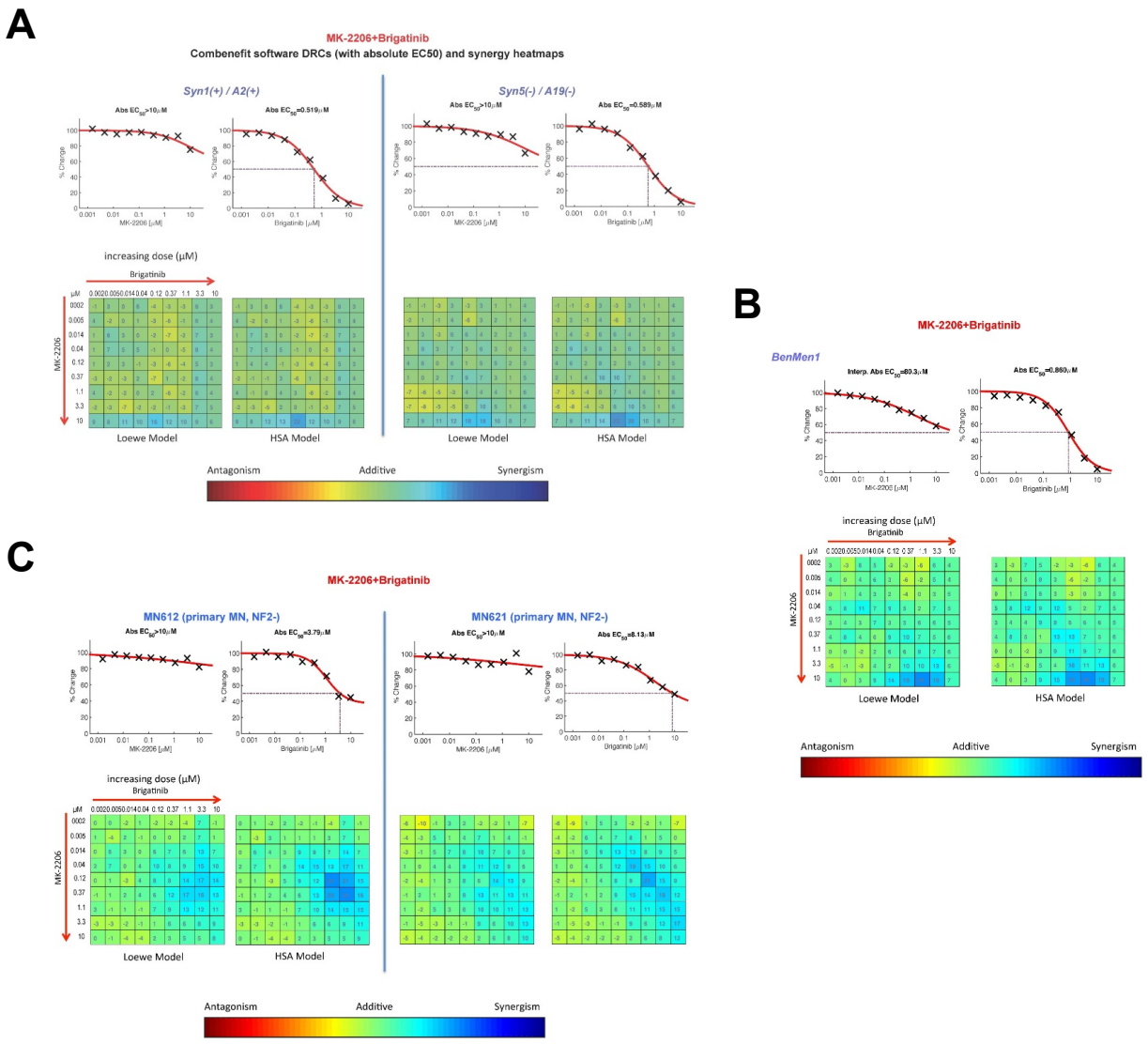
C



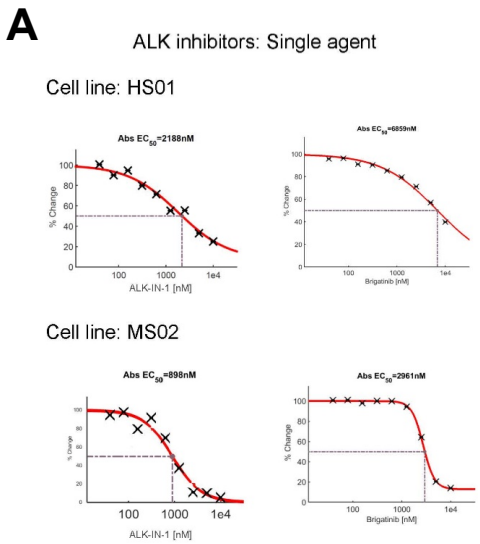
D

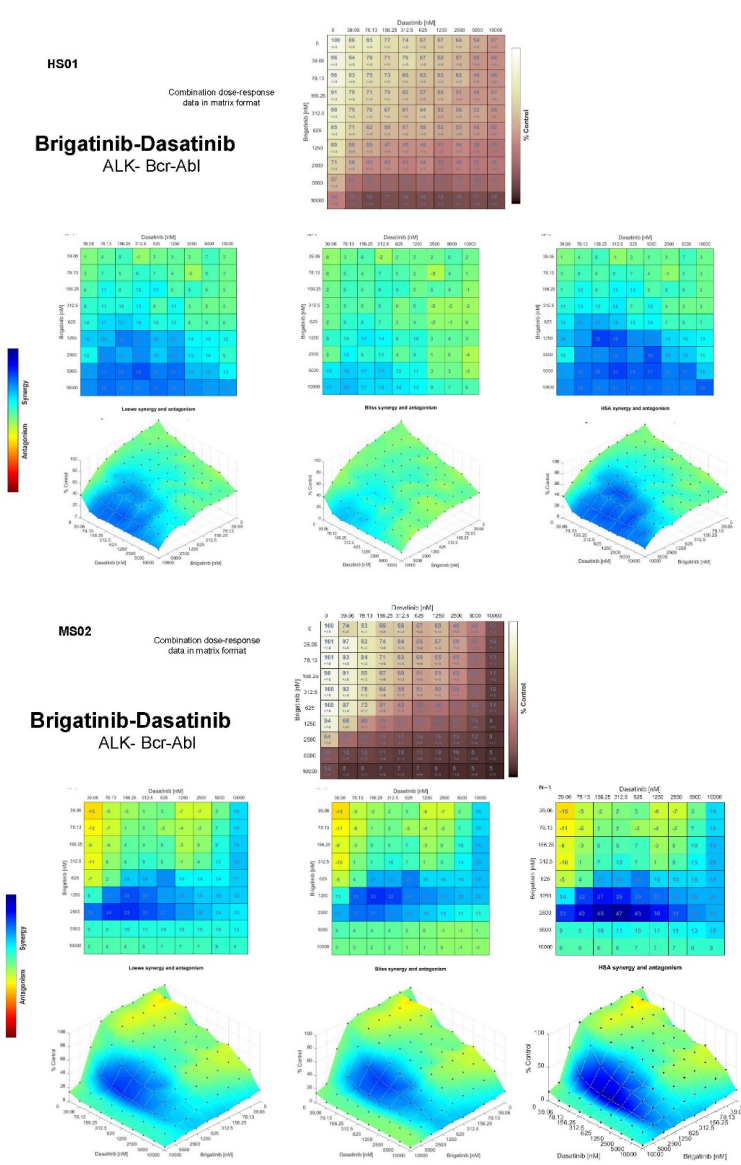


Supplementary
Figure S1

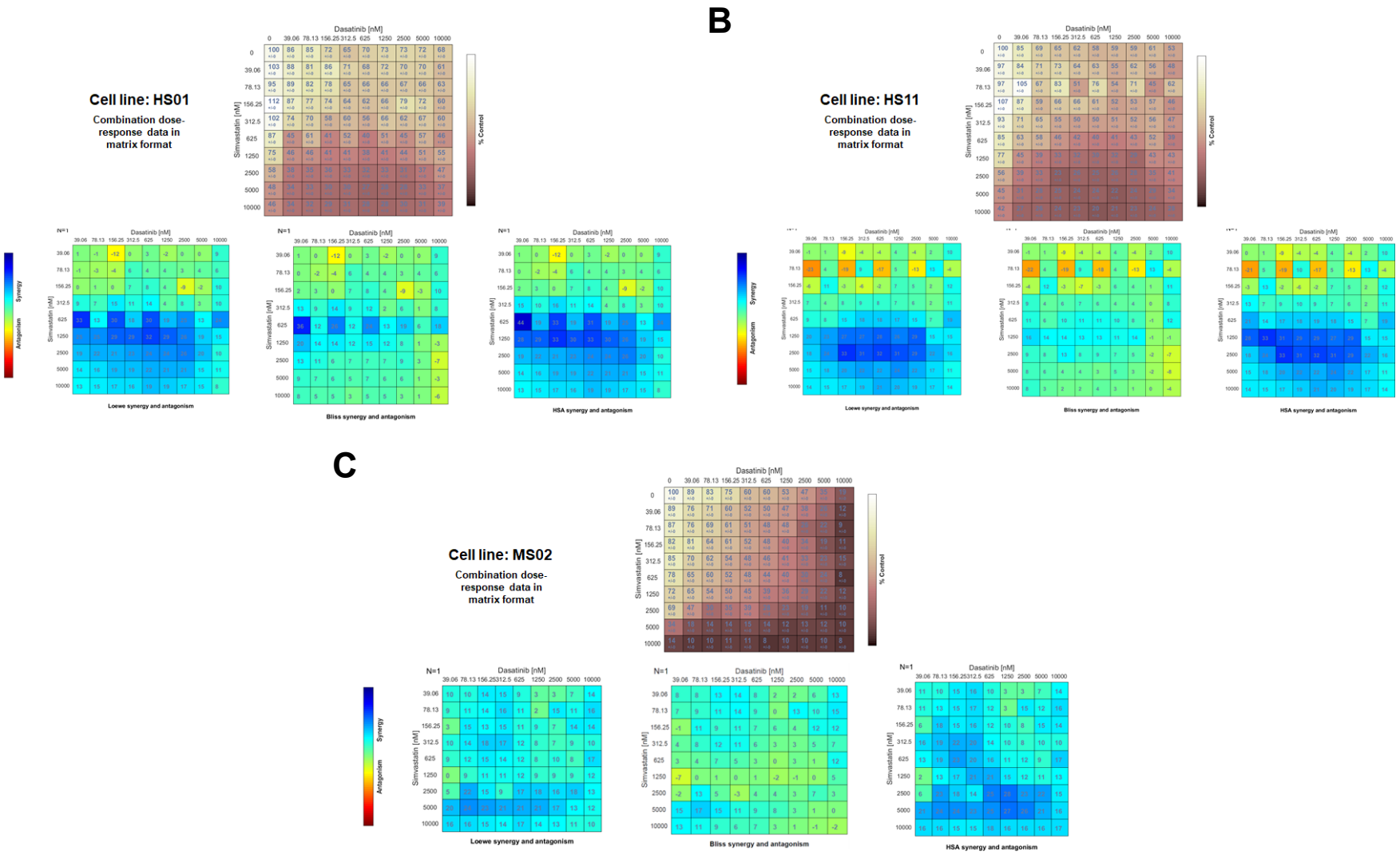


Supplementary
Figure S2





Supplementary Figure S3



Supplementary Figure S4

A

Number of Differentially Expressed Genes (DEG)

	Syn5	Syn1	Shared	Discrepant
Brigatinib				
Up	1281	242	180	0
Down	1324	318	276	0
MK-2206				
Up	0	0	0	0
Down	0	0	0	0
Brigatinib + MK-2206				
Up	1091	337	226	0
Down	1080	493	399	0

B

DEG in Untreated Syn5 vs Syn1	**DEG in Syn5+Brigatinib vs Syn5 Untreated**	
	UP (1281)	***DOWN (1324)***
UP (1034)	5	327
DOWN (1424)	653	3

DEG in Untreated Syn5 vs Syn1	**DEG in Syn5+Brigatinib +MK-2206 vs Syn5 Untreated**	
	UP (1091)	***DOWN (1080)***
UP (1034)	3	262
DOWN (1424)	567	0

C

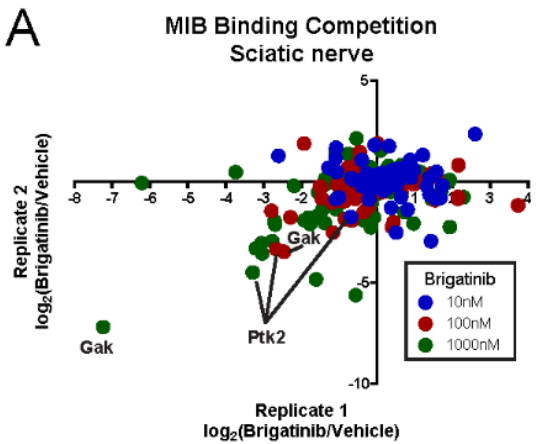
Number of Differentially Expressed Genes (DEG)

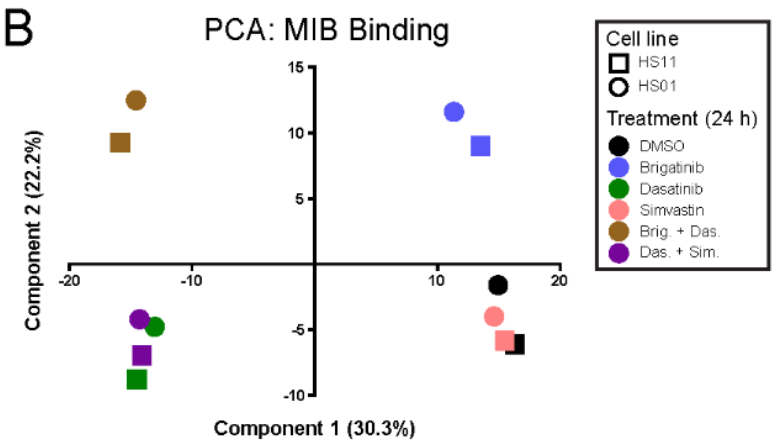
	HS01	HS11	Shared	Discrepant
Brigatinib				
Up	0	0	0	0
Down	0	1	0	0
Dasatinib				
Up	18	19	8	0
Down	7	21	2	0
Brigatinib + Dasatinib				
Up	731	451	324	0
Down	666	581	355	0
Simvastatin				
Up	35	16	12	0
Down	7	6	4	0
Dasatinib + Simvastatin				
Up	171	102	72	0
Down	174	283	108	0

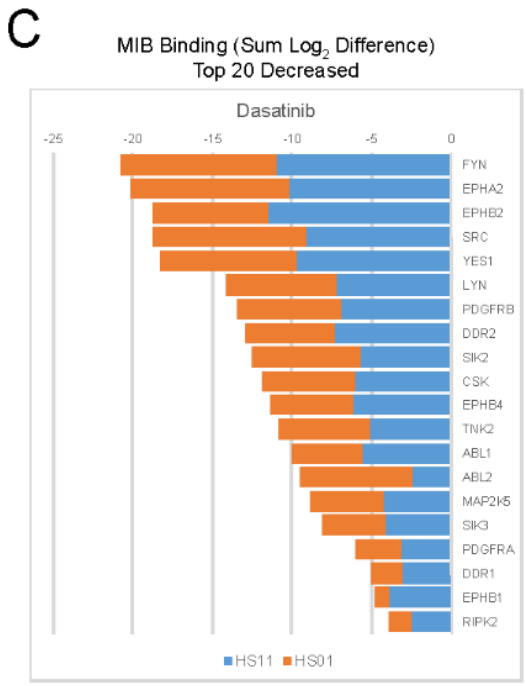
D

DEG in Untreated HS01 vs HS11	**DEG in HS01+Brigatinib +Dasatinib vs HS01 Untreated**	
	UP (731)	***DOWN (666)***
UP (40)	11	0
DOWN (15)	0	1

Supplementary Figure S5

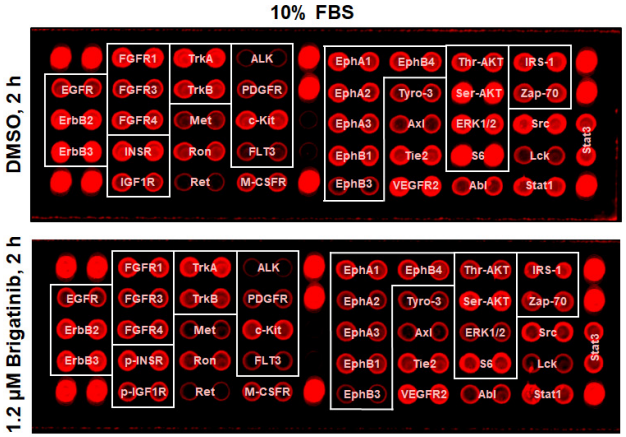






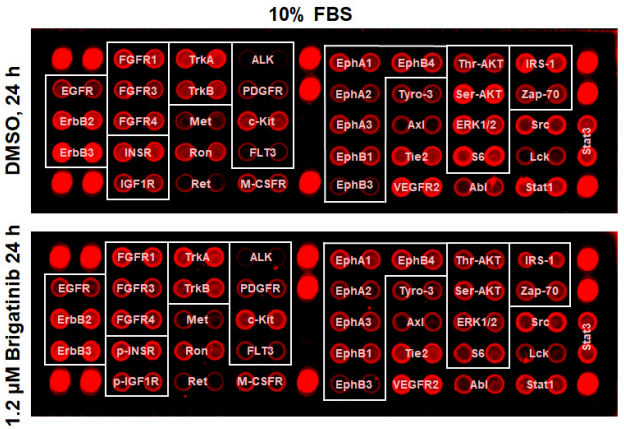
Supplementary Figure S6

A



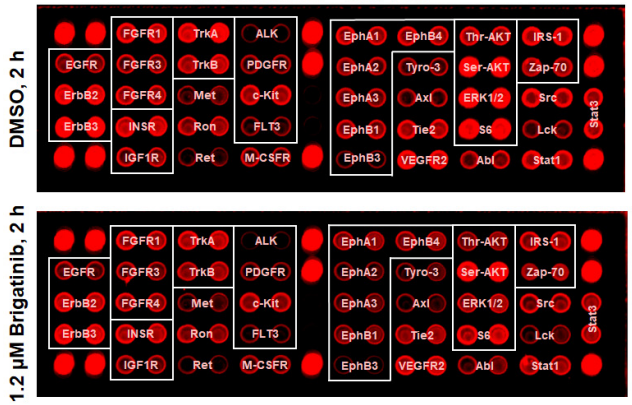
+	0.711	0.891	1.164	+	0.732	0.730	0.790	0.530	+
0.696	0.818	0.771	0.749	+	0.501	0.748	0.327	1.167	+
0.696	0.763	0.744	0.715	-	0.687	0.701	0.238	0.506	0.717
0.689	0.712	0.827	0.829	-	0.686	0.704	0.243	1.094	
+	0.771	1.073	0.787	+	0.616	0.696	0.662	0.765	+

B



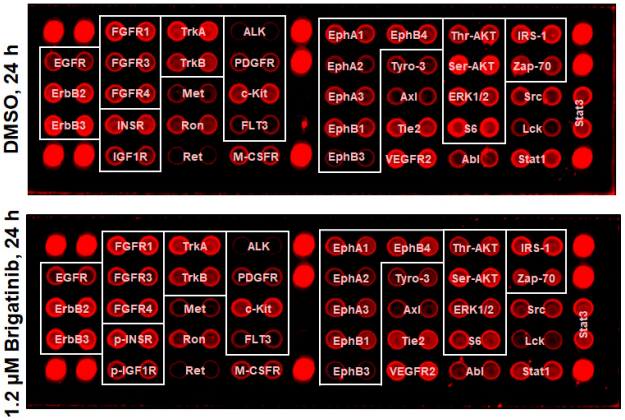
+	1.004	1.021	1.163	+	1.082	1.011	0.934	0.289	+
1.015	0.696	0.978	1.138	+	1.092	1.039	0.384	1.075	+
1.019	1.007	0.903	1.117	-	0.993	1.003	0.503	1.050	0.822
0.892	0.930	0.983	1.189	-	1.023	0.971	0.428	1.254	
+	0.977	0.868	1.023	+	1.096	0.957	0.599	0.567	+

C



+	0.764	0.665	0.618	+	0.723	0.734	0.641	0.755	+
0.790	1.187	0.770	0.742	+	0.598	0.750	0.545	0.651	+
0.783	0.843	0.868	0.811	-	0.727	0.692	0.282	0.676	0.776
0.733	0.797	0.903	0.766	-	0.705	0.728	0.397	0.769	
+	0.803	0.909	0.838	+	0.642	0.779	0.707	0.744	+

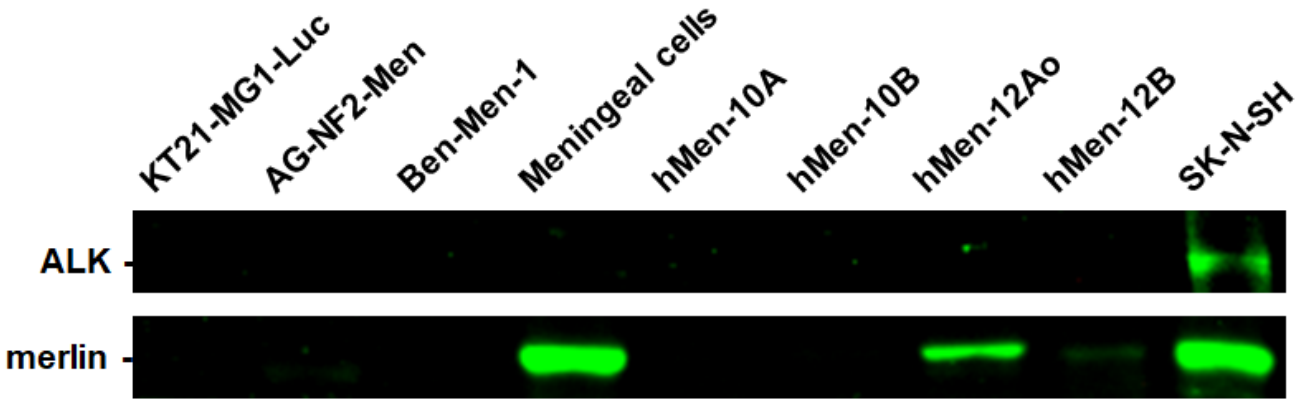
D



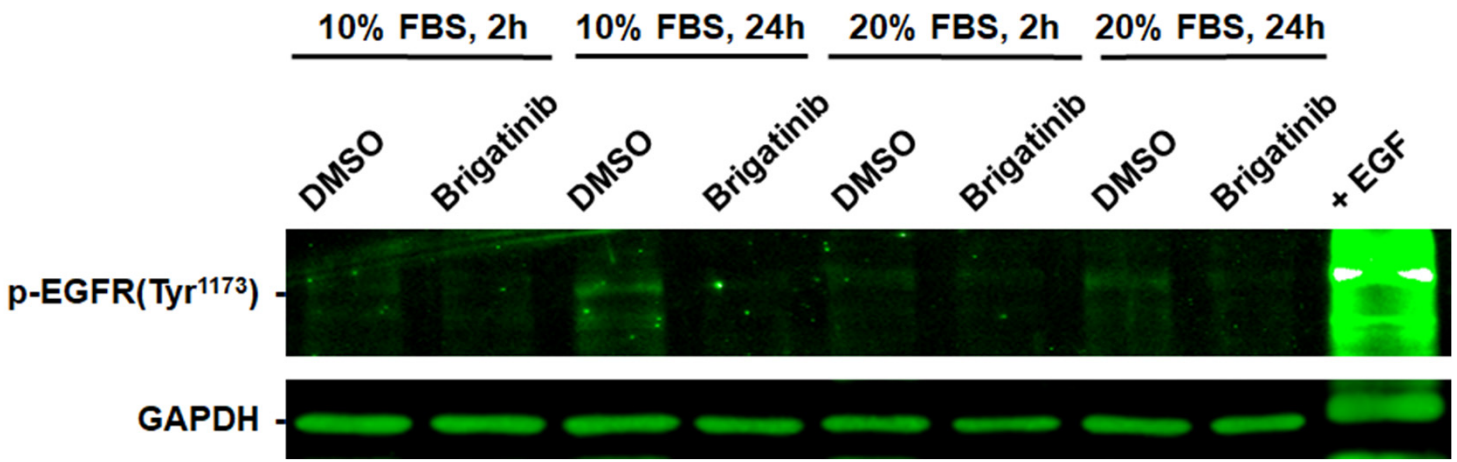
+	1.108	0.869	0.770	+	0.970	1.000	0.569	1.009	+
1.068	1.100	0.948	0.994	+	1.029	1.013	0.532	0.308	+
1.130	1.115	0.934	1.036	-	0.962	0.974	0.673	0.765	0.956
0.879	1.070	1.024	0.947	-	0.994	1.012	0.534	0.927	
+	0.969	0.818	0.899	+	1.046	0.972	0.677	0.855	+

Supplementary Figure S7

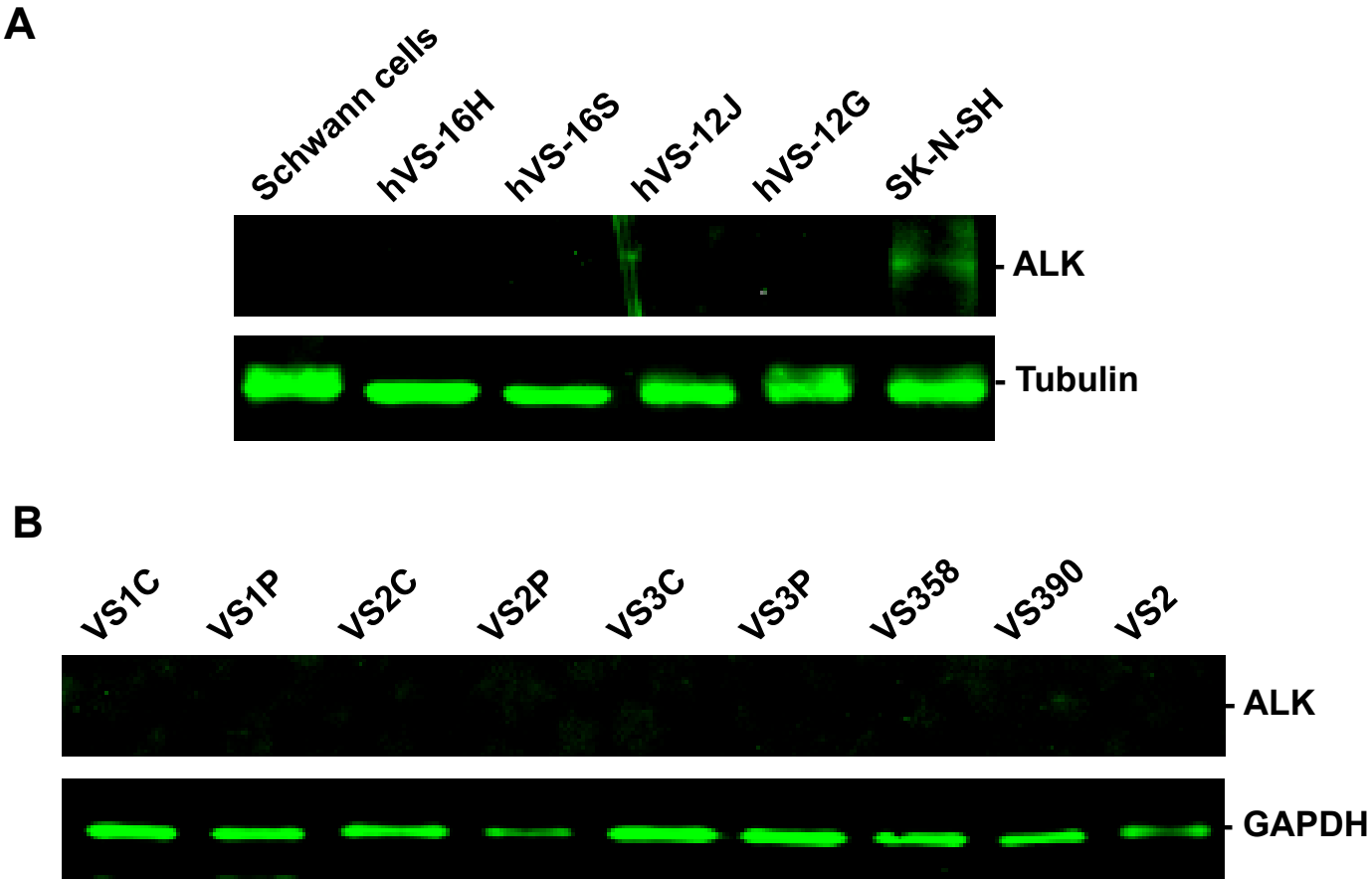
ALK was not detected in normal meningeal and *NF2*-deficient or expressing meningioma cells



Supplementary Figure S8



Supplementary Figure S9



Supplementary
Figure S10

Mouse pharmacokinetic parameters following a single oral dose of brigatinib (50 mg/kg) or MK-2206 (120 mg/kg)

Drug	PK Parameters					
	$T_{1/2}$ (h)	T_{max} (h)	C_{max} (ng/mL)	$AUC_{0-\infty}$ (h*ng/mL)	V/F (L/kg)	CL/F (L/h/kg)
Plasma						
Brigatinib	7.2	4	1311	18662	27.8	2.7
MK2206	5.6	1	2208	21286	45.3	5.6
Brain (Gross)						
	$T_{1/2}$ (h)	T_{max} (h)	C_{max} (ng/g)	$AUC_{0-\infty}$ (h*ng/g)	V/F (kg/kg)	CL/F (kg/h/kg)
Brigatinib	6.2	4	170	2319	193.3	22.6
MK2206	6.0	4	406	5462	191.5	22.0

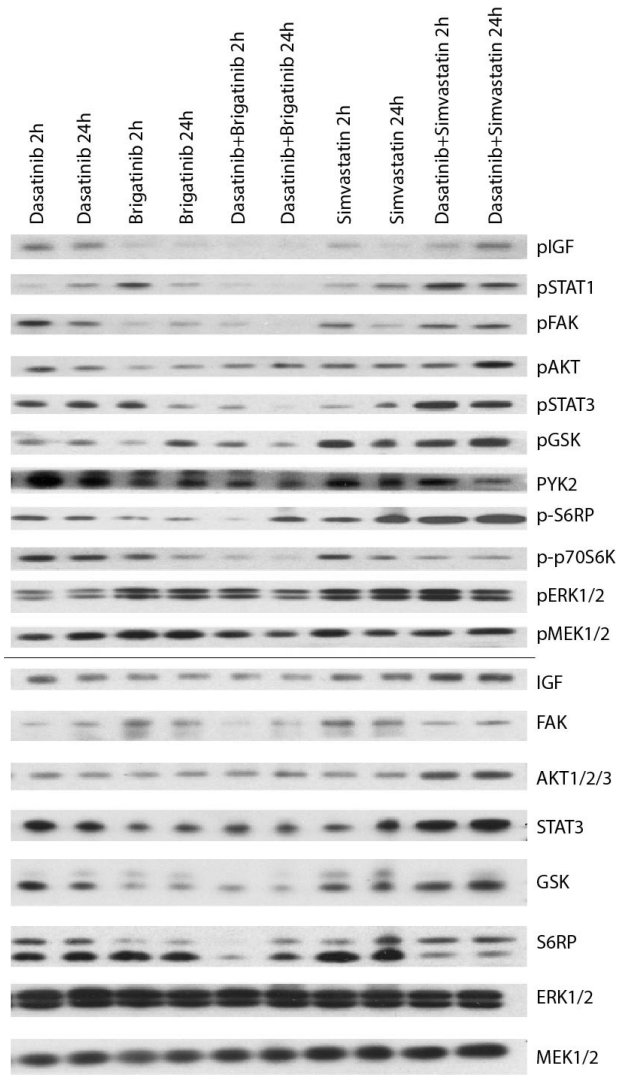
Supplementary Figure S11

Relative tumor sizes in meningioma-bearing mice prior to or after treatment with MK-2206 and brigatinib, either alone or in combination

Week	Vehicle control	SD	MK-2206	SD	Brigatinib	SD	MK-2206 + Brigatinib	SD
0	1	0	1	0	1	0	1	0
2	2.00	0.77	1.31	0.58	1.02	0.44	0.35	0.20
4	2.88	1.33	1.68	0.54	0.79	0.44	0.28	0.18
6	4.29	2.13	2.24	1.01	1.02	0.37	0.31	0.18
8	4.85	2.62	2.52	1.05	0.54	0.14	0.34	0.21
10	5.39	2.63	3.35	1.31	0.75	0.23	0.39	0.20
12	6.69	2.85	4.43	1.86	0.62	0.20	0.37	0.18

The relative tumor size shown following drug treatment was normalized to the tumor size prior to treatment (week 0), which is designated as 1 (100%).

Supplementary
Figure S12



Targeting protein translation by rocaglamide and didesmethylrocaglamide to treat MPNST and other sarcomas

Long-Sheng Chang[1,2,3,4,*], Janet L. Oblinger[1,2], Sarah S. Burns[1,2], Jie Huang[1,2], Larry W. Anderson[5], Melinda G. Hollingshead[5], Rulong Shen[4], Li Pan[6], Garima Agarwal[6], Yulin Ren[6], Ryan Roberts[1,2], Barry R. O'Keefe[5,7], A. Douglas Kinghorn[6], and Jerry M. Collins[5]

[1]Center for Childhood Cancer and Blood Diseases, Abigail Wexner Research Institute, Nationwide Children's Hospital, Columbus, OH 43205, USA; Departments of [2]Pediatrics, [3]Otolaryngology-Head & Neck Surgery, and [4]Pathology, The Ohio State University College of Medicine, Columbus, OH 43210, USA; [5]Division of Cancer Treatment and Diagnosis, Center for Cancer Research, National Cancer Institute, NIH, Frederick, MD 21702, USA; [6]Division of Medicinal Chemistry and Pharmacognosy, The Ohio State University College of Pharmacy, Columbus, OH 43210, USA; and [7]Molecular Targets Program, Center for Cancer Research, National Cancer Institute, NIH, Frederick, MD 21702, USA

Precis: Rocaglamide and didesmethylrocaglamide exhibit better drug-like properties than silvestrol and possess potent anti-tumor activity in multiple types of sarcomas

Running title: Rocaglamide and didesmethylrocaglamide for sarcoma treatment

Key words: Rocaglamide (Roc), didesmethylrocaglamide (DDR), malignant peripheral nerve sheath tumor (MPNST), Ewing sarcoma, osteosarcoma, rhabdomyosarcoma, orthotopic, cell line-derived xenograft (CDX), patient-

derived xenograft (PDX), and bioluminescence imaging (BLI)

*Corresponding author: Long-Sheng Chang, Center for Childhood Cancer and Blood Diseases, Abigail Wexner Research Institute at Nationwide Children's Hospital, 700 Children's Drive, Columbus, OH 43205, USA; Phone: 614-355-2658; Fax: 614-722-5895; E-mail: Long-Sheng.Chang@nationwidechildrens.org

Disclosure of Potential Conflicts of Interest: No potential conflicts of interest were disclosed

Authors' Contributions:

Conception and design: LSC, JLO, SSB, LWA, MGH, ADK, and JMC

Development of Methodology: LSC, JLO, SSB, JH, LWA, MGH

Acquisition of data: LSC, JLO, SSB, JH, LWA, MGH, RS, GA

Analysis and interpretation of data: LSC, JLO, SSB, LWA, ADK, JMC

Writing, review, and/or revision of the manuscript: LSC and JLO wrote the initial draft and all authors reviewed the manuscript

Administrative, technical, or material support: LSC, JLO, SSB, RR, LP, YR, BRO, ADK, JMC

Study Supervision: LSC, ADK, and JMC

Total word counts including Abstract (250 words), Introduction, Methods, Results, Discussion, and Acknowledgement: 4,825 words

Abstract

Malignant peripheral nerve sheath tumors (MPNSTs) frequently overexpress eIF4F components, and the eIF4A inhibitor silvestrol potently suppresses MPNST growth. However, silvestrol has suboptimal drug-like properties, including a bulky structure, poor oral bioavailability, sensitivity to MDR1 efflux, and pulmonary toxicity in dogs. We compared 10 silvestrol-related rocaglates lacking the dioxanyl ring and found that didesmethylrocaglamide (DDR) and rocaglamide (Roc) had growth-inhibitory activity comparable to silvestrol. Structure-activity relationship analysis revealed that the dioxanyl ring present in silvestrol was dispensable for, but may enhance, cytotoxicity. Both DDR and Roc arrested MPNST cells at G_2/M, increased the sub-G_1 population, induced cleavage of caspases and poly(ADP-ribose) polymerase, and elevated the levels of the DNA-damage response marker γH2A.X, while decreasing the expression of AKT and ERK1/2, consistent with translation inhibition. Unlike silvestrol, DDR and Roc were not sensitive to MDR1 inhibition and pharmacokinetic analysis confirmed that Roc had 50% oral bioavailability. Importantly, Roc, when administered intraperitoneally or orally, showed potent anti-tumor effects in an orthotopic MPNST mouse model and did not induce pulmonary toxicity in dogs as found with silvestrol. Treated tumors displayed degenerative changes and had more cleaved caspase 3-positive cells, indicative of increased apoptosis. Furthermore, Roc effectively suppressed the growth of osteosarcoma, Ewing sarcoma, and rhabdomyosarcoma cells and patient-derived xenografts. Both Roc- and DDR-treated sarcoma cells showed decreased levels of multiple oncogenic kinases, including IGF-1R. The more favorable drug-like properties of DDR and Roc and the potent anti-tumor activity of Roc suggest that these rocaglamides could become viable treatments for MPNST and other sarcomas.

Introduction

Malignant peripheral nerve sheath tumors (MPNSTs) are characterized as aggressive soft-tissue sarcomas with a high risk of recurrence and metastasis. Often refractory to current treatment, these tumors have a poor five-year survival rate of only about 20~50% (Kim et al., 2017). Therefore, development of more effective medical therapy that eradicate MPNSTs is of significant clinical need. MPNSTs can occur sporadically or arise from pre-existing plexiform neurofibromas in patients with neurofibromatosis type 1 (NF1), a tumor predisposition syndrome caused by mutations in the *NF1* gene which encodes the Ras-GTPase-activating protein neurofibromin. Importantly, even sporadic tumors frequently harbor mutations in the *NF1* gene or the Ras pathway. Consequently, both sporadic and NF1-associated MPNSTs exhibit upregulation of Ras downstream kinase signaling, including the phosphatidylinositol 3-kinase (PI3K)-AKT-mammalian target of rapamycin (mTOR) and Raf-MEK-ERK mitogen-activated protein kinases. MPNSTs also exhibit overexpression or aberrant activation of epidermal growth factor receptor (EGFR), platelet-derived growth factor receptor (PDGFR), and insulin-like growth factor-1 receptor (IGF-1R) (Perrone et al., 2009; Yang et al. 2011). These reports suggest that these Ras downstream kinases and deregulated receptor tyrosine kinases (RTKs) may be therapeutic targets. Additionally, recurrent mutations in the tumor suppressor genes *CDKN2A* and *TP53* and the subunits of the chromatin-modifying polycomb repressor complex-2 (PRC2), *SUZ12* and *EED*, have been identified and are important for MPNST progression (Kim and Pratilas, 2018). Inactivation of *CDKN2A* and *TP53* disables the G_1/S checkpoint. The loss of PRC2 function can lead to enhanced Ras-driven gene transcription (De Raedt et al., 2014).

As MPNSTs often exhibit hyperactive Ras activity, statins and farnesyl transferase inhibitors, which prevent localization of Ras to the membrane and inhibit MPNST cell growth (Sebti et al.,

1991; Barkan et al., 2006), have been evaluated but do not improve survival in patients with advanced cancer (Rao et al., 2004; Cloughesy et al., 2006; Hanrahan et al., 2009). Drugs that target the deregulated RTKs and mitogenic kinases have also been investigated in patients with MPNSTs; however, the results have so far been disappointing. The EGFR inhibitor erlotinib elicited poor response rates in MPNSTs with only one of 20 patients exhibiting stable disease (Albritton et al. 2006). The IGF-1R blocking antibodies, such as ganitumab, show limited objective single-agent activity (Tap et al., 2012). Sorafenib, which inhibits Raf and several RTKs, has only minimal activity in patients with sarcomas (Maki et al., 2009). The mTOR inhibitor rapamycin and its derivatives, such as everolimus, cause cytostatic responses and are being evaluated in combination with other targeted drugs. However, a recent trial showed that combination of everolimus with bevacizumab, a monoclonal antibody that binds vascular endothelial growth factor (VEGF) and prevents activation of the RTK VEGF receptor, was not effective in patients with refractory MPNSTs (Widemann et al. 2016). A phase II study is ongoing to evaluate the dual mTOR complexes 1 and 2 inhibitor TAK-228 in soft-tissue sarcomas (https://clinicaltrials.gov Identifier: NCT02987959). Collectively, the modest and transient patient responses from the completed trials indicate that targeting more than one critical pathway is likely needed to achieve a cure.

To sustain uncontrolled growth, cancer cells commonly exhibit enhanced protein translation by upregulation of the translation machinery (Malka-Mahieu et al., 2017). The most highly regulated step in the protein biosynthetic pathway occurs during translation initiation, in which the eukaryotic initiation factor 4F (eIF4F) complex is recruited to the 5' untranslated region (5'-UTR) of mRNA. This complex is composed of three subunits: eIF4G, a scaffolding protein; eIF4E, a cap-binding protein, and eIF4A, an RNA helicase which unwinds the secondary

structure of the 5'-UTR. We have shown over-expression of the three eIF4F components in multiple types of human cancer, including MPNST (Oblinger et al., 2016, 2018). Genetic inhibition of eIF4A and eIF4E using short-hairpin RNAs reduces MPNST cell proliferation. In addition, the pro-survival and pro-growth activities of several signaling pathways, such as PI3K-AKT-mTOR and Raf-MEK-ERK frequently activated in human cancer, occur in part by facilitating eIF4F-mediated translation initiation. The mTOR kinase phosphorylates and inactivates the eIF4E-binding protein (4E-BP) translational repressors (Mamane et al., 2006). Both AKT and ERKs phosphorylate eIF4B, which then associates with and increases the helicase activity of eIF4A (Chu et al., 2016). Moreover, AKT, mTOR, and the downstream ERK1/2 kinase p90 ribosomal S6 kinase can phosphorylate and inactivate an endogenous repressor of eIF4A activity, the programmed cell death 4 (PDCD4) protein. Further, the mRNAs that depend upon eIF4A for efficient translation usually contain long 5'-UTRs with guanine-rich sequences termed G-quadruplexes which can form four-stranded structures with G-tetrads stacked on one another (Malka-Mahieu et al., 2016). These eIF4A-dependent transcripts are often found in genes encoding oncoproteins, transcription factors associated with super enhancers, epigenetic regulators, and kinases (Wolfe et al., 2014). Interestingly, we found that the eIF4A inhibitor silvestrol suppresses MPNST cell growth at low nanomolar of $IC_{50,}$ decreases the levels of multiple mitogenic kinases including AKT and ERKs, and profoundly impairs the growth of MPNST xenografts (Oblinger et al., 2016). These results suggest that direct targeting of the translation initiation components, particularly eIF4A, might be an effective treatment strategy for these tumors.

Silvestrol is part of a large family of compounds termed flavaglines or rocaglates, which share a cyclopenta[*b*]benzofuran structure (Pan et al., 2014; Kinghorn et al. 2016). It possesses

potent antitumor activity in multiple other cancer models (Lucas et al. 2009; Kogure et al., 2013; Boussemart et al. 2014). However, silvestrol has some suboptimal drug-like properties. It is relatively large with a bulky dioxanyl ring, making the total synthesis of silvestrol laborious (El Sous et al., 2007; Gerard et al., 2007; Adams et al., 2009). It is a substrate for the multidrug resistance 1 (MDR1) transporter (Gupta et al. 2011) and has very limited oral bioavailability of <2% (Saradhi et al. 2011).

To search for compounds with better drug-like properties, we analyzed ten rocaglates that lack the dioxanyl moiety and examined the structure-activity relationships for this compound class. We showed that two of these compounds, rocaglamide (Roc) and didesmethylrocaglamide (DDR), exhibited potent growth inhibitory activity with IC_{50} values comparable to silvestrol. Importantly, these rocaglamides were not sensitive to MDR1 inhibition and Roc exhibited oral bioavailability and potent anti-tumor effects against multiple types of sarcomas.

Methods

Natural Compounds

Ten silvestrol-related rocaglates, inclusive of (−)-didesmethylrocaglamide, were isolated from the tropical plant *Aglaia perviridis*, collected in Vietnam as part of a multi-institutional collaborative project on the discovery of new antineoplastic natural compounds. The full structures and absolute configurations of these rocaglates were determined (Pan et al., 2013). For *in vitro* studies, purified silvestrol and related rocaglates were dissolved as a 10-mM stock in dimethyl sulfoxide (DMSO; Sigma-Aldrich). A 60-mg sample of (−)-rocaglamide (NSC326408) was prepared at the U.S. National Cancer Institute for *in vivo* studies.

Cell Lines, Cell Proliferation Assays, and Flow Cytometry

Various MPNST, Ewing sarcoma, osteosarcoma, rhabdomyosarcoma, schwannoma, meningioma, and leukemia cell lines used in this study are described in Supplementary Methods. Cell proliferation was assessed using resazurin assays and cell cycle analysis was performed with details provided in Supplementary Methods.

Western Blots

Subconfluent cells were treated with the indicated doses of Roc or DDR for 1-3 days and lysed. Equal amounts of protein lysates were analyzed by immunoblotting. Detailed procedures and the antibodies used are described in Supplementary Methods.

Pharmacokinetic (PK) analysis

Mice were administered with a 5mg/kg dose of Roc by intravenous (IV) or intraperitoneal injection (IP) or by oral gavage (PO). Blood samples were collected before and at multiple time-points after dosing (n=3). Plasma concentrations of Roc were analyzed using a sensitive liquid chromatography coupled with tandem mass spectrometry (LC/MS-MS) (Supplementary Methods).

Cell Line-Derived Xenograft (CDX) and Patient-Derived Xenograft (PDX) Models and In Vivo Efficacy

All animal work was performed according to the protocols approved by the Institutional Animal Care and Use Committee at Nationwide Children's Hospital. For animal dosing, Roc was formulated in 30% hydroxypropyl-β-cyclodextrin (HPβCD). The quantifiable, orthotopic

MPNST CDX model was generated as described previously (Burns and Chang, 2016). Mice bearing established ST8814-Luc tumors (Oblinger et al., 2016) were randomized into three groups (n=10/group) and treated with the predetermined maximum tolerated dose (MTD) of Roc at 4mg/kg by IP or 1.2mg/kg by oral gavage, or the vehicle HPβCD every other day. Tumor growth was measured weekly by BLI.

To generate PDX models, the Nationwide Children's Hospital Institutional Review Board approved the Human Subjects Protocol. Following informed patient consents, tumor specimens were used to establish PDX models according to Supplementary Methods. Mice with actively-growing PDX tumors for a Ewing sarcoma (NCH-EWS-2), an osteosarcoma (NCH-OS-7), and an alveolar rhabdomyosarcoma (NCH-ARMS-2) reaching ~100-200 mm^3 were randomized into two treatment groups (n=10/group) for each PDX model and treated with 3mg/kg of Roc or HPβCD by IP every other day, followed by tumor measurement twice weekly (Supplementary Methods).

Immunohistochemistry

Sections from Roc or vehicle-treated MPNST tumors were prepared and stained with hematoxylin and eosin (H&E) or immunostained for p-histone H3(Ser^{10}) (pH3; ab32107, Abcam) or CC3 (#9664, Cell Signaling) as previously described (Burns et al., 2013).

Results

DDR and Roc possess potent growth-inhibitory activity comparable to silvestrol.

To search for compounds with better drug-like properties, we side-by-side compared ten rocaglates lacking the dioxanyl ring (Pan et al., 2013) with silvestrol for growth-inhibitory

activity in a panel of MPNST, schwannoma, and meningioma cell lines, which we previously showed to be sensitive to the antiproliferative action of silvestrol (Oblinger et al., 2016, 2018). We found that several of these rocaglates maintained potent growth inhibition comparable to silvestrol. In particular, the IC_{50} values of Roc were slightly higher than silvestrol, while DDR reliably demonstrated ~2-fold more potent than silvestrol in all cell lines tested (Fig. 1, Table 1, and Supplementary Fig. S1), indicating that the dioxanyl moiety is dispensable for cytotoxicity. Further structure-activity comparison discerned some positions on the cyclopenta[*b*]benzofuran scaffold that affected the antiproliferative activity of rocaglates. Similar to previous observations, the substitution of a methoxy group at position 8b, as in 8b-*O*-methylrocaglaol versus rocaglaol, abolished the activity (Fig. 1). This methoxy substitution at 8b could be partly mitigated by the addition of a methylenedioxy ring to phenyl ring B. Additionally, the presence of amide or ester groups at position C-2 of the benzofuran scaffold appeared to enhance the activity, as compounds such as DDR, Roc, and methyl rocaglate were more potent than rocaglaol. Since the amide group at the C-2 position confers superior growth inhibition, we further evaluated DDR and Roc for their mechanisms of action.

Rocaglamides induce G_2/M arrest and cell death.

Flow cytometry analysis revealed that human *NF1*-expressing STS26T and *NF1*-null ST8814 MPNST cells treated with one- or two-IC_{50} doses of DDR or Roc for three days exhibited a marked increase in the G_2/M fraction (Supplementary Fig. S2A and S2B). The sub-G_1 fraction, suggestive of apoptosis, was noticeably prominent in treated STS26T cells, especially at the two-IC_{50} dose (Supplementary Fig. S2A). Phase contrast micrographs taken of cells prior to cell cycle analysis showed increased floating dead cells and debris in DDR or Roc-treated dishes. While

ST8814 cells treated for three days did not show obvious signs of cell death (Supplementary Fig. S2B), a six-day incubation resulted in increased numbers of floating dead cells with a commensurate expansion of the sub-G_1 fraction (Supplementary Fig. S2C). Collectively, these results indicate that, like silvestrol (Oblinger et al., 2016), DDR and Roc inhibit MPNST cell proliferation by inducing cell cycle arrest at G_2/M and subsequently, cell death.

DDR and Roc increase caspase and PARP cleavage and activate the DNA damage response, while suppressing mitogenic signaling pathways.

To confirm induction of apoptosis in rocaglamide-treated MPNST cells, we analyzed protein expression of several markers important for this process. STS26T cells treated for 3 days with either DDR or Roc exhibited increased cleavage of the executioner caspases-3 and 7 and their downstream substrate PARP (Fig. 2A). A concomitant decrease in the amounts of intact caspases 3 and 7 and PARP was observed, consistent with the enhanced cleavage of these apoptotic markers and possibly due to direct effects of these rocaglamides on protein translation. Likewise, the levels of the pro-survival kinases AKT and ERK1/2 were diminished in rocaglamide-treated MPNST cells. Importantly, treatment with rocaglamides also resulted in higher levels of the DNA damage response marker γH2A.X. This increase occurred as early as one day after DDR treatment before the occurrence of cell death (Fig. 2B). These results demonstrate that DDR and Roc induce apoptosis in MPNST cells, possibly subsequent to the activation of the DNA damage response.

Rocaglamides are not sensitive to MDR1 inhibition and Roc is orally bioavailable.

The MDR1/P-glycoprotein (Pgp) encoded by the *ABCB1* (ATP-binding cassette subfamily B

member 1) gene is implicated in limiting the bioavailability of several chemotherapeutics and confers drug resistance in tumors that overexpress this protein. Silvestrol is a substrate of MDR1/Pgp, which may be related to its poor oral bioavailability (Gupta et al., 2011; Saradhi et al., 2011). To determine whether there are any differences in the sensitivity to MDR1/Pgp between rocaglamides and silvestrol, we treated silvestrol-resistant 697-R leukemic cells, which overexpress MDR1/Pgp (Supplementary Fig. S3), and the parental silvestrol-sensitive 697 cells with various concentrations of each compound. Similar to previous findings (Gupta et al., 2011), we found that 697-R cells were less sensitive to silvestrol inhibition than 697 cells (26 vs 3.5nM of $IC_{50,}$ respectively; Fig. 3A). Surprisingly, DDR- and Roc-treated 697-R cells exhibited IC_{50} values very similar to those of parental 697 cells (4 vs 3nM of $IC_{50,}$ respectively, for DDR and 15 vs 8nM of $IC_{50,}$ respectively, for Roc; Figs. 3B and 3C), indicating that these rocaglamides are no longer sensitive to MDR1 inhibition.

To examine the oral bioavailability, we conducted PK studies to compare mice that had been dosed with Roc at 5mg/kg via the IV, IP, or PO route, followed by measuring Roc concentrations in blood samples collected at various times post dosing. Two separate studies with three mice at each time point for each dosing route were conducted. The maximum mean observed concentration (C_{max}) reached ~11μM for the IV route, ~4μM for the IP route, and ~0.8μM for the PO route (Fig. 4A). Areas under the plasma concentration-time curves ($AUC_{0–7h}$) produced 245μM*min of exposure in the IV route and 142μM*min of exposure in the PO route. The concentrations of Roc appeared to decline more slowly in the plasma over 24h ($T_{½}$=2.4h) with the PO route compared to those dosed by the IV route ($T_{½}$=1.5h). Based on the estimation from $AUC_{0–7h}$, Roc exhibited ~50% oral bioavailability, confirming improved bioavailability of Roc over silvestrol.

Roc, when administered intraperitoneally or orally, exhibits potent anti-tumor effects in an orthotopic MPNST model.

To evaluate the *in vivo* activity of Roc, we treated NSG mice bearing luciferase-expressing ST8814-Luc tumors implanted in the sciatic nerve with Roc at the predetermined MTD (4mg/kg by IP or 1.2mg/kg orally), or HPβCD vehicle every other day. As shown in Figs. 4B/4C, tumor bioluminescence from vehicle-treated mice steadily and rapidly increased by >10,000-fold over four-week treatment. In contrast, tumor bioluminescence from mice treated with Roc by IP only increased by an average of <10-fold, showing >99% reduction in tumor luminescence compared to controls. Similarly, Roc, when administered orally, also exhibited potent tumor inhibition with bioluminescence decreasing by >95%.

Histological analysis revealed that while MPNSTs treated with HPβCD vehicle for four weeks had large nuclei with prominent nucleoli and displayed active mitotic figures (Fig. 4D, top left panel), tumors treated with Roc by IP had pleomorphic nuclei with abundant foamy cytoplasm resembling histiocytoid degenerative changes (top middle panel). A few enlarged tumor cells that appeared multinucleated and scattered apoptosis were present. Degenerative changes and cell death were also observed in tumors treated with orally-delivered Roc (top right panel). Consistent with G_2/M arrest, tumor cells treated with IP- or orally-delivered Roc exhibited much higher prevalence of phospho-histone H3 labeling compared to vehicle-treated tumors (middle panels). In addition, Roc-treated tumors displayed increased numbers of cleaved caspase-3 positive cells which often coincided with those with multinucleated-like appearance (bottom panels). Taken together, these results indicate that Roc has oral bioavailability and possesses potent *in vivo* efficacy against MPNSTs.

Roc and DDR have broad antitumor activity against common types of pediatric sarcoma.

Since MPNSTs comprise only ~2% of all sarcomas (Farid et al. 2014), we expanded our testing of Roc and DDR to three other types of sarcomas more prevalent seen in children and young adults: Ewing sarcoma, osteosarcoma, and rhabdomyosarcoma. Using a series of commonly-used cell lines, including two Ewing sarcoma cell lines (A673 and TC32), four osteosarcoma cell lines (143B, MG-63, Saos2, and OS17), and one rhabdomyosarcoma cell line (RD), we showed that, as in MPNST cells, both rocaglamides were highly active against all of these sarcoma cell lines (Supplementary Figs. S4A-C). Also, we observed that DDR consistently exhibited lower IC_{50} values than Roc in every sarcoma cell line tested.

Subsequently, we evaluated the *in vivo* activity of Roc using PDX models for a Ewing sarcoma, an osteosarcoma, and an alveolar rhabdomyosarcoma. We discovered that Roc was highly potent in suppressing the growth of Ewing sarcoma PDXs and inhibited tumor growth by an average of ~90% over four-week treatment (Fig. 5A). Similarly, the average size of Roc-treated osteosarcoma PDX tumors was reduced by ~80% compared to those of vehicle-treated tumors (Fig. 5B). Also, Roc inhibited the growth of rhabdomyosarcoma PDXs by ~70% (Fig. 5C). Notably, the volumes of tumors in individual Roc-treated mice showed very little overlap with those in vehicle-treated mice, particularly for the Ewing sarcoma and osteosarcoma PDX models (Fig. 5). Together with the findings from the MPNST model, these results demonstrate that Roc displays significant antitumor effects against multiple types of sarcoma.

Rocaglamides decrease multiple signaling kinases and transcription factors important for sarcoma cell growth.

To further examine the molecular mechanisms underlying the antiproliferative effects of rocaglamides, we treated TC32 Ewing sarcoma, 143B osteosarcoma, and RD rhabdomyosarcoma cells with one- or two-IC_{50} dose of DDR or Roc for 1-2 days followed by Western blotting for several known drivers of cell survival and proliferation. Interestingly, we found that these rocaglamides reliably reduced the levels of the β subunit of IGF-1R, an upstream activator of PI3K-AKT signaling, in all three sarcoma cell lines (Figs. 6A-C). We also observed reduction of the IGF-1Rβ levels in rocaglamide-treated MPNST cells (Supplementary Fig. S5). In addition, both rocaglamides decreased the levels of AKT, ERKs, cyclin D1 and survivin in treated TC32, 143B, and RD cells (Fig. 6). Intriguingly, the oncogenic fusion protein EWS-FLI1, which act as an aberrant transcription factor in Ewing sarcoma (Delattre et al., 1992), was not affected in Roc- and DDR-treated TC32 Ewing sarcoma cells (Fig. 6A). Consistent with this observation, these rocaglamides did not inhibit EWS expression in 143B osteosarcoma and RD rhabdomyosarcoma cells (Figs. 6B/C). However, the levels of lysine demethylase 1 (LSD1), which modulates EWS-FLI1 transcriptional activity (Sankar et al., 2013), and NKX2.2, an EWS-FL11-regulated gene necessary for oncogenic transformation (Smith et al., 2006), were diminished by these rocaglamides in TC32 cells (Fig. 6A). Collectively, these results suggest that rocaglamides potently suppress sarcoma growth by decreasing multiple key signaling proteins important for tumor growth and survival.

Discussion

For decades, treatments for MPNSTs and other sarcomas have remained largely unchanged with current standard of care combining surgical resection with intensive multi-agent chemotherapy (Farid et al., 2014; Brown et al., 2017; Kim et al., 2017; Skapek et al., 2019).

Radiation may be used depending upon the tumor type and clinical presentation. While this multidisciplinary treatment strategy may help local control, it is not effective for metastatic and recurrent disease. Also, these multimodal regimens are associated with considerable acute and long-term toxicities that impact patients' quality of life. Despite recent advances in understanding tumor biology and targeted therapy development, an FDA-approved medical therapy for the treatment of these malignancies is still not available. We previously showed that eIF4A is a vulnerable point of disruption in MPNSTs and that the eIF4A inhibitor silvestrol potently suppresses MPNST growth (Oblinger et al., 2016). Regretfully, silvestrol exhibited an unexpected pulmonary toxicity in dogs and its further development as a cancer therapy was suspended (DM Lucas, MA Phelps, AD Kinghorn, M Grever, in preparation; Kinghorn et al., 2016). We have identified two rocaglates lacking the dioxanyl ring, Roc and DDR, with better drug-like properties than silvestrol and possessing antitumor efficacy in multiple sarcoma models, including MPNST. Most critically, a recent toxicity study conducted by the NCI Developmental Therapeutics Program revealed that Roc did not induce the toxicity found in dogs with silvestrol under the same conditions (https://dtp.cancer.gov/publications/silvestrol_rocaglamide_studies.pdf).

Our side-by-side comparison of 10 rocaglates lacking the bulky dioxanyl ring present in silvestrol has allowed us to discern certain structure-activity relationships, particularly the C-8b, C-2, and C-6 positions along the cyclopenta[*b*]benzofuran core. Consistent with previous reports (Ebada et al., 2011; Kinghorn et al., 2016), the hydroxy group at the C-8b position is essential for antiproliferative activity. This finding is consistent with the crystal structure of Roc complexed with eIF4A and polypurine RNA, which reveals hydrogen bonding between the 8b-OH of Roc and a guanine base in the RNA (Iwasaki et al., 2019). Also, the phenyl rings A and B of Roc

parallel stack with RNA bases, which may explain our finding that adding a methylenedioxy group to ring B modestly improved the growth inhibitory activity of rocaglates with methylated 8b-OH (Fig. 1). It is possible that this methylenedioxy ring may enhance the affinity of the rocaglates to the eIF4A-RNA complex, partially compensating for the loss of 8b hydrogen bonding.

Among the rocaglates lacking the dioxanyl ring that we evaluated, DDR was the most potent, suggestive of the importance of having a simple primary amide group at the C-2 position. While the presence of a dioxanyl ring instead of a methoxy group at the C-6 position enhances the potency of silvestrol compared with methyl rocaglate (Kim et al., 2006; Kinghorn et al., 2016), our data indicated that this ring is not required for cytotoxicity. However, it appears to play an important role in MDR1-induced resistance as Roc and DDR are no longer susceptible to this inhibitory effect. Consistent with this notion, we detected a higher level of MDR1 in ST8814 MPNST cells than that in STS26T cells (Supplementary Fig. S3), while the IC_{50} values of Roc and DDR in ST8814 cells were similar to those in STS26T cells (Table 1 and Supplementary Fig. S1). The MDR1 transporter binds to silvestrol and is thought to limit its oral bioavailability (Gupta et al., 2011). Our PK analysis demonstrating 50% oral bioavailability of Roc, a >25-fold improvement over silvestrol, confirms this prediction and strongly suggests a possible interaction of MDR1 with the dioxanyl moiety. The observed oral bioavailability of Roc allows a greater flexibility for dosing. More importantly, we found that Roc, when administered intraperitoneally or orally, showed potent anti-tumor effects in an orthotopic MPNST CDX mouse model and effectively suppressed the growth of PDX models for Ewing sarcoma, osteosarcoma, and rhabdomyosarcoma.

Like silvestrol, rocaglamides exert their potent growth-inhibitory and antitumor activities

mainly through inhibition of eIF4A and protein translation (Cencic et al., 2009; Sadlish et al., 2013). Consistently, we observed that Roc and DDR decreased the levels of multiple signaling proteins important for tumor growth and survival, leading to G_2/M cell cycle arrest and activation of executioner caspases. In addition to AKT and ERKs, rocaglamides reduced the levels of IGF-1R in all sarcoma cell lines tested. This decrease in IGF-1R expression, coupled with the simultaneous inhibition of AKT and ERKs, likely results in superior inhibition of IGF-1 signaling compared to the simple blockade at the receptor level. Our results further suggest that IGF-1R may serve as a biomarker for responsiveness to rocaglamides in sarcomas.

It should be noted that the effects of translation inhibition mediated by eIF4A are different from those by eIF4E, which can be activated by the AKT/mTOR pathway, a commonly deregulated event in sarcomas (Mamane et al., 2006). The mTOR inhibitor, rapamycin and its analogs, and mTOR kinase inhibitors only cause cytostatic effects and tumor stabilization (D'Abronzo and Ghosh, 2018). Also, blocking mTOR signaling is associated with activation of bypass signaling pathways that can restore critical survival signals, enabling tumor regrowth. Inhibition of eIF4E tends to decrease translation of the mRNAs with 5' terminal oligopyrimidine tracts, which encode ribosomal proteins, elongation factors, lysosomal-related and metabolic-related proteins. However, the eIF4A activity is more critical in unwinding the mRNAs with long 5'-UTRs that can form G-quadruplexes, such as *AKT* and *IGF-1R* (Wolfe et al., 2014; Malka-Mahieu et al., 2017). In addition, some transcripts, e.g., *c-MYC*, are translated from internal ribosomal entry sites that do not require the cap binder eIF4E and are insensitive to eIF4E inhibition (Wiegering et al., 2015). Thus, blocking eIF4A may have a stronger effect on tumor growth and survival.

Ewing sarcoma is frequently driven by the chimeric fusion oncogene *EWS-FLI1* due to a

chromosomal translocation that fuses an RNA-binding protein, EWSR1, with the FLI1 transcription factor (Delattre et al., 1992). Surprisingly, we found that the levels of EWS-FLI1 remained unchanged in rocaglamide-treated Ewing sarcoma cells (Fig. 6A). As a ubiquitously expressed protein, the EWSR1 levels were also not affected in other types of sarcoma cells treated with rocaglamides (Figs. 6B/C). In contrast, the levels of the epigenetic modulator LSD1, protein needed for optimal activity of the EWS-FLI1 transcriptional complex (Sankar et al., 2013), and a key EWS-FLI1 downstream target NKX2.2, a homeobox transcription factor implicated in development (Smith et al., 2006), were diminished by DDR and Roc treatment (Fig. 6). Upon inspection of these genes, we noted that the *EWSR1* transcript has a very short 5'-UTR, while the mRNAs for *NKX2.2* and *LSD1/KDM1A* contain longer G+C-rich 5'-UTRs. Therefore, we hypothesize that the *NKX2.2* and *LSD1/KDM1A* transcripts are eIF4A-dependent.

Intriguingly, prior to caspase activation, rocaglamide-treated MPNST cells exhibited increased γH2A.X, suggesting that DNA damage may be a key underlying cause of the apoptosis seen at later time points. Rocaglamides may affect prohibitin-mediated ERK activation, cause the disruption of mitochondrial integrity, and/or promote the generation of reactive oxygen species (Polier et al., 2012; Callahan et al., 2014). Alternatively, they may affect translation of the proteins responsible for DNA replication and repair, resulting in stalled replication forks or inadequate repair of DNA damage. We are presently examining these possibilities.

Roc was the first member of the cyclopenta[*b*]benzofuran class identified as a novel antileukemic agent from *Aglaia elliptifolia* by King et al. (1982). It is worth mentioning that the structures of Roc and DDR are simpler than silvestrol; therefore, they should be more amenable to chemical synthesis (Liu et al., 2012). As DDR exhibited higher *in vitro* potency against various types of sarcoma cells than Roc, we anticipate that DDR will have superior anti-tumor

efficacy. Experiments are in progress to compare these rocaglamides in various sarcoma animal models.

In summary, we have demonstrated that Roc and DDR, as eIF4A inhibitors, simultaneously suppressed multiple growth-promoting signaling pathways and induced apoptosis in tumor cells. Roc was no longer sensitive to MDR1 inhibition. It was orally bioavailable and exhibited potent anti-tumor effects in multiple sarcoma models with no overt toxicity. These promising results indicate that these rocaglamides merit further investigation as treatments for patients with MPNSTs and other sarcomas.

Acknowledgements

We sincerely thank Melissa Sammons of NCH Tumor Core for assistance with PDX models, Eva Majerova for technical help with plasma analysis, John Byrd for 697 and 697-R cells, Stephen Lessnick for Ewing sarcoma cells, and Ruoning Wang for rhabdomyosarcoma cells. This study was supported by grants from CancerFree KIDS, Sunbeam Foundation, and Department of Defense (to LSC), National Cancer Institute (P01CA125066 to ADK and P30CA16058 to The OSU Comprehensive Cancer Center), and NCI Experimental Therapeutics program (NCI Contract HHSN261200800001 to Leidos Biomedical Research).

References

Adams TE, El Sous M, Hawkins BC, Hirner S, Holloway G, Khoo ML, Owen DJ, Savage GP, Scammells PJ, Rizzacasa MA. Total synthesis of the potent anticancer *Aglaia* metabolites (-)-silvestrol and (−)-episilvestrol and the active analogue (−)-4'-desmethoxyepisilvestrol. J Am Chem Soc. 2009;131:1607-1616.

Albritton KH, Rankin C, Coffin CM, Ratner N, Budd GT, Schuetze SM, Randall RL, Declue JE, and Borden EC. Phase II study of erlotinib in metastatic or unresectable malignant peripheral nerve sheath tumors (MPNST). J Clin Oncol. 2006;24:18(suppl): 9518-9518.

Barkan B, Starinsky S, Friedman E, Stein R, Kloog Y. The Ras inhibitor farnesylthiosalicylic acid as a potential therapy for neurofibromatosis type 1. Clin Cancer Res. 2006;12:5533-5542.

Boussemart L, Malka-Mahieu H, Girault I, Allard D, Hemmingsson O, Tomasic G, Thomas M, Basmadjian C, Ribeiro N, Thuaud F, Mateus C, Routier E, Kamsu-Kom N, Agoussi S, Eggermont AM, Désaubry L, Robert C, Vagner S. eIF4F is a nexus of resistance to anti-BRAF and anti-MEK cancer therapies. Nature. 2014;513:105-109.

Burns SS, Akhmametyeva EM, Oblinger JL, Bush ML, Huang J, Senner V, Chen CS, Jacob A, Welling DB, Chang LS. Histone deacetylase inhibitor AR-42 differentially affects cell-cycle transit in meningeal and meningioma cells, potently inhibiting NF2-deficient meningioma growth. Cancer Res. 2013;73:792-803.

Burns SS, Chang L-S. Generation of noninvasive, quantifiable, orthotopic animal models for NF2-associated schwannoma and meningioma. Methods Mol Biol. 2016;1427:59-72

Callahan KP, Minhajuddin M, Corbett C, Lagadinou ED, Rossi RM, Grose V, Balys MM, Pan L, Jacob S, Frontier A, Grever MR, Lucas DM, Kinghorn AD, Liesveld JL, Becker MW, Jordan CT. Flavaglines target primitive leukemia cells and enhance anti-leukemia drug activity. Leukemia. 2014;28:1960-1968.

Cencic R, Carrier M, Galicia-Vázquez G, Bordeleau ME, Sukarieh R, Bourdeau A, Brem B, Teodoro JG, Greger H, Tremblay ML, Porco JA Jr, Pelletier J. Antitumor activity and mechanism of action of the cyclopenta[*b*]benzofuran, silvestrol. PLoS One. 2009;4:e5223.

Chu J, Cargnello M, Topisirovic I, Pelletier J. Translation initiation factors: reprogramming protein synthesis in cancer. Trends Cell Biol. 2016;26:918-933.

Cloughesy TF, Wen PY, Robins HI, Chang SM, Groves MD, Fink KL, Junck L, Schiff D, Abrey L, Gilbert MR, Lieberman F, Kuhn J, DeAngelis LM, Mehta M, Raizer JJ, Yung WK, Aldape K, Wright J, Lamborn KR, Prados MD. Phase II trial of tipifarnib in patients with recurrent malignant glioma either receiving or not receiving enzyme-inducing antiepileptic drugs: a North American Brain Tumor Consortium Study. J Clin Oncol. 2006;24:3651-3656.

D'Abronzo LS, Ghosh PM. eIF4E phosphorylation in prostate cancer. Neoplasia. 2018;20:563-573.

Delattre O, Zucman J, Plougastel B, Desmaze C, Melot T, Peter M, Kovar H, Joubert I, de Jong P, Rouleau G, Aurias A, Thomas G. Gene fusion with an ETS DNA-binding domain caused by chromosome translocation in human tumours. Nature. 1992;359:162-165.

De Raedt T, Beert E, Pasmant E, Luscan A, Brems H, Ortonne N, Helin K, Hornick JL, Mautner V, Kehrer-Sawatzki H, Clapp W, Bradner J, Vidaud M, Upadhyaya M, Legius E, Cichowski K. PRC2 loss amplifies Ras-driven transcription and confers sensitivity to BRD4-based therapies. Nature. 2014;514:247-51.

Ebada SS, Lajkiewicz N, Porco JA Jr, Li-Weber M, Proksch P. Chemistry and biology of rocaglamides (= flavaglines) and related derivatives from *Aglaia* species (Meliaceae). Prog Chem Org Nat Prod. 2011;94:1-58.

El Sous M, Khoo ML, Holloway G, Owen D, Scammells PJ, Rizzacasa MA. Total synthesis of (−)-episilvestrol and (−)-silvestrol. Angew Chem Int Ed Engl. 2007;46:7835-7838.

Farid M1, Demicco EG, Garcia R, Ahn L, Merola PR, Cioffi A, Maki RG. Malignant peripheral nerve sheath tumors. Oncologist. 2014;19:193-201.

Gerard B, Cencic R, Pelletier J, Porco JA Jr. Enantioselective synthesis of the complex rocaglate (-)-silvestrol. Angew Chem Int Ed Engl. 2007;46:7831-7834.

Gupta SV, Sass EJ, Davis ME, Edwards RB, Lozanski G, Heerema NA, Lehman A, Zhang X, Jarjoura D, Byrd JC, Pan L, Chan KK, Kinghorn AD, Phelps MA, Grever MR, Lucas DM. Resistance to the translation initiation inhibitor silvestrol is mediated by ABCB1/P-glycoprotein overexpression in acute lymphoblastic leukemia cells. AAPS J. 2011;13:357-364.

Hanrahan EO, Kies MS, Glisson BS, Khuri FR, Feng L, Tran HT, Ginsberg LE, Truong MT, Hong WK, Kim ES. A phase II study of Lonafarnib (SCH66336) in patients with chemorefractory, advanced squamous cell carcinoma of the head and neck. Am J Clin Oncol. 2009;3:274-279.

Iwasaki S, Iwasaki W, Takahashi M, Sakamoto A, Watanabe C, Shichino Y, Floor SN, Fujiwara K, Mito M, Dodo K, Sodeoka M, Imataka H, Honma T, Fukuzawa K, Ito T, Ingolia NT. The translation inhibitor rocaglamide targets a bimolecular cavity between eIF4A and polypurine RNA. Mol Cell. 2019;73:738-748.

Kim S, Salim AA, Swanson SM, Kinghorn AD. Potential of cyclopenta[*b*]benzofurans from Aglaia species in cancer chemotherapy. Anticancer Agents Med Chem. 2006;6:319-345.

Kim A, Pratilas CA. The promise of signal transduction in genetically driven sarcomas of the nerve. Exp Neurol. 2018;299(Pt B):317-325.

Kim A, Stewart DR, Reilly KM, Viskochil D, Miettinen MM, Widemann BC. Malignant Peripheral Nerve Sheath Tumors State of the Science: Leveraging Clinical and Biological Insights into Effective Therapies. Sarcoma. 2017;2017:7429697.

King ML, Chiang CC, Ling HC, Fujita E, Ochiai M, McPhail AT. X-ray crystal structure of

rocaglamide, a novel antileukemic 1*H*-cyclopenta[*b*]benzofuran from *Aglaia elliptifolia*. J Chem Soc, Chem Commun. 1982;20:1150-1151.

Kinghorn AD, DE Blanco EJ, Lucas DM, Rakotondraibe HL, Orjala J, Soejarto DD, Oberlies NH, Pearce CJ, Wani MC, Stockwell BR, Burdette JE, Swanson SM, Fuchs JR, Phelps MA, Xu L, Zhang X, Shen YY. Discovery of anticancer agents of diverse natural origin. Anticancer Res. 2016;36:5623-5637.

Kogure T, Kinghorn AD, Yan I, Bolon B, Lucas DM, Grever MR, Patel T. Therapeutic potential of the translation inhibitor silvestrol in hepatocellular cancer. PLoS One. 2013;8:e76136.

Liu T, Nair SJ, Lescarbeau A, Belani J, Peluso S, Conley J, Tillotson B, O'Hearn P, Smith S, Slocum K, West K, Helble J, Douglas M, Bahadoor A, Ali J, McGovern K, Fritz C, Palombella VJ, Wylie A, Castro AC, Tremblay MR. Synthetic silvestrol analogues as potent and selective protein synthesis inhibitors. J Med Chem. 2012;55:8859-8878.

Lucas DM, Edwards RB, Lozanski G, West DA, Shin JD, Vargo MA, Davis ME, Rozewski DM, Johnson AJ, Su BN, Goettl VM, Heerema NA, Lin TS, Lehman A, Zhang X, Jarjoura D, Newman DJ, Byrd JC, Kinghorn AD, Grever MR. The novel plant-derived agent silvestrol has B-cell selective activity in chronic lymphocytic leukemia and acute lymphoblastic leukemia *in vitro* and *in vivo*. Blood. 2009;113:4656-4666.

Maki RG, D'Adamo DR, Keohan ML, Saulle M, Schuetze SM, Undevia SD, Livingston MB, Cooney MM, Hensley ML, Mita MM, Takimoto CH, Kraft AS, Elias AD, Brockstein B, Blachère NE, Edgar MA, Schwartz LH, Qin LX, Antonescu CR, Schwartz GK. Phase II study of sorafenib in patients with metastatic or recurrent sarcomas. J Clin Oncol. 2009;27:3133-3140.

Malka-Mahieu H, Newman M, Désaubry L, Robert C, Vagner S. Molecular Pathways: The

eIF4F Translation Initiation Complex-New Opportunities for Cancer Treatment. Clin Cancer Res. 2017;23:21-25.

Mamane Y, Petroulakis E, LeBacquer O, Sonenberg N. mTOR, translation initiation and cancer. Oncogene. 2006;25:6416-6422.

Oblinger JL, Burns SS, Akhmametyeva EM, Huang J, Pan L, Ren Y, Shen R, Miles-Markley B, Moberly AC, Kinghorn AD, Welling DB, Chang L-S. Components of the eIF4F complex are potential therapeutic targets for malignant peripheral nerve sheath tumors and vestibular schwannomas. Neuro-Oncol. 2016;18:1265-1277.

Oblinger JL, Burns SS, Huang J, Pan L, Ren Y, Shen R, Kinghorn AD, Welling DB, Chang LS. Overexpression of eIF4F components in meningiomas and suppression of meningioma cell growth by inhibiting translation initiation. Exp Neurol. 2018;299(Pt B):299-307.

Pan L, Acuña UM, Li J, Jena N, Ninh TN, Pannell CM, Chai H, Fuchs JR, Carcache de Blanco EJ, Soejarto DD, Kinghorn AD. Bioactive flavaglines and other constituents isolated from *Aglaia perviridis*. J Nat Prod. 2013;76:394-404.

Pan L, Woodard JL, Lucas DM, Fuchs JR, Kinghorn, AD. Rocaglamide, silvestrol, and related bioactive compounds from *Aglaia* species. Nat Prod Rep. 2014:31;924-931.

Perrone F, Da Riva L, Orsenigo M, Losa M, Jocollè G, Millefanti C, Pastore E, Gronchi A, Pierotti MA, Pilotti S. PDGFRA, PDGFRB, EGFR, and downstream signaling activation in malignant peripheral nerve sheath tumor. Neuro Oncol. 2009;11:725-736.

Polier G, Neumann J, Thuaud F, Ribeiro N, Gelhaus C, Schmidt H, Giaisi M, Köhler R, Müller WW, Proksch P, Leippe M, Janssen O, Désaubry L, Krammer PH, Li-Weber M. The natural anticancer compounds rocaglamides inhibit the Raf-MEK-ERK pathway by targeting prohibitin 1 and 2**.** Chem Biol. 2012;19:1093-1104**.**

Rao S, Cunningham D, de Gramont A, Scheithauer W, Smakal M, Humblet Y, Kourteva G, Iveson T, Andre T, Dostalova J, Illes A, Belly R, Perez-Ruixo JJ, Park YC, Palmer PA. Phase III double-blind placebo-controlled study of farnesyl transferase inhibitor R115777 in patients with refractory advanced colorectal cancer. J Clin Oncol. 2004;22:3950-3957.

Sadlish H, Galicia-Vazquez G, Paris CG, Aust T, Bhullar B, Chang L, Helliwell SB, Hoepfner D, Knapp B, Riedl R, Roggo S, Schuierer S, Studer C, Porco JA Jr, Pelletier J, Movva NR. Evidence for a functionally relevant rocaglamide binding site on the eIF4A-RNA complex. ACS Chem Biol. 2013;8:1519-1527.

Sankar S, Bell R, Stephens B, Zhuo R, Sharma S, Bearss DJ, Lessnick SL. Mechanism and relevance of EWS/FLI-mediated transcriptional repression in Ewing sarcoma. Oncogene. 2013;32:5089-5100.

Saradhi UV, Gupta SV, Chiu M, Wang J, Ling Y, Liu Z, Newman DJ, Covey JM, Kinghorn AD, Marcucci G, Lucas DM, Grever MR, Phelps MA, Chan KK. Characterization of silvestrol pharmacokinetics in mice using liquid chromatography-tandem mass spectrometry. AAPS J. 2011;13:347-56.

Sebti SM, Tkalcevic GT, Jani JP. Lovastatin, a cholesterol biosynthesis inhibitor, inhibits the growth of human H-ras oncogene transformed cells in nude mice. Cancer Commun. 1991;3:141-147.

Skapek SX, Ferrari A, Gupta AA, Lupo PJ, Butler E, Shipley J, Barr FG, Hawkins DS. Rhabdomyosarcoma. Nat Rev Dis Primers. 2019;5:1.

Smith R, Owen LA, Trem DJ, Wong JS, Whangbo JS, Golub TR, Lessnick SL. Expression profiling of EWS/FLI identifies NKX2.2 as a critical target gene in Ewing's sarcoma. Cancer Cell. 2006;9:405-416.

Tap WD, Demetri G, Barnette P, Desai J, Kavan P, Tozer R, Benedetto PW, Friberg G, Deng H, McCaffery I, Leitch I, Badola S, Chang S, Zhu M, Tolcher A. Phase II study of ganitumab, a fully human anti-type-1 insulin-like growth factor receptor antibody, in patients with metastatic Ewing family tumors or desmoplastic small round cell tumors. J Clin Oncol. 2012;30:1849-1856.

Widemann BC, Meyer CF, Cote GM, Chugh R, Milhem MM, Van Tine BA, Kim A, Turpin B, Dombi E, Jayaprakash N, Okuno SH, Helman LJ, Onwudiwe N, Steinberg SM, Reinke DK, Cichowski K, and Perentesis JP. SARC016: phase II study of everolimus in combination with bevacizumab in sporadic and neurofibromatosis type 1 (NF1) related refractory malignant peripheral nerve sheath tumors (MPNST). J Clin Oncol. 2016;34(15_suppl):11053-11053.

Wiegering A, Uthe FW, Jamieson T, Ruoss Y, Hüttenrauch M, Küspert M, Pfann C, Nixon C, Herold S, Walz S, Taranets L, Germer CT, Rosenwald A, Sansom OJ, Eilers M. Targeting translation initiation bypasses signaling crosstalk mechanisms that maintain high MYC levels in colorectal cancer. Cancer Discov. 2015;5:768-781.

Wolfe AL, Singh K, Zhong Y, Drewe P, Rajasekhar VK, Sanghvi VR, Mavrakis KJ, Jiang M, Roderick JE, Van der Meulen J, Schatz JH, Rodrigo CM, Zhao C, Rondou P, de Stanchina E, Teruya-Feldstein J, Kelliher MA, Speleman F, Porco JA Jr, Pelletier J, Rätsch G, Wendel HG. RNA G-quadruplexes cause eIF4A-dependent oncogene translation in cancer. Nature. 2014;513:65-70.

Yang J, Ylipää A, Sun Y, Zheng H, Chen K, Nykter M, Trent J, Ratner N, Lev DC, Zhang W. Genomic and molecular characterization of malignant peripheral nerve sheath tumor identifies the IGF1R pathway as a primary target for treatment. Clin Cancer Res.

2011;17(24):7563-73.

Figure Legends

Figure 1. Identification of didesmethylrocaglamide and rocaglamide with potent growth-inhibitory activity comparable to silvestrol. The structure of each rocaglate is shown along with its IC_{50} value in STS26T MPNST cells as determined in Table 1. Structure-activity comparison revealed that the dioxanyl (dioxanyloxy) ring is dispensable but may enhance the cytotoxicity of rocaglates. An unmethylated C-8b hydroxyl group (arrow) and the amide functionality (rectangle) of didesmethylrocaglamide and rocaglamide are important for optimum antiproliferative activity, while methylation of the C-8b hydroxyl group (oval) substantially impaired the activity.

Figure 2. DDR and Roc increase caspase and PARP cleavage and elevate the levels of γH2A.X while decreasing AKT and ERK expression in MPNST cells. (A) Protein lysates prepared from STS26T cells treated for 3 days with 1- or 2-IC_{50} of DDR or Roc were analyzed by Western blots for caspase-3/7, PARP, AKT, ERK1/2, and GAPDH as a loading control. (B) Protein lysates from STS26T cells treated for 1 and 2 days with 1- or 2-IC_{50} of DDR were probed for the expression of phosphorylated H2A.X (γH2A.X). As a positive control, lysates from HMS-97 human malignant schwannoma cells irradiated with 4 Grays (Gy) of X-ray were used.

Figure 3. Unlike silvestrol, DDR and Roc inhibits proliferation of MDR1-overexpressing 697-R leukemic cells at IC_{50} values similar to parental 697 cells. Cell proliferation was measured on 697-R and 697 cells treated for 3 days with various concentrations of silvestrol (A), DDR (B), and Roc (C). Each treatment was performed in six replicates, and each experiment was repeated twice. Shown are representative dose-response growth inhibition

curves for all three drugs from experiments run in parallel. The insets show the IC_{50} values for each compound.

Figure 4. Roc has 50% oral bioavailability and potently suppresses the growth of orthotopic MPNST xenografts. (A) Plasma concentration-time profiles of Roc were obtained by PK analysis according to Methods. The mean concentration of Roc with standard deviation (SD) in mouse plasma for each time point after IV, IP, and PO administration was plotted. For each dosing route, two independent studies were performed. (B) Shown are representative BL images of ST8814-Luc MPNST-bearing mice prior to (PreTx) and 4 weeks (wks) after treatment with Roc at 4mg/kg by IP, 1.2mg/kg by PO, or HPβCD vehicle every other day. (C) The relative tumor-emitted BL signals were denoted as % of total flux after treatment relative to the total flux prior to treatment designated as one (100%). The data are shown as mean ± SD. For each treatment group, at least 7 mice completed the full treatment schedule. Note that tumor bioluminescence from vehicle-treated mice rapidly increased by an average of ~17,000-fold over four weeks. However, tumor bioluminescence from the Roc IP group grow only by ~3-fold and from the Roc PO group increased ~470-fold on average. (D) H&E staining show that while vehicle-treated xenografts contained large vesicular nuclei with prominent nucleoli and mitotic activity, tumors treated with Roc by IP had pleomorphic nuclei and many enlarged tumor cells had abundant foamy cytoplasm resembling histiocytoid degenerative changes along with scattered apoptosis (top panels). Degenerative tumor cells were also present in tumors treated with orally-delivered Roc. Tumor necrosis with necrotic debris separating mostly degenerative tumor cells with viable vasculature was also observed. Immunostaining revealed abundant phospho-histone H3 (pH3)-labeled cells in Roc-treated tumors compared to vehicle-treated

tumors (middle panels). Increased numbers of cleaved caspase-3 (CC3)-positive cells were detected in Roc-treated tumors (bottom panels).

Figure 5. Roc exhibits potent anti-tumor effects in multiple sarcoma PDX models. Mice with growing Ewing sarcoma (A), osteosarcoma (B), and rhabdomyosarcoma (C) PDXs were treated with 3mg/kg of Roc or HPβCD vehicle by IP every other day. Tumor diameters were measured twice weekly and volumes calculated according to Methods. The normalized tumor volume, denoted as the ratio of the calculated tumor volume after treatment relative to the volume prior to treatment designated as one, was plotted as the mean tumor volume of the entire treatment group at each time point with SD (A, C, and E). The calculated tumor volume for each individual mouse over time was also plotted (B, D, and F).

Figure 6. DDR and Roc reduce multiple signaling proteins important for sarcoma cell growth and survival. Protein lysates from TC32 Ewing sarcoma (A), 143B osteosarcoma (B), and RD rhabdomyosarcoma (C) cells treated for 1 and 2 days with the indicated concentrations of DDR or Roc were analyzed by Western blotting for various oncogenic driver proteins. GAPDH was used as a loading control.

Supplementary Figure Legends

Supplementary Figure S1. Dose-response growth inhibition curves of DDR and Roc in MPNST cells. *NF1*-expressing STS26T (blue lines) and *NF1*-deficient ST8814 (red lines) MPNST cells were treated with various concentrations of DDR or Roc, followed by determination of cell proliferation as described in Methods. Experiments were performed in six replicates and were repeated three times. Data shown are the mean of replicates from one representative experiment for each cell line and compound. The graph inset shows the mean IC_{50} values derived from three independent experiments.

Supplementary Figure S2. DDR and Roc induce G_2/M arrest and increase sub-G_1 fraction in MPNST cells. (A) STS26T cells were treated with the indicated concentrations of DDR and Roc for three days, and phase-contrast images of treated cells were taken, followed by cell harvesting for flow cytometry analysis as described in Methods. Cell-cycle histograms of propidium iodide-labeled cells revealed a prominent increase in the G_2/M and sub-G_1 peaks after treatment. (B-C) Flow cytometry analysis and phase-contrast images of ST8814 cells treated with DDR or Roc for three (B) or six days (C) were conducted and showed an increased G_2/M fraction in treated cells. Also, a large increase in the sub-G_1 fraction was observed in cells treated for six days.

Supplementary Figure S3. Expression of the MDR1/Pgp protein in 697 and 697-R leukemic cells, various MPNST cell lines (ST8814, STS26T, S462, and T265), and primary human Schwann cells. Western blot analysis was conducted as described in Methods. GAPDH was used as a loading control.

Supplementary Figure S4. DDR and Roc possess potent growth inhibitory activities against various Ewing sarcoma, osteosarcoma, and rhabdomyosarcoma cell lines. Cell proliferation assays were performed on the osteosarcoma cell lines 143B, MG-63, Saos2, and OS17 (A), the Ewing sarcoma cell lines A673 and TC32 (B), and the rhabdomyosarcoma cell line RD (C) treated with various concentrations of DDR (squares) or Roc (triangles) according to Methods. Each treatment was conducted in six replicates and the mean of replicates was calculated and used to generate the dose-response growth inhibition curve. Shown are representative curves for each cell line and treatment. The graph inset show the mean IC_{50} values derived from two independent experiments.

Supplementary Figure S5. DDR and Roc decrease the expression of IGF-1R, AKT and ERKs in MPNST cells. Protein lysates prepared from ST8814 cells treated for 3 days with 1- or 2-IC_{50} of DDR or Roc were analyzed by Western blots as described in Methods. GAPDH served as a loading control.

Supplementary Methods

Cell lines

The human MPNST cell lines (ST8814, STS26T, S462, T265, and luciferase-expressing ST8814-Luc), the human *NF2*-deficient meningioma cell line Ben-Men-1, the *Nf2*$^{-/-}$ mouse schwannoma cell line Sch10545, and primary human Schwann cells were propagated as previously described (Burns et al., 2013; Burns and Chang, 2016; Oblinger et al., 2016, 2018). The Ewing sarcoma cell line A673 and the osteosarcoma cell lines, 143B and MG-63, were grown in Dulbecco's Modified Eagle's (DME) medium (Millipore-Sigma) supplemented with 10% fetal bovine serum (FBS; Atlanta Biological). The silvestrol-sensitive 697 and silvestrol-resistant 697-R pre-B acute lymphoblastic leukemia cells (Gupta et al., 2011), the Ewing sarcoma cell line TC32, the osteosarcoma cell lines, Saos2 and OS17, and the rhabdomyosarcoma cell line RD were cultivated in RPMI 1640 medium (Millipore-Sigma) plus 10% FBS.

Cell Proliferation Assays and Flow Cytometry

Actively-growing cells were seeded in 96-well plates (Sarstedt) at 2,000 cells/well for Ben-Men-1 and RD cells, 30,000 cells/well for 697 and 697-R cells, and 4,000 cells/well for all other cell lines. The following day, cells were treated with various concentrations of each compound or and 0.05% of DMSO as the control for six days for MG-63 cells or three days for all remaining cell lines. Cell proliferation was assessed using resazurin assays and the IC_{50} value calculated (Oblinger et al., 2016). Cell cycle analysis was performed as previously described (Burns et al., 2013).

Western Blots

Subconfluent cells were treated with the indicated doses of Roc or DDR for 1-3 days and then harvested in cell lysis buffer (Cell Signaling Technology) containing 1 mM phenylmethylsufonylfluoride and protease inhibitor cocktail (Sigma-Aldrich). The protein content in cleared lysates was quantitated using the microBCA assay (ThermoFisher). Equal amounts of protein were run in sodium dodecyl sulfate-polyacrylamide gels and electrotransferred onto Immobilon-FL PVDF membranes (Millipore). The antibodies used were directed against: AKT (#9272), caspase-3 (#9662), caspase-7 (#9492), cleaved caspase-7 (#9491), ERK1/2 (#4695), glyceraldehyde-3-phosphate dehydrogenase (GAPDH; #5174), phospho-histone H2A.X (pH2A.X[Ser^{139}]; #9718), insulin-like growth factor-1 receptor β subunit (IGF-1Rβ; #9750), MDR1/ABCB1 (#13978), poly(ADP-ribose) polymerase (PARP; #9532), and cleaved PARP (#5625; all from Cell Signaling Technology), LSD1 (sc-136174), NKX2.2 (sc-514161), and survivin (sc-17779; Santa Cruz Biotechnology), and cleaved caspase-3 (CC3; ab32042) and FLI1 (ab15289; Abcam). Protein bands were detected using IRDye® infrared fluorescent dye-labeled secondary antibodies and scanning on an Odyssey CLx imaging system (LI-COR Biosciences) using the appropriate fluorescent channel at a resolution of 84 μm.

Pharmacokinetic (PK) analysis

Mice were administered with a 5 mg/kg dose of Roc by intravenous (IV) or intraperitoneal injection (IP) or by oral gavage (PO). Blood samples were collected prior to and at multiple indicated time-points after dosing (n = 3). Plasma samples were obtained by centrifugation and stored at -80ºC. To measure plasma concentrations of Roc, a sensitive liquid chromatography coupled with tandem mass spectrometry (LC/MS-MS) detection method was developed. The

reference compounds Roc (NSC326408) and pipernyl rocaglate (NSC784086) were provided by the NCI Developmental Therapeutics Program with pipernyl rocaglate used as the internal standard for quantitation. Plasma samples were processed by taking 100 µl of plasma and adding 300 µl of methanol containing 0.05 µM of internal standard. The samples were vortexed and centrifuged at 10,000xg for 10 min. The supernatant was collected and evaporated to dryness. Dried samples were reconstituted in 100 µl of 1:1 water:acetonitrile and centrifuged at 10,000xg for 3 min, followed by injecting 10 µl into an HPLC instrument. Compounds of interest were separated on a Kinetex EVO C18 column (150 x 2.1 mm) with a flow rate of 0.25 ml/min. Mobile phase consisted of 80% ammonium formate (1 g/L) and 20% acetonitrile at the start of the run, and a linear gradient to 10% ammonium formate/90% acetonitrile was applied over 14 min. Roc and the internal standard were identified by MS/MS using a Thermo Vantage TSQ run in positive ion mode. The transitions used were m/z 506 to m/z 352 (Roc) and m/z 570 to m/z 450 (internal standard). Standard curves constructed in blank mouse plasma were found to be linear over the range of 0.001 µM (Limit of Quantitation) to 2.5 µM of Roc. Samples found to be above 2.5 µM of Roc were reanalyzed after dilution with blank plasma. Absolute recoveries of Roc from plasma were >98%. Areas under the curve (AUC) estimations were made manually using the trapezoidal method of integration.

Orthotopic Cell Line-Derived Xenograft (CDX) and Patient-Derived Xenograft (PDX) Models and In Vivo Efficacy

All animal work was performed according to the protocols approved by the Institutional Animal Care and Use Committee at Nationwide Children's Hospital. For animal dosing, Roc was formulated in 30% hydroxypropyl-β-cyclodextrin (HPβCD; CTD, Inc.). To generate the

orthotopic MPNST CDX model, ST8814-Luc cells were injected into the sciatic nerves of NSG mice (*NOD.Cg-Prkdc^{scid} Il2rg^{tmlWjl}/SzJ*; The Jackson Laboratory), followed by bioluminescence imaging (BLI) to monitor tumor growth (Burns and Chang, 2016). Mice bearing established ST8814-Luc tumors, as defined by increasing bioluminescence signals over at least two time points (Burns et al., 2013), were randomized into three groups (n = 10/group) and treated with the predetermined maximum tolerated dose (MTD) of Roc at 4 mg/kg by IP or 1.2 mg/kg by oral gavage, or the vehicle HPβCD every other day. Tumor growth was measured weekly by BLI. Following 4 weeks of treatment, tumors were harvested for histological analysis.

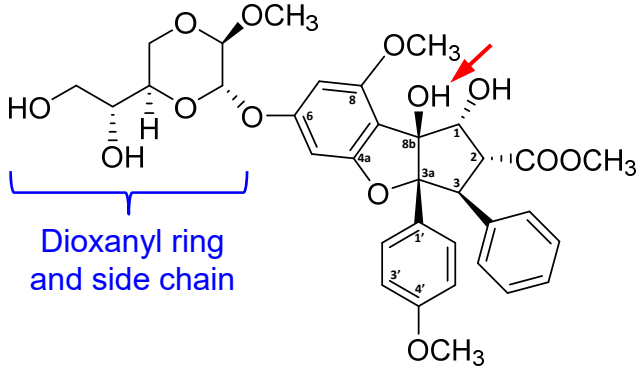
To generate PDX models, the Nationwide Children's Hospital Institutional Review Board approved the Human Subjects Protocol for the acquisition of surgically-removed tumor specimens from patients and informed patient consents were obtained. Shortly after resection, fresh tumor tissues with their histological types confirmed by a specialized pathologist were placed in Dulbecco's-modified Eagle (DME) medium (Invitrogen) and brought to the research laboratory. A piece of tumor fragment was implanted subcutaneously on the dorsal right flank area in an eight-to-ten week-old immunodeficient mouse under anesthesia. Tumors were allowed to grow until established, at which time the established PDX tumors were repeatedly passed from one animal to the next or cryopreserved. For Roc treatment, actively-growing PDXs for a Ewing sarcoma (NCH-EWS-2), an osteosarcoma (NCH-OS-7), and an alveolar rhabdomyosarcoma (NCH-ARMS-2) were excised and cut into 5-mm pieces. Each tumor piece was re-implanted into an NSG mouse and tumor growth was monitored. Once noted, the tumor sizes in the axial plane at its greatest dimension (L) and the orthogonal short dimension (S) were measured twice weekly using a Fowler Ultra-Cal Electronic Caliper. Approximated tumor volumes were calculated using the formula $V = (L \times S^2)/2$. Mice with growing tumors reaching ~100-200 mm^3

were randomized into two treatment groups (10 mice/group) for each PDX model and treated with 3mg/kg of Roc or HPβCD by IP every other day, followed by tumor measurement twice weekly.

Table 1. The growth-inhibitory activity of silvestrol and 10 related rocaglates lacking the dioxanyl ring in *NF1*$^{+/+}$ STS26T and *NF1*$^{-/-}$ ST8814 MPNST, *Nf2*$^{-/-}$ schwannoma, and *NF2*$^{-/-}$ meningioma cells. The average IC_{50} value of each rocaglate was determined by 3-day resazurin proliferation assays as described in Methods. Didesmethylrocaglamide (DDR) and rocaglamide (Roc) were found to possess growth-inhibitory activity similar to or more potent than silvestrol. ND, not determined.

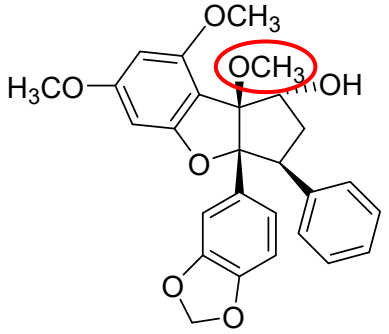
Compound	MW (Da)	IC_{50} (nM)			
		Sch10545 *Nf2*$^{-/-}$ schwannoma cells	**Ben-Men-1** *NF2*$^{-/-}$ meningioma cells	**STS26T** *NF1*$^{+/+}$ MPNST cells	**ST8814** *NF1*$^{-/-}$ MPNST cells
Silvestrol	**654**	**70**	**10**	**10**	**40**
8b-*O*-methyl-4'-demethoxy-3',4'-methylenedioxyrocaglaol	**462**	**>2,500**	**>2,500**	**5,000**	**10,000**
Methyl 8b-*O*-methyl-4'-demethoxy-3',4'-methylenedioxyrocaglate	**520**	**1,900**	**3,800**	**1,300**	**2,000**
Rocaglaol	**434**	**60**	**100**	**40**	**90**
Methyl rocaglate	**492**	**50**	**55**	**25**	**35**
4'-demethoxy-3',4'-methylenedioxyrocaglaol	**448**	**65**	**85**	**55**	**120**
Methyl 4'-demethoxy-3',4'-methylenedioxyrocaglate	**506**	**60**	**80**	**35**	**70**
8b-*O*-methylrocaglaol	**448**	**>20,000**	**>20,000**	**>20,000**	**>20,000**
Didesmethylrocaglamide	**477**	**10**	**5**	**5**	**5**
Methyl 8b-*O*-methylrocaglate	**506**	**9,300**	**>10,000**	**≥10,000**	**>20,000**
Rocaglamide	**506**	**ND**	**15**	**15**	**20**

Figure 1



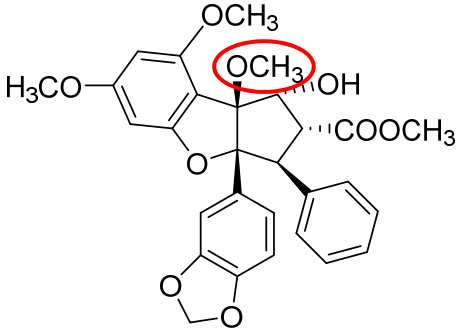
Silvestrol
(MW = 654)

IC_{50} = 10 nM



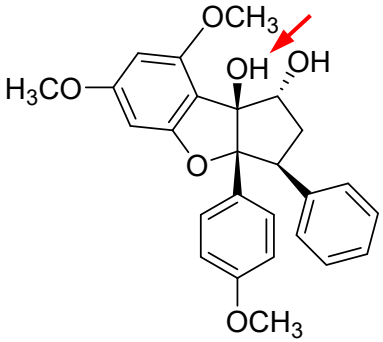
8b-*O*-methyl-4'-demethoxy-3',4'-methylenedioxyrocaglaol
(MW = 462)

5000 nM



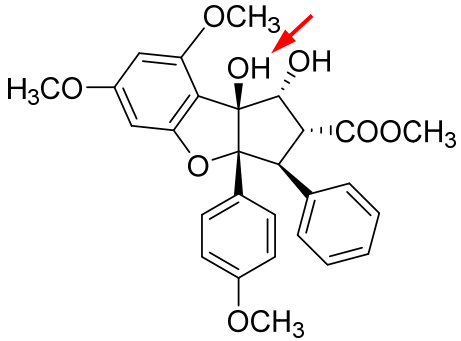
Methyl 8b-*O*-methyl-4'-demethoxy-3',4'-methylenedioxyrocaglate
(MW = 520)

1300 nM



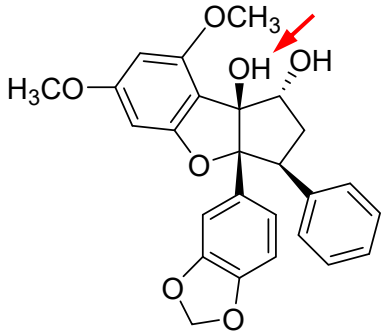
Rocaglaol
(MW = 434)

40 nM



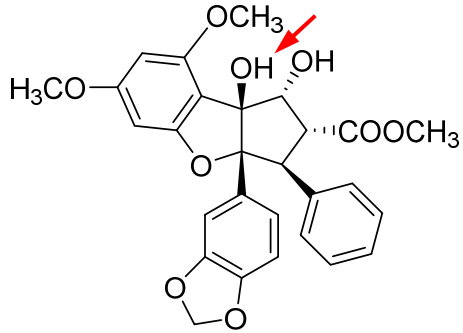
Methyl rocaglate
(MW = 492)

25 nM



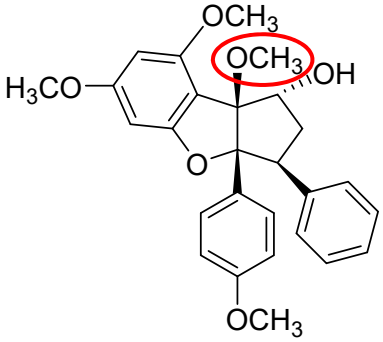
4'-demethoxy-3',4'-methylenedioxyrocaglaol
(MW = 448)

55 nM



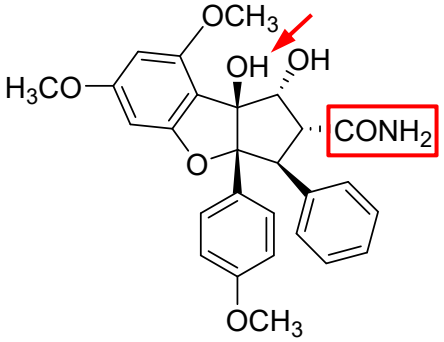
Methyl 4'-demethoxy-3',4'-methylenedioxyrocaglate
(MW = 506)

35 nM



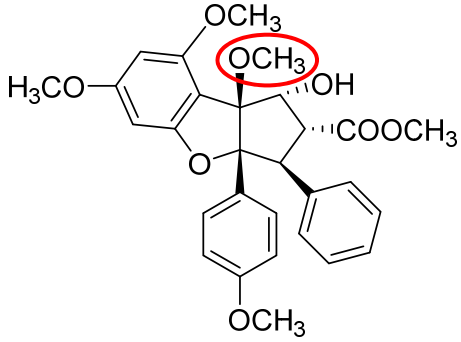
8b-*O*-methylrocaglaol
(MW = 448)

>20,000 nM



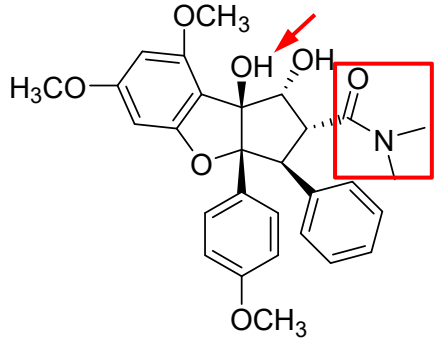
Didesmethylrocaglamide
(MW = 477)

5 nM



Methyl 8b-*O*-methylrocaglate
(MW = 506)

≥10,000 nM



Rocaglamide (MW = 506)

15 nM

Figure 2A

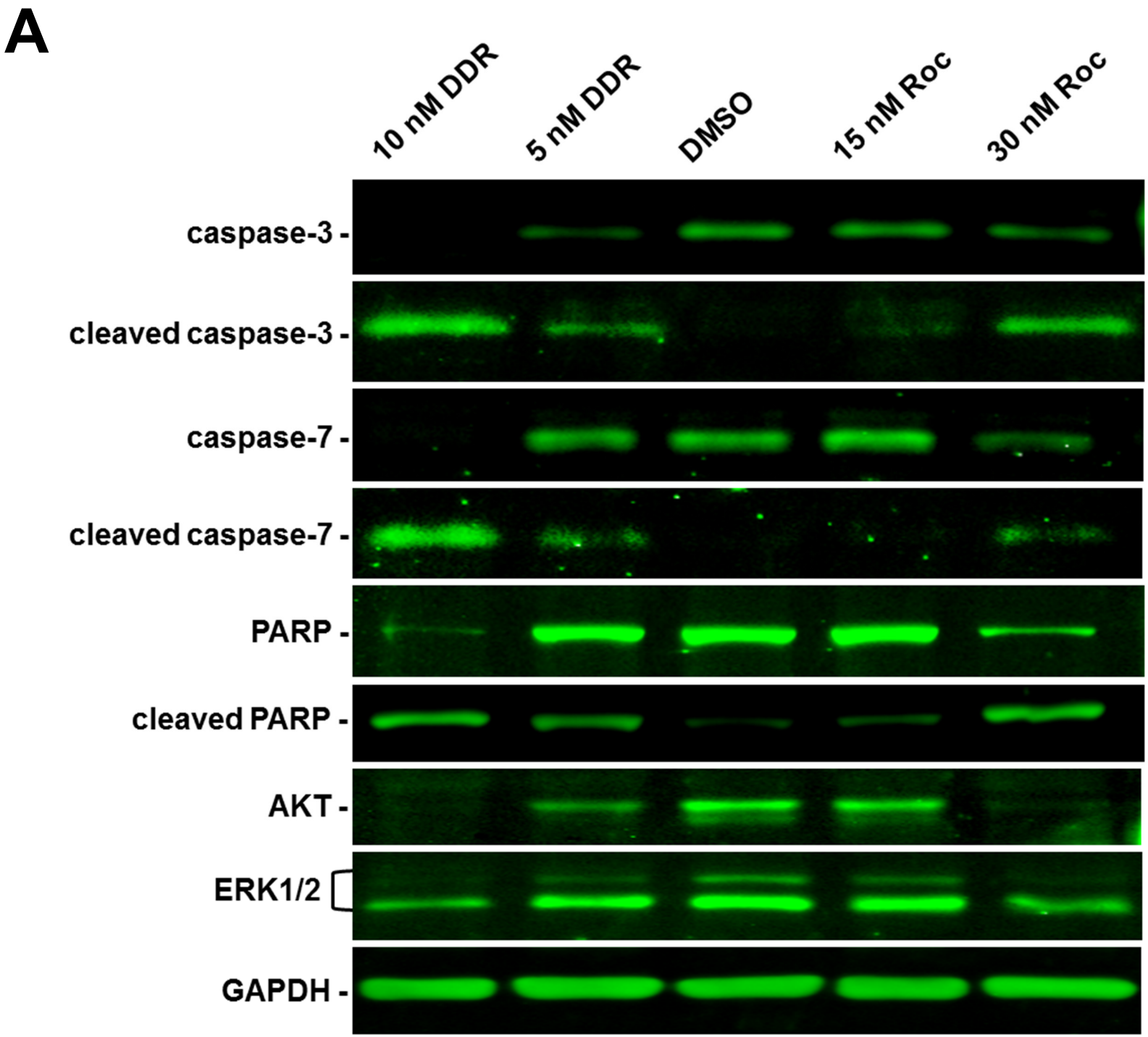

A
10 nM DDR
5 nM DDR
DMSO
15 nM Roc
30 nM Roc
caspase-3 -
cleaved caspase-3 -
caspase-7 -
cleaved caspase-7 -
PARP -
cleaved PARP -
AKT -
ERK1/2
GAPDH -

Figure 2B

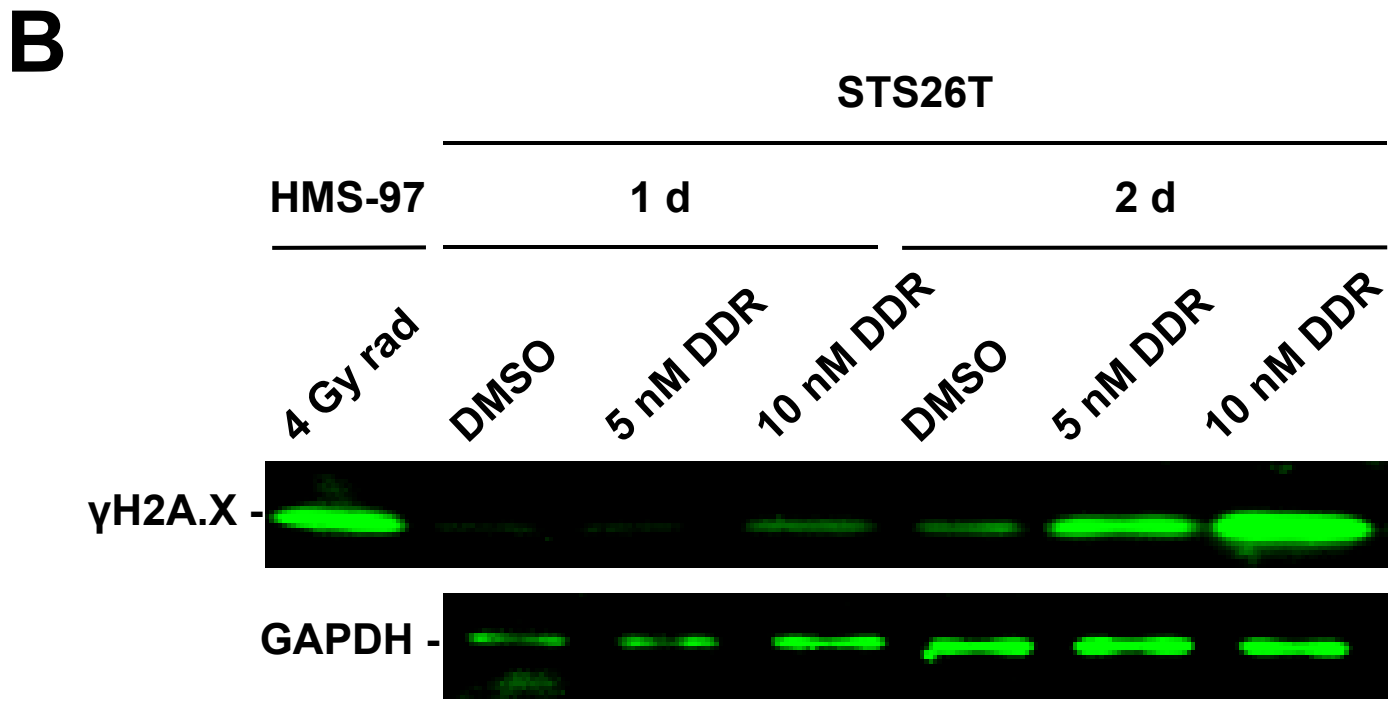

B
STS26T
HMS-97
1 d
2 d
4 Gy rad
DMSO
5 nM DDR
10 nM DDR
DMSO
5 nM DDR
10 nM DDR
γH2A.X -
GAPDH -

Figure 3

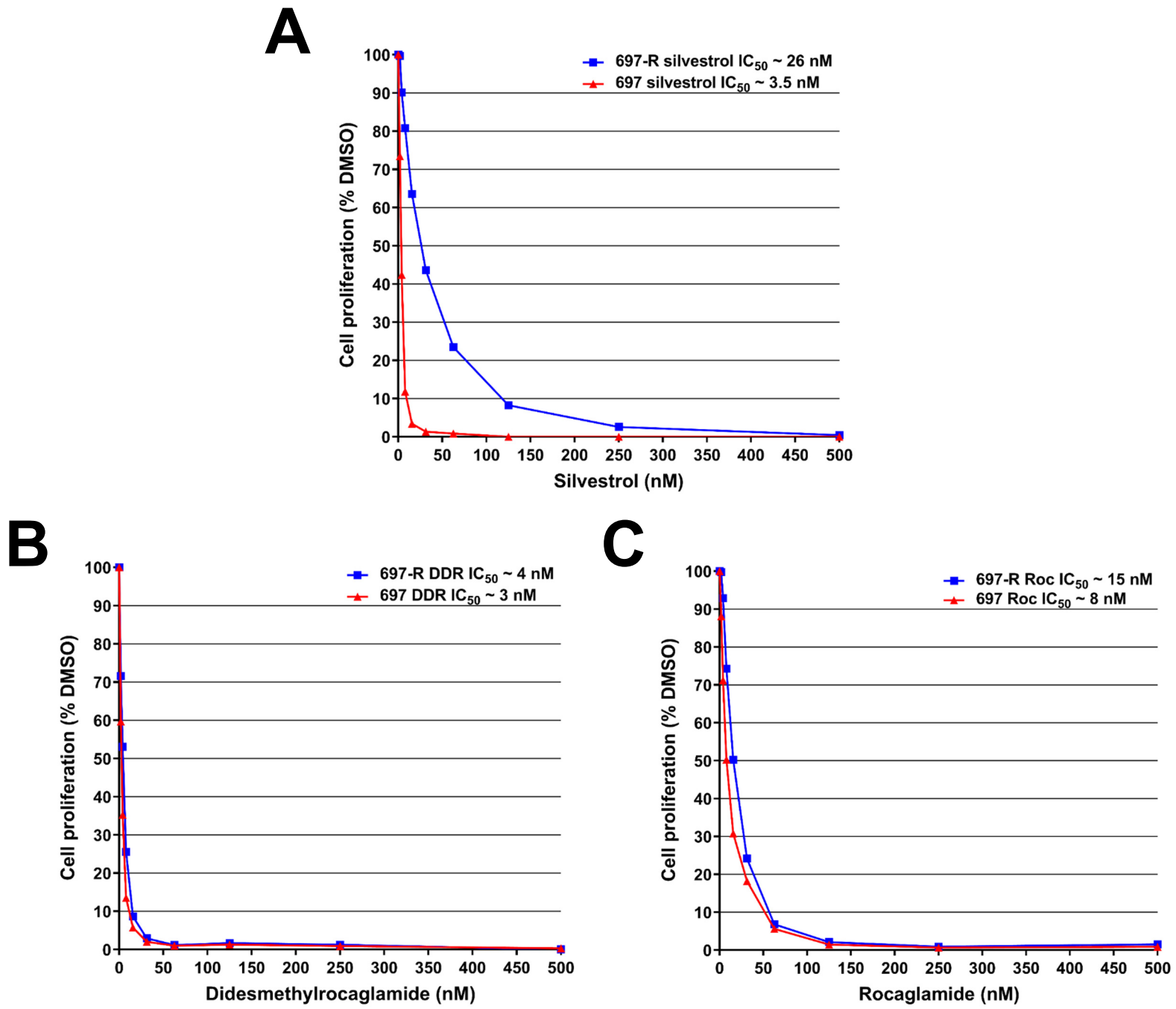

A
697-R silvestrol IC50 ~ 26 nM
697 silvestrol IC50 ~ 3.5 nM
Cell proliferation (% DMSO)
Silvestrol (nM)
B
697-R DDR IC50 ~ 4 nM
697 DDR IC50 ~ 3 nM
Cell proliferation (% DMSO)
Didesmethylrocaglamide (nM)
C
697-R Roc IC50 ~ 15 nM
697 Roc IC50 ~ 8 nM
Cell proliferation (% DMSO)
Rocaglamide (nM)

Figure 4ABC

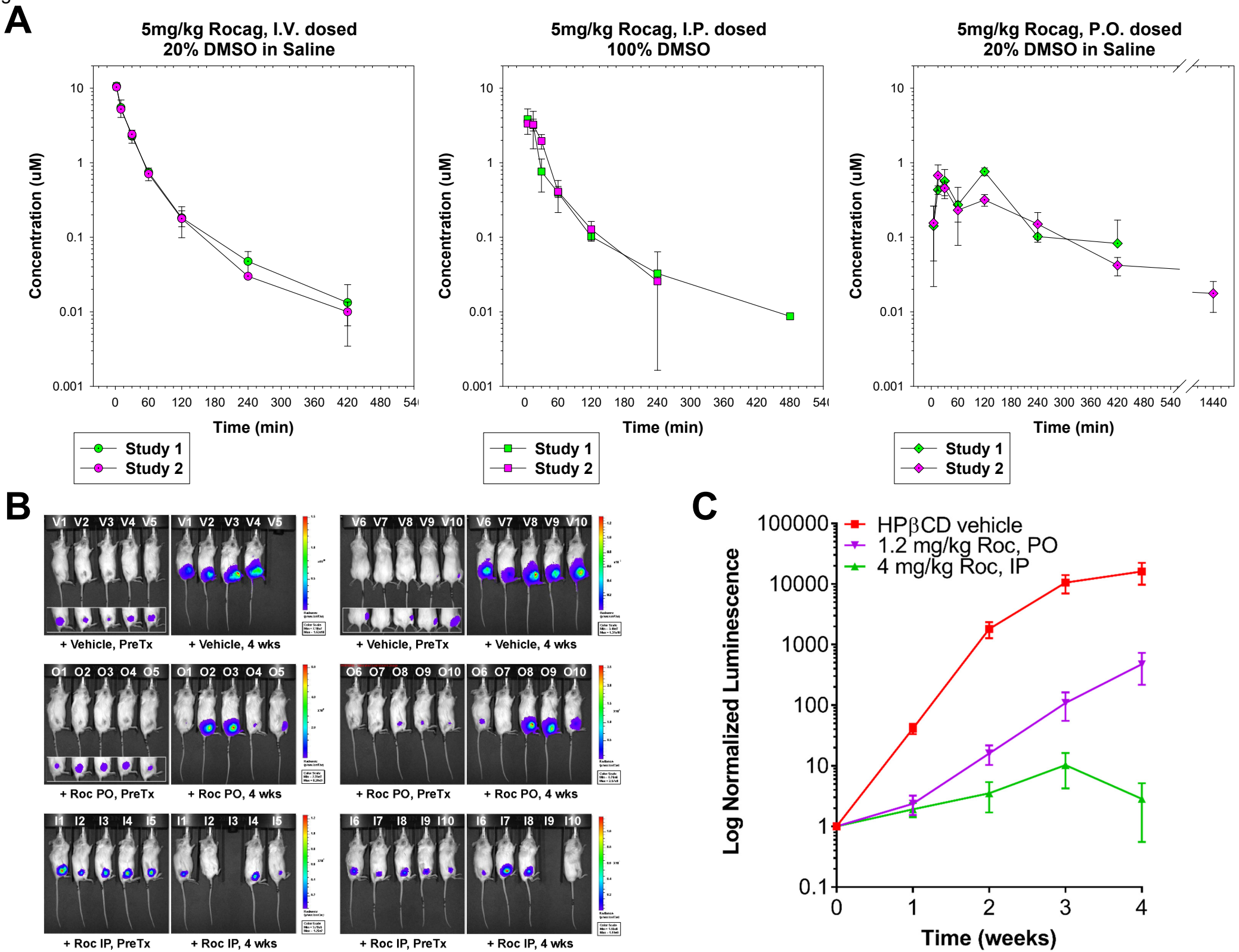

A
5mg/kg Rocag, I.V. dosed
20% DMSO in Saline
5mg/kg Rocag, I.P. dosed
100% DMSO
5mg/kg Rocag, P.O. dosed
20% DMSO in Saline
Concentration (uM)
Time (min)
Study 1
Study 2
B
+ Vehicle, PreTx
+ Vehicle, 4 wks
+ Roc PO, PreTx
+ Roc PO, 4 wks
+ Roc IP, PreTx
+ Roc IP, 4 wks
C
HPβCD vehicle
1.2 mg/kg Roc, PO
4 mg/kg Roc, IP
Log Normalized Luminescence
Time (weeks)

Figure 4D

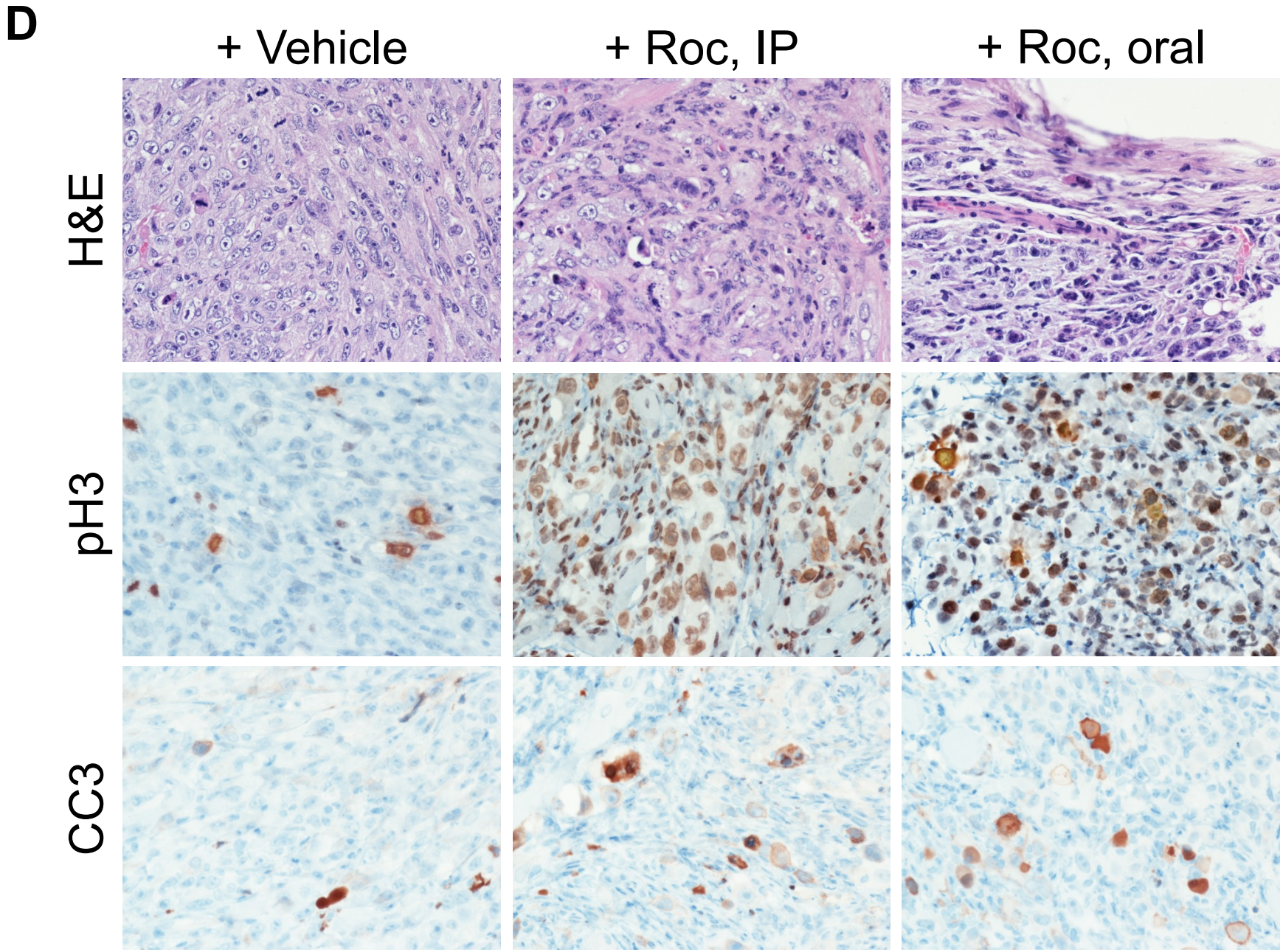
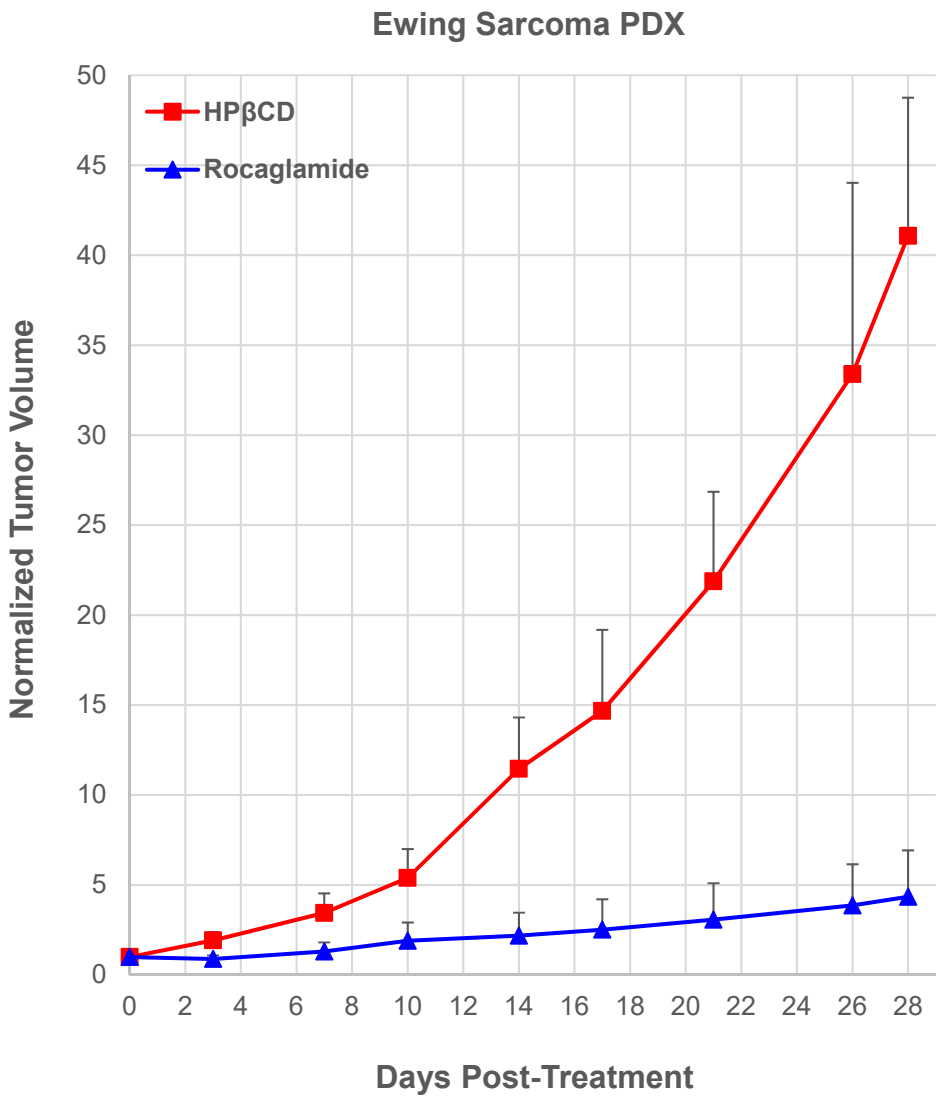


Figure 5A


Ewing Sarcoma PDX
HPβCD
Rocaglamide
Normalized Tumor Volume
Days Post-Treatment
0
5
10
15
20
25
30
35
40
45
50
0 2 4 6 8 10 12 14 16 18 20 22 24 26 28

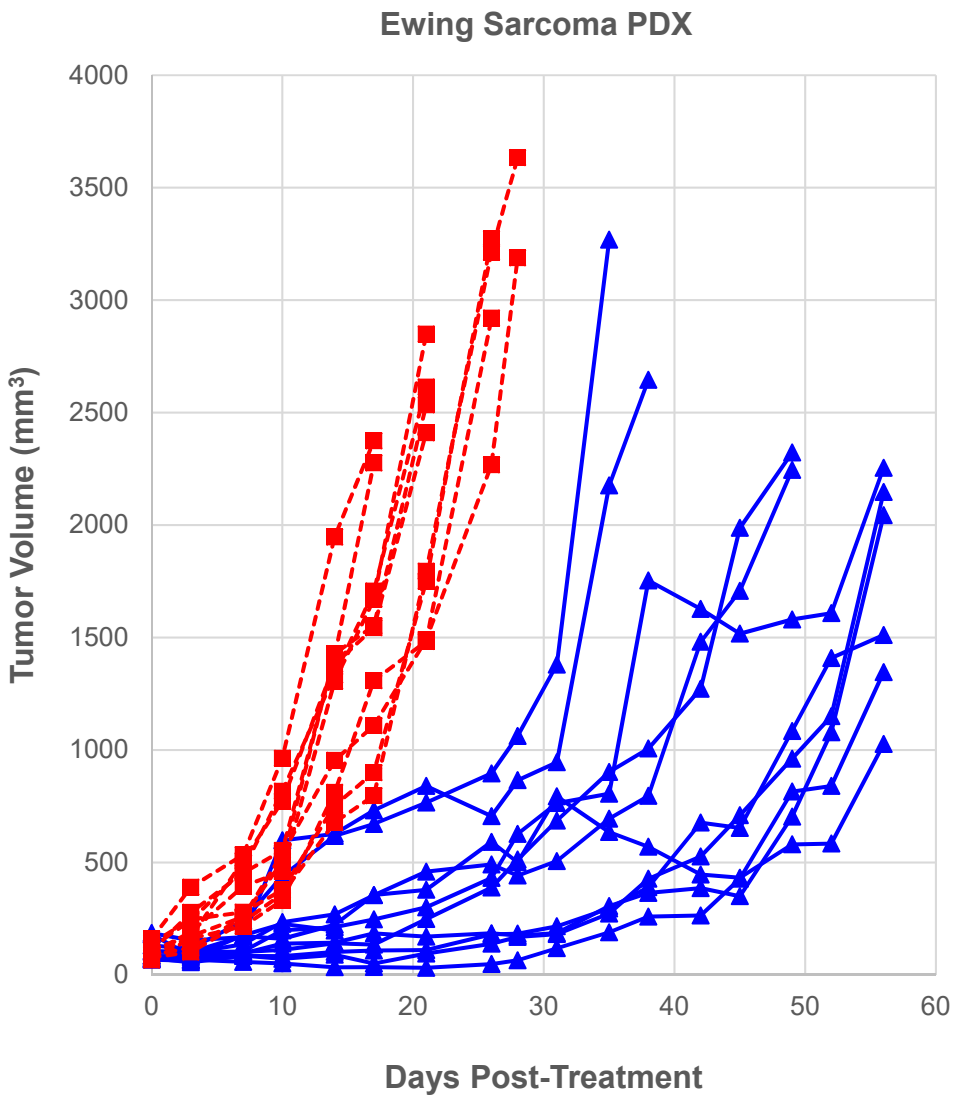
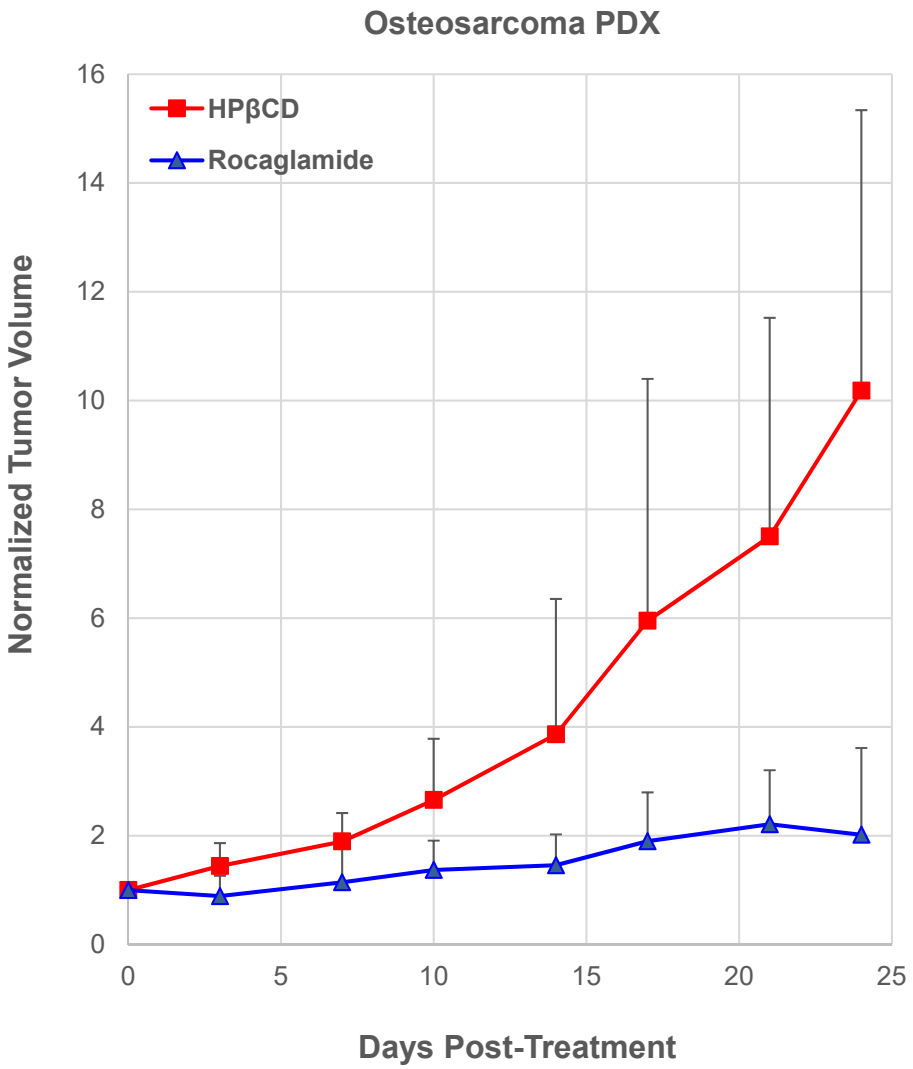

Ewing Sarcoma PDX
Tumor Volume (mm³)
Days Post-Treatment
0
500
1000
1500
2000
2500
3000
3500
4000
0 10 20 30 40 50 60

Figure 5B


Osteosarcoma PDX
HPβCD
Rocaglamide
Normalized Tumor Volume
Days Post-Treatment
0
2
4
6
8
10
12
14
16
0
5
10
15
20
25

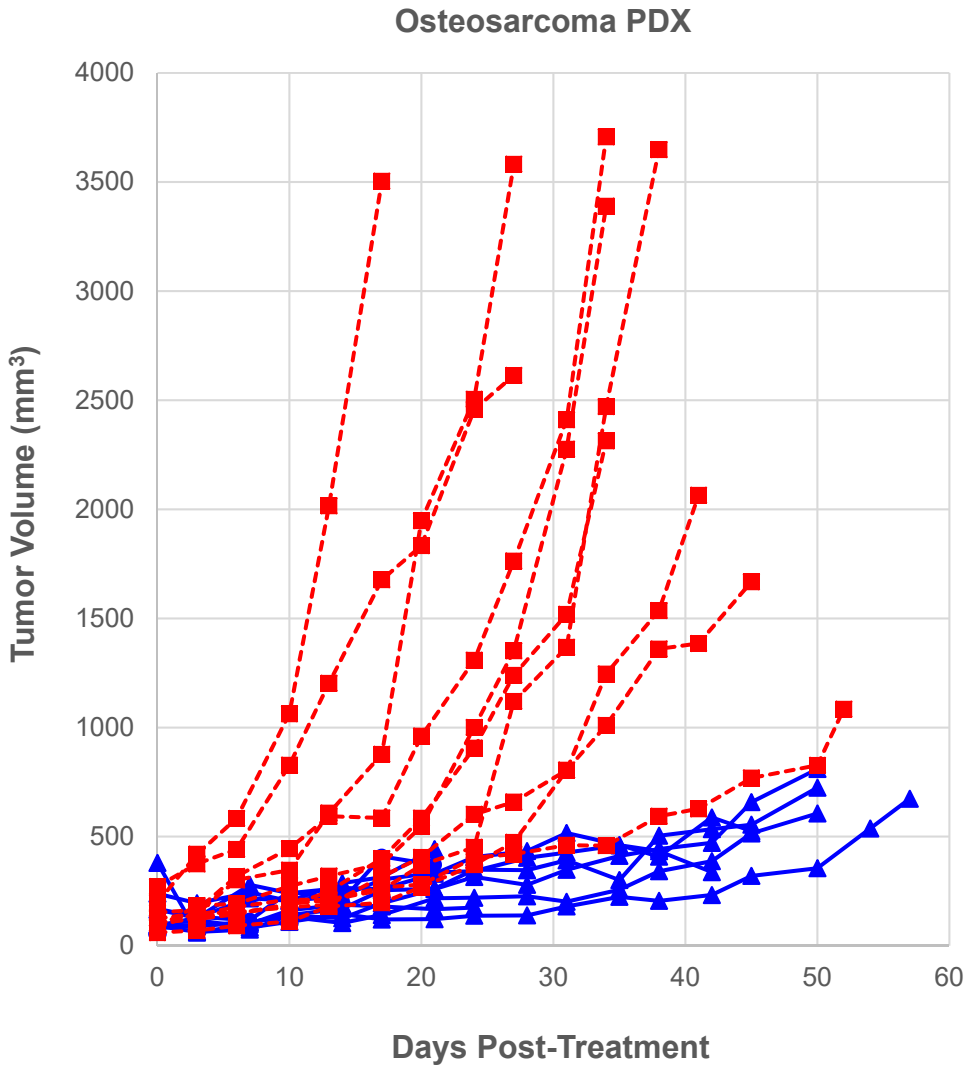
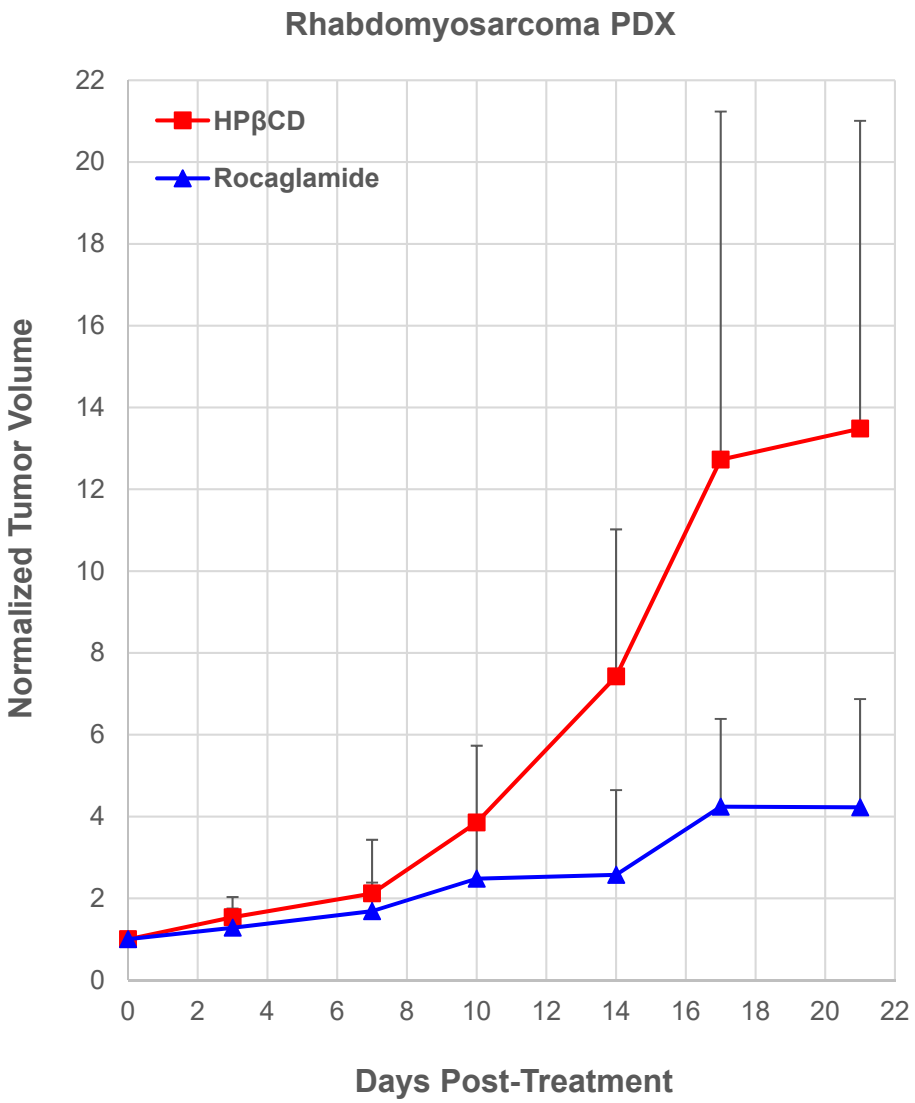

Osteosarcoma PDX
Tumor Volume (mm³)
Days Post-Treatment
0
500
1000
1500
2000
2500
3000
3500
4000
0
10
20
30
40
50
60

Figure 5C


Rhabdomyosarcoma PDX
HPβCD
Rocaglamide
Normalized Tumor Volume
Days Post-Treatment
0
2
4
6
8
10
12
14
16
18
20
22

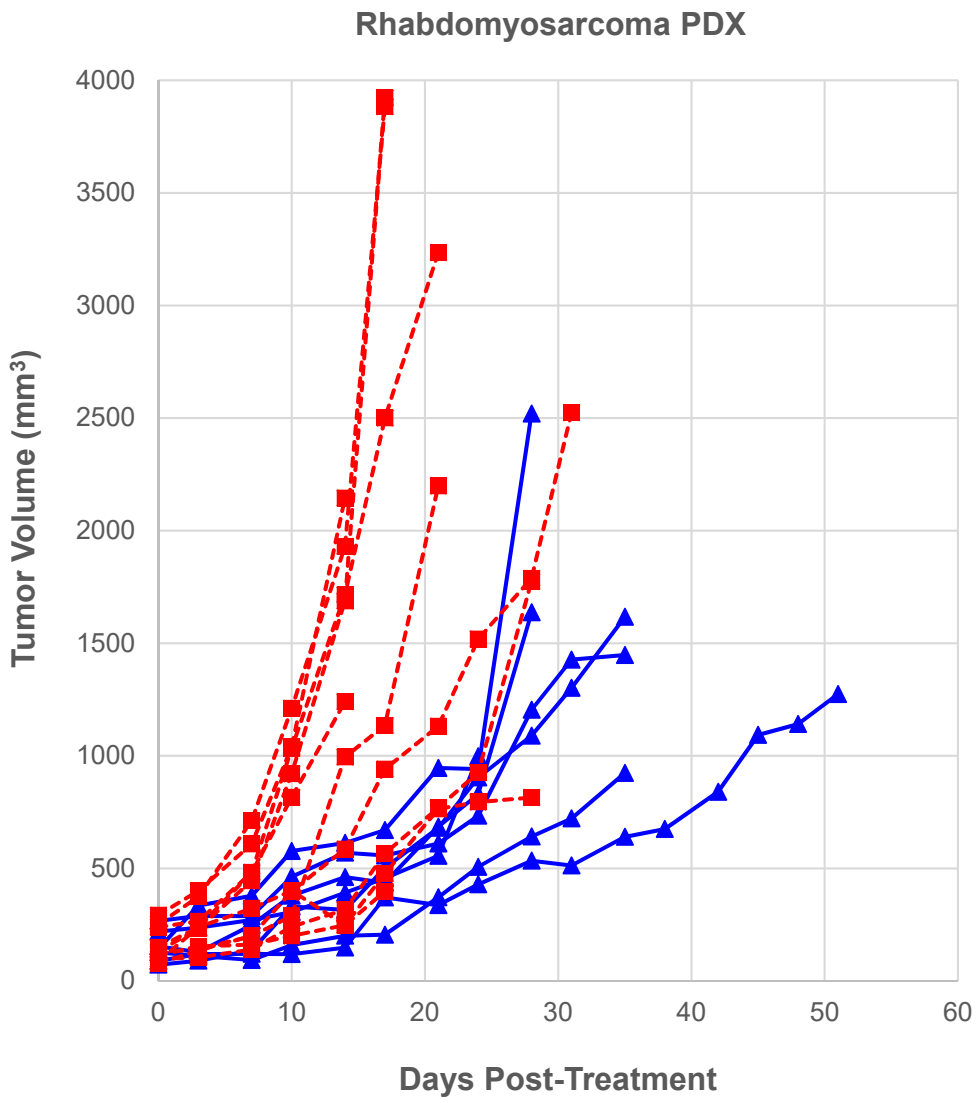

Rhabdomyosarcoma PDX
Tumor Volume (mm³)
Days Post-Treatment
0
500
1000
1500
2000
2500
3000
3500
4000
0
10
20
30
40
50
60

Figure 6A

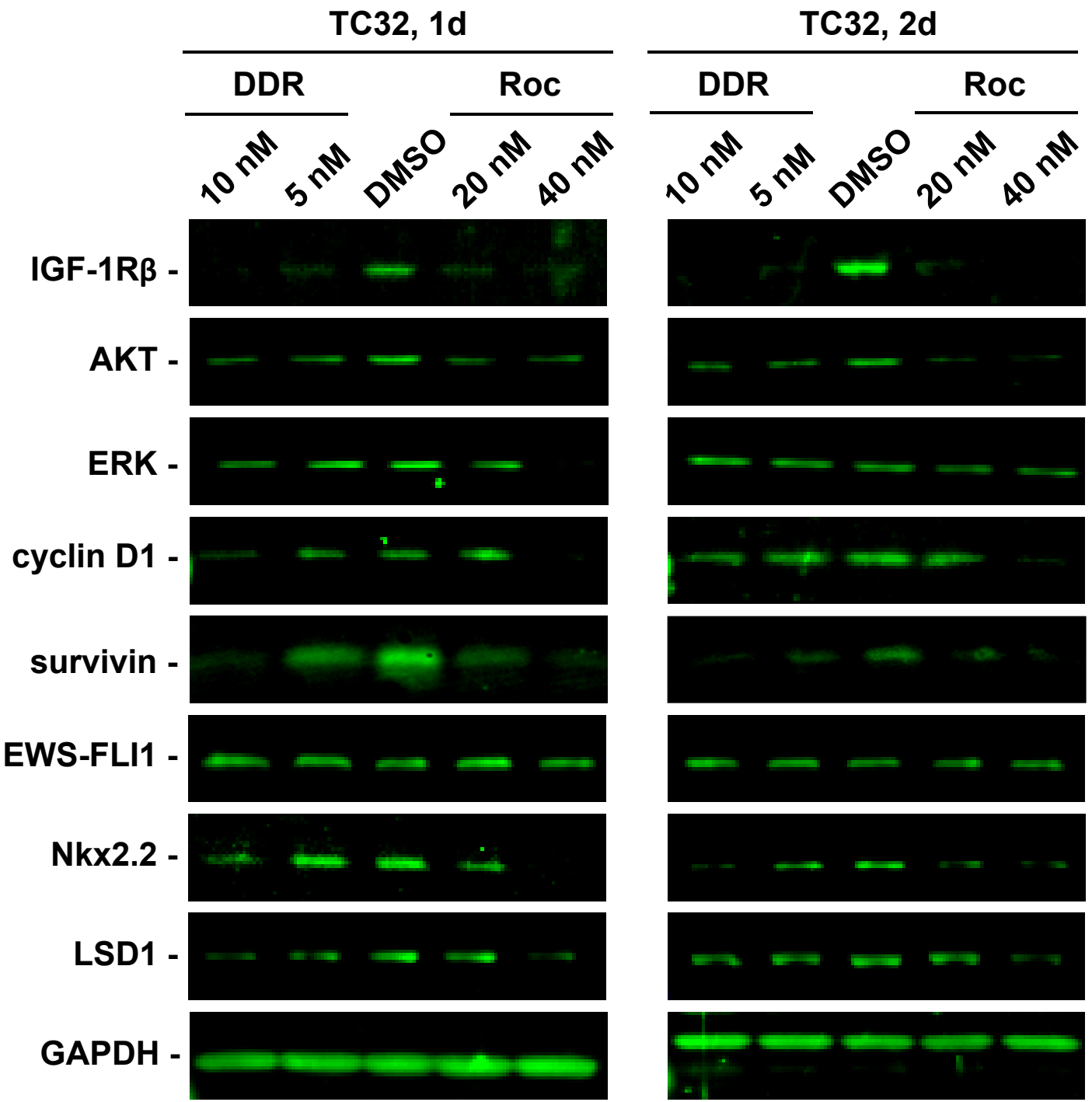

TC32, 1d
TC32, 2d
DDR
Roc
DDR
Roc
10 nM
5 nM
DMSO
20 nM
40 nM
10 nM
5 nM
DMSO
20 nM
40 nM
IGF-1Rβ -
AKT -
ERK -
cyclin D1 -
survivin -
EWS-FLI1 -
Nkx2.2 -
LSD1 -
GAPDH -

Figure 6B

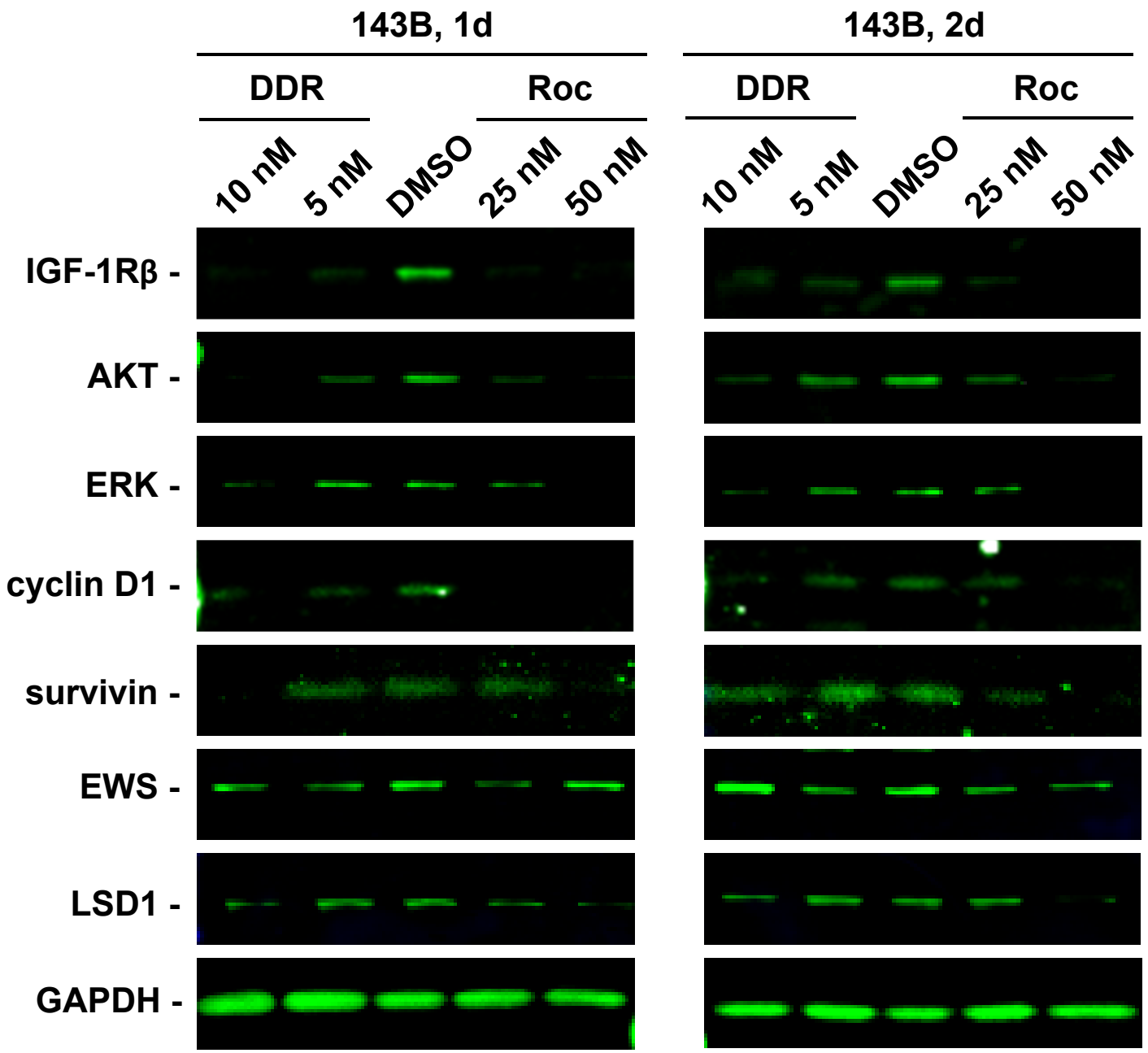
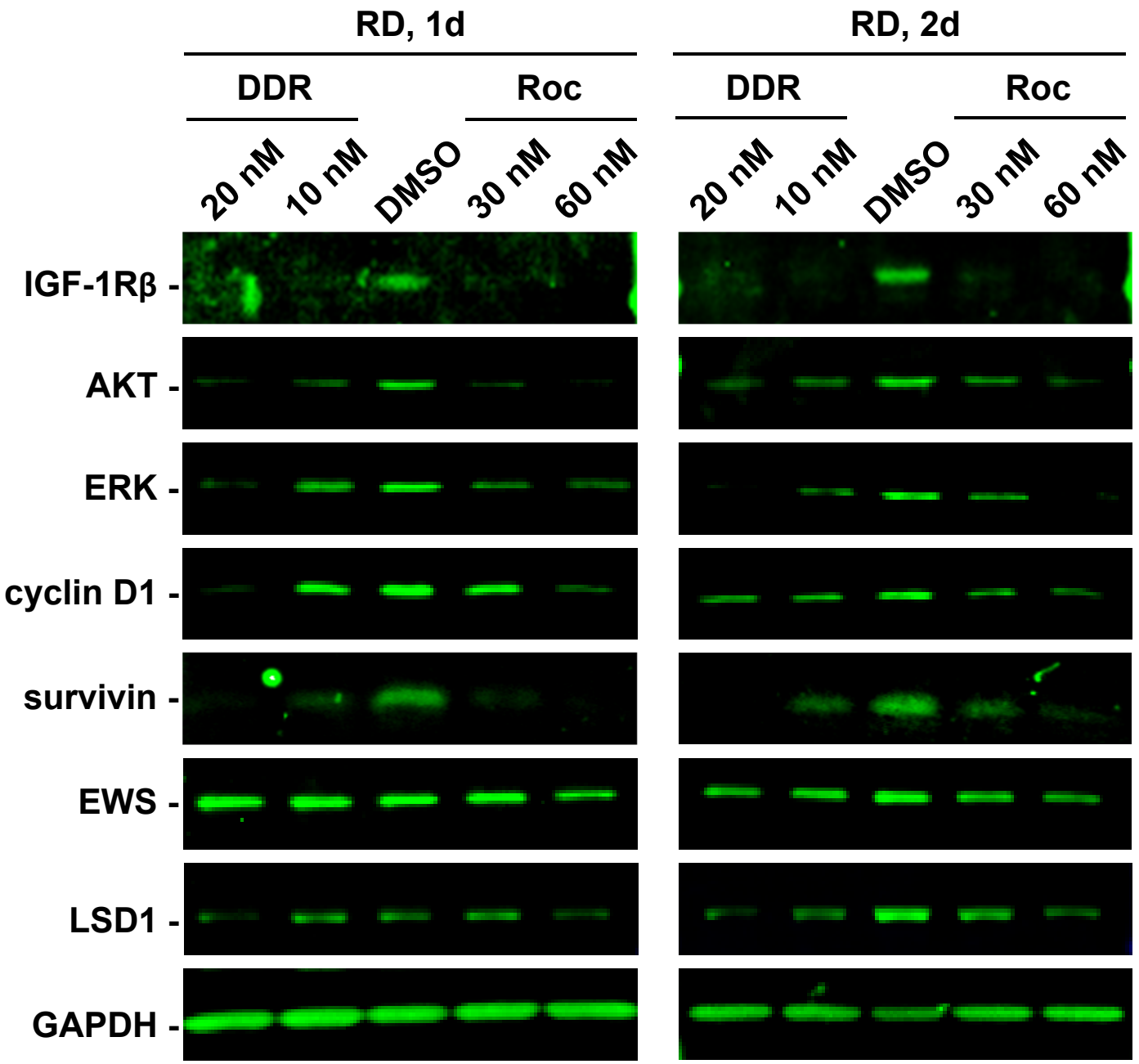
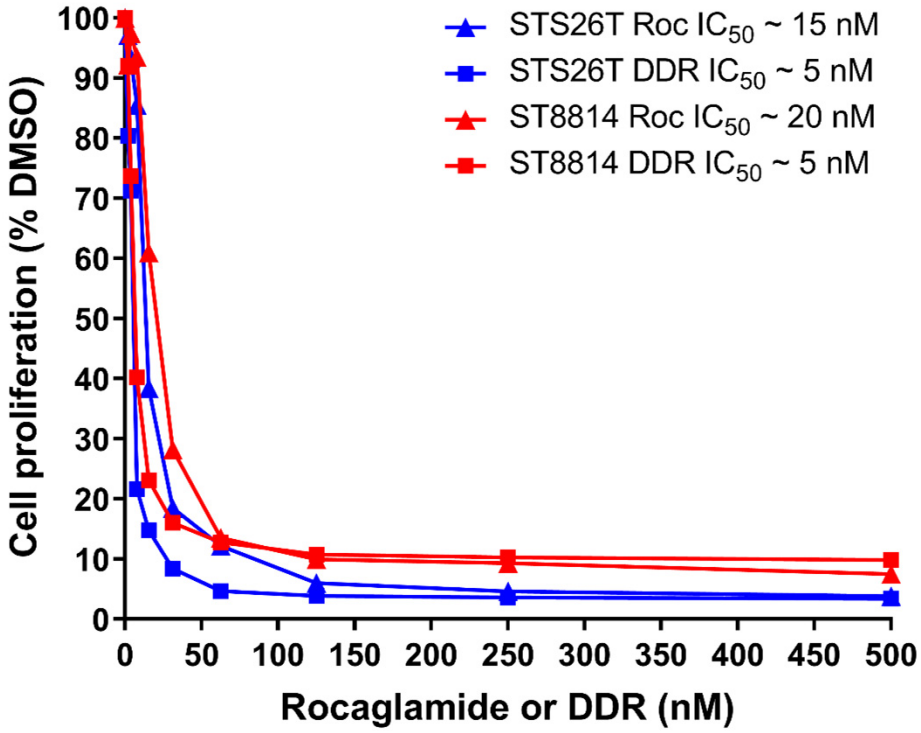

143B, 1d
143B, 2d
DDR
Roc
DDR
Roc
10 nM
5 nM
DMSO
25 nM
50 nM
10 nM
5 nM
DMSO
25 nM
50 nM
IGF-1Rβ -
AKT -
ERK -
cyclin D1 -
survivin -
EWS -
LSD1 -
GAPDH -

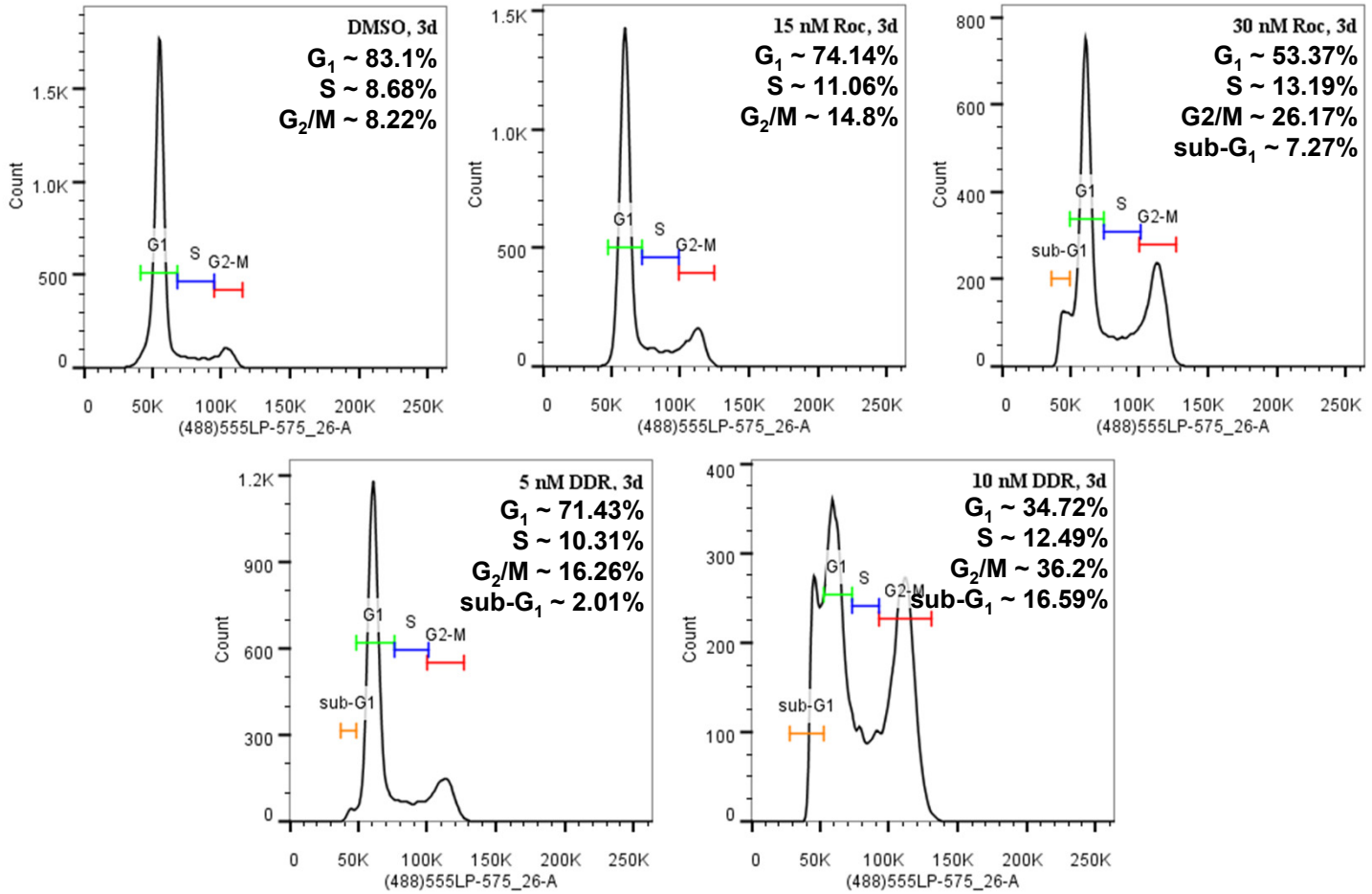
Figure 6C

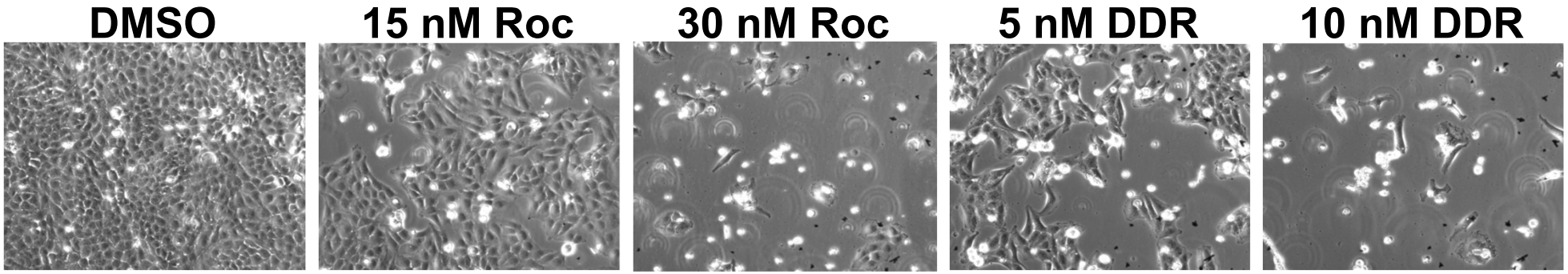

RD, 1d
RD, 2d
DDR
Roc
DDR
Roc
20 nM
10 nM
DMSO
30 nM
60 nM
20 nM
10 nM
DMSO
30 nM
60 nM
IGF-1Rβ -
AKT -
ERK -
cyclin D1 -
survivin -
EWS -
LSD1 -
GAPDH -

Supplementary Fig. S1

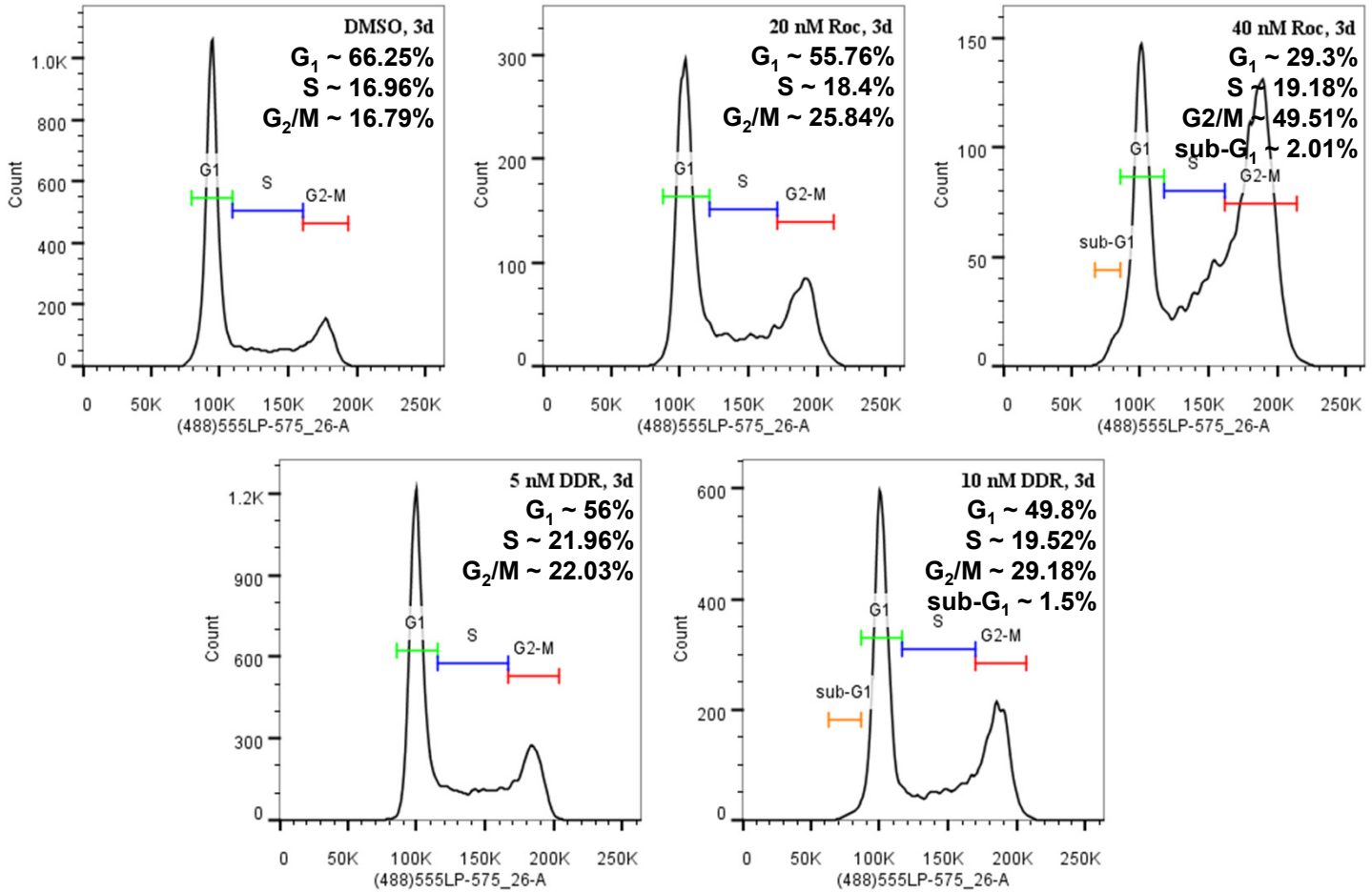


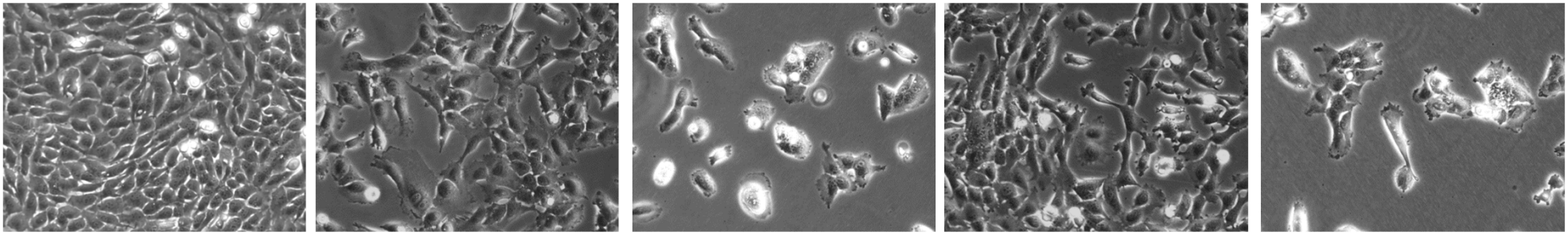
Supplementary Fig. S2A



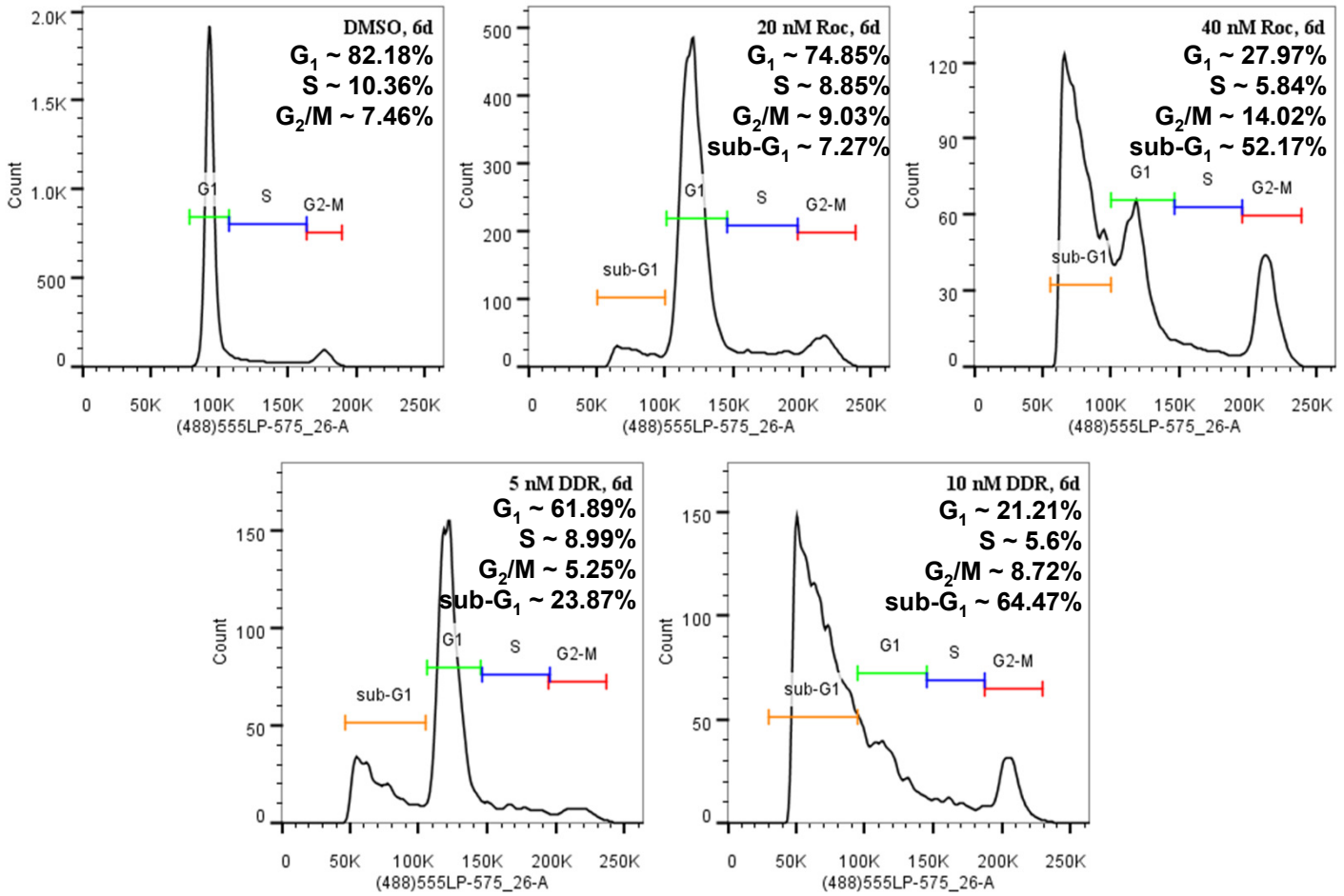


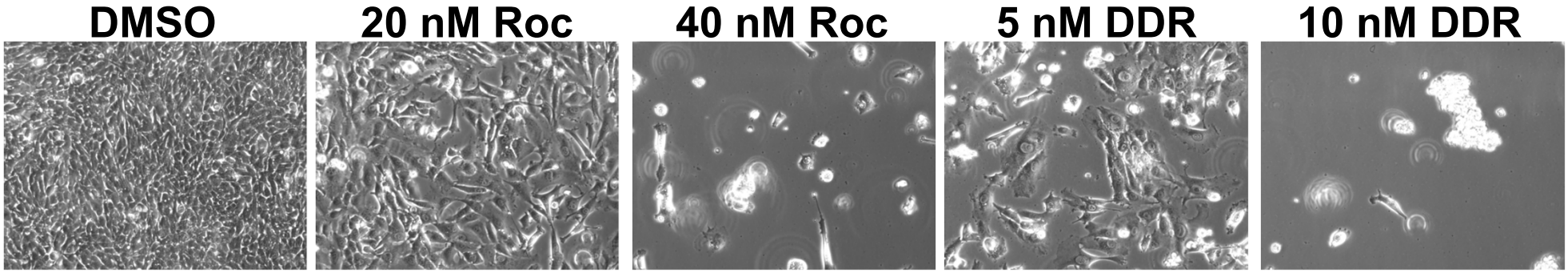
Supplementary Fig. S2B



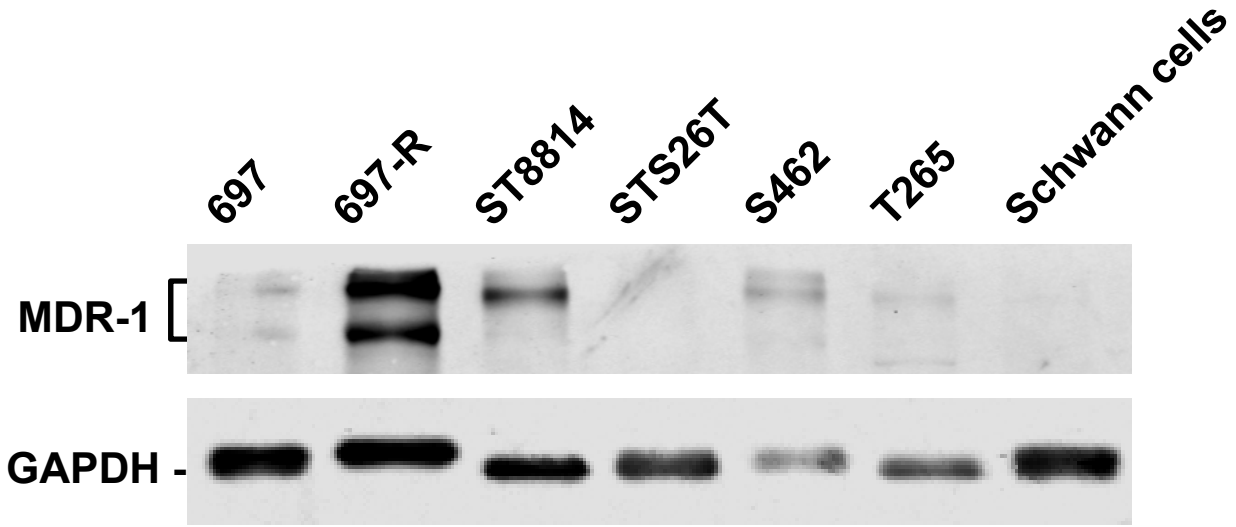


Supplementary Fig. S2C

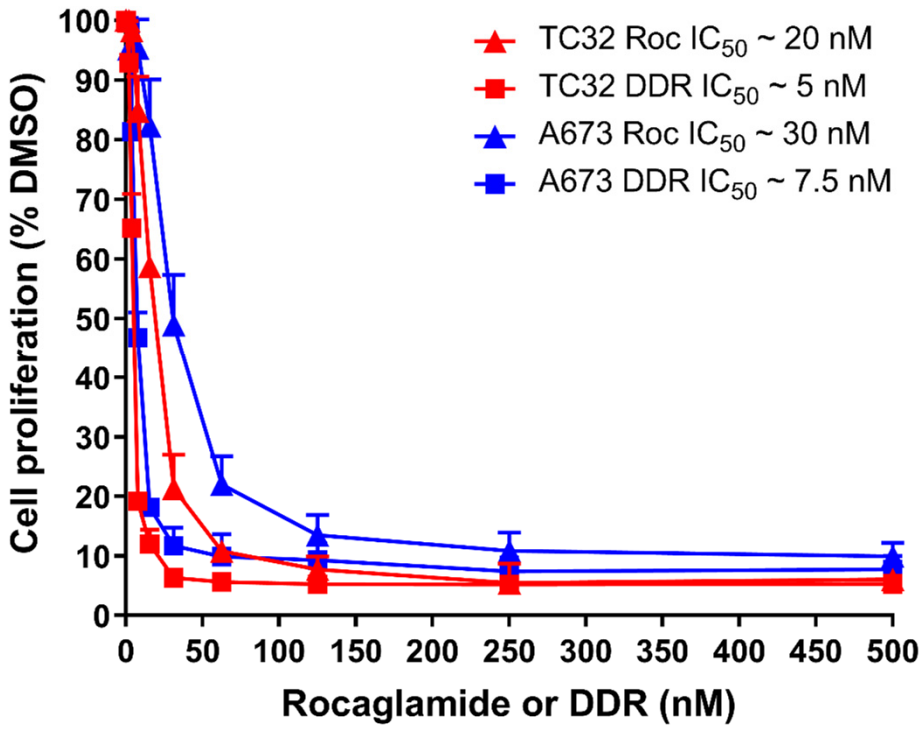




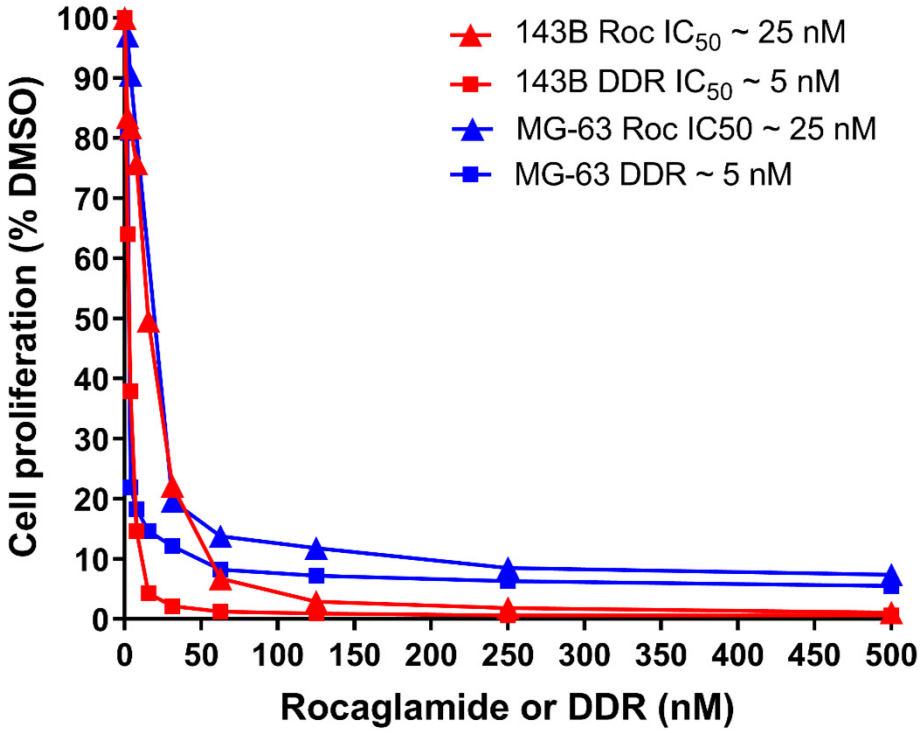
Supplementary Fig. S3

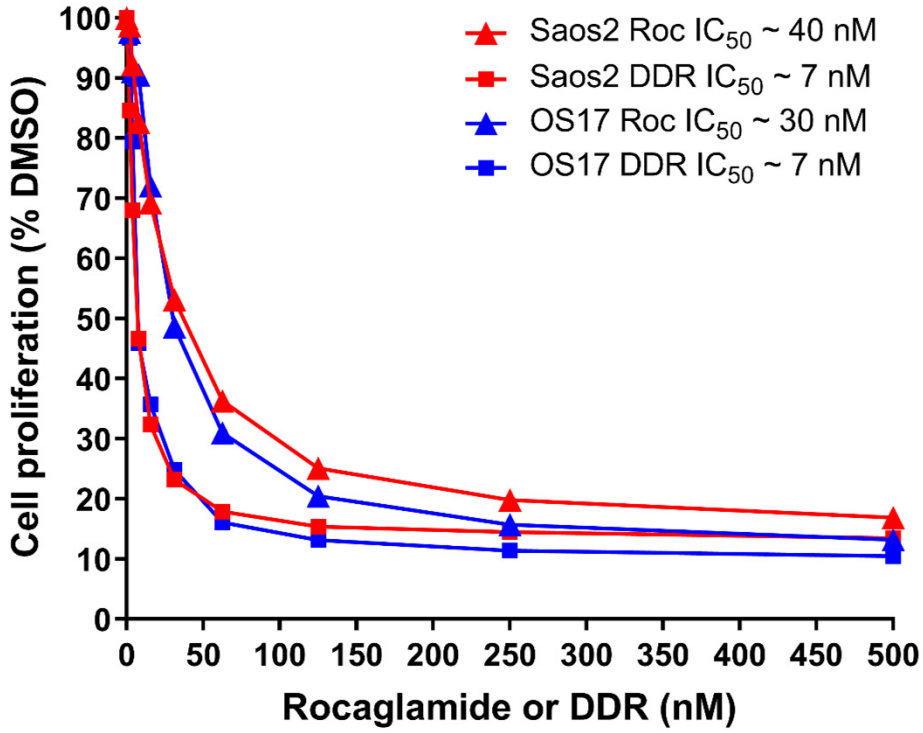


Supplementary Fig. S4A

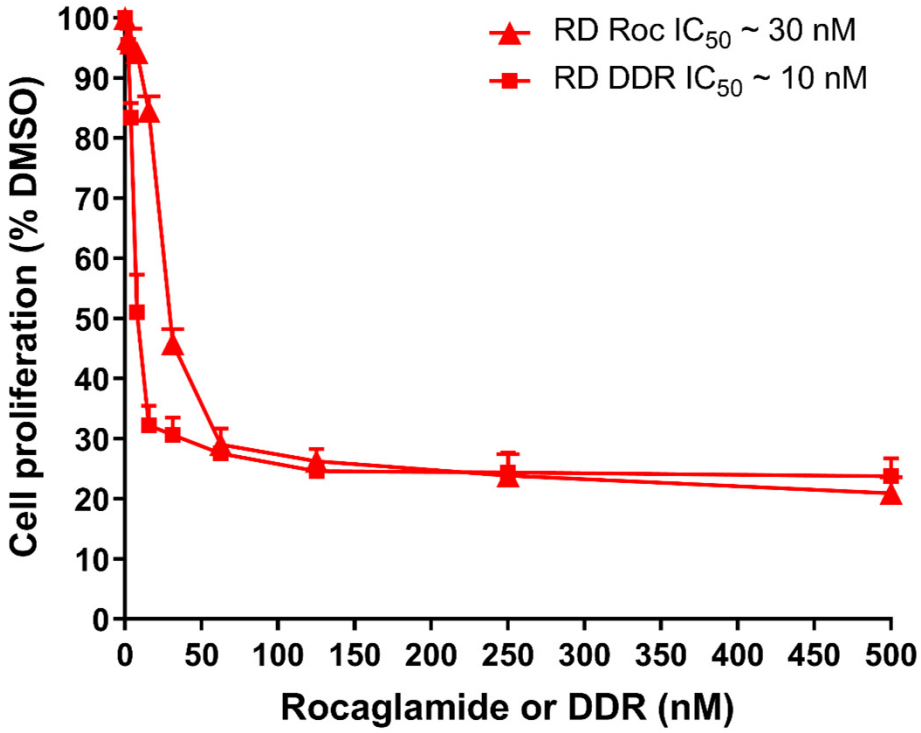


Supplementary Fig. S4B

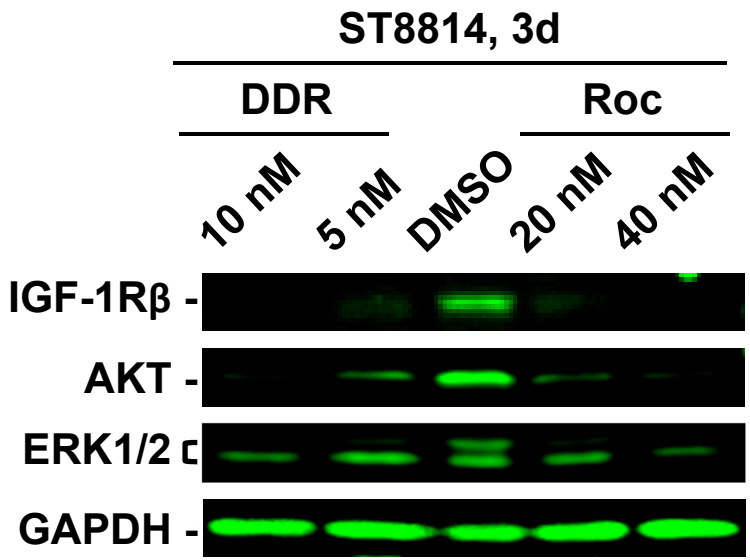




Supplementary Fig. S4C



Supplementary Fig. S5



Abstract Submission

Basic and translational research

NF2/Schwannomatosis

NF2018/ABS-184

Novel drug discovery for NF2-deficient meningiomas: Brigatinib causes tumor shrinkage in NF2-deficient meningiomas

Long-Sheng Chang[*1], Sarah S Burns[1], Janet L Oblinger[1], Marc Ferrer[2], Jie Huang[1], Ming Poi[3], Vijaya Ramesh[4], On behalf of the Synodos for NF2 Consortium[5] and Full list of Investigators of the Children's Tumor Foundation (CTF)-supported Synodos for NF2 Consortium: https://www.synapse.org/#!Synapse:syn2343195/wiki/62126

[1]Center for Childhood Cancer & Blood Diseases/Department of Pediatrics, The Res Inst at Nationwide Children's Hosp/The Ohio State Univ College of Medicine, Columbus, OH, [2]National Center for Advancing Translational Sciences, NIH, Bethesda, MD, [3]Division of Pharmacy Practice & Science , The Ohio State Univ College of Pharmacy, Columbus, OH, [4]Center for Genomic Medicine and Department of Neurology, Massachusetts General Hospital, Boston, MA, [5]The CTF-supported Synodos for NF2 Consortium, NY, United States

Select your prefered type of presentation: Platform presentation

Background: Originating from meningothelial cells of the arachnoid layer lining the brain, meningiomas cause significant morbidities by compressing adjacent brain tissues, cranial nerves, and blood vessels. Meningiomas can occur spontaneously or are frequently found in NF2 patients carrying *NF2* mutations. As an FDA-approved drug is presently not available for *NF2*-deficient meningioma, we aimed to identify novel targeted drugs that delay tumor progression or cause tumor shrinkage.

Methods: A panel of isogenic *NF2*$^-$ and *NF2*$^+$ arachnoidal cells and *NF2*$^-$ meningioma cells was used to screen ~2000 compounds of diverse mechanisms of action. The anti-tumor activity of the selected drug combination, pharmacokinetic (PK) analysis, PathScan RTK Signaling Antibody Arrays, and Western blots were performed.

Results: From the single agent screen, 45 potent compounds were selected for further combination screening, and 33 drug combinations, including the combination of brigatinib, an inhibitor of multi-RTKs including ALK, and MK2206, an AKT inhibitor, were identified that exhibited a greater synergistic growth inhibition in *NF2*$^-$ cells versus *NF2*$^+$ cells. As a single agent, brigatinib effectively blocked tumor growth and reduced tumor size in the intracranial *NF2*-deficient Ben-Men-1-LucB meningioma model, while MK2206 only modestly suppressed tumor growth. Combined treatment with brigatinib and MK2206 further reduced tumor size. Upon cessation of treatment, the tumors treated with brigatinib or the brigatinib/MK2206 combination regrew. Importantly, these regrown tumors were responsive to these drugs when retreated again. PK analysis revealed that both brigatinib and MK2206 crossed the blood-brain barrier and accumulated in tumor-containing brain tissues. Intriguingly, Ben-Men-1 cells did not express ALK but expressed several phospho-RTKs (p-RTKs) with strong expression of p-ErbB2, ErbB3, FGFR1, TrkA, and VEGFR2. Brigatinib treatment reduced the levels of most of these p-RTKs with the most significant reduction in EGFR, ErbB2, ErbB3, VEGFR2, several Eph receptor members, as well as FAK. In addition, brigatinib treatment attenuated the downstream signals of these kinases, including p-AKT and p-ERKs.

Conclusions: The anti-tumor effects of brigatinib in *NF2*-deficient meningiomas are mediated through inhibition of multiple growth-promoting RTKs but not ALK. Brigatinib and its combination with an AKT inhibitor should be further evaluated in patients with *NF2*-deficient meningiomas (Support: the CTF and US Department of Defense)

Disclosure of Interest: None Declared

Keywords: None

Abstract Submission

Basic and translational research

NF1

NF2018/ABS-185

Identification of silvestrol-related rocaglates with better bioavailability and high potency against malignant peripheral nerve sheath tumors

Long-Sheng Chang[*1], Janet L Oblinger[1], Sarah S Burns[1], Jie Huang[1], Larry Anderson[2], Rulong Shen[3], Li Pan[4], Yulin Ren[4], Barry R O'Keefe[5], A Douglas Kinghorn[4], Jerry M Collins[2]

[1]Center for Childhood Cancer & Blood Diseases/Department of Pediatrics, The Research Institute at Nationwide Children's Hospital/The Ohio State University College of Medicine, Columbus, OH, [2]Division of Cancer Treatment and Diagnosis, National Cancer Institute, NIH, Bethesda, MD, [3]Department of Pathology, The Ohio State University College of Medicine, [4]Division of Medicinal Chemistry and Pharmacognosy, The Ohio State University College of Pharmacy, Columbus, OH, [5]Division of Cancer Treatment and Diagnosis and Molecular Targets Program, Center for Cancer Research, National Cancer Institute, NIH, Bethesda, MD, United States

Select your prefered type of presentation: Platform presentation

Background: Malignant peripheral nerve sheath tumors (MPNSTs) frequently overexpress eIF4F components, and the eIF4A inhibitor silvestrol effectively suppresses MPNST growth. However, silvestrol has suboptimal drug-like properties, including a bulky structure and poor oral bioavailability. Our objectives are to identify potent silvestrol-related rocaglates and to determine their bioavailability, anti-tumor effects, and mechanisms of action.

Methods: *NF1*$^{+/+}$ STS26T and *NF1*$^{-/-}$ ST8814 MPNST and 697 and silvestrol-resistant 697-R leukemic cells were treated with various concentrations of each rocaglate. Cell proliferation assays, flow cytometry, Western blots, and pharmacokinetic (PK) analysis were performed. A quantifiable, orthotopic *NF1*-deficient MPNST mouse model and immunohistochemistry were conducted to assess antitumor effects.

Results: Among 10 silvestrol-related rocaglates lacking the dioxanyl ring examined, didesmethylrocaglamide (DDR) and rocaglamide (ROC) had potent growth-inhibitory activity comparable to silvestrol in MPNST cells. Structure-activity relationship analysis revealed that the dioxanyl ring in silvestrol was dispensable while the C-8b hydroxyl group was essential for cytotoxicity. DDR and ROC arrested MPNST cells at G_2/M and significantly increased the sub-G_1 fraction. Accordingly, these rocaglamides induced cleavage of caspases 3 and 7 and poly(ADP-ribose) polymerase, while decreasing total protein levels of these apoptotic markers, consistent with translation inhibition. Additionally, DDR and ROC reduced the levels of mitogenic kinases AKT and ERK1/2. Unlike silvestrol, DDR and ROC inhibited proliferation of silvestrol-resistant 697-R leukemic cells, which over-express the MDR1 multidrug transporter, at IC_{50} values similar to silvestrol-sensitive 697 cells, suggesting that these rocaglamides may be more bioavailable. PK analysis confirmed that ROC had 50% oral bioavailability. Importantly, ROC, when administered intraperitoneally or orally, potently suppressed the growth of luciferase-expressing *NF1*$^{-/-}$ ST8814-Luc MPNST xenografts with no overt toxicity. Treated tumors had abundant phospho-histone H3 labeling and more cleaved caspase 3-positive cells, consistent with G_2/M arrest and indicative of increased apoptosis, respectively.

Conclusions: The more favorable drug-like properties and potent anti-tumor effects suggest that ROC and DDR have potential to become viable MPNST treatments. (Support: CancerFree Kids, the US Department of Defense, and National Cancer Institute, NIH)

Disclosure of Interest: None Declared

Keywords: None

Abstract Submission

Basic and translational research

NF2/Schwannomatosis

NF2018/ABS-151

Preclinical Assessment of MEK1/2 Inhibitors for Neurofibromatosis Type 2-Associated Schwannomas Reveals Differences in Efficacy and Drug Resistance Development.

Cristina Fernandez-Valle[*1], Marisa Fuse[1], Christine Dinh[2], Jeremie Vitte[3], Joanna Kirkpatrick[4], Thomas Mindos[4], Stephani Campion[5], Konstantin Brnjos[1], Maria Clara Franco[6], Jie Huang[7], Juan Young[2], Alejandra Petrilli[1], Denise Yan[2], Rahul Mittal[2], Rulong Shen[8], Fred Telischi[2], Long-Sheng Chang[7], Helen Morrison[4], Marco Giovannini[3], Xue-Zhong Liu[2]

[1]University of Central Florida, Orlando, [2]University of Miami Miller School of Medicine, Miami, [3]David Geffen School of Medicine, UCLA, Los Angeles, United States, [4]Leibniz Institute on Aging, Jena, Germany, [5]Orlando Health , Orlando, [6] Oregon State University, Corvallis, [7]Nationwide Children's Hospital, [8]Ohio State University, Columbus, United States

Select your prefered type of presentation: Platform presentation

Background: Neurofibromatosis type 2 (NF2) is a genetic tumor disorder caused by loss of function of the *NF2*/merlin tumor suppressor gene. A hallmark of NF2 is formation of bilateral vestibular schwannomas (VS) for which no FDA-approved drug is presently available. Because merlin modulates activity of the Ras/Raf/MEK/ERK pathway, we investigated repurposing drugs targeting MEK1/2 to treat NF2-associated schwannomas.

Methods: Mouse and human merlin-deficient Schwann cell (MD-MSC/HSC) lines were screened against six MEK1/2 inhibitors. Efficacious drugs were tested in orthotopic allograft and *NF2* transgenic mouse models. Proteome and pathway analyses were conducted. Drug efficacy was examined in primary human VS cells with *NF2* mutations and correlated with differential DNA methylation patterns.

Results: Trametinib, PD0325901, and cobimetinib were the most potent in reducing MD-MSC/HSC viability. Each decreased pERK1/2 and cyclin $D_{1,}$ increased p27, and induced caspase 3 cleavage in MD-MSCs. Proteome analysis was consistent with cell cycle arrest and activation of pro-apoptotic pathways in trametinib-treated MD-MSCs. The three inhibitors slowed the growth of MD-MSC allografts compared to controls. However, decreased pERK1/2, cyclin $D_{1,}$ and Ki67 levels were observed in PD0325901 and cobimetinib, but not trametinib treated grafts. Eight weeks of trametinib treatment reduced tumor burden and average tumor size compared to controls in the *NF2* transgenic mouse model; tumors did not exhibit reduced pERK1/2 staining compared to control. Both trametinib and PD0325901 modestly reduced viability of several primary human VS cells with *NF2* mutations. DNA methylation analysis of PD0325901-resistant versus -susceptible VS identified differentially methylated regions in genes that could contribute to drug-resistance.

Conclusions: This comprehensive pre-clinical study demonstrates efficacy differences and possible emergence of drug resistance among MEK inhibitors in schwannoma models and supports further investigation of MEK inhibitors alone and in combination with other targeted drugs as treatments for NF2-associated schwannomas.

Disclosure of Interest: None Declared

Keywords: None

Abstract Submission

Clinical research

NF2/Schwannomatosis

NF2018/ABS-215

Phase 1 and Phase 0 studies of AR-42, a pan histone deacetylase inhibitor, in subjects with neurofibromatosis type 2 (NF2)-associated vestibular schwannomas and meningiomas

D. Bradley Welling*[1], Sarah Burns[2], Janet Oblinger[3], Beth Miles-Markley[4], Amir Mortazavi[5], Amy Quinkert[6], Jaishri Blakeley[7], S. Alireza Monsouri[8], Brian Neff[9], Robert Jackler[10], Long-Sheng Chang[2,3,4]

[1]Otolaryngology, Harvard Medical School, Massachusetts Eye and Ear, Massachusetts General Hospital, Boston, [2]Departments of Pediatrics, [3]Center for Childhood Cancer, Nationwide Children's Hospital, [4]Otolaryngology Head & Neck Surgery, [5]Internal Medicine, The Ohio State University, Columbus, [6]Otolaryngology, Harvard University/MEEI, Boston, [7]Departments of Neurology, Neurosurgery and Oncology, [8]Neurosurgery, Johns Hopkins University, Baltimore, [9]Department of Otolaryngology, Mayo Clinic, Rochester, [10]Department of Otolaryngology, Stanford University, Palo Alto, United States

Select your prefered type of presentation: Platform presentation

Background: Patients with NF2 frequently develop bilateral vestibular schwannomas (VS) and multiple meningiomas. Presently, an FDA-approved medical therapy is not available. The histone deacetylase inhibitor AR-42 suppresses schwannoma growth and causes tumor shrinkage in meningiomas in preclinical models.

Methods: As part of a phase I trial of AR-42 in patients with advanced or recurrent solid tumors for which no standard therapy is available or patients who decline available standard treatment options, patients with NF2-associated VS and meningiomas were enrolled and received AR-42 treatment 3 times weekly for 3 weeks followed by 1-week break. Subsequently, a phase 0 exploratory evaluation of AR-42 for intratumoral pharmacodynamics and pharmacokinetics in VS and meningiomas was performed.

Results: In the phase I trial, 5 NF2 patients were recruited. AR-42 was overall well-tolerated, and the maximum tolerated dose (MTD) was defined at 60 mg. AR-42 demonstrated anti-tumor activity mostly in the form of tumor stability. In one NF2 patient treated for 10 months, AR-42 significantly reduced tumor size in meningiomas and slowed VS growth rates. After cessation of treatment, meningiomas remained small, but VS quickly resumed growth. Tissue samples including bilateral right and left VS, a skull base meningioma, and an optic meningioma from this patient as well as a VS from a second person with NF2 were collected. These 5 tumors underwent comprehensive genomic profiling via FoundationOne. Mutations in *NF2* and *NUP98* were found. A phase 0 study with the primary objective to estimate p-AKT and $p16^{INK4A}$ levels after 3 weeks of oral AR-42 at 40 mg every other day, 3 times a week for 3 weeks preceding surgery, in NF2-related and sporadic VS and meningiomas, as well as control tumor samples from a tissue bank is ongoing. The secondary objectives include assessment of audiometric changes and volumetric tumor reduction and determination of plasma and intra-tumoral AR-42 concentrations. So far, 5 patients were studied. AR-42 concentrations in the plasma and VS of treated patients reached levels around the IC_{50} value determined *in vitro* and was more preferentially concentrated in the tumors. AR-42 decreased the levels of p-AKT, pERK1/2, p-PRAS40, and p-S6 in treated VS.

Conclusions: **Conclusions:**AR-42 achieves therapeutic concentrations in the tumors and hits its targets. Further investigation of AR-42 as an NF2 treatment is ongoing.

(Funding: The US Department of Defense, The Galloway Family, and Advocure NF2)

Disclosure of Interest: None Declared

Keywords: None

Abstract presented at the 2019 NF Conference, San Francisco, CA. (Sept. 2019)

Brigatinib as a potential therapy for malignant peripheral nerve sheath tumors

Janet Oblinger, Ph.D.
Nationwide Children's Hospital & The Ohio State University

MPNSTs are highly aggressive soft-tissue sarcomas that have a high risk of recurrence and metastasis and are refractory to current treatment. These tumors can arise spontaneously or from pre-existing plexiform neurofibromas in patients with neurofibromatosis type 1 (NF1), a tumor predisposition syndrome caused by inactivating mutations in the *NF1* tumor suppressor gene which encodes a Ras-GTPase-activating protein. Importantly, even sporadic tumors often incur mutations in the *NF1* gene or the Ras pathway. As a consequence, MPNSTs exhibit upregulation of Ras downstream kinase signaling, including the phosphatidylinositol 3-kinase (PI3K)-AKT-mammalian target of rapamycin (mTOR) and Raf-MEK-ERK mitogen-activated protein kinases. MPNSTs also harbor other genetic alterations, such as aberrant activation of epidermal growth factor receptor (EGFR) and insulin-like growth factor-1 receptor (IGF-1R), suggesting that these receptor tyrosine kinases (RTKs) may be therapeutic targets. Previously we showed that the FDA-approved ALK inhibitor brigatinib (ALUNBRIG™) suppresses multiple RTKs and non-RTKs, including focal adhesion kinase (FAK). Here we demonstrate that brigatinib exhibited growth-inhibitory activity in *NF1*-deficient ST8814 and *NF1*-expressing STS26T MPNST cells. Combination of brigatinib with the dual mTORC1/2 inhibitor INK128 (sapanisertib) yielded enhanced anti-proliferative effects. Treatment of ST8814 cells with brigatinib decreased p-EGFR and p-IGF-1R and their downstream p-AKT and p-S6. Treatment with INK128 also profoundly inhibited p-AKT and p-S6. Interestingly, combination of brigatinib and INK128 further reduced the phosphorylation of these signaling mediators and p-FAK compared to either monotherapy, suggesting cooperation in suppressing the AKT-mTOR pathway. However, we did not detect ALK expression in ST8814 and STS26T cells, indicating that brigatinib mediates growth inhibition via targeting of other tyrosine kinases. Experiments are in progress to investigate the anti-tumor activity of brigatinib in patient-derived xenograft (PDX) models for MPNST. Collectively, our data suggest that brigatinib should be further evaluated as a potential treatment for MPNST.

Full List Authors: Janet Oblinger[1,2] and Long-Sheng Chang[1,2,3]

[1]Center for Childhood Cancer and Blood Diseases, Abigail Wexner Research Institute at Nationwide Children's Hospital and Depts of [2]Pediatrics & [3]Otolaryngology-Head & Neck Surgery, The Ohio State University

Funding: CancerFree KIDS, Department of Defense

Abstract presented at the 2019 NF Conference, San Francisco, CA. (Sept. 2019)

Targeting protein translation with rocaglamide and didesmethylrocaglamide to treat NF1 and NF2 tumors

Long-Sheng Chang
Nationwide Children's Hospital & The Ohio State University

To sustain uncontrolled growth, cancer cells exhibit enhanced protein synthesis by upregulation of the protein translation machinery. Previously we reported that NF1-associated malignant peripheral nerve sheath tumors (MPNSTs) and NF2-related vestibular schwannomas and meningiomas exhibit elevated expression of eIF4A, eIF4E, and eIF4G, components of the eIF4F translation initiation complex, and that the eIF4A inhibitor silvestrol potently suppresses the growth of these tumor cells. Studies by others also show strong anti-tumor activity of silvestrol in several other cancer models, suggesting that it may be a potential cancer treatment. However, silvestrol has suboptimal drug-like properties, including a bulky structure, sensitivity to inhibition by the MDR1 multidrug-resistant transporter, and poor oral bioavailability. By screening 10 silvestrol-related rocaglates lacking the dioxanyl ring, we identified rocaglamide (Roc) and didesmethylrocaglamide (DDR) with potent growth-inhibitory activity comparable to silvestrol in MPNST cells. Structure-activity relationship analysis revealed that the dioxanyl ring present in silvestrol was dispensable for, but may enhance, cytotoxicity. Both Roc and DDR arrested MPNST cells at G_2/M, significantly increased the sub-G_1 fraction, and induced cleavage of caspases 3 and 7 and poly(ADP-ribose) polymerase, while decreasing total protein levels of these apoptotic markers and mitogenic kinases AKT and ERK1/2, consistent with translation inhibition. Additionally, these rocaglamides elevated the levels of γH2AX, a marker of the DNA damage response. Unlike silvestrol, Roc and DDR were not sensitive to MDR1 inhibition. Pharmacokinetic analysis confirmed that Roc had 50% oral bioavailability. Importantly, Roc, when administered intraperitoneally or orally, potently suppressed the growth of orthotopic *NF1*-deficient MPNST xenografts with no overt toxicity. Treated MPNSTs had abundant phospho-histone H3 labeling and more cleaved caspase 3-positive cells, consistent with G_2/M arrest and indicative of increased apoptosis, respectively. In addition, Roc exhibited anti-tumor effects in patient-derived xenograft models for several types of sarcomas, including Ewing sarcoma, osteosarcoma, and rhabdomyosarcoma. Western blot analysis revealed that Roc and DDR decreased multiple oncogenic kinases, including IGF-1R, in sarcoma cells. Further, these rocaglamides potently inhibited proliferation of *NF2*-deficient schwannoma and meningioma cells. The more favorable drug-like properties and potent anti-tumor effects of Roc and DDR suggest that these rocaglamides have potential to become viable treatments for NF1- and NF2-associated tumors, including MPNST, as well as other sarcomas.

Full List Authors: Long-Sheng Chang[1], Janet L Oblinger[1], Sarah S Burns[1], Jie Huang[1], Larry Anderson[2], Rulong Shen[3], Li Pan[4], Yulin Ren[4], Ryan Roberts[1], Barry R O'Keefe[5], A Douglas Kinghorn[4], Jerry M Collins[2]

[1]Ctr for Childhood Cancer & Blood Diseases, Nationwide Children's Hospital/Dept of Pediatrics, The Ohio State Univ, [2]Div of Cancer Treatment and Diagnosis, National Cancer Institute, NIH, [3]Dept of Pathology, The Ohio State Univ, [4]Div of Medicinal Chemistry and Pharmacognosy, The Ohio State Univ Coll of Pharmacy, [5]Div of Cancer Treatment and Diagnosis and Molecular Targets Program, Ctr for Cancer Research, National Cancer Institute, NIH

Funding: CancerFree KIDS, Sunbeam Foundation, Department of Defense